

INFORMATION TO USERS

This manuscript has been reproduced from the microfilm master. UMI films the text directly from the original or copy submitted. Thus, some thesis and dissertation copies are in typewriter face, while others may be from any type of computer printer.

The quality of this reproduction is dependent upon the quality of the copy submitted. Broken or indistinct print, colored or poor quality illustrations and photographs, print bleedthrough, substandard margins, and improper alignment can adversely affect reproduction.

In the unlikely event that the author did not send UMI a complete manuscript and there are missing pages, these will be noted. Also, if unauthorized copyright material had to be removed, a note will indicate the deletion.

Oversize materials (e.g., maps, drawings, charts) are reproduced by sectioning the original, beginning at the upper left-hand corner and continuing from left to right in equal sections with small overlaps. Each original is also photographed in one exposure and is included in reduced form at the back of the book.

Photographs included in the original manuscript have been reproduced xerographically in this copy. Higher quality 6" x 9" black and white photographic prints are available for any photographs or illustrations appearing in this copy for an additional charge. Contact UMI directly to order.

UMI

A Bell & Howell Information Company
300 North Zeeb Road, Ann Arbor MI 48106-1346 USA
313/761-4700 800/521-0600

UNIVERSITY OF ALBERTA

CREEP ANALYSIS OF THE LEANING TOWER OF PISA

BY

JUNLI BAI



A thesis submitted to the Faculty of Graduate Studies and Research in partial fulfillment
of the requirements for the degree of Doctor of Philosophy

IN

GEOTECHNICAL ENGINEERING

DEPARTMENT OF CIVIL AND ENVIRONMENTAL ENGINEERING

Edmonton, Alberta

Spring 1998



National Library
of Canada

Acquisitions and
Bibliographic Services

395 Wellington Street
Ottawa ON K1A 0N4
Canada

Bibliothèque nationale
du Canada

Acquisitions et
services bibliographiques

395, rue Wellington
Ottawa ON K1A 0N4
Canada

Your file Votre référence

Our file Notre référence

The author has granted a non-exclusive licence allowing the National Library of Canada to reproduce, loan, distribute or sell copies of this thesis in microform, paper or electronic formats.

The author retains ownership of the copyright in this thesis. Neither the thesis nor substantial extracts from it may be printed or otherwise reproduced without the author's permission.

L'auteur a accordé une licence non exclusive permettant à la Bibliothèque nationale du Canada de reproduire, prêter, distribuer ou vendre des copies de cette thèse sous la forme de microfiche/film, de reproduction sur papier ou sur format électronique.

L'auteur conserve la propriété du droit d'auteur qui protège cette thèse. Ni la thèse ni des extraits substantiels de celle-ci ne doivent être imprimés ou autrement reproduits sans son autorisation.


0-612-29022-0

Canada

UNIVERSITY OF ALBERTA

FACULTY OF GRADUATE STUDIES AND RESEARCH

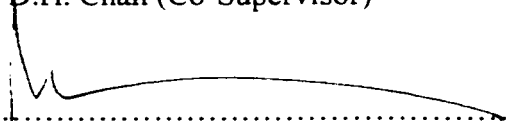
The undersigned certify that they have read, and recommend to the Faculty of Graduate Studies and Research for acceptance, a thesis entitled CREEP ANALYSIS OF THE LEANING TOWER OF PISA submitted by Junli Bai in partial fulfillment of the requirements for the degree of Doctor of Philosophy in Geotechnical Engineering.



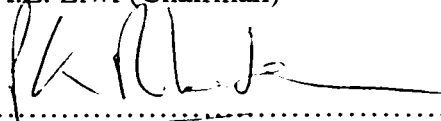
.....
Dr. N.R. Morgenstern (Supervisor)




.....
Dr. D.H. Chan (Co-Supervisor)



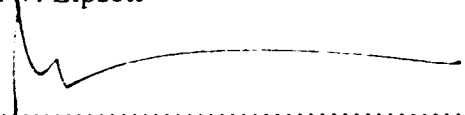
.....
Dr. A.E. Elwi (Chairman)



.....
Dr. P.K. Robertson



.....
Dr. A.W. Lipsett



.....
Prof. M.B. Jamiolkowski (External-examiner)

Date... March 12, 1998

To my father, my mother
my husband Jingsheng, and my daughter Sandy
-For their continuous Love, Encouragement, and Support.

ABSTRACT

This research aims at studying the leaning mechanism of the Leaning Tower of Pisa and analyzing the creep behavior of the soil beneath the foundation of the tower under both two and three-dimensional conditions.

The existing literature on creep modeling was reviewed and the double-yield surface Cam-clay plasticity (DYSCP) model was studied in detail. This model was modified by changing the intrinsic time variables. The modified model was tested by simulating a series of triaxial drained creep tests. Results show that the modified model can provide a more accurate and reasonable approximation of the time-dependent effect of the Singh and Mitchell parameter m .

Simulations of the time-dependent deformation of the soil beneath the tower's foundation in both the two-dimensional plane strain and fully three-dimensional conditions were carried out. An extensive model parameter study was conducted. The creep effect has been found to account for 1.5° out of the total 5.5° of the tower's inclination. It causes mean effective stresses to increase and deviatoric stresses to decrease in the clay layers, resulting in the stress state to move further away from the critical state line. It was also found that the deformation behavior of the soil beneath the tower's foundation is not sensitive to any specific model parameter in the DYSCP model. The total tilting angle of 5.5° could not be simulated by simply changing the values of these parameters. There must be other reasons that contribute to the tilting of the tower which are almost impossible to be considered in a single constitutive model.

Nevertheless, as the only fully three-dimensional creep analysis ever carried out, the current study could calculate the tilting history of the tower within reasonable accuracy during its construction period and illustrate more or less the same trend for the last four centuries. The model also could match the observed maximum settlement on top of the upper clay layers extremely well. Therefore, this study provides considerable insight into the deformation history of the soil beneath the foundation and the stresses that likely exist within it.

ACKNOWLEDGMENTS

It has been an excellent experience to have worked under the direction of Dr. N.R. Morgenstern. I am deeply grateful to him for his continuous support, guidance and enthusiasm in the subject. His ideas and supervision throughout this research will be appreciated forever.

I wish to express my gratitude to Dr. D.H. Chan for his support and patience since the beginning of this work. His supervision, discussions, suggestions, and comments were invaluable to the accomplishment of this research.

I am also very grateful to the other faculty members in the Geotechnical Engineering Group at the University of Alberta, such as Dr. P.K. Robertson, Dr. D.C. Sego, and Dr. Z. Eisenstein for their support. Technical support given by Doug Booth and Gerry Cyre in computer facilities is appreciated.

My six-year old daughter Sandy has been growing up with this thesis. Great thanks to her for her cooperation and understanding in helping me to balance my efforts as a mother and a Ph. D. student, especially during the last two and half years when I have been alone with her.

I owe special thanks to my husband Jingsheng and to my parents for their understanding and their sacrifices on my behalf. I was, I am, and I will always be grateful to them.

TABLE OF CONTENTS

Chapter	Page
1 Thesis scope and objectives	
1.1 Introduction.....	1
1.2 Research scope.....	4
1.3 Research objective and anticipated contributions.....	5
1.4 Thesis outline.....	5
2 Literature review	
2.1 Introduction.....	8
2.2 Review of creep models.....	9
2.2.1 Review of the existing creep models.....	9
2.2.2 Double-yield surface Cam-clay plasticity (DYSCP) model.....	13
2.3 Construction history and physical observation of Pisa Tower.....	21
2.3.1 Construction history.....	21
2.3.2 History of tilting and major perturbations.....	22
2.4 Subsurface conditions.....	24
2.5 Major research efforts about the tower.....	26
2.5.1 The leaning of the tower.....	26
2.5.2 Stabilization measures.....	28
2.5.3 Previous numerical analysis.....	29
2.5.4 Creep test of the Pisa clay.....	31
2.6 Summary.....	32

3	Numerical simulation of drained creep tests on Pisa clay	
3.1	Introduction.....	58
3.2	Geotechnical properties of Pisa Soils	59
3.3	Modification of a time-dependent constitutive model	60
3.3.1	Original constitutive model	60
3.3.2	Modification of the intrinsic time variables.....	63
3.4	Verification of the modified model using Bishop’s drained creep tests	66
3.4.1	Model parameters	67
3.4.2	Simulation results by varying the Singh and Mitchell parameter m	68
3.4.3	Numerical simulation of Bishop’s drained creep tests	68
3.5	Verification of the modified model using Mitchell’s drained creep tests.....	69
3.5.1	Model parameters	70
3.5.2	Simulation results	71
3.6	Conclusions.....	71
4	Numerical analyses of time-dependent behavior of Pisa Tower	
4.1	Introduction.....	88
4.2	Overview of Pisa Tower	89
4.2.1	Construction history.....	89
4.2.2	Soil profile and soil parameters	90
4.2.3	Stabilization measures	92
4.2.4	Previous numerical investigation.....	94
4.3	Time-dependent constitutive model.....	95
4.4	Plane strain elastic and elasto-plastic analysis.....	98
4.4.1	Finite element	99

4.4.2	Stress distributions in the soil beneath the foundation	101
4.4.3	Displacements of the footing	102
4.4.4	Sensitivity analysis of correction factors	103
4.5	Plane strain visco-plastic analysis.....	104
4.5.1	Input parameters	104
4.5.2	Stress distributions in the soil beneath the foundation	105
4.5.3	Displacements of the footing	106
4.6	Summary and conclusion	107

5 Deformation behavior of Pisa Tower--parameter sensitivity studies

5.1	Introduction.....	143
5.2	The Leaning Tower of Pisa.....	144
5.2.1	History of construction	145
5.2.2	Subsurface conditions.....	145
5.3	The constitutive model.....	146
5.4	Sensitivity analyses of time-independent parameters	147
5.4.1	Virgin compression index C_c	149
5.4.2	The angle of internal friction ϕ'	149
5.4.3	Failure ratio R_f	150
5.4.4	Reference void ratio e_a	152
5.5	Sensitivity analyses of time-dependent parameters	152
5.5.1	Volumetric creep parameter C_α	154
5.5.2	Singh and Mitchell creep parameter A	155
5.5.3	Singh and Mitchell creep parameter m	155
5.5.4	Singh and Mitchell creep parameter $\bar{\alpha}$	156
5.6	Summary and conclusions	157

6	Three-dimensional visco-plastic analyses of Pisa Tower	
6.1	Introduction.....	197
6.2	The constitutive model.....	198
6.2.1	Yielding surfaces	198
6.2.2	Numerical stability criteria	198
6.3	Ground profile and construction history of Pisa Tower.....	200
6.4	Historic tilting and major disturbance of Pisa Tower	201
6.5	Three dimensional visco-plastic analysis.....	204
6.5.1	Finite element	205
6.5.2	Simulation results	206
6.6	Sensitivity analyses	210
6.6.1	Influence of Singh and Mitchell creep parameter $\bar{\alpha}$ and m.....	210
6.6.2	Influence of hyperbolic parameter a	211
6.7	Three dimensional visco-plastic analysis with the super-structure.....	211
6.8	Summary and conclusions	213
7	Conclusions and recommendations	
7.1	Conclusions.....	247
7.2	Recommendations for further work.....	249
	BIBLIOGRAPHY	250

LIST OF TABLES

Table		Page
2.1	Physical and index properties	35
3.1	Model parameters for 19m sample	72
3.2	Atterberg limits of 19m sample	72
3.3	Atterberg limits of drained creep test samples (Mitchell and Soga 1995).....	73
3.4	Model parameters for Test-1 (6m sample)	74
3.5	Model parameters for Test-2 (10m sample)	74
3.6	Applied step loads and duration	75
4.1	Weight, overturning moment and rigid tilt versus time.....	109
4.2	Loading conditions for elastic and elasto-plastic analyses (CF=24, $I_c = 1.27$).....	109
4.3	Soil parameters for elastic analysis.....	110
4.4	Cam-clay parameters for the clay layers	111
4.5	Soil parameters for the sand layers	112
4.6	Singh and Mitchell parameters (from Mitchell and Soga 1995).....	112
5.1	Possible range of time-independent parameters	159
5.2	Cam-clay parameters for the clay layers	160
5.3	Soil parameters for the sand layers	161
5.4	Singh and Mitchell parameters (from Mitchell and Soga 1995).....	161
5.5	Time-independent parameters used in FEA analyses	162
5.6	Sensitivity analyses results of time-independent parameters.....	162

5.7	Possible range of time-dependent parameters	163
5.8	Time-dependent parameters used in FEA analyses	164
5.9	Sensitivity analyses results of time-dependent parameters.....	164
6.1	Cam-clay parameters for the clay layers.....	215
6.2	Soil parameters for the sand layers.....	215
6.3	Singh and Mitchell parameters (from Mitchell and Soga 1995)	216
6.4	Weight, overturning moment and rigid tilt versus time.....	217
6.5	Three-dimensional loading increments.....	218

LIST OF FIGURES

Figure		Page
2.1	Schematic show of main aspects of viscous behavior (after Burghignoli et al. 1994)	36
2.2	Schematic show of existing approach of creep modeling.....	37
2.3	Definition of primary and secondary consolidation and immediate and delayed (modified after Borja and Kavazanjian 1985).....	38
2.4	Kavazanjian's general volumetric model (modified after Kavazanjian 1978).....	39
2.5	Normalized soil properties (modified after Ladd and Foott 1974).....	40
2.6	Equivalent consolidation pressure(ECP) concept (modified after Hsieh 1987)	41
2.7 (a)	Schematic representation of Singh and Mitchell creep function.....	42
2.7 (b)	Influence of deviatoric stress level on creep strain rate.....	42
2.8	Stress-strain behavior following a period of sustained shear loading (Hirst 1968).....	43
2.9	Kavazanjian's general deviatoric model (modified after Kavazanjian 1978).....	43
2.10	The critical state line and state boundary surface.....	44
2.11	Consolidation curves on e-lnp space	45
2.12	Three-Dimensional representation of double-yield-surface criteria in principal stress space (Hsieh et al. 1990)	45

2.13	Weight and geometrical characteristics of Pisa Tower (from Jamiolkowski et al. 1993).....	46
2.14	Construction history (from Jamiolkowski et al. 1993).....	47
2.15	Correction during construction (from Jamiolkowski et al. 1993)	48
2.16	History of rigid tilt (Burland 1991)	49
2.17	Tilting history of Pisa Tower.....	50
2.18	Comparison of cone resistance profiles (after Burland and Potts 1995)	51
2.19	Probable initial soil profile at the site of Pisa Tower (Calabresi et al. 1992).....	52
2.20	Atterberg limits of Pisa soil (after Calabresi et al. 1992)	53
2.21	Temporary structural strengthening (light circumferential prestressing).....	54
2.22	Counterweight on north edge of foundation position of lead weights	54
2.23	Comparison between measured and predicted strain (after Mitchell and Soga 1995).....	55
2.24	Axial strain versus Time for the creep test by Bishop and Lovenburry (after Mitchell and Soga 1995).....	56
2.25	Axial strain versus Log time relationship of maximum stress cases (after Mitchell and Soga 1995).....	57
3.1	Probable initial soil profile at the site of Pisa Tower (Calabresi et al. 1992).....	76
3.2	Projection of double yield surface on p-q plane	77
3.3	Projection of double yield surface on p- γ plane	77

3.4	Evaluation of deviatoric age (modified after Borja and Kavazanjian 1985).....	78
3.5	Singh and Mitchell creep parameters	79
3.6	Numerical simulation of triaxial test on Pisa clay.....	80
3.7	Axial strain versus time for the creep test by Bishop and Lovenburry (after Mitchell and Soga 1995).....	81
3.8	Numerical results of axial strain versus time relationship for 75% loading case (before correction).....	82
3.9	Numerical results of axial strain versus time relationship for 75% loading case (after correction).....	82
3.10	Axial strain versus time relationship.....	83
3.11	Volumetric strain versus time relationship.....	83
3.12	Location of undisturbed sample boring and seismic cone tests	84
3.13	Stress path of Test-1 (6m sample) (after Mitchell and Soga 1995).....	85
3.14	Stress path of Test-2 (10m sample) (after Mitchell and Soga 1995).....	85
3.15	Axial strain versus Log time relationship of maximum stress cases (after Mitchell and Soga 1995).....	86
3.16	Axial strain versus time curve for Test-1 (6m sample, layer A ₁) (Maximum stress case).....	87
3.17	Axial strain versus time curve for Test-2 (10m sample, layer B ₁) (Maximum stress case).....	87
4.1	Geometrical characteristics of Pisa Tower (after Jamiolkowski et al. 1993).....	113

4.2	Construction history (from Jamiolkowski et al. 1993).....	114
4.3	Probable initial soil profile at the site of Pisa Tower (after Calabresi et al. 1992)	115
4.4	Comparison of cone resistance profiles to the north and south of the tower (Burland and Potts 1995)	116
4.5	Current soil condition at the tower (after Mitchell and Soga 1995)	117
4.6	Schematic show of existing approaches of creep modeling	118
4.7	Definition of primary and secondary consolidation and immediate and delayed compression (after Borja and Kavazanjian 1985)	119
4.8	Projection of double yield surface on p-q plane	120
4.9	Finite element mesh for two-dimensional analyses.....	121
4.10	Conversion of three dimensional condition to plane strain condition (Mitchell and Soga 1995).....	122
4.11	In-situ stress versus depth.....	123
4.12	Vertical stress contours (elasto-plastic analysis).....	124
4.13	Mean stress contours (elasto-plastic analysis).....	125
4.14	Deviatoric stress contours (elasto-plastic analysis).....	126
4.15	Mean stress distribution at various depths (elasto-plastic analyses)	127
4.16	Deviatoric stress distribution at various depths (elasto-plastic analyses).....	128
4.17	Stress ratio distribution at various depths (elasto-plastic analyses)	129
4.18	Settlement of the footing (CF=24, Ic=1.27, elasto-plastic analyses)	130
4.19	Influence of CF on the settlement of the footing (for Ic=1.27)	131

4.20	Influence of I_c on the settlement of the footing (for $CF=24$)	131
4.21	Pisa Tower weight and overturning moment versus time	132
4.22	Vertical stress contours (visco-plastic analysis).....	133
4.23	Mean stress contours (visco-plastic analysis).....	134
4.24	Deviatoric stress contours (visco-plastic analysis).....	135
4.25(a)	Stress path at 9.8m South	136
4.25(b)	Stress path at 9.8m North	137
4.26	Mean stress distribution at various depths (visco-plastic analyses)	138
4.27	Deviatoric stress distribution at various depths (visco-plastic analyses).....	139
4.28	Stress ratio distribution at various depths (visco-plastic analyses)	140
4.29	Settlement of the footing ($CF=24$, $I_c=1.27$, visco-plastic analyses)	141
4.30	Comparison of the settlement of the footing (for $CF=24$, $I_c=1.27$)	141
4.31 (a)	Tilting history of the tower.....	142
4.31 (b)	Settlement versus time relationship.....	142
5.1	Construction history (from Jamiolkowski et al. 1993)	165
5.2	Probable initial soil profile at the site of Pisa Tower (after Calabresi et al. 1992)	166
5.3	Projection of double yield surface on p-q plane	167
5.4	Cam-clay compression index λ vs depth (Mitchell and Soga 1995).....	168
5.5	Cam-clay compression index κ vs depth (Mitchell and Soga 1995).....	169
5.6	Cam-clay compression index M vs depth (Mitchell and Soga 1995)	170
5.7	Cam-clay compression index N vs depth (Mitchell and Soga 1995)	171

5.8	Finite element idealization of the Pisa foundation (part)	172
5.9	Consolidation curves on e-lnp space	173
5.10	FEA results for different value of C_c at layer A_1 and B_1	174
5.11(a)	MCCM yielding surface for A_1 layer	176
5.11(a)	MCCM yielding surface for B_1 layer	176
5.12	FEA results for different value of ϕ' at layer A_1 and B_1	177
5.13(a)	Stress-strain curves from Hyperbolic model for A_1 layer	179
5.13(b)	Stress-strain curves from Hyperbolic model for A_1 layer	179
5.14	FEA results for different value of R_f at layer A_1 and B_1	180
5.15	FEA results for different value of ea at layer A_1 and B_1	182
5.16	Creep strain curves for maximum stress cases (Mitchell and Soga 1995)	184
5.17	C_α / C_c vs. depth (Calabresi et al. 1992)	185
5.18	Initial void ratio vs. Depth (Mitchell and Soga 1995)	186
5.19	FEA results for different value of C_α at layer A_1 and B_1	187
5.20	Singh and Mitchell creep parameters A and $\bar{\alpha}$	189
5.21	FEA results for different value of A at layer A_1 and B_1	190
5.22	FEA results for different value of m at layer A_1 and B_1	192
5.23	FEA results for different value of $\bar{\alpha}$ at layer A_1 and B_1	194
5.24	Sensitivity of model parameters in terms of final inclination	196
5.25	Sensitivity of model parameters in terms of final settlement	196
6.1	Projection of double yield surface on p-q plane	219
6.2	Weight and geometrical characteristics of Pisa Tower	

	(from Jamiolkowski et al. 1993).....	220
6.3	Probable initial soil profile at the site of Pisa Tower (after Calabresi et al. 1992)	221
6.4	Construction history (from Jamiolkowski et al. 1993).....	222
6.5	Tilting history of the tower (observed).....	223
6.6	Change in inclination of the foundation since 1911 (after Jamiolkowski et al. 1993)	224
6.7	Daily movement of the tower due to change of temperature (after Jamiolkowski et al. 1993)	225
6.8	Relative settlement over the piazza dei Miracoli (after AGI 1991)	226
6.9	Three dimensional finite element model of the Pisa foundation.....	227
6.10	20-node rectangular element for 3D analysis.....	228
6.11	8-node rectangular element for 3D analysis.....	228
6.12	Pisa Tower weight and overturning moment versus time relationship	229
6.13	Three dimensional mesh of the Pisa foundation (part).....	230
6.14(a)	Shear stress-strain relationship at 6.5m deep (layer A ₁ , element 508)	231
6.14(b)	Shear stress-strain relationship at 6.5m deep (layer A ₁ , element 503)	231
6.15(a)	Shear stress-strain relationship at 12m deep (layer B ₁ , element 331)	232
6.15(b)	Shear stress-strain relationship at 12m deep (layer B ₁ , element 326)	232
6.16(a)	Mean stress distribution at depth of 6.5m (layer A ₁).....	233
6.16(b)	Mean stress distribution at depth of 12m (layer B ₁).....	233
6.17(a)	Deviatoric stress distribution at depth of 6.5m (layer A ₁).....	234
6.17(b)	Deviatoric stress distribution at depth of 12m (layer B ₁)	234

6.18(a)	Volumetric strain distribution at depth of 6.5m (layer A ₁).....	235
6.18(b)	Volumetric strain distribution at depth of 12m (layer B ₁).....	235
6.19(a)	Deviatoric strain distribution at depth of 6.5m (layer A ₁).....	236
6.19(b)	Deviatoric strain distribution at depth of 12m (layer B ₁).....	236
6.20(a)	Stress path at 9.8m south of the footing center. 6.5m (clayey silt layer A ₁).....	237
6.20(b)	Stress path at 9.8m south of the footing center. 12m (upper clay layer B ₁).....	237
6.21(a)	Stress path at 9.8m north of the footing center. 6.5m (clayey silt layer A ₁).....	238
6.21(b)	Stress path at 9.8m north of the footing center. 12m (upper clay layer B ₁).....	238
6.22	Comparison for the settlement of the footing under different element type (plastic analysis).....	239
6.23	Comparison for the settlement of the footing under different element type (creep analysis)	239
6.24	Tilting history of the tower (original parameters. update coordinates. with 8 weak elements from stage two).....	240
6.25	Tilting history of the tower (original material parameters).....	240
6.26	Influence of Singh and Mitchell parameter m on tilting angle.....	241
6.27	Influence of Singh and Mitchell parameter $\bar{\alpha}$ on tilting angle	241
6.28	Stress strain relationship under different hyperbolic parameter a	242
6.29	Three dimensional finite element model of Pisa Tower	

	and its foundation	243
6.30	Three dimensional finite element model of Pisa Tower and its foundation (part)	244
6.31 (a)	Tilting history of the tower (8 weak elements from stage 2)	245
6.31 (b)	Tilting history of the tower (8 two-order of weak elements from stage 2)	245
6.32	Predicted settlement profile on the top of clay layers	246

CHAPTER 1

THESIS SCOPE AND OBJECTIVES

1.1 Introduction

The time-dependent response of a soil may assume a variety of forms owing to the complex interaction among soil structure, stress history, drainage conditions, and changes in temperature, pressure, and biochemical environment over time. There are two main types of time-dependent behavior: primary consolidation, which is due to the interaction of free pore water and the soil skeleton; and viscosity, which is brought about by the apparent viscous characteristics of the soil skeleton. Soil viscosity includes rate sensitivity, stress relaxation, and creep. Primary consolidation, stress relaxation and creep are more significant in soft or normally consolidated soils than in stiff or overconsolidated soils.

When the total stress in the soil is increased under undrained condition, excess pore pressure is generated. This pore pressure subsequently dissipates with time, resulting in an increase in both deformation and strength. This phenomenon is called primary consolidation. Its rate depends on how fast the pore water can escape. Primary consolidation is a well-studied process. Terzaghi's (1943) and Biot's (1941) theories of consolidation can be used to evaluate the consolidation deformation.

Soil has rate sensitive characteristics. The undrained shear strength as well as the residual strength of a soil increases with an increase in strain rate. The effect of strain rate on undrained shear strength has been studied by Kulaway and Mayne (1990). Their results indicated that the magnitude of the effect was about 10% for each order of magnitude increase in the strain rate. The effect of strain rate on residual strength has been studied by Wedage (1995). In this case, the use of the rate-dependent model in

certain field cases was found to provide a satisfactory basis for simulating slope movement.

Stress relaxation is used to describe the phenomenon when the applied state of deformation is held constant and stresses decrease with time, while the term "creep" is used to describe the time-dependent deformation of soil under sustained loads or stresses. Stress relaxation and creep are often treated as two separate phenomena although physical considerations suggest that one process could be responsible for bringing about the other. A rate-constitutive model can be used for both creep and stress relaxation (Borja 1992).

Creep and stress relaxation are important in geotechnical problems when long-term behavior under sustained loading is of interest. In general, the higher the clay content and the more active the clay minerals, the more important are creep and stress relaxation. At higher water content or higher temperature, creep rates increase, and the relaxation stresses corresponding to specific values of strain decrease. Test type and prior stress history also have an effect on the creep deformations and relaxation stresses.

Creep can be further divided into volumetric creep and deviatoric creep. In consolidation tests, the void ratio keeps decreasing with time, even though the effective stress remains constant after all excess pore pressure has been dissipated. This phenomenon is called volumetric creep or secondary consolidation.

If shear stress is kept constant in triaxial tests, shear strain will increase with time. These time-dependent shear deformations are usually referred to as deviatoric creep or shear creep. If additional load is applied, soil strength can be higher or lower than its original value depending on the drainage condition.

Creep has been studied more extensively than stress relaxation because most geotechnical problems involve application of a sustained load and not of a sustained state of deformation. A characteristic relationship between strain rate and time exists for most soils. A general pattern of the logarithm of strain rate versus the logarithm of time has

been observed for undisturbed and remolded clay, wet or dry clay, normally consolidated and overconsolidated clay and sand (Singh and Mitchell 1968). Application of stress first leads to a period of transient creep, during which the strain rate decreases continuously with time, followed by creep, which appears to be at nearly a constant rate over a period of time. If the shear stresses are high enough, an acceleration in creep rate may occur under certain drainage conditions, leading to creep failure. These three stages are denoted as primary, secondary, and tertiary creeps.

Various models with different assumptions regarding constitutive behavior of soils are available including empirical curve fitting models, extension of rate process theory, rheological models, and advanced theories of visco-elasticity and plasticity. But, unfortunately, most of them still remain at the research level. The double-yield surface Cam-clay plasticity (DYSCP) model is the only one to be capable of simulating creep behavior of soft clays in certain field cases (Borja et al. 1990, Morsy et al. 1995). This model introduces an additional horizontal deviatoric yield surface inside the modified Cam-clay volumetric yield surface to account for the shear deformation developed during loading inside the modified Cam-clay yield surface. An important numerical implication of this horizontal yield surface is that it results in a non-associated plastic flow rule. Creep deformation consists of volumetric and deviatoric components. The total creep strain rate is evaluated by employing the non-associative flow rule on both deviatoric and volumetric yield surfaces and forcing the creep strain rate to satisfy empirical volumetric and deviatoric creep functions simultaneously. This model is adopted here to analyze the time-dependent deformation behavior of the soil underneath the Leaning Tower of Pisa.

Pisa Tower is 58.4 meters high with a foundation diameter of 19.6 meters. It started to lean southward following the second construction stage. Over the past 800 years, the south side has settled more than the north side, giving about a 2m differential settlement and a 5.5° inclination. At present, the seventh cornice overhangs the first one

by about 4.1m. The factor of safety with respect to the overturning moment is very close to 1.0. It has tilted enough to raise serious concerns about a complete failure.

Recently, the tower has stopped leaning southward as a result of the application of the lead counterweights at the north side as a temporary remedial measure. The permanent solution to save the tower, ground freezing operations followed by soil extraction, began in April 1995 but it was stopped after five months. The ground did not respond as expected. Many questions still need to be answered. These questions include the following: What mechanism controls the deformation behavior of the tower? What are the long-term effects of these stabilization methods? In order to provide insights to these problems, a numerical model is required. Up to now, various numerical models have been proposed, but they all fail to give satisfactory results about time-dependent deformation characteristics, even though previous creep tests on Pisa clay have shown the importance of these characteristics.

1.2 Research scope

The research scope of this thesis focuses on the study of creep effects on the deformation behavior and the stress-strain response beneath the tower's foundation. The DYSCP model is adopted to investigate time-dependent deformation behavior of the soil beneath the foundation. This model has been initially incorporated into the computer program named PISA-FORTRAN by Morsy (1994). In this thesis, the original model was modified by changing the intrinsic time variables. Then the modified model was extended to handle three-dimensional cases. The input data used in this study were determined based mainly on Calabresi's (1992) study and Mitchell and Soga's (1995) creep tests.

First, a series of triaxial drained creep tests conducted by Bishop and Lovenbury (1969) and Mitchell and Soga (1995) were simulated to verify the modified model. Then this model was used for two-dimensional plane strain analysis. Finally, the existing two-dimensional model was extended to handle three-dimensional problems. Fully three-

dimensional visco-plastic analyses with and without the super-structure cases were carried out.

It must be kept in mind that the actual situation of the tower is very complex. Many disturbances have happened over the course of time which have increased its inclination. Moreover, there may be more than one mechanism controlling its deformation behavior. It is almost impossible to account for all aspects in a single model. Nevertheless, laboratory tests on the Pisa clay have already shown the importance of its creep characteristics. It is worth knowing how much this type of effect will contribute to the tower's deformation.

1.3 Research objective and anticipated contributions

The objectives of this research include the following: studying the leaning mechanism of the tower and analyzing the time-dependent behavior of the soil beneath the foundation by extending the existing two-dimensional DYSCP model to the three-dimensional case.

There are several anticipated contributions that this research can offer. It provides a better understanding of the physical mechanisms of the creep phenomenon. The time-dependent deformation properties of Pisa soil is studied. The existing two-dimensional DYSCP model is modified and extended to three-dimensional cases. The observed foundation deformation of the tower is simulated from the construction stage to the present day.

1.4 Thesis outline

This thesis is written in a mixed format. It is organized as follows:

Chapter one first briefly describes the background information about the time-dependent deformation behavior of soils. It reviews the current situation of Pisa Tower

and the state-of-the-art work in this area. The research scope, objectives, and anticipated contributions are described. The last part of the chapter presents an outline of the thesis.

Chapter two consists of three parts: the first presents various existing creep models to provide a better understanding of the creep phenomenon. One of the existing models named the DYSCP model is addressed in detail. This model is adopted to study the creep phenomenon of the soil beneath the tower's foundation. The second part introduces the construction history of Pisa Tower, its subsoil conditions, and some physical observations about the changes in its inclination. The last part describes the major research efforts about the tower, such as the investigations of the mechanisms which triggered the initial tilt, various stabilization measures to save the tower, and the creep tests on the Pisa clay. The most recent research results by Burland and Potts (1995) and Mitchell and Soga (1995) are highlighted. From these previous works, some useful conclusions can be drawn.

Chapter three presents the modification to the double-yield surface model by changing the intrinsic time variables. The modified model is then tested to simulate a series of triaxial drained creep tests conducted by Bishop and Lovenbury (1969) and Mitchell and Soga (1995). Numerical results are compared with the test data. Excellent agreement is obtained.

Chapter four presents the results of two-dimensional plain strain analyses. A brief review of Pisa Tower, including its subsurface condition, its construction history, physical disturbances, and some stabilization measures is presented. The main features of the DYSCP model are introduced. Two-dimensional elastic and elasto-plastic analyses are conducted to investigate the stress paths as well as stress levels in each soil layer. The DYSCP model is then applied to study the time-dependent deformation behavior of the tower. Creep effects in stress distribution and displacement are investigated. Sensitivity analyses on some correction factors are conducted to look at the possibility of obtaining better displacement results.

Chapter five presents an extensive model parameter sensitivity study, conducted through sixteen visco-plastic plain strain FEM analyses, to enhance the limited experience in transforming model parameters into field behavior when combining elastic, plastic and creep response. The clayey silt layer A_1 and the upper clay layer B_1 are focused on in this study due to their significance in the deformation behavior of the soil and the scatter characteristics of their model parameters. The effects of the model parameters including time-independent as well as time-dependent ones on the calculated strain and the total deformation of the foundation are discussed. A better understanding is provided.

Chapter six presents the results of the three-dimensional visco-plastic analyses using the DYSCP model. Finite element models with and without the super-structure are studied. Node coordinates are updated after each time step. The capability of the numerical model in predicting the stress-strain-time behavior under the fully three-dimensional field case is illustrated. Creep effects on the deformation behavior and the stress-strain response of the soil beneath the tower's foundation are studied in detail. Sensitivity analyses on Singh and Mitchell creep parameters $\bar{\alpha}$ and m and the hyperbolic parameter a are carried out to investigate the possibility of improving the simulated results by simply changing these material parameters. The possible reasons which cause the difference between the calculated values and the observed ones are discussed to provide a better understanding of the deformation mechanism of the tower.

Chapter seven summarizes the conclusions from the entire thesis and presents recommendations for further work.

CHAPTER 2

LITERATURE REVIEW

2.1 Introduction

It is well known that soil has viscous behavior. A survey of the literature shows that the main aspects of viscous behavior that have been investigated in the past are as follows (see Figure 2.1): the effects of the viscosity of the soil skeleton on one-dimensional consolidation; the factors affecting the coefficient of secondary consolidation C_{α} ; the coupling of volumetric and deviatoric components of creep deformations; and the influence of the viscosity of the soil skeleton on the earth pressure coefficient at rest K_0 . This study belongs to the third category--the coupling of volumetric and deviatoric components of creep deformations.

Creep deformation of soils is an important consideration in a wide variety of geotechnical problems, such as time-dependent settlements of foundations after all excess pore pressure has been dissipated, and time-dependent deformation of soft embankment foundations which may eventually fail in creep rupture before excess pore pressure has been dissipated.

This research focuses on the study of creep effects on the deformation behavior of the Leaning Tower of Pisa. The first part of this chapter reviews various existing creep models to provide a better understanding of the creep phenomenon. A general phenomenological model developed by Kavazanjian and Mitchell (1977) is presented in detail. Then, the development of the double-yield surface Cam-clay plasticity (DYSCP) model is introduced. This model will be modified to study creep behavior of the soil beneath the tower's foundation.

The last part of this chapter gives an overview of Pisa Tower. As a case study of time dependent behavior, the tower's construction history, negative events which influence the inclination history, and its subsurface conditions have been investigated. The major research efforts about the tower, such as those focusing on the mechanisms which triggered the initial tilt, various stabilization measures to save the tower, and creep tests of the Pisa clay, have been presented. The most recent research results by Burland and Potts (1995) and Mitchell and Soga (1995) are highlighted.

2.2 Review of creep models

2.2.1 Review of the existing creep models

Time-dependent phenomena in soils have been studied during the last fifty years. Various creep models have been developed mainly based on four mechanisms (Buisman 1940 and Barden 1969): (1) the viscous soil skeleton; (2) jumping of bonds; (3) structural viscosity; and (4) micropore-macropore structure. Figure 2.2 presents the major category of the existing creep models

2.2.1.1 Fundamental approach

The fundamental approach studies creep behavior of soils on a particle level. It can be divided into three categories: (1) viscosity of adsorbed water; (2) cavity channel network; and (3) rate process theory.

The concept of structural viscosity assumes that the structure of a clay has an inherent viscosity that presumably originates at the contacts between individual particles. Adsorbed water around clay particles is assumed to be the cause of the viscosity. This mechanism forms the basis of adsorbed water approach (Terzaghi 1941, Barden 1965, Walker 1969). The work done by Leonard and Girault (1961) and Mesri (1973) showed

that the presence of adsorbed water is not necessary in order for secondary consolidation to occur.

The concept of micropore-macropore structure assumes that a soil has more than one level of structure. Creep is caused by the slow drainage of pore water from a micropore into a macropore system. This mechanism forms the basis of the cavity channel network model (De Jong 1968). Due to the complexity of this model, it has only been employed by a few other researchers (Holzer et al. 1973).

The concept of jumping of bonds assumes that the fundamental bonding unit of a granular medium is preferentially displaced when work is done on the soil. This mechanism forms the basis of rate process theory (Eyring 1936, Murayama and Shibata 1961, Mitchell 1964, Christensen and Wu 1964, Pusch and Feltham 1980 and 1981, Feda 1989, and Kuhn and Mitchell 1993). Due to its complexity, rate process theory has not been widely used in practice and still remains primarily a research tool.

2.2.1.2 Rheological approach

The viscous soil skeleton mechanism forms the basis of rheological approaches. In this model, the viscous grain skeleton is represented by elements containing springs and dashpots. The spring represents soil elasticity, and the dashpot represents soil viscosity. Different combinations of springs and dashpots form different rheological models (Murayama and Shibata 1958, Schiffman 1959, Christensen and Wu 1964, Abdel-Hady and Herrin 1966, and Yoshikuni et al. 1994). The rheological models are generally limited to a particular soil, for a particular range of variable, and do not permit easy extrapolation. They are not used extensively in creep modeling of soil.

2.2.1.3 Overstress approach

The overstress model assumes that when the rate of visco-plastic deformation is not zero, a dynamic yield surface which differs from the static yield surface exists, and its

position depends on the amount of hardening experienced by the material. The salient feature of this theory is that the magnitude of the visco-plastic strain rate is a function of the overstress, which is the stress increase due to the rate effects above a reference value (Perzyna 1963, Adachi and Okano 1974, Adachi and Oka 1982, Dafalias 1982, Katona 1984, Kaliakin and Dafalias 1990, and Kutter and Sathialingam 1992).

2.2.1.4 Flow surface approach

Flow surface or non-stationary yield surface models assume that there exists a loading function f which depends on the state of stress, the plastic history of the material through the plastic strains, and a scalar parameter β . This parameter β embodies time dependent alteration of the material properties. The visco-plastic strain rates are given by the sum of two contributions. The first one relates to stress rates and the second one to elapsing time (Perzyna 1966, Zienkiewicz and Corneau 1974, Sekiguchi 1977, Nova 1982, Katon and Mulert 1984, Matsui and Abe 1985, and Desai et al. 1995).

2.2.1.5 Incremental non-linear approach

An incremental non-linear approach was proposed by Darve (1978). In order to take into account of the viscous phenomena, a time dependent strain rate component was simply added to the strain rate which is originally stress rate dependent (Darve 1978, Darve and Vuailat 1982, and Kolymbas 1987)

2.2.1.6 Endochronic approach

The endochronic approach is an inelastic constitutive relation. It is formulated from the concept of internal state variables based on the assumption that there exists a group of such variables that fully defines a continuous free energy. Those state variables can be qualitatively interpreted in terms of microscopic processes. Intrinsic time has been chosen as a state variable. This approach is convenient and flexible in treating unloading.

cyclic loading, strain-softening, and cross-hardening (Valanis 1971, Bazant and Krizek 1976, Ansal et al. 1979).

2.2.1.7 Phenomenological approach

The phenomenological approach is the endeavor to produce empirical relationships that predict creep behavior based solely on observed creep behavior in the laboratory. This approach can be subdivided into three groups: (a) volumetric scaling; (b) deviatoric scaling; and (c) volumetric and deviatoric coupled scaling.

Kavazanjian and Mitchell (1977) postulated that strain tensors can be decomposed into volumetric and deviatoric components. Further, the volumetric and deviatoric strain components can be decomposed into immediate and delayed components based on Bjerrum's (1967) concept (see Figure 2.3).

The volumetric scaling procedure is based on Taylor's (1948) secondary creep law. The increments of volumetric viscous deformation are calculated based on this secondary creep law. The deviatoric components of viscous deformation are computed by the normality rule. With this, the deviatoric creep strain increments will be overestimated, especially at high values of the stress ratio η . For $\eta=M$, the deviatoric creep strain increments are infinite. Thus this procedure can only be used at low values of η (Kavazanjian and Mitchell 1977, Borja and Kavazanjian 1985, Yin and Graham 1991, and Burghignoli et al. 1994).

The deviatoric scaling procedure is based on Singh and Mitchell's (1968) creep equation. The deviatoric viscous deformation is computed as a function of time using Singh and Mitchell's equation. The volumetric component is obtained by introducing normality. In this procedure, the volumetric creep strain increments will be overestimated at low values of the stress ratio η . For isotropic stress states, the volumetric creep strain

increments will be infinite. This procedure can only be used at high values of η (Chang et al. 1974. Burke 1983. and Borja and Kavazanjian 1985)

As mentioned earlier, the volumetric scaling procedure is only suitable at low values of η , while the deviatoric one is only suitable at high values of η . To avoid this problem, Borja et al. (1990) and Hsieh et al. (1990) proposed a new scaling procedure that can simultaneously satisfy both the volumetric and deviatoric creep relationships. This procedure will be used in this study, and will be discussed in detail later in the next section.

2.2.2 Double-yield surface Cam-clay plasticity (DYSCP) model

General phenomenological representations for volumetric and deviatoric soil deformations, including the effect of time, were first postulated by Kavazanjian and Mitchell (1977). In 1978, they developed the general theory within the theoretical framework of pseudo-linear elasticity. In 1985, Borja and Kavazanjian proposed a consistency law based on the C_α creep law (volumetric scaling) at low values of the stress ratio η and the Singh and Mitchell creep equation (deviatoric scaling) at larger values of η . They extended the general phenomenological theory within the classical theory of plasticity. The time-independent stress-strain behavior is evaluated using the ellipsoidal yield surface of the modified Cam-clay model (Roscoe and Burland 1968). The time-independent plastic strain and time-dependent total strain (creep) are obtained by the normality condition and the consistency requirement on the yield surface. Consistency requires that the creep strain rate reduces to phenomenological creep rate expressions for isotropic or undrained triaxial stress conditions.

In 1984, Borja demonstrated the concept of a horizontal deviatoric yield surface represented by the Von-Mises model within the ellipsoid of the modified Cam-clay model. In 1990, Hsieh et al. extended this concept to include time-dependent effects. They introduced this cylindrical yield surface into Borja and Kavazanjian's general

stress-strain-time model to account for the plastic shear distortion that occurs without volume change below the state boundary surface. Thus, a double-yield surface Cam-clay plasticity (DYSCP) model was postulated. This theory is used to evaluate both the time-independent and time-dependent components of strains.

2.2.2.1 General volumetric model

Kavazanjian and Mitchell (1980) generalized Bjerrum's one-dimensional compression model to three-dimensional states of stress. The vertical effective stress in Bjerrum's plot was changed to volumetric (mean), or octahedral effective stress. It was assumed that a similar plot could be constructed for volumetric deformations at any constant deviatoric stress level and that the isochrones on all such plots would have the same slope C_c .

If there were no hydrodynamic lag, the immediate volumetric compression would occur instantaneously upon load application. Generally, immediate volumetric deformations cannot be determined directly due to hydrodynamic lag. Rules for delayed volumetric deformations must be developed first, then immediate deformations can be back calculated by subtracting the delayed contribution from primary deformations. Since secondary compression consists solely of delayed deformations, laws governing the delayed volumetric compression of soils can be deduced from observations of secondary compression. Taylor's (1948) secondary compression law is adopted to evaluate the delayed volumetric part.

$$[2.1] \quad \dot{\epsilon}_v = \frac{\psi}{(1+e)t_v}$$

where $\dot{\epsilon}_v$ is the volumetric strain rate; ψ is the secondary compression coefficient, in natural logarithm scale; e is the void ratio; and t_v is the volumetric age, relative to an initial reference time (t_v),

Kavazanjian and Mitchell's (1980) general volumetric model assumes that C_{α} (secondary compression coefficient in \log_{10} scale) is independent of both deviatoric and volumetric stresses and that C_c (virgin compression index) is also constant. The schematic representation of the volumetric model is shown in Figure 2.4. In void ratio-log stress-log time space, at constant deviatoric stress levels, deformation is described as a series of parallel planes. These planes are assumed to represent a unique relationship among void ratio, effective stress, and time under sustained loading of an element of cohesive soils. The spacing of these planes is governed by the values of the virgin compression index C_c and the coefficient of secondary compression C_{α} .

In this model, it was assumed that upon an instantaneous increase in volumetric effective stress, the state of a normally consolidated soil moves along the virgin compression line with slope C_c in the void ratio-log stress plot. The response of an overconsolidated soil is governed by the quasi-preconsolidation concept. Under unloading and reloading conditions, soil state moves along a straight line with slope C_r (assuming the recompression ratio and the swelling ratio are the same). During the consolidation stage, the rate of volumetric change can be evaluated on the basis of soil permeability and pore pressure boundary.

2.2.2.2 General deviatoric model

Since pore water pressure is isotropic, it does not affect the value of the deviatoric stress. Thus the problem of hydrodynamic lag does not enter into the determination of immediate and delayed components of the deviatoric deformations.

The general deviatoric model evaluates both the immediate and delayed deformations as a function of the deviatoric stress level \bar{D} . Immediate deviatoric deformation can be evaluated by Konder's (1963) hyperbolic model in conjunction with Ladd and Foott's (1974) normalization technique and Hvorslev's (1960) equivalent consolidation concepts.

After studying the results of the consolidated-undrained triaxial compression tests conducted by Perloff (1962) at various overconsolidation ratios under various rates of strain. Konder (1963) found that the nonlinear stress-strain curves of both clay and sand can be approximated by a hyperbola.

Ladd and Foott (1974) found that dividing the deviatoric stress by the effective confining pressure in isotropically consolidated undrained triaxial tests would yield a unique stress-strain curve, which is independent of the effective confining pressure. An idealized triaxial compression test plot is shown in Figure 2.5. This normalized soil property concept is incorporated to account for stress-dependence of shear modulus.

By adopting Hvorslev's (1960) equivalent consolidation pressure concept, Kavazanjian and co-worker (1978,1980b) extend normalized behavior from normally consolidated soils to overconsolidated soils. They postulated that the deviatoric stress versus axial strain behavior of lightly overconsolidated clay is the same as for the clay normally consolidated at the same void ratio, regardless of whether the soil has been overconsolidated by unloading or through a quasi-preconsolidation process, as shown in Figure 2.6.

By combining the normalized soil properties concept with the equivalent consolidation concept, Kavazanjian (1978) postulated the following equation for evaluating the immediate deviatoric deformations

$$[2.2] \quad (\sigma_1 - \sigma_3) = \frac{\varepsilon_a p_c R_f}{a + b\varepsilon_a}$$

where σ_1 and σ_3 are the major and minor principal stresses, respectively; ε_a is the axial strain; a is the reciprocal of the initial tangent modulus; b is the reciprocal of the

asymptotic value of stress difference at infinite strain: R_f is the failure ratio.

$$R_f = \frac{(\sigma_1 - \sigma_3)_{\text{failure}}}{(\sigma_1 - \sigma_3)_{\text{ultimate}}}; \text{ and } p_e \text{ is the equivalent consolidation pressure.}$$

After studying Atchafalaya and Boston Blue clay, Kavazanjian and co-workers (1980 b) found that the above equation works well for overconsolidation ratio less than 4.

The delayed deviatoric deformations can be evaluated through the Singh and Mitchell (1968) creep model.

$$[2.3] \quad \dot{\epsilon}_a = A \exp(\bar{\alpha}\bar{D}) \left[\frac{(t_d)_i}{t_d} \right]^m$$

where $\dot{\epsilon}_a$ is the axial strain rate; A, $\bar{\alpha}$, and m are Singh and Mitchell parameters; \bar{D} is the deviatoric stress level, $\bar{D} = \frac{(\sigma_1 - \sigma_3)}{(\sigma_1 - \sigma_3)_{\text{ultimate}}}$; and t_d is the deviatoric age, relative to an initial reference time $(t_d)_i$.

Since this creep model describes delayed deformations as a function of deviatoric stress level, it is compatible with the immediate deformation model. It can provide a good representation of real soil behavior (Kavazanjian and Mitchell 1980a). On the other hand, it is simple: only three parameters are necessary. Figure 2.7 schematically illustrates this model.

The delayed deviatoric model can be generalized to three dimensions by assuming isotropic material behavior. Kavazanjian and Mitchell (1977, 1980a) developed rules for superposition of deviatoric stress increments based on the work of Hirst (1968). Hirst found that cohesive soils subjected to a sustained deviatoric stress will show a quasi-resistance to subsequent immediate deformation. He described this behavior as a stiffening of the soil skeleton or work hardening. In the absence of thixotropic and structural changes, the soil will eventually return to the immediate deviatoric deformation

curve (see Figure 2.8). Lade and Musante (1976) assume that in the unload-reload region, cohesive soils deform essentially as a linearly elastic solid with a modulus equal to the initial tangent modulus E_t (neglecting hysteresis effects). By adopting this assumption, Kavazanjian and Mitchell (1980) postulated a general deviatoric model, which is shown in Figure 2.9.

Under initial loading condition, the soil stress-strain relationship will follow a hyperbola. Under sustained loading, soil will creep according to the Singh and Mitchell relationship. Under unloading-reloading conditions, soil will behave like an elastic material with an initial modulus E_t .

2.2.2.3 Critical state concept and Cam-clay model

Cam-clay models are the most widely used plasticity models for characterizing the stress-strain behavior of normally to lightly overconsolidated cohesive soil. They are developed based on the critical state concept.

A soil sample, if allowing volume change, will dilate or contract in a shearing test, depending on its initial state of density. As it continues to shear, it will reach a point at which the rate of volume change diminishes. This constant volume state is called the critical state.

When the effective stress paths of the triaxial tests are plotted on the (p, q) plane, the final constant volume states lie on a straight line with a slope of M . This straight line is called the critical state line. The trace of drained and undrained test paths in (p, q, e) space will define the general surface which is called the Roscoe Surface (see Figure 2.10).

It has been known since the 1930s that a plot of the void ratio at isotropic consolidation state and the void ratio at the critical state versus the natural logarithm of

hydrostatic effective stress p are approximately two parallel straight lines (see Figure 2.11).

Two equations are used to characterize the critical state

$$[2.4] \quad q = M p$$

$$[2.5] \quad e = \Gamma - \lambda \ln(p)$$

where Γ is the critical void ratio at $p = 1$; and λ is the slope on a natural logarithm plot.

The equation for the isotropic consolidation line is

$$[2.6] \quad e = e_a - \lambda \ln(p)$$

where e_a is the void ratio at $p = 1 \text{ kPa}$.

A clay will be 'wet' when its state point lies between these lines, and will be 'dry' when its state point is inside the critical state line.

Based upon this critical state concept, Roscoe et al. (1963) developed the original Cam-clay theory by assuming that there is no recoverable component of shear distortion. The yield surface is as follows:

$$[2.7] \quad q = \frac{Mp}{\lambda - \kappa} (e_a - e - \lambda \ln(p))$$

where κ is the slope of the reloading and swelling line on an e - $\ln(p)$ plot.

This yield surface has a bullet shape. It has a number of shortcomings, one of which is that it has a corner along the isotropic effective stress axis. At this corner, plastic strain increments are not well defined.

To overcome the shortcoming of the original Cam-clay model, Burland (1965) proposed a modified Cam-clay theory. The equation for the new yield surface is as follows

$$[2.8] \quad \frac{q^2}{M^2} + p(p - p_c) = 0$$

where p_c is the preconsolidation stress. This equation represents an ellipse in (p, q) space with center at $p_c/2$.

Roscoe and Burland (1968) found that the modified Cam-clay model made a distinct improvement in prediction of the triaxial compression behavior of normally consolidated Kaolin, but the shear strain was under-predicted. This is due to the assumption of the modified Cam-clay theory, which assumes no shear distortion can be associated with a stress path beneath the state boundary surface. Experimental results obtained by London (1967), and Wroth and London (1967) contradicted this assumption. They found that considerable plastic shear distortions take place for stress paths inside the yield surface. To account for this, Roscoe and Burland (1968) proposed the concept of horizontal yield surface inscribed in the Cam-clay ellipsoid as shown in Figure 2.12. This horizontal yielding surface can be expressed as

$$[2.9] \quad G = q - q_c = 0$$

where q_c is the shear yield stress based on the Von-Mises yield criterion.

Hsieh (1987) extended this theory to include time-dependent deformations. The time-independent and time-dependent components of strains are both evaluated by this double-yield surface criterion.

2.2.2.5 Basic assumption and limitation of DYSCP model

The basic assumptions of the DYSCP model are summarized as follows. (1) isotropy: since the modified Cam-clay model and Von-Mises model are both isotropic, the resulting model (DYSCP model) is also isotropic; (2) Uncoupling: volumetric deformation is independent of deviatoric stress level, and vice versa. With this assumption, Bjerrum's one-dimensional compression concept and the Singh and Mitchell equation can be generalized to three-dimensional cases; (3). constant C_α or ψ : this assumption is correct only if soil is normally consolidated with low sensitivity, and principal stress ratios are between the hydrostatic case (isotropic triaxial consolidation) and the one-dimensional case. For principal stress ratios greater than those encountered in one-dimensional compression, C_α may increase significantly (Ladd and Preston 1965); and (4) neglect hysteresis effects: hysteresis effects of soils have been neglected by assuming that the recompression ratio and the swelling ratio are the same.

Due to the above basic assumptions, some limitations of this model are expected: (1) it can only be used for soil on the 'wet' side (NC or slightly OC); (2) it cannot be used for any anisotropically consolidated soils or those stress paths that involve significant rotation of the principal stress directions; (3) it cannot predict creep rupture due to the validation of Singh and Mitchell model. It can only be used for stress levels between 20% to 80% of maximum; and (4) it cannot be used for cyclic loading due to the neglect of hysteresis effects on soils.

2.3 Construction history and physical observation of Pisa Tower

As one of the seven wonders of the world, the Leaning Tower of Pisa has drawn attention for many years. Starting from its second construction stage, the south side of the foundation has settled more than the north side, presently giving a southward tilt of 5.5° . Its safety against a sudden collapse has created a serious concern.

2.3.1 Construction history

The purpose of the construction of the tower was to complete a religious monumental complex, which included the Cathedral and the Baptistery. The Cathedral was erected one hundred years earlier and the Baptistery twenty years earlier than the tower. The weight and geometry of the tower are shown in Figure 2.13.

Figure 2.14 shows the construction process of the tower. It started in August 1173. Five years later (1178), the works were interrupted at the middle of the fourth level due to political reasons. If the construction had continued much further, the foundation would have experienced an undrained bearing capacity failure. The interruption lasted about one century by which time the strength of the ground had increased due to consolidation under the weight of the tower (Burland and Potts 1995). In 1272, the second construction stage was started and six years later, the tower was brought almost to completion, up to the seventh cornice. It was during this construction phase that the deviation of the tower axis began to appear. This is reflected by the attempt of the architects to correct the constant inclination by progressively changing the thickness of the stone element (called "ricorso"), see Figure 2.15. In 1278 the construction of the tower was again interrupted by political problems. Once again if the work had continued, the tower would have fallen over. The third stage of construction (the bell chamber) started in 1360 and ended in 1370. The whole construction lasted for nearly 200 years. Even if it is unintentional, the erection of the tower represents an excellent example of stage construction, which might deserve a careful re-examination by means of appropriate numerical analyses (Jamiolkowski et al. 1993).

2.3.2 History of tilting and major perturbations

Burland's (1991) endeavor to infer the evolution of the inclination of the tower during its construction from the variation of the thickness of "ricorsi" is shown in Figure 2.16. This figure assumes that during construction the masons made continuous

adjustments to keep the floors horizontal at each storey. The figures and data from Cambefort (1978) and Leonards (1979) showed that during the first construction stage the tower experienced random inclinations in different directions. Starting from only the second construction stage, the southward leaning became evident, and this kind of movement has been continuous ever since.

Figure 2.17 shows the evolution of the tower inclination over time. The displayed data have been highly qualitative until 1758. The random inclinations in the early construction stage have been neglected. At present the tower is inclined to the south at about 5.5° . From 1370 to 1550, there is an abrupt increase in inclination. It is certain that something happened during that time, since the tilting angle of the tower increased by more than 3° . Unfortunately, there are no historic records available before 1838. The only clue is related to the Meloria War during which Pisa city suffered a disastrous defeat by Genoa.

Another possible explanation for the discontinuity of the tower inclination is that after the tower reached its full height, leaning instability occurred, which caused the tower to rotate around a center above the foundation (Burland and Potts 1995). This kind of pure rotation amplifies the tower's inclination.

During the Second World War, the town was subjected to notable destruction from heavy bombing raids. Some artistic treasures including the Piazza dei Miracoli were seriously damaged (Verlag La Torre s.r.l. 1984). Even though there are no detailed records available relating to the direct damage of Pisa Tower, it is likely that the tower might at least suffer from bomb explosion shocks. This kind of dynamic influence may have caused the tower to tilt more.

Among the recorded events, the excavation of the catino in 1834 appears to have caused an increase in tilting by 0.5° . In this century, the inclination of the tower has been increasing due to various events. The foundation masonry grouting in 1933 caused a

sudden increase in tilt by 31 seconds. The soil and masonry drilling in 1966 caused 6 seconds increase. Ground water lowering from 1970 to 1974 caused 41 seconds increase. A masonry boring in 1985 caused an increase in tilt by 10 seconds. The current rate of tower inclination has doubled since the 1930's. The tower is very sensitive to even the smallest ground disturbance.

Due to the complicated situation of the tower, such as the above mentioned disturbances and different deformation mechanisms, it is almost impossible to account for all the aspects in a single model.

2.4 Subsurface conditions

Geotechnical exploration of the subsurface conditions underlying the tower's foundation has been carried out since 1913. The most complete set of data on the subsurface soil was collected by the committee chaired by Polvani since 1965. Further investigations were executed in the late mid-eighties. The results were published in part by Lancellotta and Pepe (1990). A comprehensive interpretation of those data was undertaken recently by Calabresi et al. (1992). They summarized the geotechnical information obtained up to 1990.

A careful study of the detailed sample descriptions given by the Polvani Report suggests that beneath the tower in Formation A, there exists a lens of clayey silt which thins from south to north. Figure 2.18 shows a comparison between two cone tests at 30m from the north and south sides of the tower axis. It reveals a significant non-homogeneity of this formation. Apart from that, the rest of the layers are fairly uniform. The separation surfaces are flat and the thickness of each layer is almost constant. The initial soil profile underneath the tower's foundation proposed by Calabresi et al. (1992) is shown in Figure 2.19. It contains three main formations:

Formation A: About 10m in thickness. clayey silt and silty sand. It can be subdivided into three layers: (1) MG, top soil and made ground; (2) layer A_1 , loose to very loose yellow sandy silt to clayey silt without stratification. It is formed by a first layer of clayey silts A_1^I , 1.4m thick (elev. 0 to -1.4m), overlying the silty sands A_1^{II} , 4.0m thick (elev. -1.4 to -5.4m). The second clayey silt layer A_1^I is included in the silty sands layer A_1^{II} . Its thickness increases linearly from 0, at 60m north of the tower axis, to 3.0m at 35m south of the tower axis; and (3) layer A_2 , uniform gray sand with inter-bedded clay layers and broken fossils, 2.0m thick (elev. -5.4 to -7.4m). Formation A is believed to be of major significance affecting the lean due to its significant inhomogeneity.

Formation B: About 30m in thickness, predominantly clayey. It can be subdivided into four layers: (1) upper clay or Pancone clay, about 11m thick (elev. -7.4m to -17.8m), including layer B_1 , B_2 , and B_3 , high plasticity clays, normal consolidated or slightly overconsolidated clay; (2) intermediate clay, about 4m thick (elev. -17.8m to -22.0m), including layer B_4 and B_5 , dark gray to yellow, low plasticity clayey silts, overconsolidated with OCR of 1.8; (3) intermediate sand (B_6), about 2.5m thick (elev. -22.0m to -24.4m), gray, sometimes yellow; and (4), lower clay, about 13m thick (elev. -24.4m to -37.0m), clays and silts, including layer B_7 to B_{10} , blue gray to gray with yellow zones, medium plasticity, normal consolidated clay. Formation B is very uniform laterally. It is believed to be the seat of a major part of the tower settlement.

Formation C: Slightly silty sand, encountered at a depth of 40m and extends to a depth greater than the deepest boring.

The index properties of Pisa soil are summarized in Table 2.1. The Atterberg limits are shown in Figure 2.20. They are based on the evaluation of the Polvani Committee made from 1965 to 1971 (MLW 1971) and by the Design Group from 1986 to 1988 (Lancellotta and Pepe 1990). It can be seen that the unit weight γ progressively decreases with depth. An abrupt increase is observed in the upper clays. The higher values of specific gravity G_s are observed in the upper clays. The highest average values

of the plasticity index PI as well as the highest water content values are found in the upper clays. In the intermediate clays the plasticity index PI is very low and water content is close to the plastic limit. The clay fraction CF decreases in B₂, B₅, and B₈ to B₉. Most of the measured activity data are in the range of 0.5 to 1.0. Those are typical values for medium to active clays.

X-ray diffraction analysis conducted by Mitchell and Soga (1995) reveals that the mineralogical compositions of Formation A and Formation B are the same. The clay minerals are mainly kaolinite, illite, and vermiculite. The non-clay fraction is dominated by quartz.

2.5 Major research efforts about the tower

Pisa Tower has drawn attention for many years. Throughout its history, thousands of ideas and projects have been submitted from time to time, from everywhere of the world. A large amount of data has been provided by these previous investigations.

2.5.1 The leaning of the tower

Many investigators have studied the mechanisms which caused the tower to lean. The proposed mechanisms are summarized in the following.

Terzaghi (1934) attributed the cause of leaning to differential consolidation of the underlying soft highly plastic clay. He pointed out that both the inadequate bearing capacity and the erosion hypotheses should produce abrupt movements, but the real tower did not deform like that.

Mitchell et al. (1977, 1995) proposed that southward leaning of the tower was initiated by differential immediate settlements within the stratified silty sands with clay seams (layer A₁¹ in Formation A). The resulting eccentricity in loading caused additional tilting in the same direction due to differential consolidation of the underlying clay. The

non-homogeneity of Formation A determines the leaning direction. The underlying clay in Formation B is the main seat of settlement.

Cambefort (1978) proposed that the progressive tilting of the tower can only come from the creep of the soft soil. Sample tests conducted by Bishop and Lovenbury (1969) and Mitchell and Soga (1995) show that creep is important in the soil beneath the tower's foundation, especially in the clayey silt layer A_1 and the highly plastic clay layer B_1 .

Nathan (1978), Schultze (1973), and Kerisel (1975) proposed that there is probably a slip band within the layer whereby the center of gravity of the tower is shifted more and more towards the south. The additional moment induces the additional settlement at the south end.

Leonards (1979) proposed that local shear failure in the upper clay stratum was the cause of the large tilt that occurred as the seventh story was being completed in the year 1278. The tower did not collapse because yielding was restricted to a thin zone near the top of the clay and was limited to a small area. The results of a careful re-examination have contradicted this hypothesis.

After studying the observed data, Lancellotta (1993) and Burland and Potts (1995) drew the conclusion that the seat of the continuing long-term tilting of the tower lies in Formation A, not Formation B. The fundamental mechanism underlying the behavior of the tower is leaning instability triggered by a small geometrical imperfection in the construction. The tower is subjected to a rigid body motion during steady-state creep-rotation. They think that if the inclination had been due to the nonuniform properties of Formation A, it would have developed much earlier rather than after the height exceeded the sixth cornice.

Some investigators attribute the initial reason for the leaning to non-uniform dewatering of the foundation soil, or to non-uniform surface loads due to the stockpiling

of the building stones, or to various disturbances due to earthquake, wind, temperature, traffic and visitors. There is insufficient evidence to support these mechanisms.

According to Mitchell et al. (1979), to determine with certainty the true mechanism responsible for the differential settlement would require measures at various times and locations of strain, stress, pore water pressure, and soil parameters. Since such measures do not exist, no one can state with certainty the cause of the leaning.

To investigate the cause of the initial leaning is beyond the scope of this research, but from previous studies, including recent investigations by Burland and Potts (1995) and Mitchell and Soga (1995), the following conclusions can be drawn: the mechanisms of both creep and leaning instability exist in the foundation soil; The existence of one mechanism does not mean the other can be neglected.

2.5.2 Stabilization measures

The regular monitoring showed that the rate of southward inclination of the tower in 1990 had doubled since the 1930's. After a similarly constructed bell tower at the Cathedral of Pavia collapsed without warning in 1989, the safety of the Pisa Tower became a big issue. In the early 1990, the tower was closed to the general public due to its critical situation. A special commission, composed of Italian and foreign experts, was brought together by the Prime Minister of Italy to develop and implement new measures for stabilizing the tower. The ultimate goal of the commission is not to straighten the tower but to reduce the tower's lean by half a degree and hold it there. The tower curves like a banana and will never stand truly up right. The reduced half a degree tilting will be enough to keep this landmark standing into the next century (Wheeler 1993, and Heiniger 1995).

The current Commission has implemented two temporary measures to slightly improve the safety of the tower: (1) the installation of temporary local reinforcement

(post-tensioned cables) at the first cornice to prevent local buckling as shown in Figure 2.21; and (2) the improvement of the foundation stability against overturning by placing a 6MN lead counterweight at the north rim of the tower base, as shown in Figure 2.22, which caused tilt towards the north by about 50 seconds of arc.

Following the temporary solutions, some permanent solutions have been studied. Among various possible approaches, the one inducing controlled settlement below the north side of the tower was highly recommended, along with two alternatives: an electro-osmotic consolidation treatment and a controlled soil extraction technique. The first alternative, proposed by Mitchell (1991), would induce the settlement of the tower at the north side by causing the reduction of the volume in the top most part of the Pancone clay. The second one, postulated by Terracina (1962), would obtain a similar effect by drilling into the soil at an angle and by removing small volumes with a sampling tool. Trials close to the tower showed that the controlled soil extraction method looks encouraging and is being adopted. The final selected solution includes three phases: (1) the freezing of the ground using liquid nitrogen and excavating the ground; (2) the casting of a post tensioned concrete ring beam to embrace the tower's foundation and applying ground anchors on the north side of the beam; and (3) the excavation of bore-holes. The anchored ring beam will replace the function of the temporary measure of 6MN lead weight placed on the tower's up-tilt side. Then, the controlled subsidence to the north of the tower will be achieved by excavating bore-holes. The implementation of this solution started in April 1995 but was suspended five months later because the excavation unearthed a 1m thick mass of boulders, rocks and bricks bound together by a lime mortar. It also discovered undocumented old steel grout tubes tying the tower's foundation to a surrounding walkway. The tower did not react as expected. The stabilization work caused the tower to move back to the south side by 3.5 arc seconds (Oliver 1995, and Parker 1995). The commissioners decided to skip the second phase and move directly to the last phase of bore-hole excavation.

2.5.3 Previous numerical analysis

There are mainly four groups of people dealing with numerical modeling of Pisa tower (Jamiolkowski 1994): Calabresi et al. at the University of Rome. Burland and Potts at Imperial College. Borja, Mitchell, and Schiffman at various American institutions, and Lancellota and Pepe at the Politecnico di Torino. Results so far obtained are not quite satisfactory. The reasons are linked to some peculiar issues, such as the tower's three-dimensional nature and the relevance of creep and coupling between shear stress and volumetric strain on one side, and the mean effective stress and shear strain on the other. Of these four groups, only Burland's and Mitchell's work have been released.

2.5.3.1 Burland's work

Burland and Potts (1995) conducted a numerical study of the tower using the time-independent modified Cam-clay model with coupled consolidation. A plane strain approach was used. The model can generate its own overturning moment in response to any change of inclination.

Finite element analysis results showed that large strain analysis did not differ significantly from a traditional infinitesimal strain analysis but introduced time consuming complications. Thus, infinitesimal strain approach was used. The predicted inclination history was different from the observed one, although the final 5.44 degrees tilting was very close to that observed. The final average settlement of the foundations was about 3.8 m, while the actual observed one was about 3.0 m. They thought that the difference between the predicted and measured values were due largely to the values of G/p_0' (G is the shear modulus and p_0' is the initial mean effective stress) used in FEA, which were determined empirically. On the other hand, the model cannot take time-dependent deformation behavior into consideration. It is a plane strain analysis rather than a three dimensional one.

2.5.3.2 Mitchell's work

Mitchell and Soga (1995) did three-dimensional and plane strain finite element analyses using elastic and elasto-plastic models. After comparing the computed stress distributions and displacements, they found that no simple two-dimensional representation can represent the actual behavior of the tilting tower. Three-dimensional analysis is necessary. Elasto-plastic analysis should be used to predict the stress-strain behavior of the tower.

FEA results showed some stress concentration in Formation A, which supported Mitchell's hypothesis about the leaning. The predicted final rotation in year 1990 was 3.5 degrees, but the observed one was 5.5 degrees. The final maximum settlement in 1990 was 1.6m, while the measured one was 2.8m. They thought that the difference could be caused by two factors. One is creep behavior, especially in the clayey silt layer (A_1) and the Pancone clay layers (B_1 and B_3) which the time-independent Cam-clay model could not predict. Figure 2.23 shows the influence of creep deformations. The other was due to the use of small strain formulation in FEA. They found the deviatoric strain at some points could reach up to 40%.

2.5.4 Creep test of the Pisa clay

2.5.4.1 Bishop's creep tests

Bishop and Lovenbury (1969) investigated creep behavior of the Pisa clay at the depth of approximately 19 meters, which belongs to the highly structured layer B3 as shown in Figure 2.19. Six drained creep tests under constant loads of 50, 75, and 85% of the drained strength of the clay were conducted, two for each stress level. The approximate size of the samples was 7.62 cm in diameter and 15.24 cm in height. The applied confining pressure was 152 kPa. The primary consolidation ended in less than

two days after the final loading. The volume change data were unreliable due to a water leakage problem.

Test results showed that all the samples exhibited sudden increases in strains for a length of time at some stage, as shown in Figure 2.24, which reflects the structural breakdown of the Pisa clay carbonates. After that, the axial strain rates were in the range of 1 to 1.5% per logarithmic time cycle.

2.5.4.2 Mitchell's creep tests

Mitchell and Soga (1995) conducted a total of nine triaxial creep tests on the Pisa clay. The undisturbed samples were obtained from Borehole L2, located southwest of the Pisa Tower. Four of them were taken from four different depths of 6m, 10m, 14m, and 19m corresponding to layers A_1 , B_1 , B_2 , and B_3 respectively, as indicated in Figure 2.19. The size of the cylindrical specimens was approximately 3.4 cm in diameter and 8.9 cm in height. The applied loads were obtained from the results of three dimensional elasto-plastic analysis of the Pisa tower. They were applied in steps to simulate the construction sequence of the tower. For each step, a constant load was applied instantly then was allowed to last for 7 days. Primary consolidation was considered not to require more than one day. Thus fully drained conditions were expected to be achieved after one day of constant loading. In order to avoid drying, the specimens were covered by a membrane and put into the triaxial cell which was filled with water during the test. Drainage was allowed at the top and bottom of the specimen (one dimensional flow). Throughout the test, a back pressure of 98 kPa was applied to maintain saturation. Some water leakage was observed during the test. Thus, the volume change data were very unreliable.

The measured axial strains with log time relationship are shown in Figure 2.25. It can be seen that the 10m sample exhibited very large axial strain (up to 16%) due to its highly plastic nature and the relatively large tower loads. The 6m sample also exhibited large deformations (up to 9%) due to very large tower load increments.

2.6 Summary

This chapter covers the major creep phenomena studied over the past five decades. Different approaches used to study soil creep behavior have been reviewed to provide context.

One of these approaches-the phenomenological approach-was later generalized into three dimensions. It unifies the existing volumetric and deviatoric models. Each model component is assumed to consist of immediate and delayed contributions based on Bjerrum's (1967) concept. The immediate volumetric model is developed by generalizing Bjerrum's one-dimensional compression model to a three-dimensional state of stress. The immediate deviatoric deformation is evaluated by Konder's (1963) hyperbolic model in conjunction with Ladd and Foott's (1974) normalization technique. The delayed volumetric and deviatoric deformation can be evaluated by Taylor's (1948) secondary creep law and Singh and Mitchell's (1968) creep equation, respectively.

Borja and Kavazanjian (1985) extend the general phenomenological theory within the classical theory of plasticity. The modified Cam-clay model is used to calculate the time-independent deformation component of cohesive soil. Later the idea of introducing a horizontal deviatoric yield surface is adopted to predict the plastic shear distortion that occurs without volume change below the state boundary surface. Thus, the DYSCP model was developed. This model will be used in this research to study creep phenomena beneath the Leaning Tower of Pisa.

As a case study for time dependent behavior, Pisa Tower's construction history, as well as some major negative events, has been studied. Some physical observations about subsoil conditions and the inclination of the tower have been investigated. Various mechanisms to explain the leaning of the tower have been presented. Among them, creep phenomena are believed to be one of the major reasons.

In order to save the tower, different stabilization measures have been proposed. Some temporary solutions have been implemented. The last option-ground freezing operations followed by ground-anchored in-situ concrete collar construction and soil extraction-was initiated, but suspended after five months. This operation will move directly to the soil extraction stage.

Numerical modeling conducted by Burland and Potts (1995) and Mitchell and Soga (1995) show that three-dimensional elasto-plastic small strain analysis is necessary in order to predict the deformation behavior of the tower. Creep deformation should be included in the analysis.

Creep tests by Bishop and Lovenbury (1969) and Mitchell and Soga (1995) show that creep is important in the Pisa clay especially in layers A_1 and B_1 . Samples from the B_1 layer exhibited very large axial strain (up to 16%) due to its highly plastic nature and the relatively large tower loads. Samples from the A_1 layer also exhibited large deformations (up to 9%) due to very large tower load increments.

Table 2.1 Physical and index properties

layer	elevation (m)	γ (kN/m ³)	G_s	w (%)	S_r	I.L. (%)	PI (%)	CF (%)	activity
MG	+3.0 to 0.0	18.2 to 19.5	2.63 to 2.69	25.4 to 34.1	0.87 to 1.00	30 to 43	6 to 19	16 to 27	0.40 to 1.20
A ₁	-0.90 to -6.10	15.8 to 19.9	2.67 to 2.75	25.4 to 40.1	0.87 to 1.00	28 to 44	3 to 18.7	3 to 23	0.30 to 1.71
A ₂	-4.35 to -7.95	15.5 to 19.5	2.65 to 2.74	10.7 to 57.7	0.88 to 0.99	55 to 60	28 to 32	2 to 29	1.10
B ₁	-7.45 to -11.50	16.6 to 18.8	2.76 to 2.81	36.6 to 60.6	0.96 to 1.00	53 to 87	28 to 56	24 to 72	0.62 to 1.17
B ₂	-10.90 to -13.20	16.9 to 18.4	2.74 to 2.77	31.2 to 51.2	0.86 to 1.00	32 to 66	10 to 37	18 to 54	0.40 to 0.70
B ₃	-12.55 to -17.75	15.2 to 18.1	2.65 to 2.80	41.0 to 66.5	0.95 to 1.00	53 to 103	20 to 61	24 to 74	0.56 to 1.13
B ₄	-17.85 to -19.10	19.2 to 20.3	2.67 to 2.76	22.3 to 30.9	0.91 to 1.00	43 to 72	25 to 47	24 to 60	0.64 to 1.13
B ₅	-18.60 to -22.40	19.0 to 20.7	2.71 to 2.77	20.0 to 32.6	0.94 to 0.99	28 to 56	8 to 36	13 to 55	0.43 to 1.16
B ₆	-22.15 to -24.40	18.3 to 19.5	2.68 to 2.72	25.6 to 33.3	0.94 to 1.00	27 to 35	3 to 11	8 to 14	0.43 to 0.55
B ₇	-24.50 to -28.60	17.4 to 20.2	2.70 to 2.82	24.5 to 52.8	0.97 to 1.00	35 to 83	14 to 57	23 to 78	0.41 to 0.98
B ₈	-29.20 to -31.20	17.8 to 20.4	2.65 to 2.74	24.7 to 39.7	0.93 to 0.99	45 to 57	13 to 35	12 to 40	0.72 to 1.17
B ₉	-32.30 to -33.90	16.3 to 20.3	2.53 to 2.74	24.7 to 50.2	0.96 to 1.00	45 to 70	24 to 39	20 to 44	0.68 to 1.95
B ₁₀	-34.55 to -36.40	18.1 to 19.8	2.68 to 2.78	26.8 to 36.5	0.96 to 1.00	43 to 67	22 to 44	32 to 68	0.57 to 0.72
C	-37.2 to -57.25	16.0 to 22.0	2.47 to 2.68	13.1 to 53.3	0.89 to 1.00	15 to 18	1 to 5	4 to 12	0.80 to 0.56

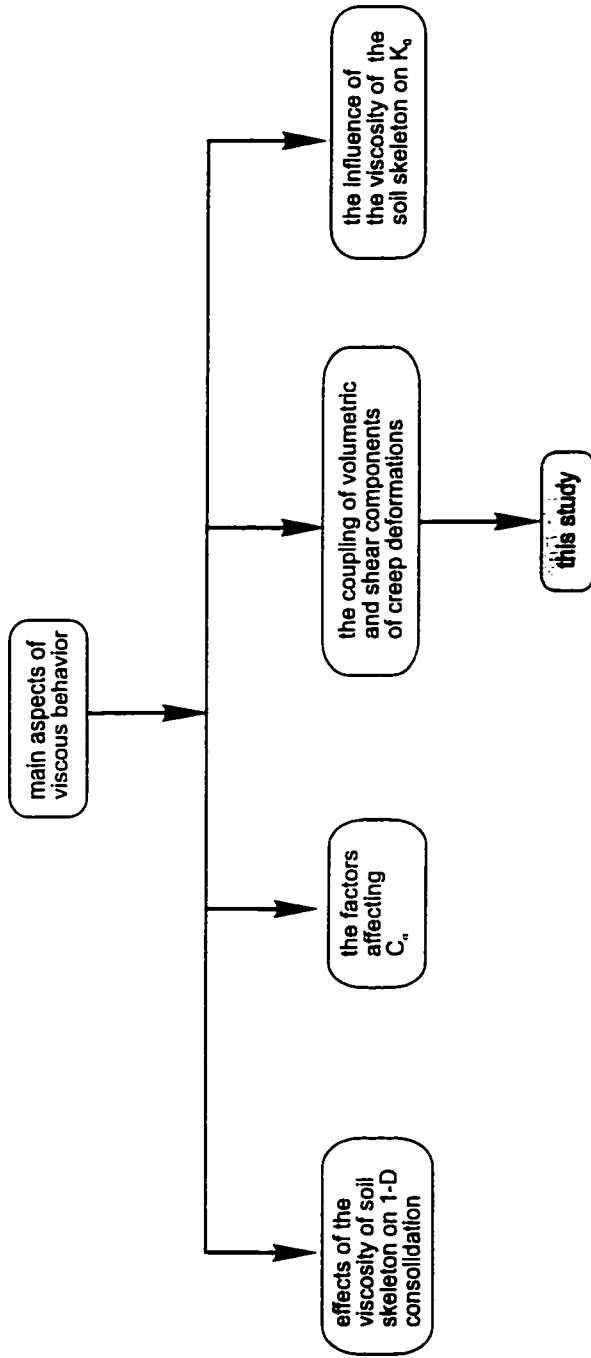


Fig. 2.1 Schematic show of main aspects of viscous behavior (after Burghignoli, et al. 1994)

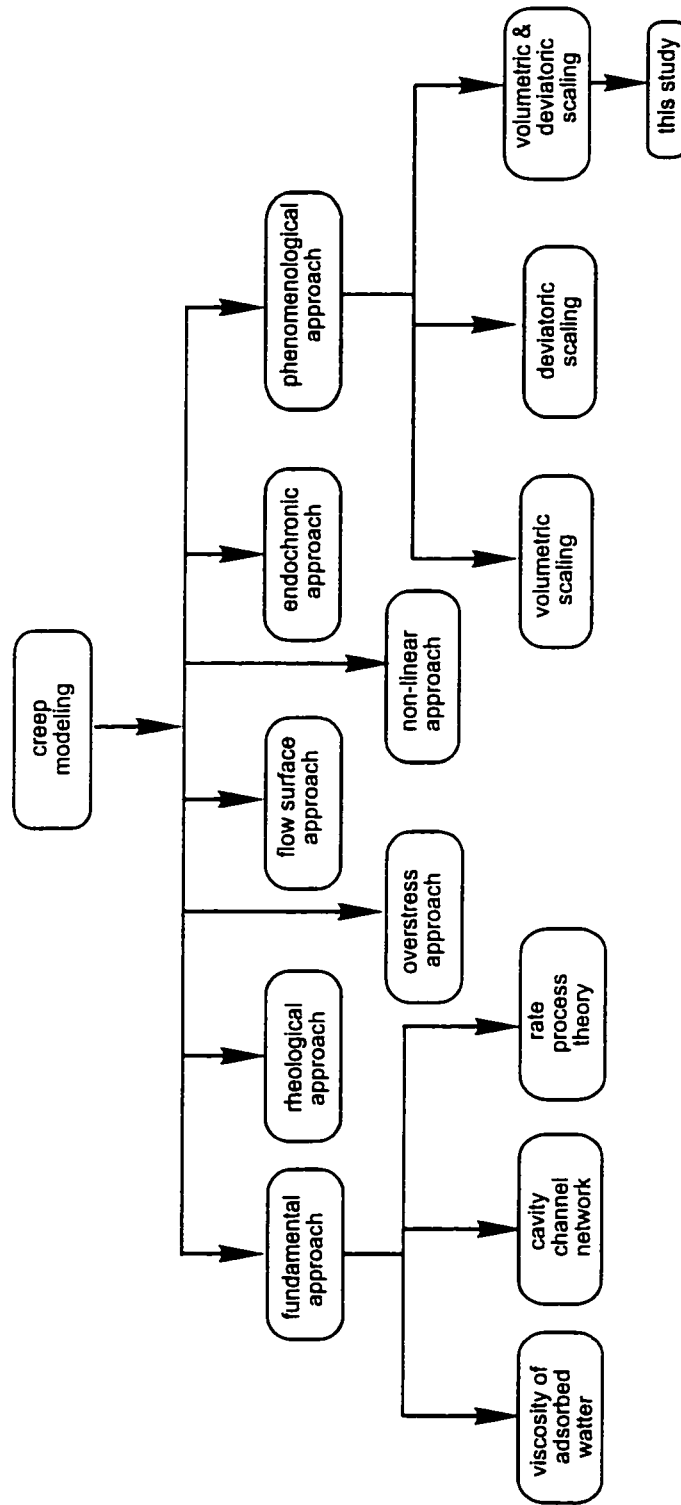


Fig. 2.2 Schematic show of existing approaches of creep modelling

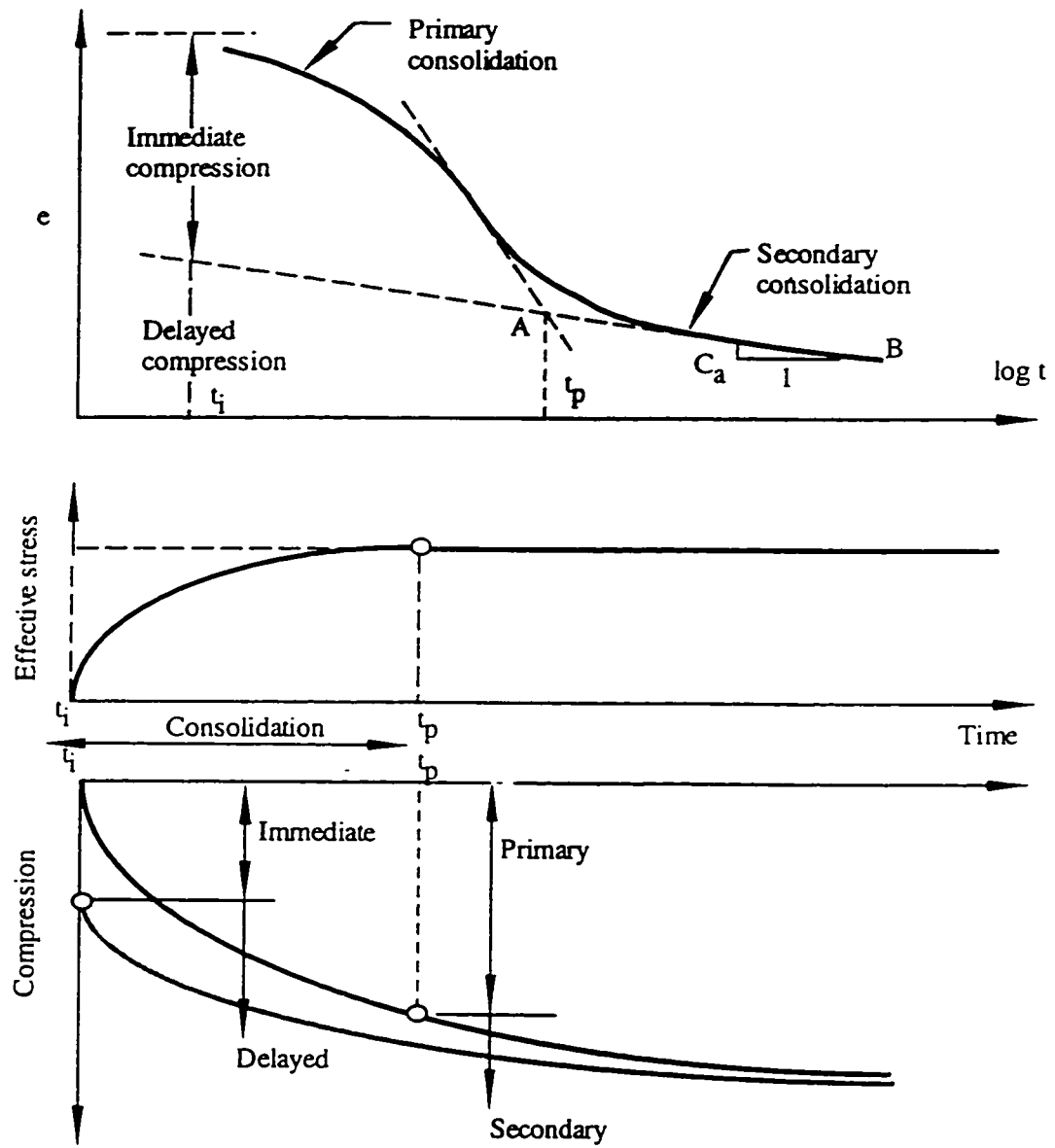


Fig. 2.3 Definition of primary and secondary consolidation and immediate and delayed compression (modified after Borja and Kavazanjian, 1985)

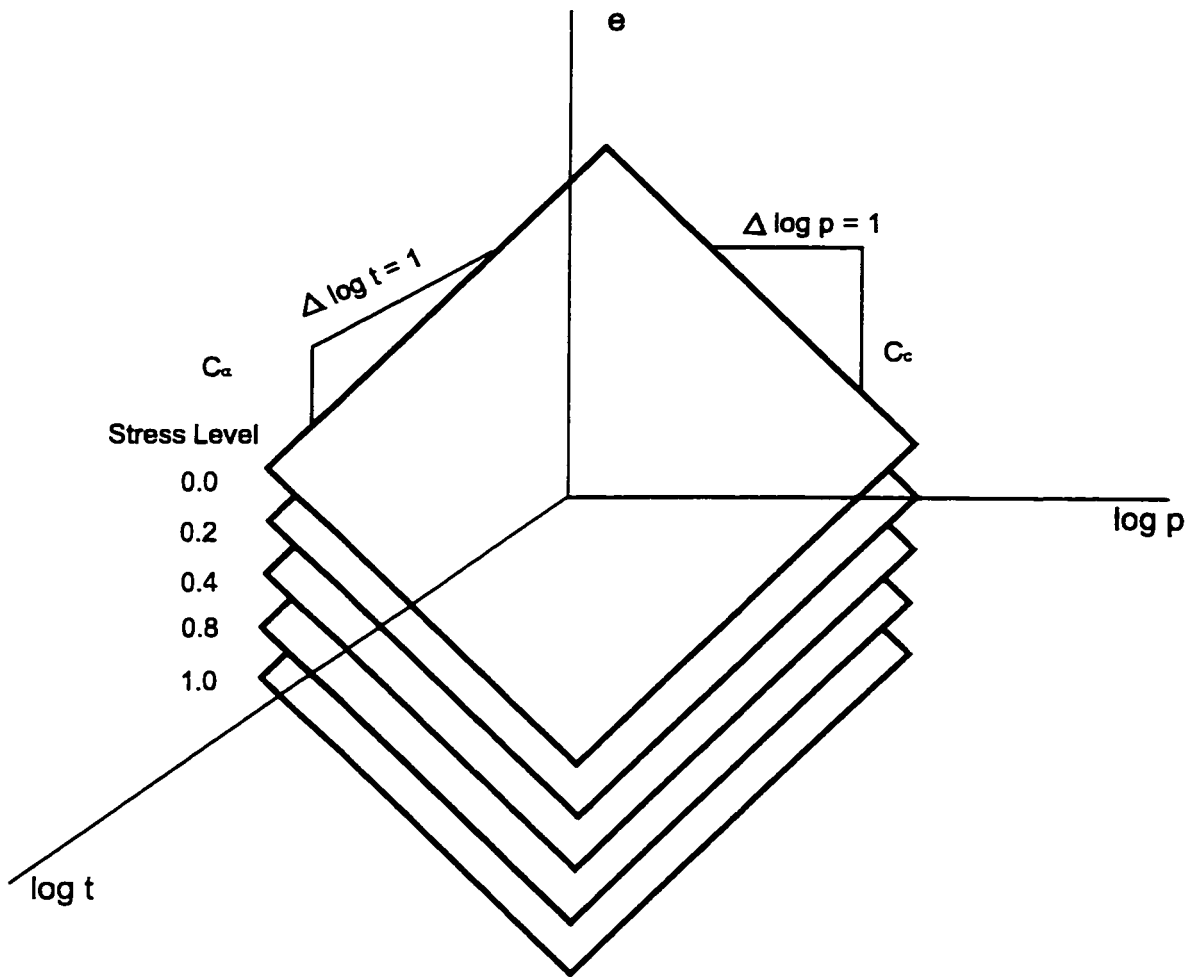


Fig. 2.4 General volumetric model (modified after Kavazanjian, 1978)

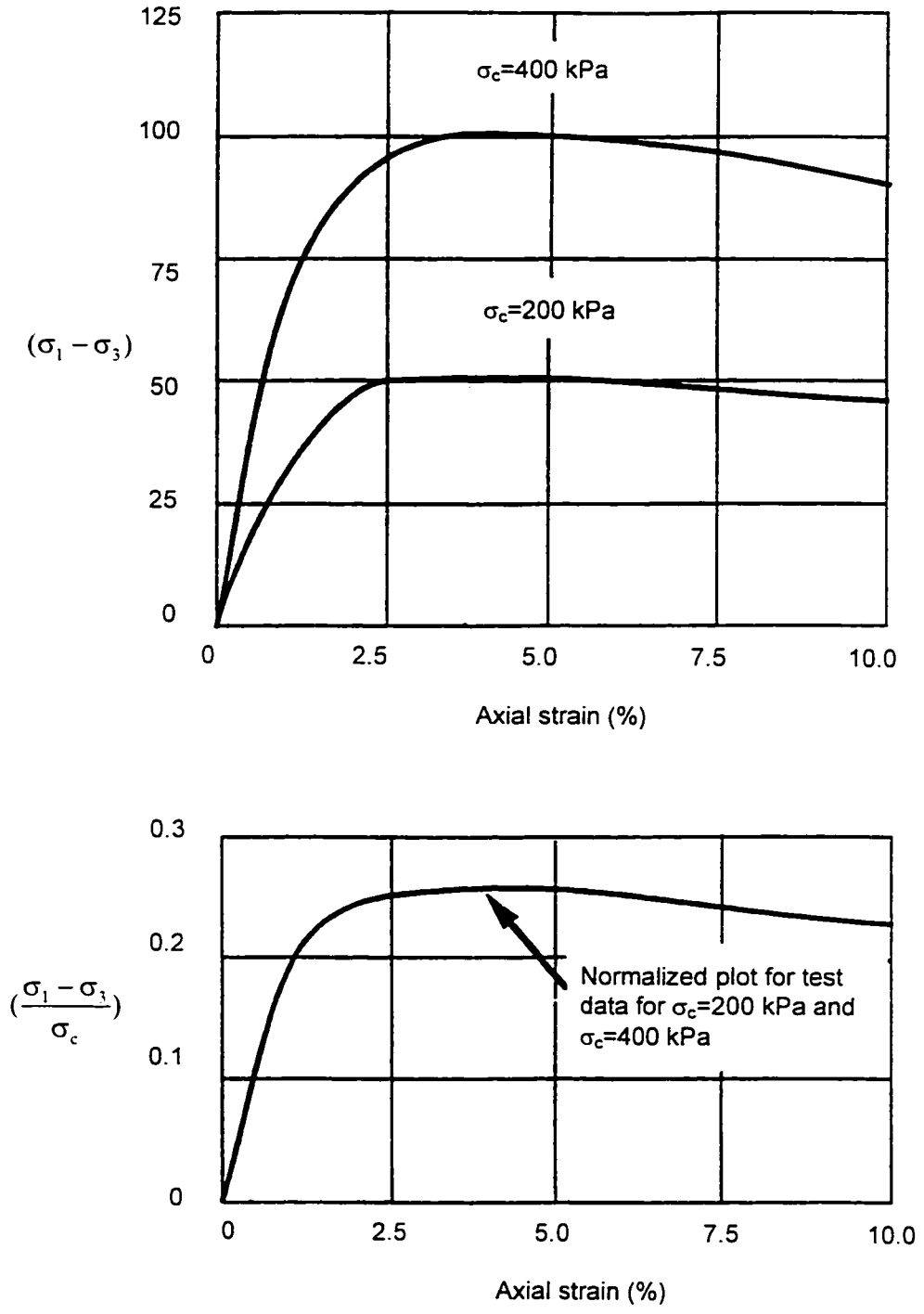


Fig. 2.5 Normalized soil properties (modified after Ladd and Foott, 1974)

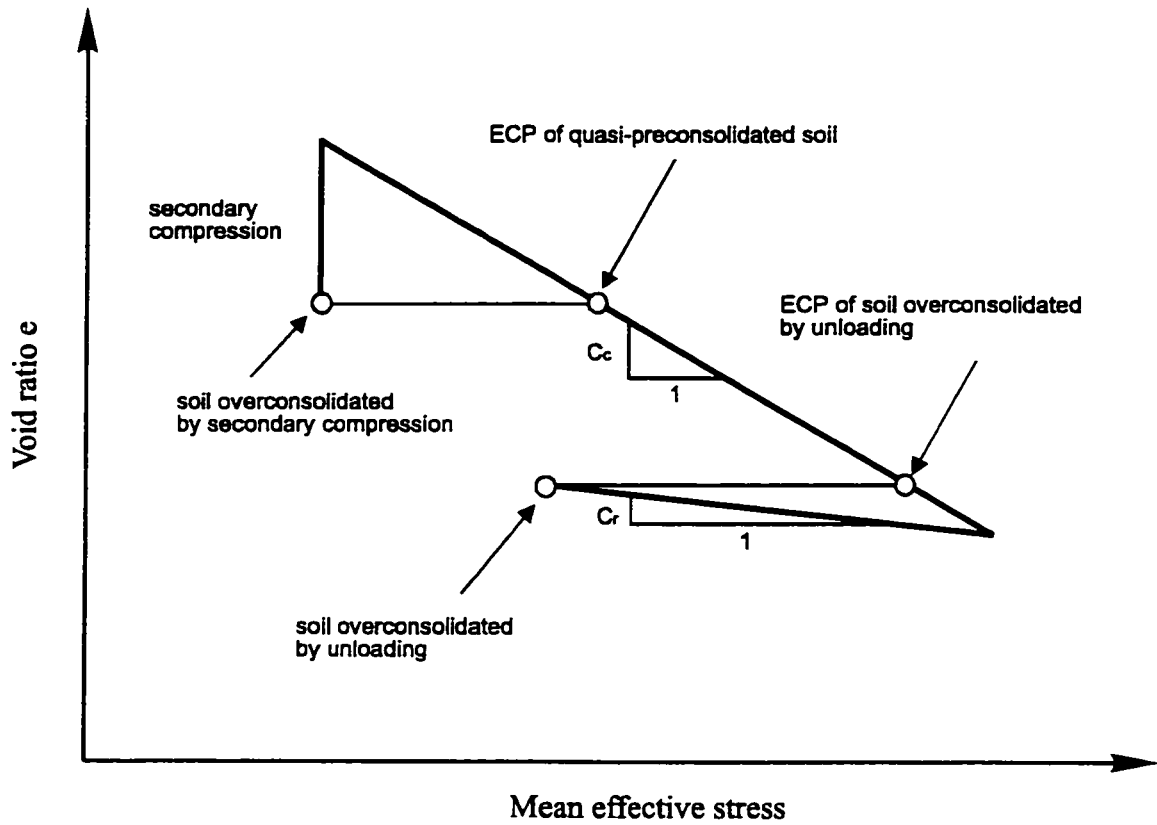


Fig. 2.6 Equivalent consolidation pressure (ECP) concept (modified after Hsieh, 1987)

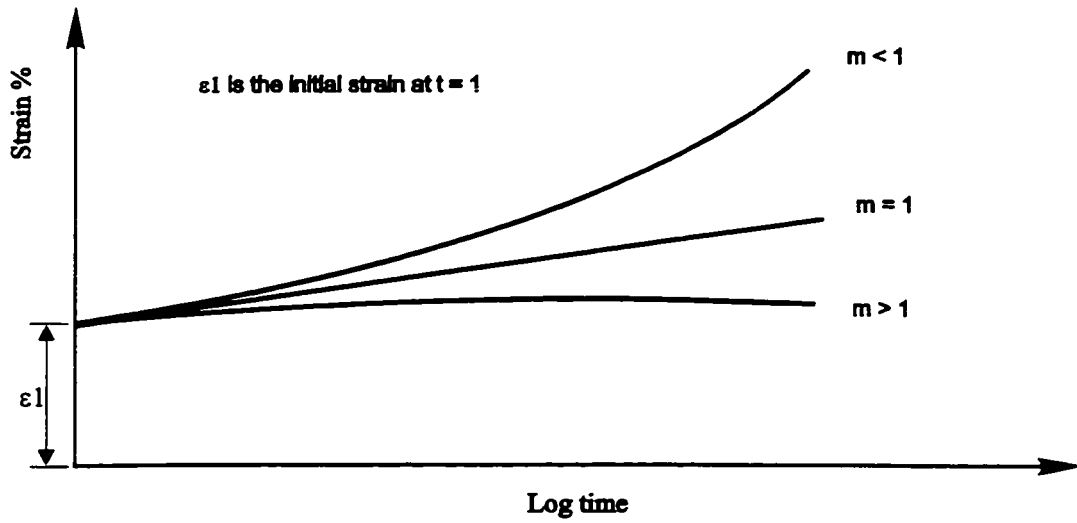


Fig. 2.7 (a) Schematic representation of Singh-Mitchell creep function

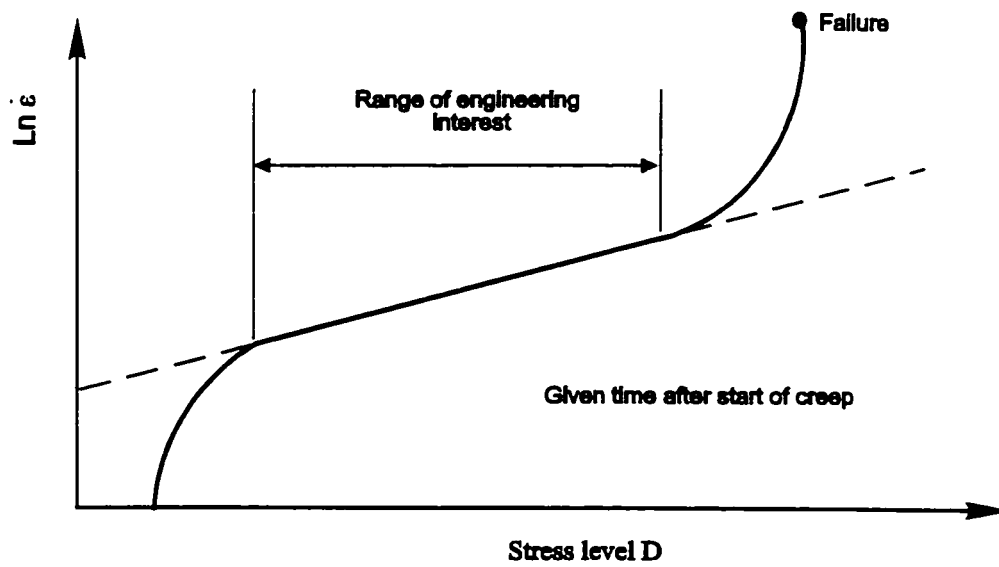


Fig. 2.7 (b) Influence of deviatoric stress level on creep strain rate

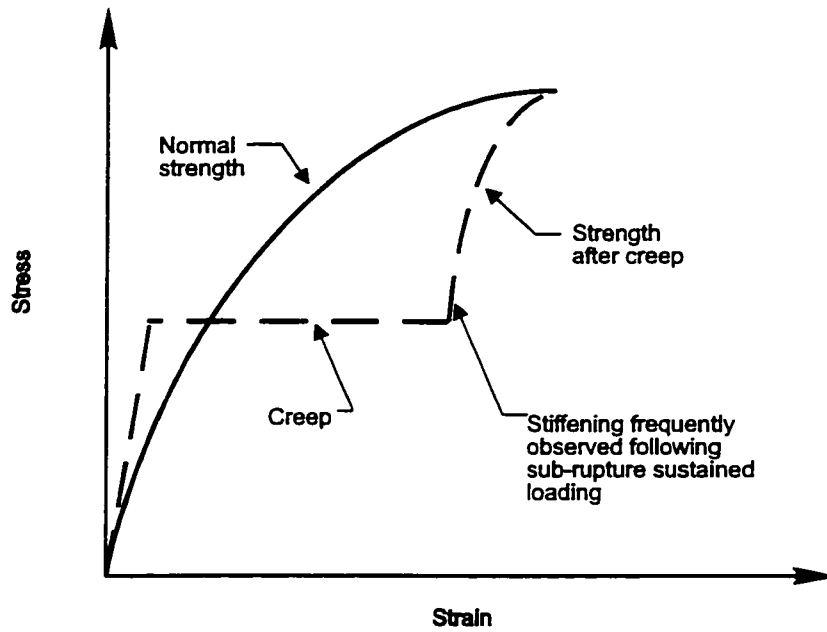


Fig. 2.8 Stress-strain behavior following a period of sustained shear loading (modified after Hirst, 1968)

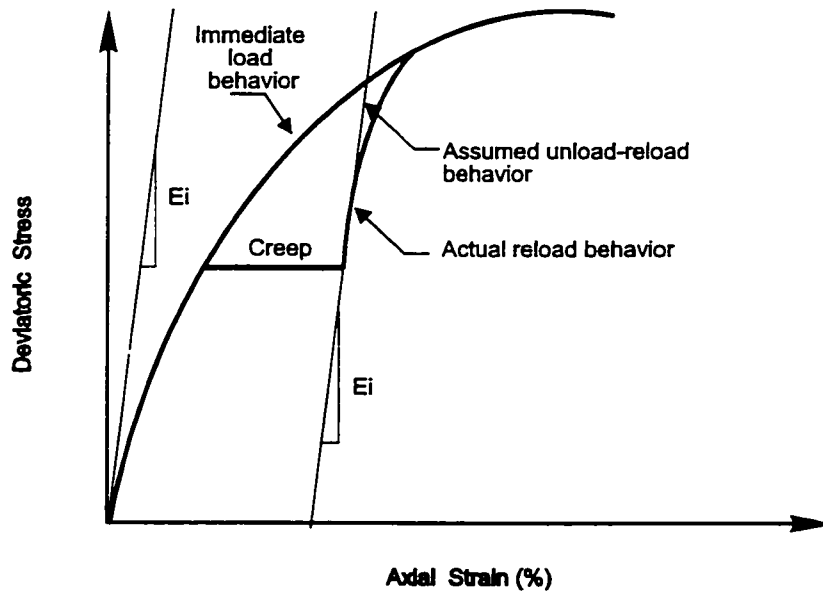


Fig. 2.9 Kavazanjian's general deviatoric model (modified after Kavazanjian, 1978)

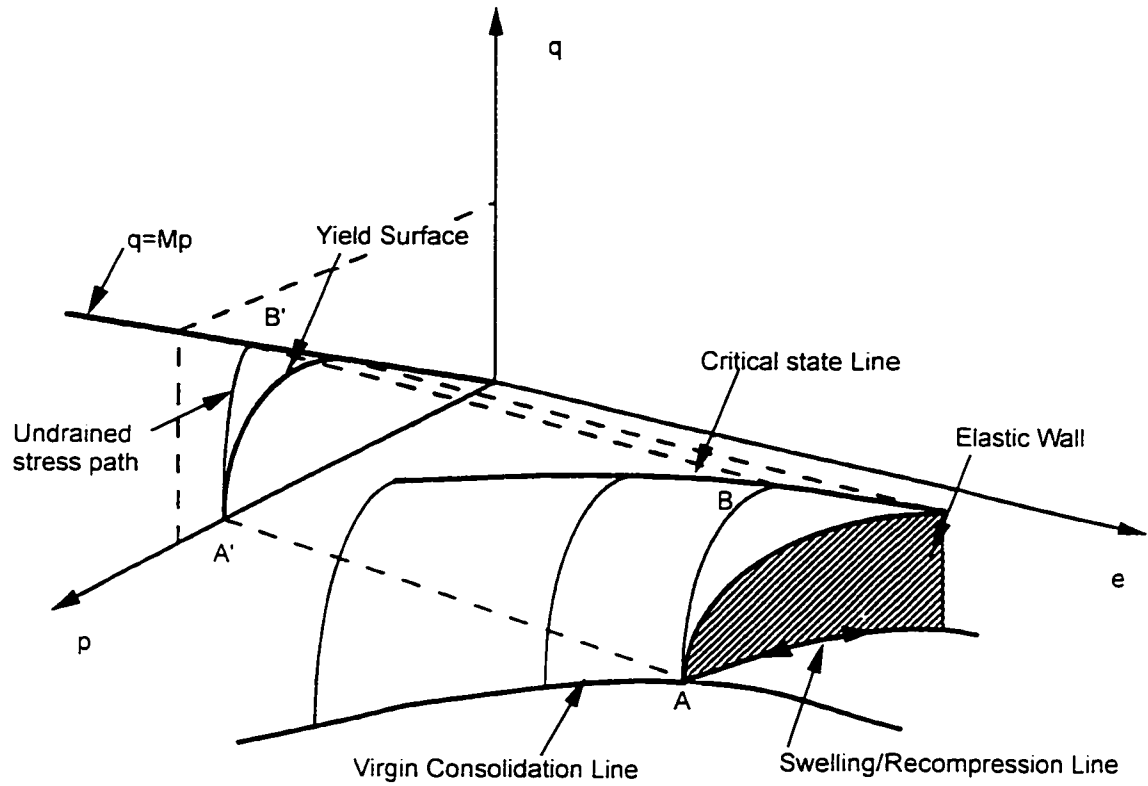


Fig. 2.10 The critical state line and the state boundary surface (modified after Morsy, 1994)

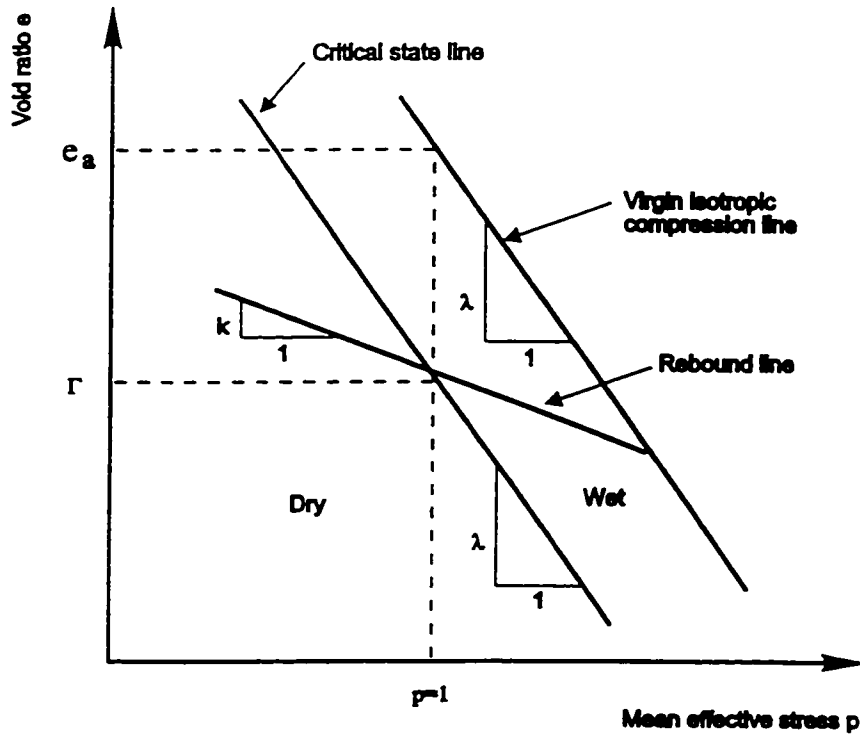


Fig. 2.11 Consolidation curves on e - $\ln p$ space

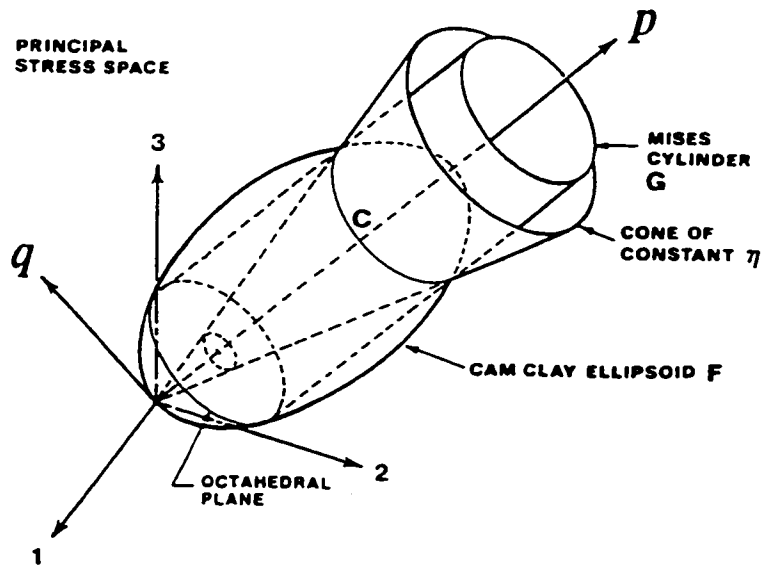


Fig. 2.12 Three-dimensional representation of Double-Yield-Surface criteria in principal stress space (Hsieh, et al., 1990)

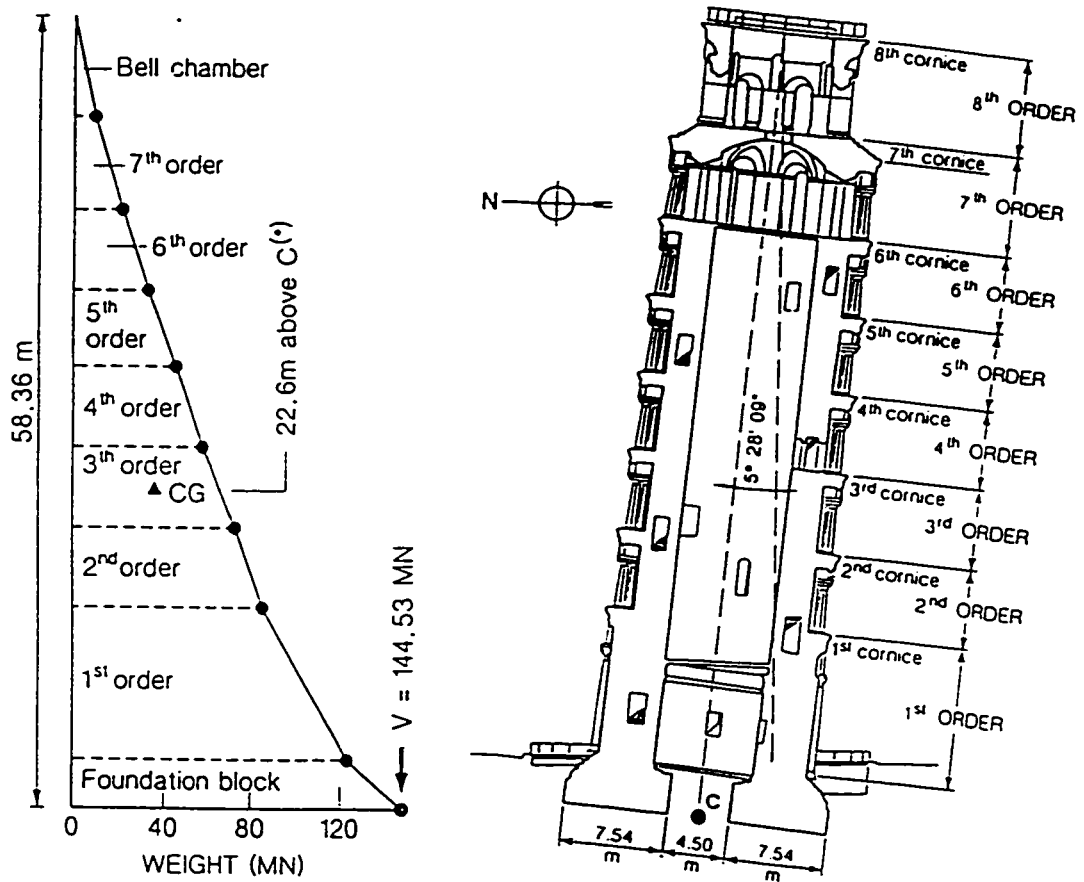


Fig. 2.13 Weight and geometrical characteristics of Pisa Tower (after Jamiolkowski et al., 1993)

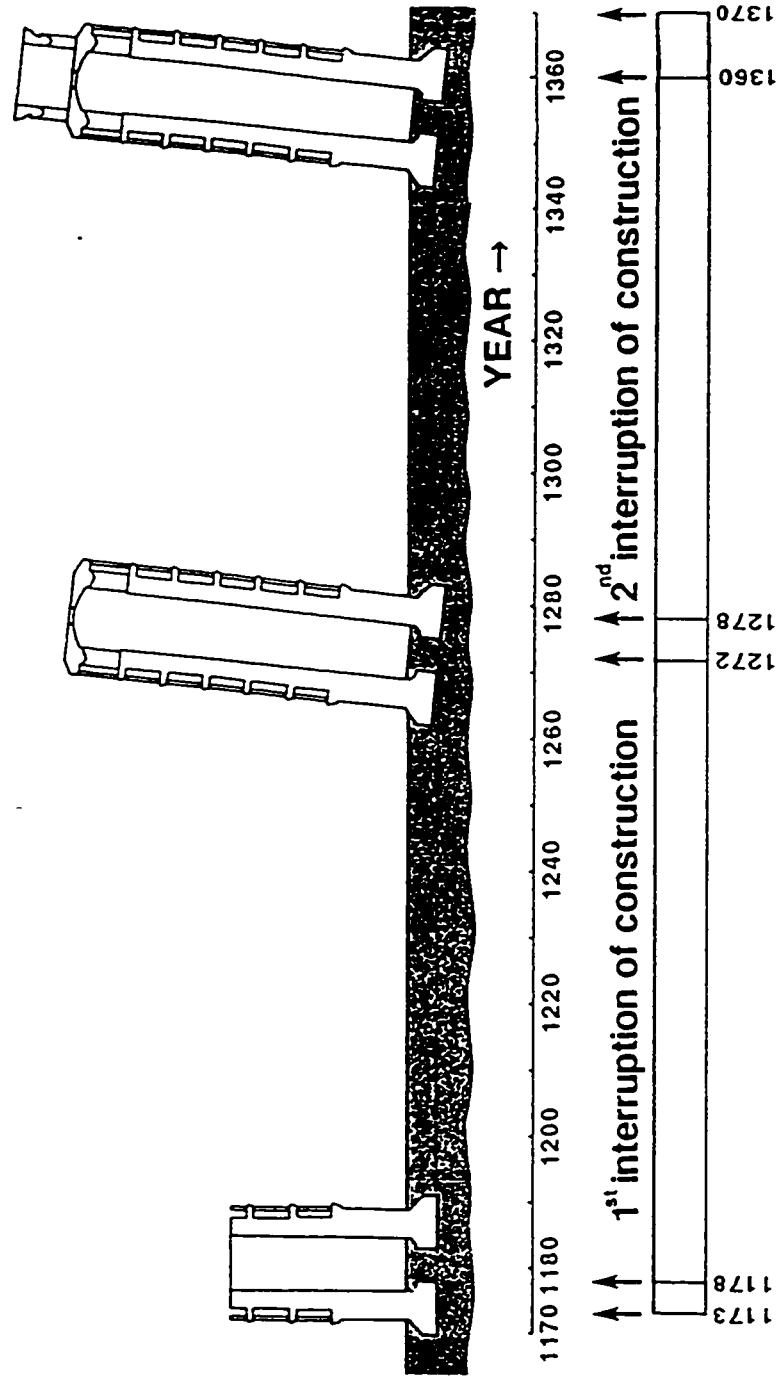


Fig. 2.14 Construction history (after Jamiołkowski et al., 1993)

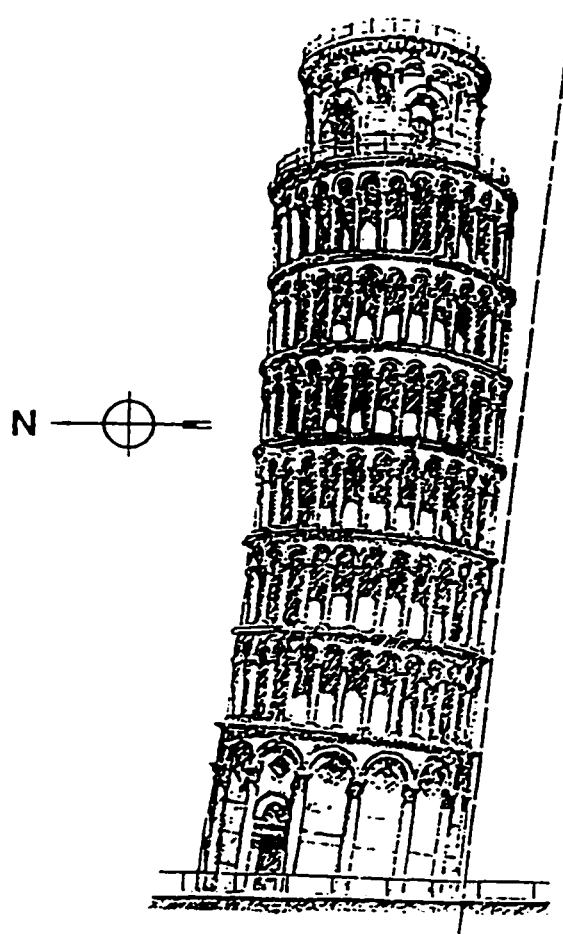


Fig. 2.15 Correction during construction
(after Jamiolkowski et al. 1993)

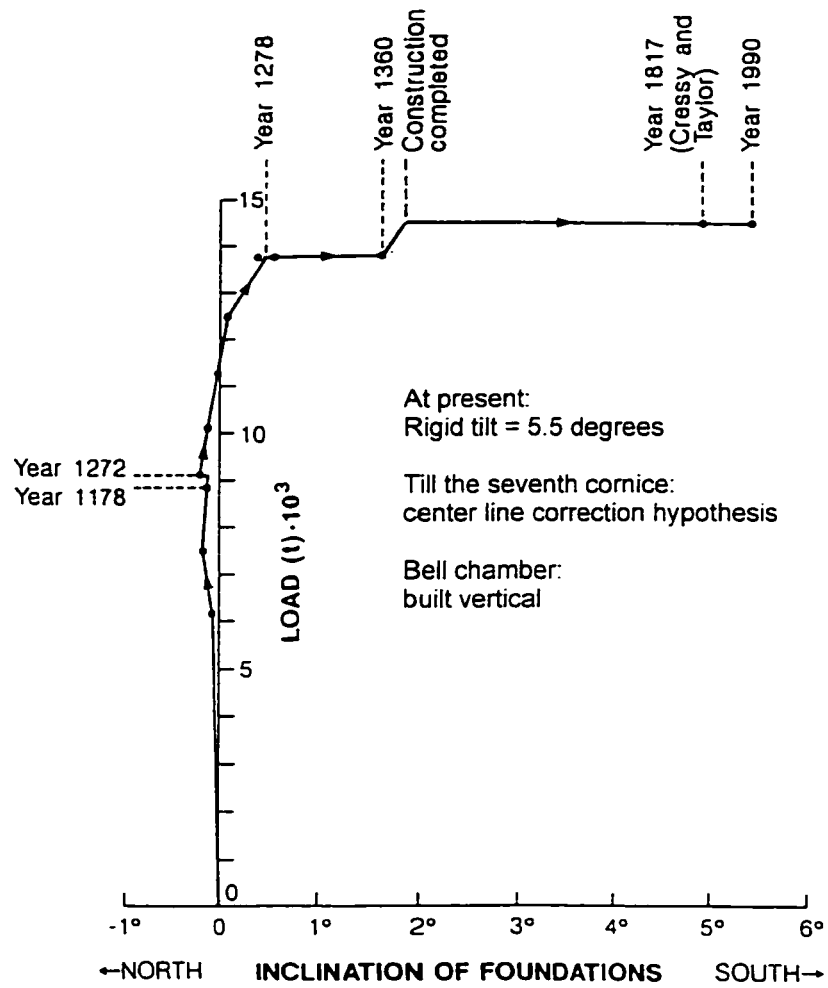


Fig. 2.16 History of rigid tilt (after Burland, 1991)

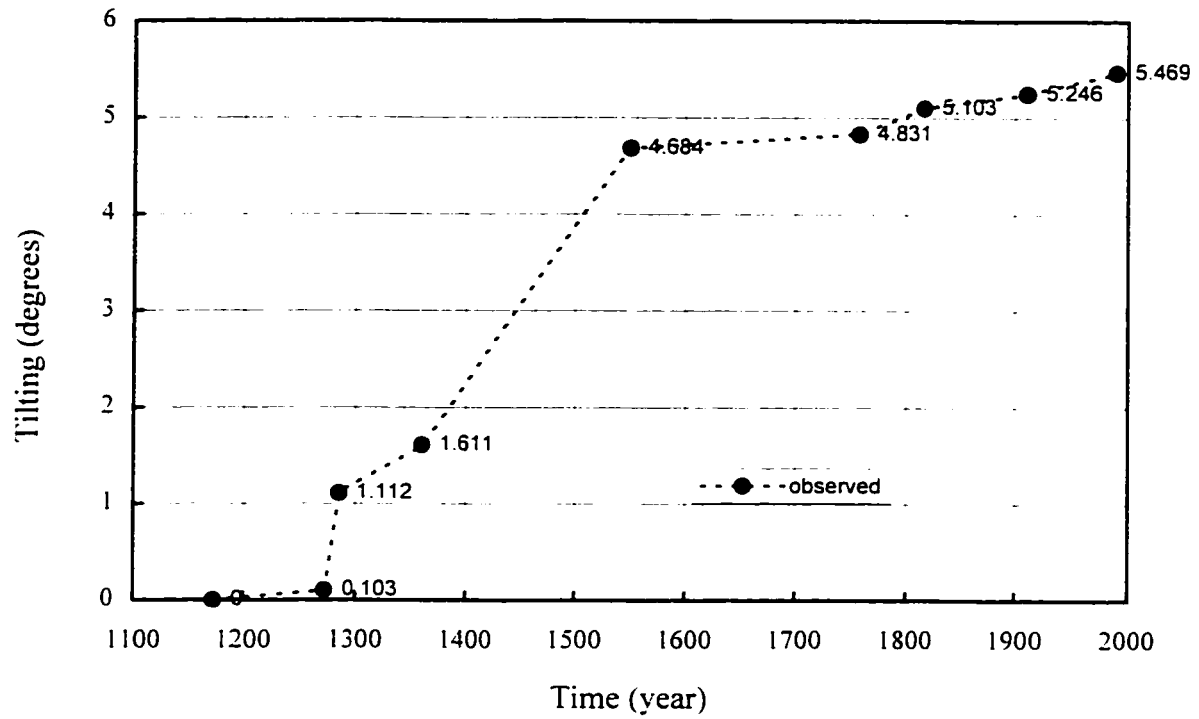


Fig. 2.17 Tilting history of Pisa Tower

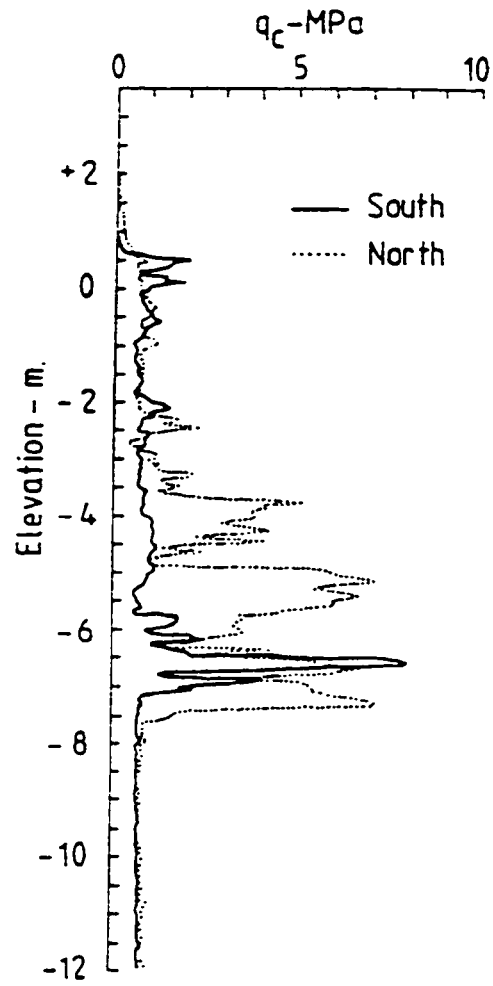


Fig. 2.18 Comparison of cone resistance profiles to the north and south of the tower (Burland and Potts, 1994)

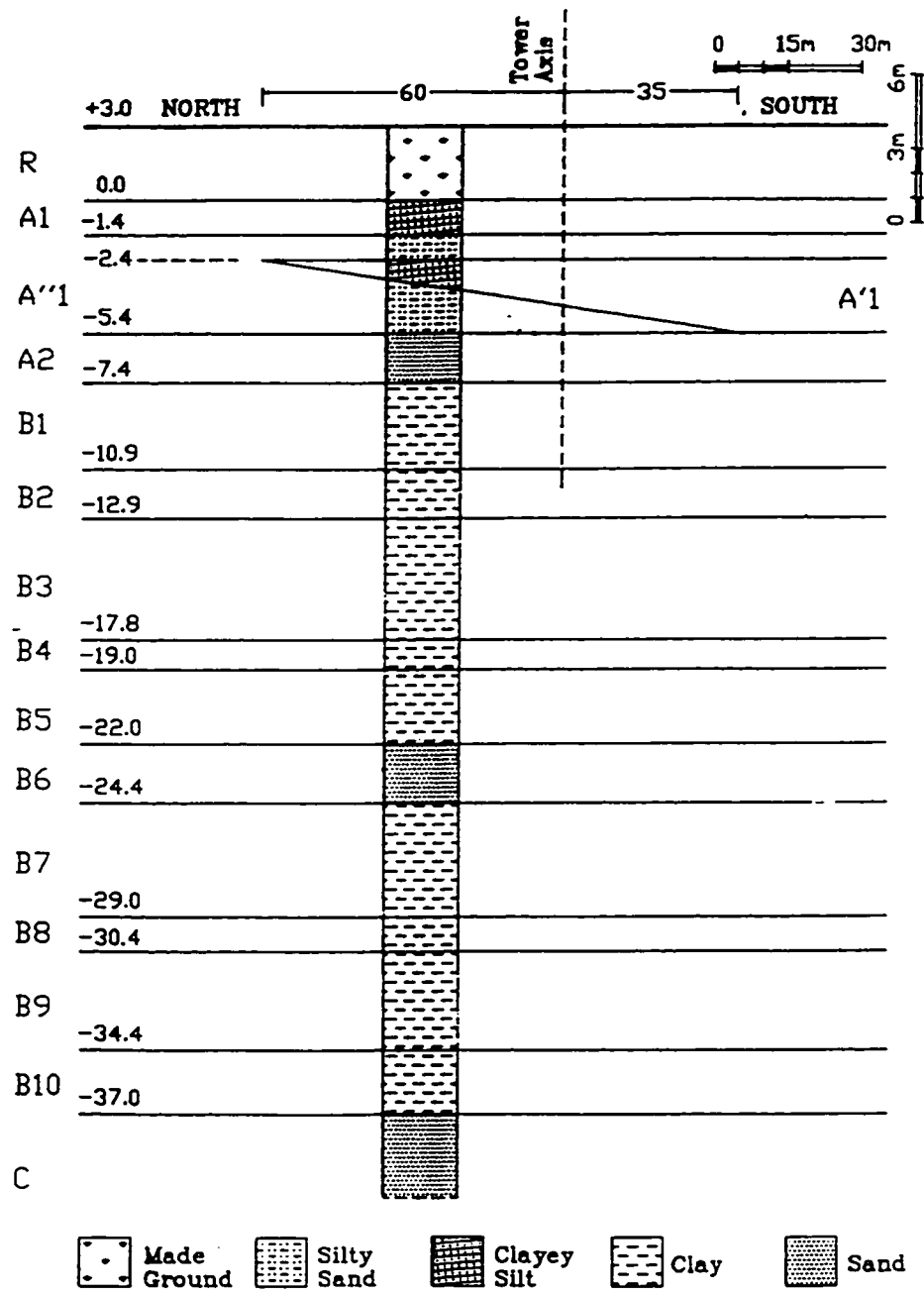


Fig. 2.19 Probable initial soil profile at the site of Pisa Tower (Calabresi et al., 1992)

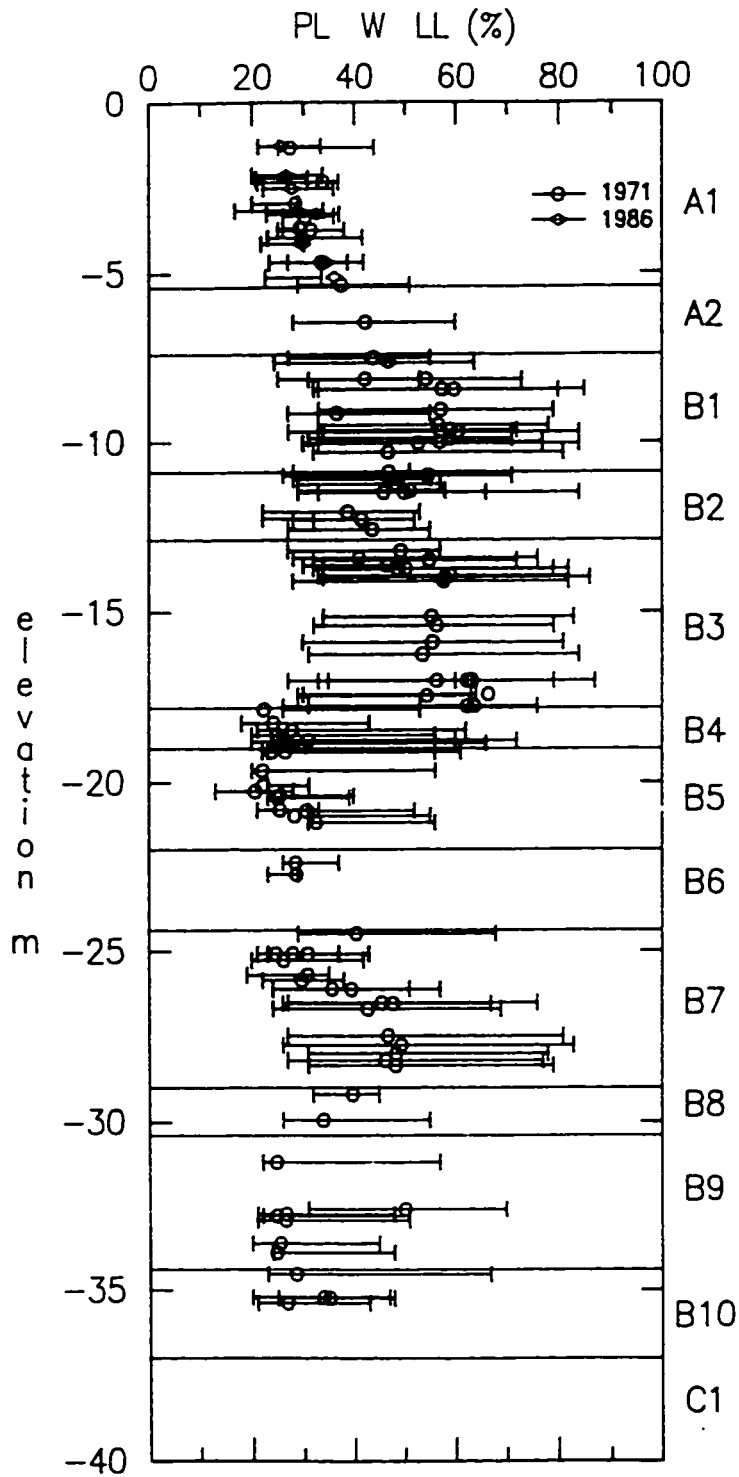


Fig. 2.20 Atterberg limits of Pisa soil (after Calabresi et al., 1992)

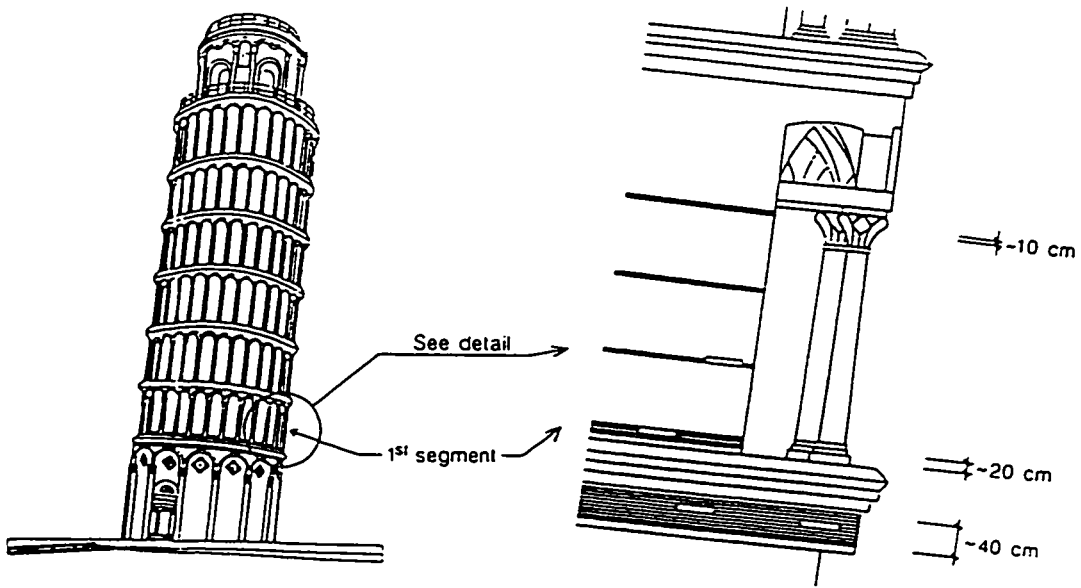


Fig. 2.21 Temporary structural strengthening (light circumferential prestressing)

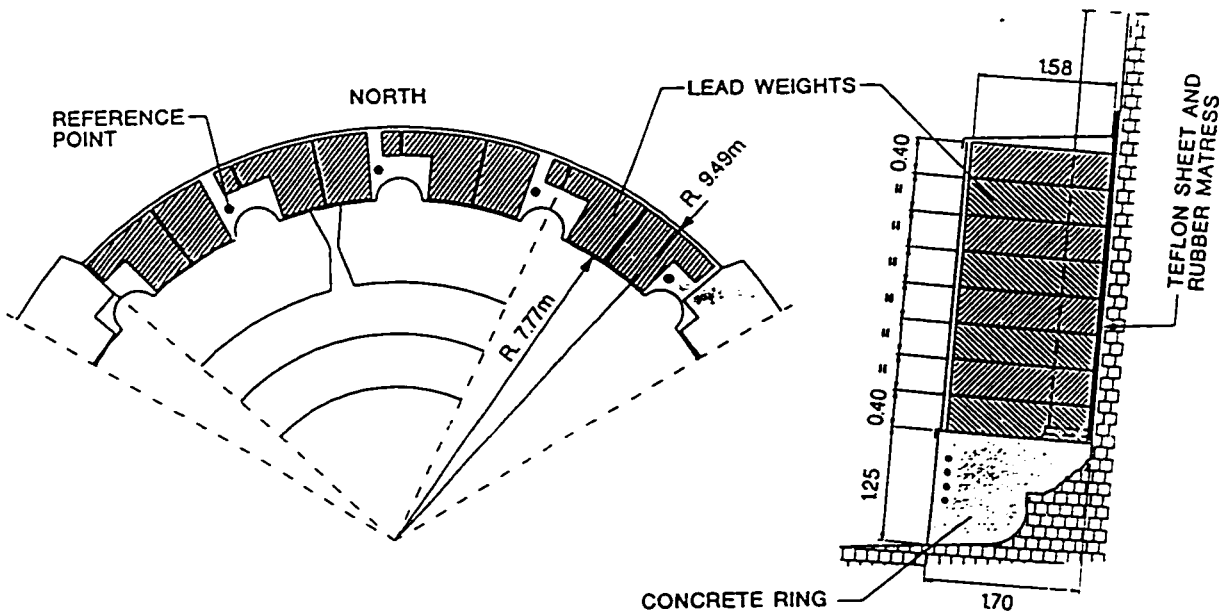


Fig. 2.22 Counterweight on North edge of foundation position of lead weights

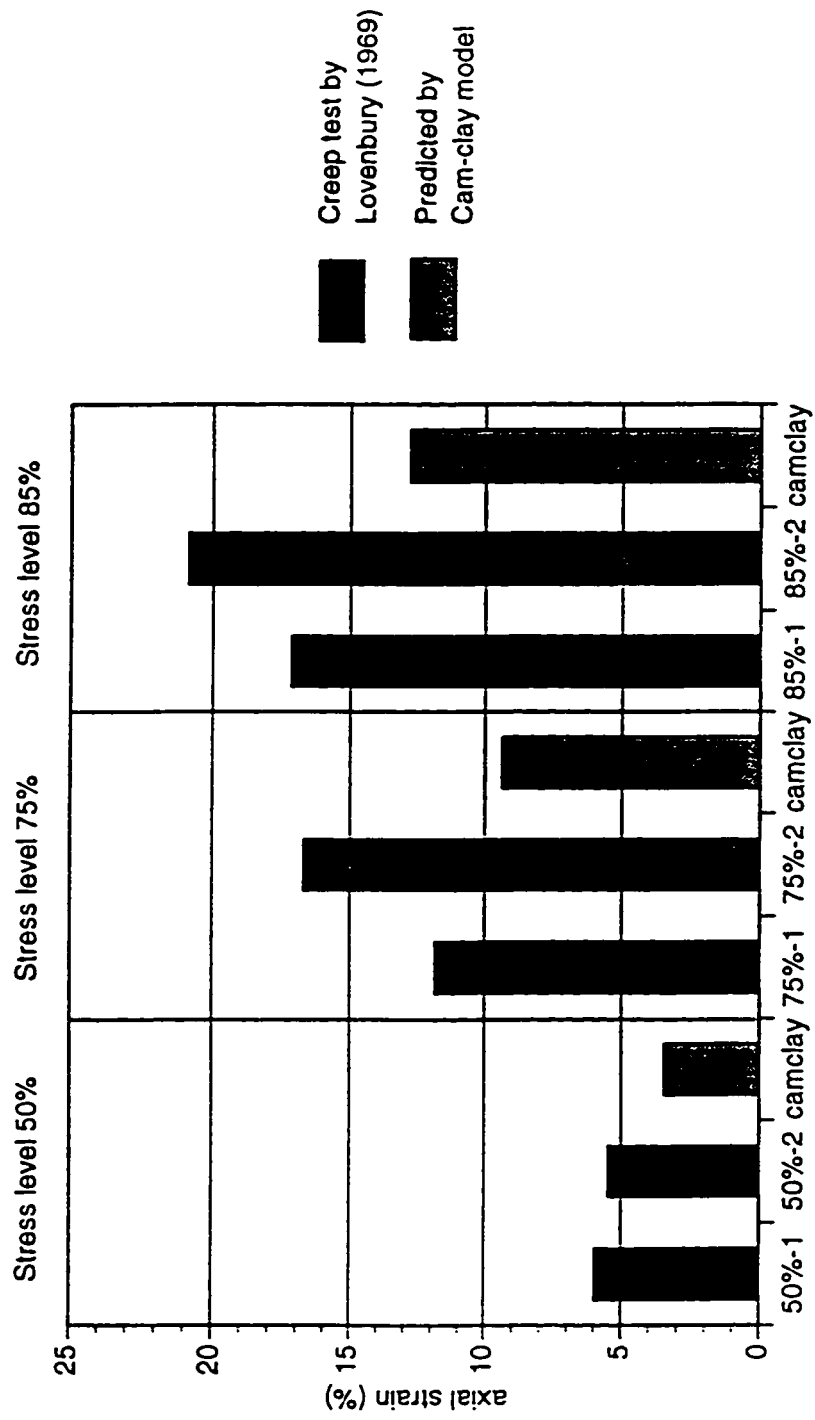
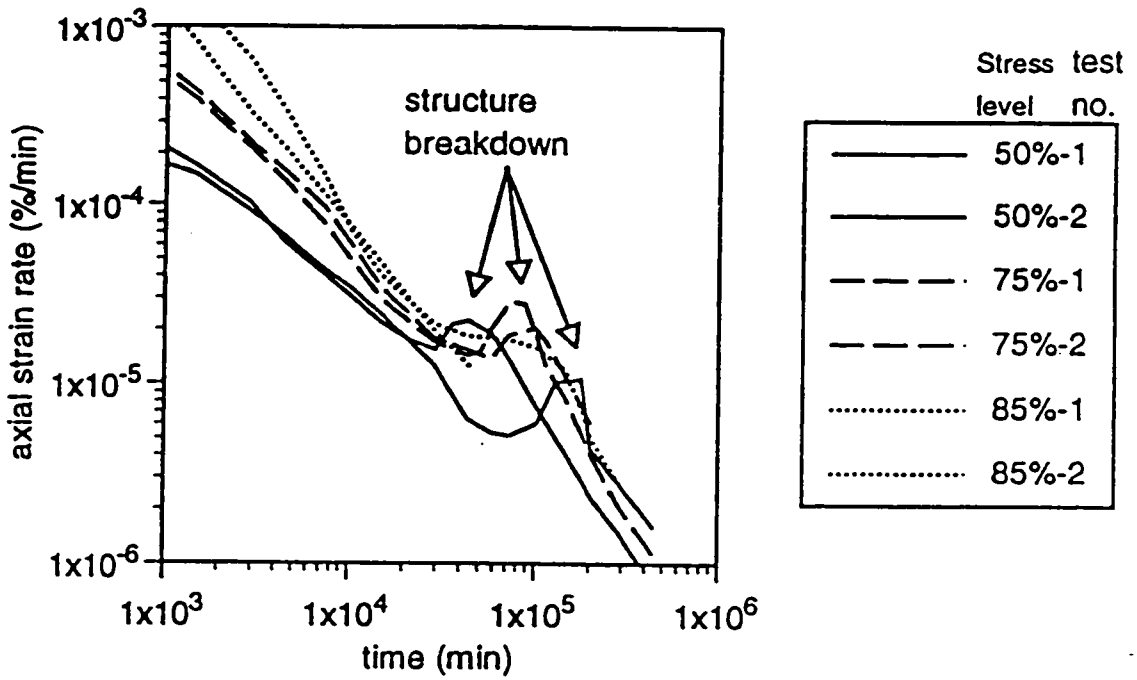


Fig. 2.23 Comparison between measured and predicted strain (after Mitchell and Soga, 1995)



(b) magnified
1,000 to 1,000,000 minutes

Fig. 2.24 Axial strain rate versus time for the creep test by Bishop and Lovenburry (1969) (after Mitchell and Soga, 1995)

Pisa creep test results
Axial strain
Maximum stress case

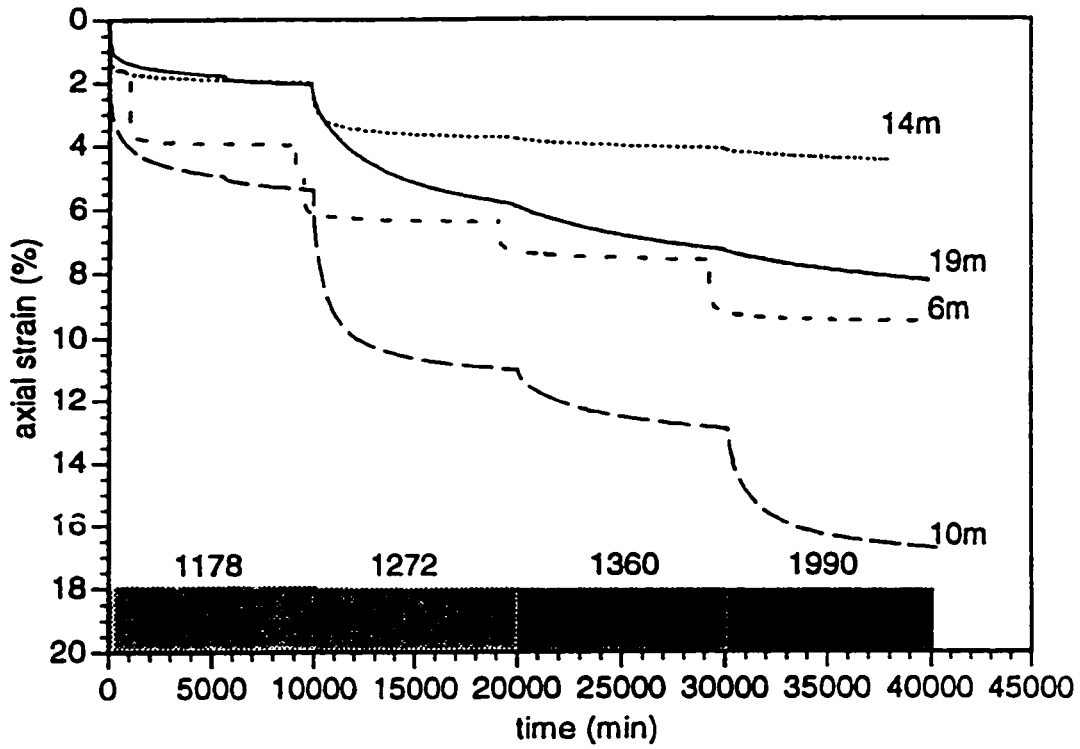


Fig. 2.25 Axial strain vs. log time relationship of maximum stress cases (after Mitchell and Soga, 1995)

CHAPTER 3

NUMERICAL SIMULATION OF DRAINED CREEP

TESTS ON PISA CLAY

3.1 Introduction

In order to study the time-dependent behavior of Pisa clay, a series of triaxial drained creep tests were conducted by Bishop and Lovenbury (1969) and Mitchell and Soga (1995). In this chapter, numerical simulations of the laboratory tests were carried out using a double-yield surface model, which includes the modified Cam-clay ellipsoid with the Von-Mises cylinder inscribed in it. This model was first developed by Hsieh (1987) and was cast in a manner to satisfy a unified phenomenological model for the stress-strain-time behavior of soft clays developed by Kavazanjian and Mitchell (1980). The model parameters are all readily obtainable from standard laboratory tests or from correlation with index properties of the soil, which are familiar to most geotechnical engineers. Borja and Kavazanjian (1985) showed that this constitutive model along with volumetric scaling can predict accurately the stress-strain-time behavior of Weald Clay under drained triaxial compression condition and undisturbed San Francisco Bay mud under both drained triaxial and undrained plane strain conditions. Morsy et al. (1995) used this model with volumetric and deviatoric coupled scaling to model accurately the stress-strain-time behavior of Tar Island Clay under drained triaxial conditions. Brandes et al. (1996) used this model with deviatoric scaling to simulate an undisturbed deep sea clay from the North Central Pacific tested under both drained triaxial creep and one-dimensional creep conditions. Good agreement was observed between test results and axial strain predictions. In this study, the constitutive model was modified first by changing the intrinsic time variables. Then the modified model was used to simulate the triaxial drained creep tests conducted by Bishop and Lovenbury (1969) and Mitchell and

Soga (1995). The capability of this modified model in assessing the stress-strain-time behavior of Pisa clay beneath the tower's foundation was illustrated.

3.2 Geotechnical properties of Pisa Soils

The initial soil profile underneath the tower's foundation contains three main formations, as shown in Figure 3.1.

Formation A is 10m thick, and contains rather variable clayey silt and silty sand. It can be subdivided into three layers: (1) MG, top soil and made ground, about 3.0m thick; (2) layer A_1 , loose to very loose yellow sandy silt to clayey silt without stratification. It is formed by a first layer of clayey silts A_1' , 1.4m thick, overlying the silty sands A_1'' , 4.0m thick. The second clayey silt layer A_1' is included in the silty sands layer A_1'' , its thickness increasing linearly from 0.0m at 60m north of the tower axis, to 3.0m at 35m south of the tower axis; and (3) layer A_2 , uniform gray sand with inter-bedded clay layers and broken fossils, 2.0m thick.

Formation B is about 30m thick, and contains predominantly clay. It can be subdivided into four layers: (1) upper clay or Pancone clay (B_1 to B_3), about 11m thick, high plasticity, normal consolidated or slightly overconsolidated clay; (2) intermediate clay (B_4 and B_5), dark gray to yellow, low plasticity clayey silts, overconsolidated with OCR of 1.8; (3) intermediate sand (B_6), about 2.5m thick, gray, sometimes yellow; and (4) lower clay (B_7 to B_{10}), about 13m thick, clays and silts, blue gray to gray with yellow zones, medium plasticity, normal consolidated clay.

Formation C is slightly silty sand, and is encountered at a depth of 40m. It extends to a depth greater than the deepest boring.

3.3 Modification of a time-dependent constitutive model

3.3.1 Original constitutive model

The constitutive model presented herein is called the double-yield surface Cam-clay plasticity (DYSCP) model. It implements the concept of double-yield criteria

represented by the ellipsoid of the modified Cam-clay model and the Von-Mises cylinder inscribed in this ellipsoid. in order to account for the plastic shear distortion that occurs without volume change below the state boundary surface (Roscoe and Burland 1968. Hsieh 1987). A detailed derivation of this model can be found in Hsieh et al. (1990) and Morsy et al. (1995). Here only the main features and equations are presented.

Central to the formulation is the assumption that the total-strain-rate tensor can be decomposed into an immediate part ($\dot{\underline{\underline{\epsilon}}}$, $\dot{\underline{\underline{\epsilon}}}_F^p$, and $\dot{\underline{\underline{\epsilon}}}_G^p$) and a delayed part ($\dot{\underline{\underline{\epsilon}}}$) based on Bjerrum's (1967) concept.

$$[3.1] \quad \dot{\underline{\underline{\epsilon}}} = \dot{\underline{\underline{\epsilon}}}^e + \dot{\underline{\underline{\epsilon}}}_F^p + \dot{\underline{\underline{\epsilon}}}_G^p + \dot{\underline{\underline{\epsilon}}}^t$$

where superscripts e and p denote the time-independent elastic and plastic components, respectively; superscript t denotes the time-dependent (creep) component; and subscripts F and G denote the MCCM ellipsoid and the Von-Mises cylinder, respectively. The projection of the yield surfaces F and G on the p-q plane is shown in Figure 3.2.

$$[3.2] \quad F = F(\sigma_{ij}, p_c) = \frac{q^2}{M^2} + p'(p' - p_c) = 0$$

$$[3.3] \quad G = G(\sigma_{ij}, q_c) = q - q_c = 0$$

where F denotes the first yield surface given by MCCM ellipsoid; G denotes the second yield surface given by the Von-Mises cylinder; σ_{ij} denotes the effective stress components; p_c denotes the isotropic preconsolidation pressure which defines the size of the ellipsoid; p' denotes the mean stress, $p' = (\sigma_1 + \sigma_2 + \sigma_3) / 3$; $\sigma_1, \sigma_2, \sigma_3$ denote effective principal stress components; q denotes the shear stress in terms of the stress invariant, $q = \frac{1}{\sqrt{2}} \sqrt{(\sigma_1 - \sigma_2)^2 + (\sigma_2 - \sigma_3)^2 + (\sigma_3 - \sigma_1)^2}$; q_c denotes the shear yield stress based on the Von-Mises yield criterion. It defines the size of the cylinder. In Figure 3.2, $\eta = q_c / p'$; and M denotes the slope of the critical state line in the p-q plane.

This double-yield surface theory is used to evaluate both the time-independent and time-dependent strain components (Hsieh 1987). Since both the yielding surfaces F and G are isotropic, the resulting model is also isotropic and is not expected to provide a good prediction of anisotropically consolidated soils or those stress paths that involve rotation of the principal-stress direction.

The elastic part of the time-independent components $\underline{\dot{\epsilon}}^e$ is evaluated by applying generalized Hooke's law and by assuming that the trace of the MCCM surface on the q - γ plane is a hyperbola of the form (see Figure 3.3):

$$[3.4] \quad q = \frac{\gamma p_c}{a + b\gamma} R_f$$

where γ denotes the shear strain. $\gamma = \frac{\sqrt{2}}{3} \sqrt{(\epsilon_1 - \epsilon_2)^2 + (\epsilon_2 - \epsilon_3)^2 + (\epsilon_3 - \epsilon_1)^2}$; a and b denotes the hyperbolic stress-strain parameters; and R_f denotes the failure ratio.

$$R_f = \frac{(\sigma_1 - \sigma_3)_{\text{failure}}}{(\sigma_1 - \sigma_3)_{\text{ultimate}}}$$

The immediate plastic deformation $\underline{\dot{\epsilon}}_F^p$ and $\underline{\dot{\epsilon}}_G^p$ can be evaluated based on the current stress state with respect to the double-yield surfaces F and G (Hsieh et al. 1990). The time-dependent strain rate tensor $\underline{\dot{\epsilon}}^t$ can be divided into distinct but interdependent volumetric and deviatoric parts (Kavazanjian and Mitchell 1980):

$$[3.5] \quad \underline{\dot{\epsilon}}^t = \underline{\dot{\epsilon}}_v^t + \underline{\dot{\epsilon}}_d^t$$

Taylor's (1948) secondary creep law and Singh and Mitchell's (1968) creep equation can be used to evaluate these components:

$$[3.6] \quad \dot{\epsilon}_v^t = \frac{\psi}{(1+e)t_v}$$

$$[3.7] \quad \dot{\epsilon}'_d = Ae^{\bar{\alpha}\bar{D}} \left[\frac{(t_d)_i}{t_d} \right]^m$$

where ψ denotes the secondary compression coefficient, in natural logarithm scale; e denotes the void ratio; t_v denotes the volumetric age, relative to the initial reference time $(t_v)_i$ (usually set to unity). It is a measure of void ratio reduction due to creep as shown in Figure 3.4; $\bar{\alpha}$, and m denote Singh and Mitchell creep parameters, as shown in Figure 3.5; $(t_d)_i$ denotes the instant deviatoric time, usually set to unity; t_d denotes the deviatoric age relative to $(t_d)_i$. It is a measure of the shear strain due to overconsolidation as shown in Figure 3.3; and \bar{D} denotes the deviatoric stress level, $\bar{D} = \frac{(\sigma_1 - \sigma_3)}{(\sigma_1 - \sigma_3)_{ultimate}}$.

The total creep strain rate tensor is evaluated by employing an associated flow rule for both the equivalent volumetric and deviatoric yield surfaces F and G and by forcing it to satisfy the secondary creep law for volumetric creep and the Singh and Mitchell law for deviatoric creep simultaneously, i.e., volumetric and deviatoric coupled scaling process. The resulting creep strain is perpendicular neither to F nor to G and, therefore, the flow rule for creep strains is always non-associative.

$$[3.8] \quad \dot{\underline{\epsilon}}' = \frac{\psi}{3(1+e)t_v} \underline{I} + \sqrt{\frac{3}{2}} Ae^{\bar{\alpha}\bar{D}} \left[\frac{(t_d)_i}{t_d} \right]^m \hat{\underline{n}}$$

where \underline{I} denotes the second-order identity tensor; $\hat{\underline{n}} = \frac{\underline{\sigma}}{\|\underline{\sigma}\|}$; and $\|\underline{\sigma}\|$ denotes the

Euclidean norm.

This constitutive model has thirteen parameters to define the material property. Seven of them are used for defining material in the absence of creep: the remaining six are used for the presence of creep. The values of these parameters can be obtained from isotropic triaxial tests, consolidation tests, triaxial creep tests, and correlation with index properties of soil.

3.3.2 Modification of the intrinsic time variables

The above constitutive model needs two intrinsic time variables, the volumetric age and the deviatoric age, to determine the rate of growth of p'_c , q_c and the attendant evaluation of the creep strain rate. The two intrinsic time variables can be represented in the following equations (Borja and Kavazanjian 1985, Hsieh et al. 1990, and Morsy et al. 1994):

$$[3.9] \quad t_v = (t_v)_i \exp\left(\frac{e_2 - e_1}{\psi}\right)$$

$$[3.10a] \quad t_d = \left[\frac{(\gamma_1 - \gamma_2)(1 - m)}{A \exp(\bar{\alpha}D)(t_d)_i^m} \right]^{1/(1-m)} \quad \text{for } m \neq 1$$

$$[3.10b] \quad t_d = (t_d)_i \exp\left(\frac{\gamma_1 - \gamma_2}{A \exp(\bar{\alpha}D)}\right) \quad \text{for } m = 1$$

The definitions of e_1 , e_2 , γ_1 , and γ_2 are shown in Figures 3.3 and 3.4.

Comprehensive computations carried out in this study demonstrated that Equation [3.10] cannot respond correctly to variable values of the Singh and Mitchell parameter m . In order to identify the problem, the following derivation is developed:

3.3.2.1 Volumetric age

From the definition of volumetric strain,

$$[3.11] \quad \dot{\varepsilon}_v = \frac{\dot{e}^p}{(1 + e)}$$

Comparing this relationship with Taylor's secondary compression, Equation [3.6] yields

$$[3.12] \quad \dot{e}^p = -\frac{\psi}{t}$$

The negative sign is added here because as time progresses, the void ratio tends to decrease.

Integration of Equation [3.12] yields

$$[3.13] \quad e^p = -\psi \ln t + c$$

where c is the integration constant.

Let void ratio e_2 correspond to the reference volumetric time $(t_v)_i$ associated with the virgin consolidation curve (see Figure 3.4). If $t = (t_v)_i$, $e^p = e_2$, then

$$[3.14] \quad c = e_2 + \psi \ln(t_v)_i$$

Substituting this back into Equation [3.13] yields

$$[3.15] \quad e^p = -\psi \ln \frac{t}{(t_v)_i} + e_2$$

Let the void ratio e_1 correspond to the current state with time t_v . If $t = t_v$, $e^p = e_1$, then

$$[3.16] \quad t_v = (t_v)_i \exp\left(\frac{e_2 - e_1}{\psi}\right)$$

Equation [3.16] is identical with Equation [3.9].

3.3.2.2 Deviatoric age

Integration of the Singh and Mitchell Equation [3.7] yields two different mathematical forms:

$$[3.17a] \quad \varepsilon_a = A \exp(\bar{\alpha} \bar{D})(t_d)_i^m \left(\frac{1}{1-m}\right) t^{1-m} + c_1 \quad \text{for } m \neq 1$$

$$[3.17b] \quad \varepsilon_a = A \exp(\bar{\alpha} \bar{D})(t_d)_i \ln t + c_2 \quad \text{for } m = 1$$

In the three-dimensional case, the above equation becomes:

$$[3.18a] \quad \gamma = A \exp(\bar{\alpha D})(t_d)_i^m \left(\frac{1}{1-m}\right) t^{1-m} + c_1 \quad \text{for } m \neq 1$$

$$[3.18b] \quad \gamma = A \exp(\bar{\alpha D})(t_d)_i \ln t + c_2 \quad \text{for } m = 1$$

where γ is the shear strain. c_1 and c_2 are integration constants.

Let shear strain γ_1 correspond to the current state with time t_d . Let strain γ_2 correspond to an instant time $(t_d)_i$ with a hyperbolic relationship on the q - γ plane (see Figure 3.3).

$$[3.19] \quad \gamma_2 = \frac{qa}{p'_c R_f - qb}$$

For the $m \neq 1$ case, if $t = (t_d)_i$, $\gamma = \gamma_2$, integration constant c_1 can be obtained from Equation [3.18a] as follows:

$$[3.20] \quad c_1 = \gamma_2 - \frac{A}{1-m} \exp(\bar{\alpha D})(t_d)_i$$

Substituting c_1 back into Equation [3.18a], and setting $t = t_d$ and $\gamma = \gamma_1$, the deviatoric age t_d can be obtained as.

$$[3.21] \quad t_d = \left[\frac{(\gamma_1 - \gamma_2)(1-m)}{A \exp(\bar{\alpha D})(t_d)_i^m} + (t_d)_i^{1-m} \right]^{1/(1-m)} \quad \text{for } m \neq 1$$

For the $m = 1$ case, if $t = (t_d)_i$, $\gamma = \gamma_2$, integration constant c_2 can be obtained from Equation [3.18b] as:

$$[3.22] \quad c_2 = \gamma_2 - A \exp(\bar{\alpha D})(t_d)_i \ln(t_d)_i$$

Substituting c_2 back into Equation [3.18b] and let $t = t_d$ and $\gamma = \gamma_1$ yields:

$$[3.23] \quad t_d = (t_d)_i \exp\left(\frac{(\gamma_1 - \gamma_2)}{A \exp(\bar{\alpha} D)(t_d)_i}\right) \quad \text{for } m = 1$$

Comparing Equations [3.21] and [3.23] with [3.10], one can see that Equation [3.10a] misses the term $(t_d)_i^{1-m}$ in the bracket, which is a function of the parameter m . Equation [3.10b] misses the term $(t_d)_i$ in the denominator part of the exponential. Only when $(t_d)_i = 1$, Equation [3.23] takes the same form as Equation [3.10b]. Equations [3.21] and [3.23] are the correct forms for the intrinsic time variables. This will be further verified through a series of creep tests as presented in the following sections.

3.4 Verification of the modified model using Bishop's drained creep tests

In order to verify the modified constitutive model, the triaxial drained creep tests of Pisa clay conducted by Bishop and Lovenbury (1969) are simulated through the finite element program named PISA-FORTRAN developed by Chan and Morgenstern (1992) and Morsy (1994). The four eight-node element mesh used in this study is shown in Figure 3.6.

Bishop and Lovenbury (1969) investigated creep behavior of Pisa clay at a depth of approximately 19 meters from the ground surface, which belongs to the highly structured layer B3 as shown in Figure 3.1. Six drained creep tests under constant loads of 50, 75, and 85% of the drained strength of the clay were conducted, two for each stress level. The applied confining pressure was 152 kPa. The primary consolidation ended in less than two days after final loading. The approximate size of the samples was 7.62 cm in diameter and 15.24 cm in height. Test results showed that all the samples exhibited sudden increases in strains for a length of time at some stage during the test as shown in Figure 3.7. Bishop and Lovenbury (1969) concluded that this phenomenon reflected the structural breakdown of Pisa clay carbonates. After the structural breakdown, the axial strain rates were in the range of 1 to 1.5% per logarithmic time cycle, which was consistent with Mitchell and Soga's (1995) triaxial drained creep tests.

3.4.1 Model parameters

Table 3.1 presents the values of thirteen material parameters required in the DYSCP model. Parameters C_c , C_r , ϕ , and e_a are determined based on Calabresi's (1992) and Tamagnini's (1993) study; Singh and Mitchell parameters A , $\bar{\alpha}$, and m are obtained from the strain rate controlled undrained triaxial tests conducted by Mitchell and Soga (1995); and parameter C_α is determined from Mitchell and Soga's (1995) drained creep tests. The hyperbolic parameters a and b are calculated from the following formulas:

$$[3.24] \quad a = \frac{p_c' \cdot R_f}{3G}$$

$$[3.25] \quad b = R_f \cdot \frac{2^{(1-\frac{C_r}{C_c})}}{M}$$

where p_c' is the preconsolidation pressure; G is the shear modulus; M is the Cam-clay parameter. $M = \frac{6 \sin \phi}{3 - \sin \phi}$; and R_f is the failure ratio. R_f is in the range of 0.7 to 1.0.

Here it is assumed to be 0.80.

Since Bishop's samples have lower water content, lower liquid and plastic limits (as show in Table 3.2), the value of C_c is modified from 0.615 to 0.515 and the value of m from 0.75 to 0.95 to best match the laboratory data.

3.4.2 Simulation results by varying Singh and Mitchell parameter m

The intrinsic time variable relationships expressed in both Equation [3.10] and Equations [3.21] and [3.23] are incorporated into the finite element program separately. Bishop and Lovenbury's (1969) drained creep tests under a constant load of 75% of the drained strength are selected as an example to investigate the impact of these two different intrinsic time relationships. Eight scenarios are conducted under different values of the Singh and Mitchell parameter m (0.75, 0.80, 0.85, 0.90, 0.95, 0.99, 1.0, and 1.2). The calculated axial strain versus time are plotted in Figures 3.8 and 3.9, with Figure 3.8

based on Equation [3.10] and Figure 3.9 based on Equations [3.21] and [3.23], respectively.

Theoretically, a low value of m should result in a high value of axial strain because the strain rate decreases at a smaller rate as the m value decreases, as expressed by the Singh and Mitchell relationship (see Equation [3.7] or Figure 3.5). As m approaches 1.0, Equations [3.10a] and [3.10b] should result in identical curves. Figure 3.9 does follow all these rules. However, Figure 3.8 shows that high values of m return to high axial strains for m value less than 1.0 cases. When m equals 1.0, axial strain drops dramatically. Moreover, when m takes the values of 0.99 and 1.0, a big difference in the axial strain results. All those phenomena imply that the modified model provides a better representation for the intrinsic time variables than Equation [3.10].

3.4.3 Numerical simulation of Bishop's drained creep tests

Using the same material parameters as listed in Table 3.1, Bishop's drained creep tests were simulated under different constant loads: 50%, 75%, and 85% of the drained strength of the clay. The results, together with measured data, are plotted in Figures 3.10 and 3.11.

Figure 3.10 shows an excellent agreement between the numerical and laboratory results for the relationship of axial strain versus time under both 50% and 75% stress levels. Under the 85% stress level, the results slightly under-predict the axial strain before 20 days, but show the same trend after that time. For the volumetric strain versus time relationship (see Figure 3.11), numerical results could not precisely follow the laboratory data. Under the 85% stress level, it over-predicts the volumetric strain before one day of creep, then under-predicts it after that time. Under both the 50% and 75% stress levels, numerical results over-predict the volumetric strain before 200 days, and follow the same trend after that time.

There are two main reasons for these discrepancies. One is that the volumetric strains from laboratory data are unreliable because of the leakage problem, as might be expected from the long duration test. The other is due to the highly structured nature of

the soil itself, as shown in Figure 3.7. Overall, numerical results still could match the trend of laboratory data.

3.5 Verification of the modified model using Mitchell's drained creep tests

Mitchell and Soga (1995) conducted a total of nine triaxial drained creep tests for Pisa clay. The undisturbed samples were obtained from Borehole L2, located Southwest of the Pisa Tower, as shown in Figure 3.12. The samples were taken at four different locations, 6m, 10m, 14m, and 19m depths corresponding to layers A_1 , B_1 , B_2 , and B_3 , respectively, as indicated in Figure 3.1. The size of the cylindrical specimens was approximately 3.4 cm in diameter and 8.9 cm in height. The applied loads were obtained based on the results of a three-dimensional elasto-plastic analysis. They were applied in steps to simulate the construction sequence of the tower. For each step, a constant load was applied instantly which was allowed to last for 7 days. Figures 3.13 and 3.14 show the stress paths of samples named Test-1 (6m sample from layer A_1) and Test-2 (10m sample from layer B_1). During each step, after the instant load was applied, samples experienced stages from undrained deformation at the beginning of the loading, through partially drained consolidation, to fully drained conditions after the dissipation of excess pore pressure. Primary consolidation was considered not to require more than one day. Thus, fully drained conditions were expected to be achieved after one day of constant loading. In order to avoid drying, the specimens were covered by a membrane and put into the triaxial cell which was filled with water during the test. Drainage was allowed at the top and bottom of the specimen (one dimensional flow). Throughout the test, a back pressure of 98 kPa was applied to maintain saturation. Some water leakage was observed during the test. Thus, the volume change data were unreliable.

The measured axial strain with logarithm time relationships of the four samples named Test-1 to Test-4 corresponding to the four different depths are shown in Figure 3.15. It can be seen that the 10m sample (Test-2) exhibits very large axial strain (up to 16%) due to its highly plastic nature and the relatively large tower loads. The 6m sample (Test-1) also exhibits large deformations (up to 9%) due to very large tower load increments. Creep deformation is not significant for the 14m sample (Test-3) due to its

relatively low plasticity characteristics. Creep deformation is important for the 19m sample (Test-4). Since it belongs to highly structural layer B₃, and it was already simulated through Bishop and Lovenbury's (1969) creep tests in the previous section, it will not be simulate again. Thus, here only the 6m and 10m samples are selected to conduct the numerical simulation, due to their significance in the deformation behavior of the soil beneath the tower's foundation and relatively high creep characteristics. The Atterberg limits of these two samples are indicated in Table 3.3.

3.5.1 Model parameters

In order to simulate the drained creep tests named Test-1 and Test-2, a four eight-node element mesh was employed. The model parameters for the 6m and 10m samples are listed in Tables 3.4 and 3.5 respectively. As previously mentioned, the values of parameter C_c , C_r , ϕ , and e_a are determined based on Calabresi's (1992) and Tamagnini's (1993) study. The values of Singh and Mitchell parameters A , $\bar{\alpha}$, and m are obtained from Mitchell and Soga's (1995) strain rate controlled undrained triaxial tests. The value of C_α is determined from Mitchell and Soga's (1995) drained creep tests. The values of a and b are calculated based on the hyperbolic relationship with R_f of 0.89. Due to the difference in the Atterberg limits (see Table 3.3), the compression index C_c of the 6m sample was modified from 0.205 to 0.155 to match the laboratory data. Table 3.6 shows the triaxial loading case converted from using the following equation:

$$[3.26] \quad \sigma_1 = p' + \frac{2}{3}q$$

$$[3.27] \quad \sigma_3 = p' - \frac{1}{3}q$$

3.5.2 Simulation results

The calculated axial strain versus time relationships are plotted in Figures 3.16 and 3.17 for the 6m and 10m samples, respectively. The numerical results match the laboratory data very well for different loading steps, especially at the second and third

loading stages. There are some discrepancies in the 1178 and 1990 loading stages. For the 6m sample, numerical results tend to under-predict the axial strain under the 1178 loading stage, while they over-predict the axial strain under the year 1990 loading stage. For the 10m sample, numerical results tend to over-predict the axial strain under the 1178 loading stage, while they under-predict the axial strain under the 1990 loading stage. Over all, the discrepancies are fairly small compared with the total values. The modified model gives a very good prediction of the stress-strain-time behavior of Pisa clay.

3.6 Conclusions

From the above laboratory test results and the numerical analyses, the following conclusions can be drawn:

1. The modified equations for the intrinsic time variables have been proven theoretically, as well as by simulating some laboratory results, to be able to provide more accurate and reasonable approximation in order to reflect the effect of the Singh and Mitchell parameter m .
2. Creep deformation is important in the soil beneath the tower's foundation. It can cause axial strain to increase up to 16% in the highly plastic layer.
3. The double-yield surface model can accurately predict the stress-strain-time behavior of Pisa clay.

Table 3.1 Model parameters for 19m sample

parameter	symbol	value
virgin compression index	C_c	0.515 (0.615)
recompression index	C_r	0.081
secondary compression coefficient	C_α	0.0154
hyperbolic stress-strain parameters	a, b, R_f	0.0057, 1.348, 0.80
Singh and Mitchell creep parameters	A, $\bar{\alpha}$, m	$2.15 \cdot 10^{-3}$ %/day, 8.82, 0.95(0.75)
internal friction angle	ϕ	26.54
void ratio at $p_c=1$ kPa	e_a	2.73
instant volumetric and deviatoric time	$(t_v)_i$, $(t_d)_i$	1.0 day, 1.0 day

Table 3.2 Atterberg limits of 19m sample

items	Bishop's*	Tamagnini's or Mitchell's**
Water content (%)	49.5	62
liquid limit (%)	76	96
plastic limit (%)	29	41

* from Table 1, Bishop and Lovenbury (1969);

** from Table 5-1 and 5-2, Mitchell and Soga (1995).

Table 3.3 Atterberg limits of drained creep test samples (Mitchell and Soga 1995)

(a). Mitchell's test

Tests sample	depth (m)	layer	water content (%)	liquid limit (%)	plastic index (%)
Test-1 (6m)	6.41-6.61	A ₁	28.7-30.6	39	12.9
Test-2 (10m)	10.69-10.89	B ₁	59.5-66.1	92	48.4

(b). Calabresi's test

Tests sample	depth (m)	layer	water content (%)	liquid limit (%)	plastic index (%)
Test-1 (6m)	6.41-6.61	A ₁	25-33	28-44 (36.0)	3-32 (14.0)
Test-2 (10m)	10.69-10.89	B ₁	40-60	55-87 (74.5)	28-56 (44.0)

Table 3.4 Model parameters for Test-1 (6m sample)

parameter	symbol	value
virgin compression index	C_c	0.155 (0.205)
recompression index	C_r	0.021
secondary compression coefficient	C_α	0.0051
hyperbolic stress-strain parameters	a, b, R_f	0.0046, 1.22, 0.89
Singh and Mitchell creep parameters	A, $\bar{\alpha}$, m	$2.19 \cdot 10^{-2}$ %/min, 5.86, 0.95
internal friction angle	ϕ	33.67
void ratio at $p_c=1$ kPa	e_a	1.29
instant volumetric and deviatoric time	$(t_v)_i, (t_d)_i$	1.0 min, 1.0 min

Table 3.5 Model parameters for Test-2 (10m sample)

parameter	symbol	value
virgin compression index	C_c	0.615
recompression index	C_r	0.081
secondary compression coefficient	C_α	0.0154
hyperbolic stress-strain parameters	a, b, R_f	0.0063, 1.548, 0.89
Singh and Mitchell creep parameters	A, $\bar{\alpha}$, m	$1.62 \cdot 10^{-2}$ %/min, 6.33, 0.83
internal friction angle	ϕ	26.54
void ratio at $p_c=1$ kPa	e_a	2.73
instant volumetric and deviatoric time	$(t_v)_i, (t_d)_i$	1.0 min, 1.0min

Table 3.6 Applied step loads and duration

	initial	1	2	3	4	5	6
year	1173		1178		1272	1360	1990
Test-1 6m sample	(65,12)	(116,81) 1 day (1440 min)	(166.3,149) 6 days (8640 min)	(230,223) 1 day (1440 min)	(293.3,296) 6 days (8640 min)	(365.3,392) 7 days (10080 min)	(469.7,565) 7 days (10080 min)
year	1173	1178	1272	1360	1990		
Test-2 10m sample	(102,9)	(128,78) 7 days (10080 min)	(163.7,106) 7 days (10080 min)	(177.7,121) 7 days (10080 min)	(201.7,148) 7 days (10080 min)		

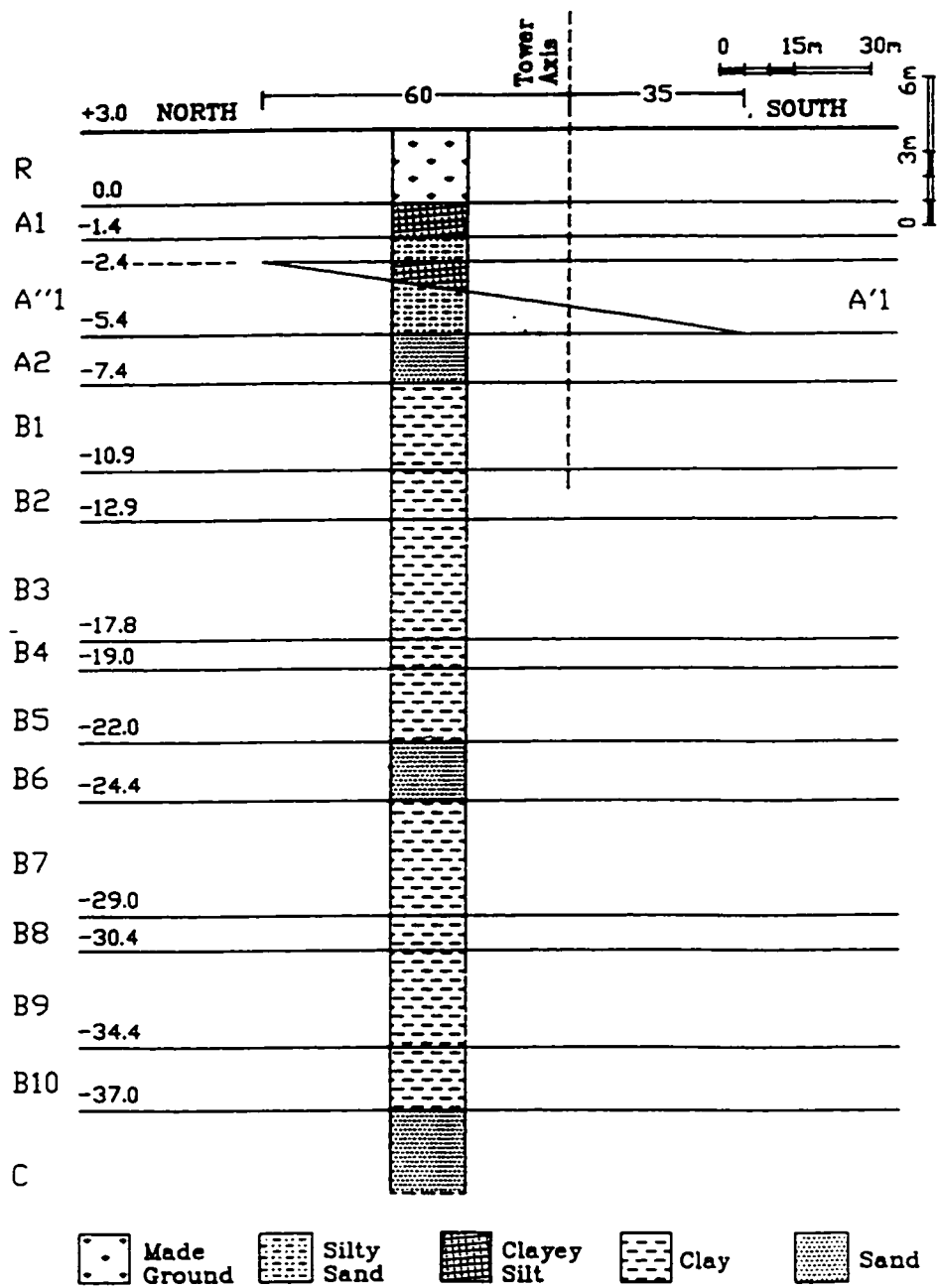


Fig. 3.1 Probable initial soil profile at the site of Pisa Tower (Calabresi et al., 1992)

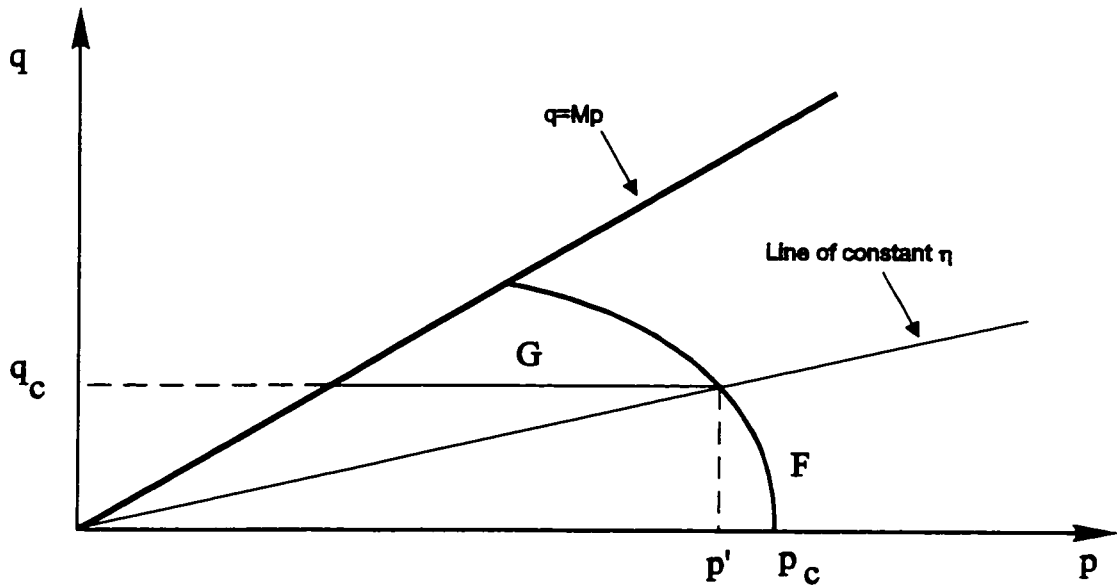


Fig. 3.2 Projection of double yield surface on p-q plane

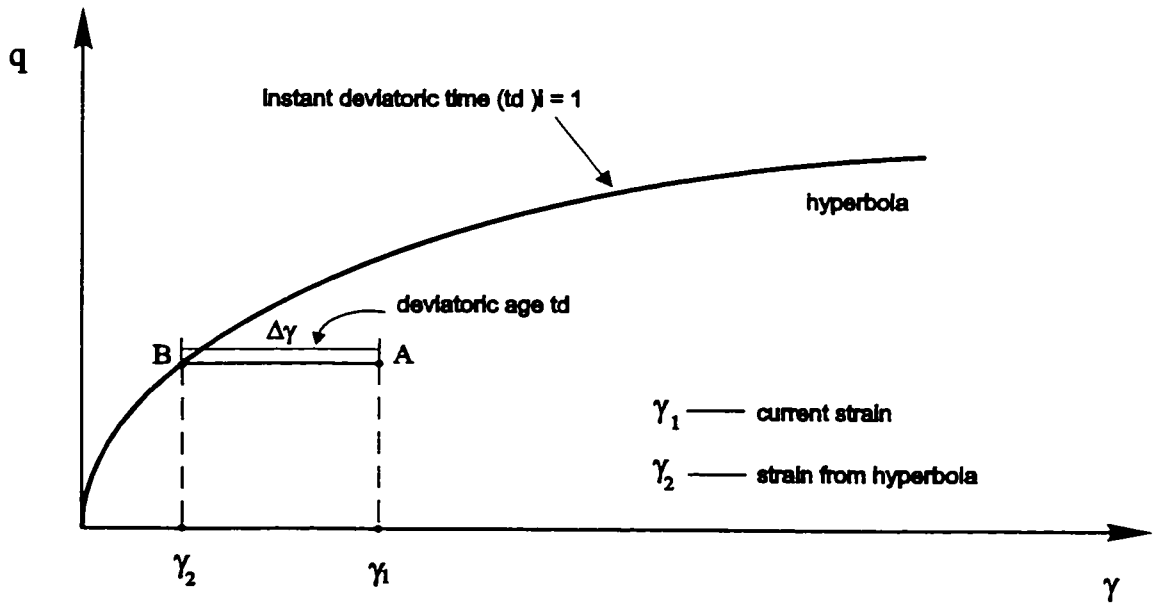


Fig. 3.3 Projection of double yield surface on p- γ plane

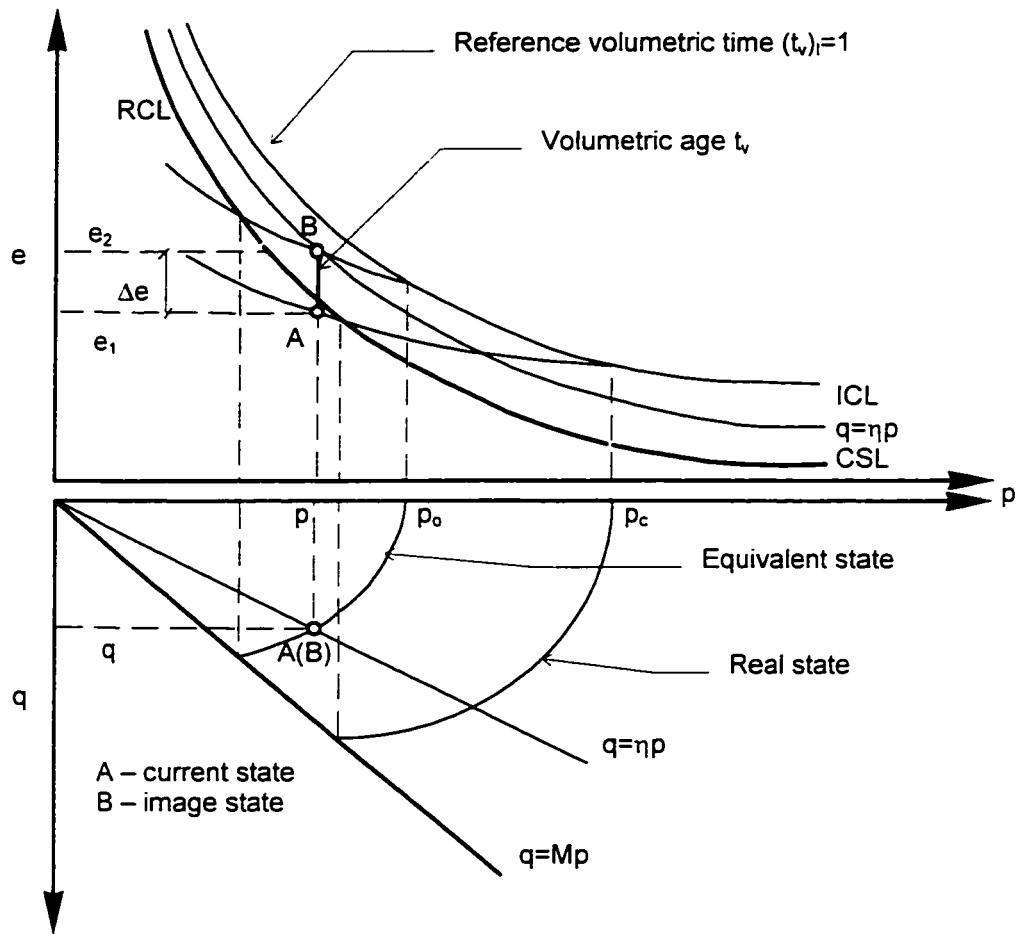


Fig. 3.4 Evaluation of volumetric age (modified after Borja and Kavazanjian 1985)

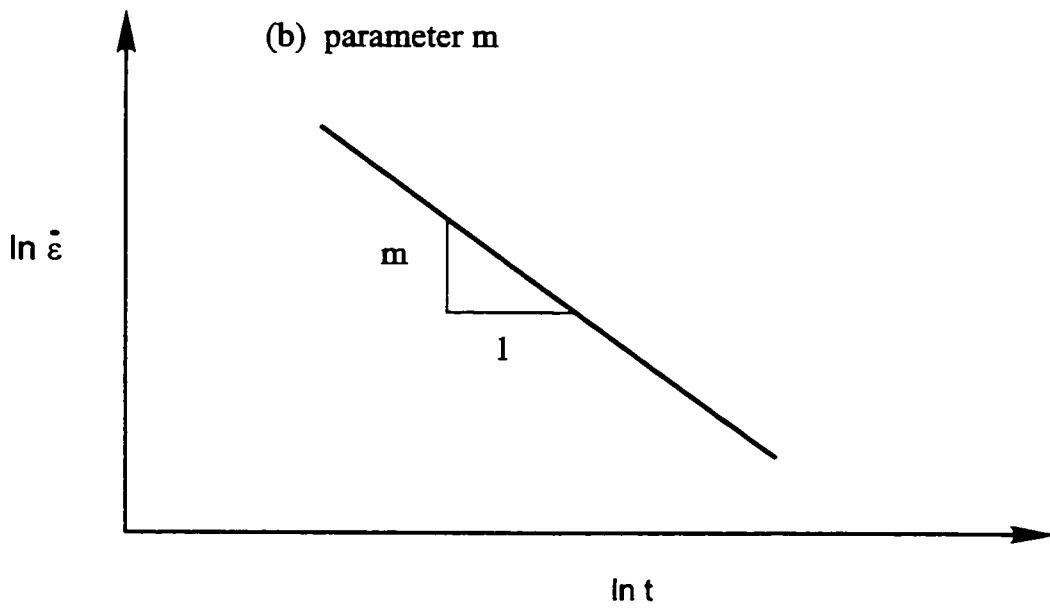
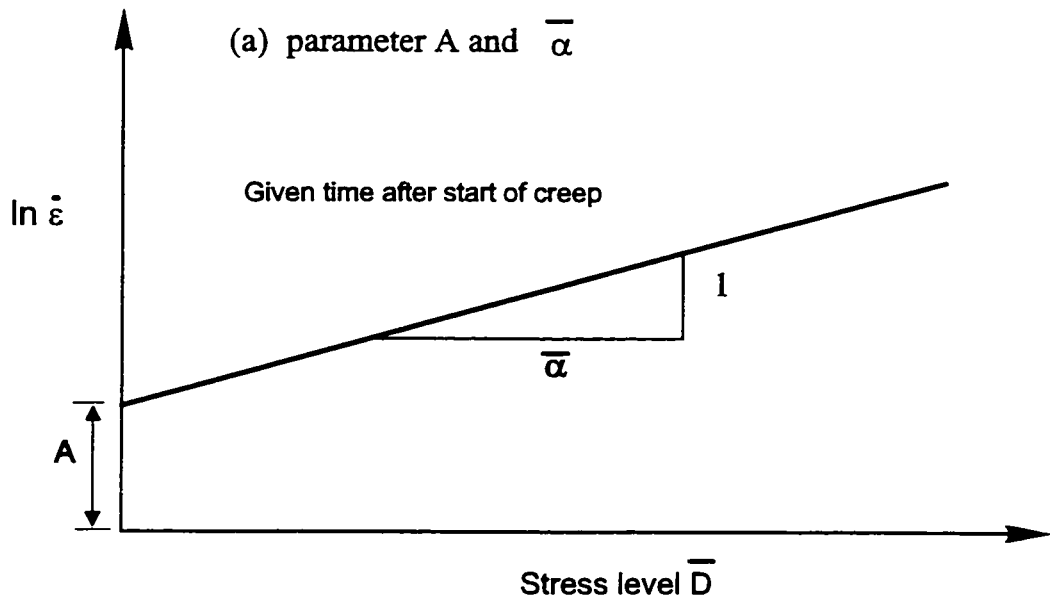


Fig. 3.5 Singh Mitchell creep parameters

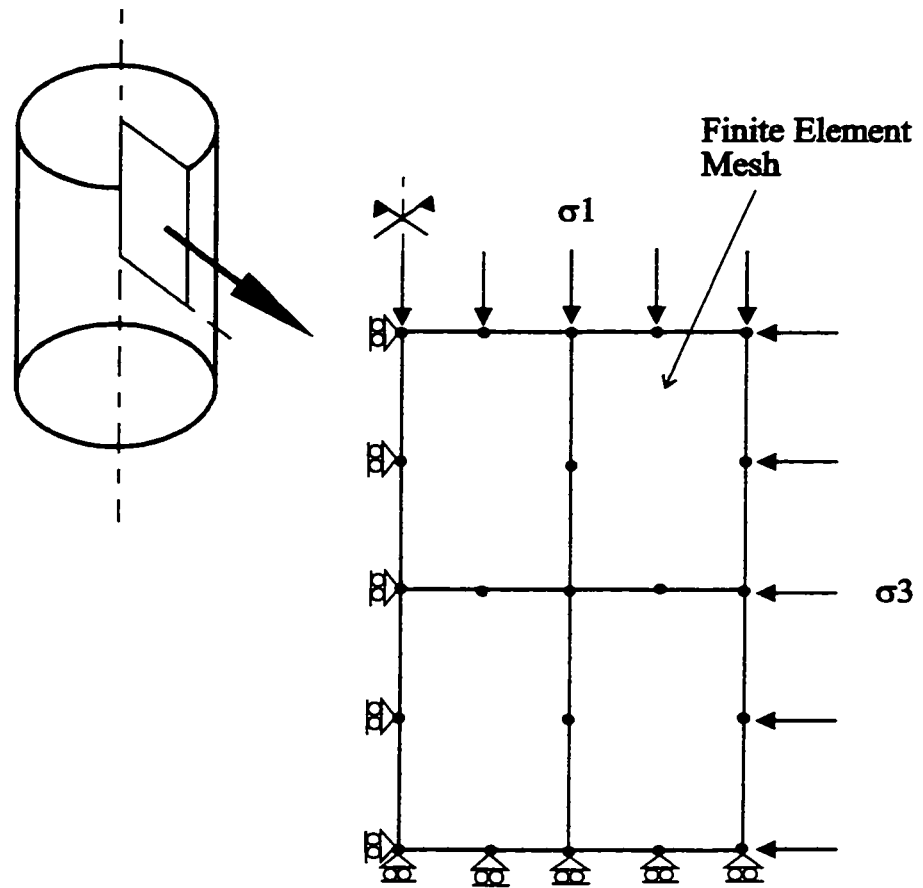
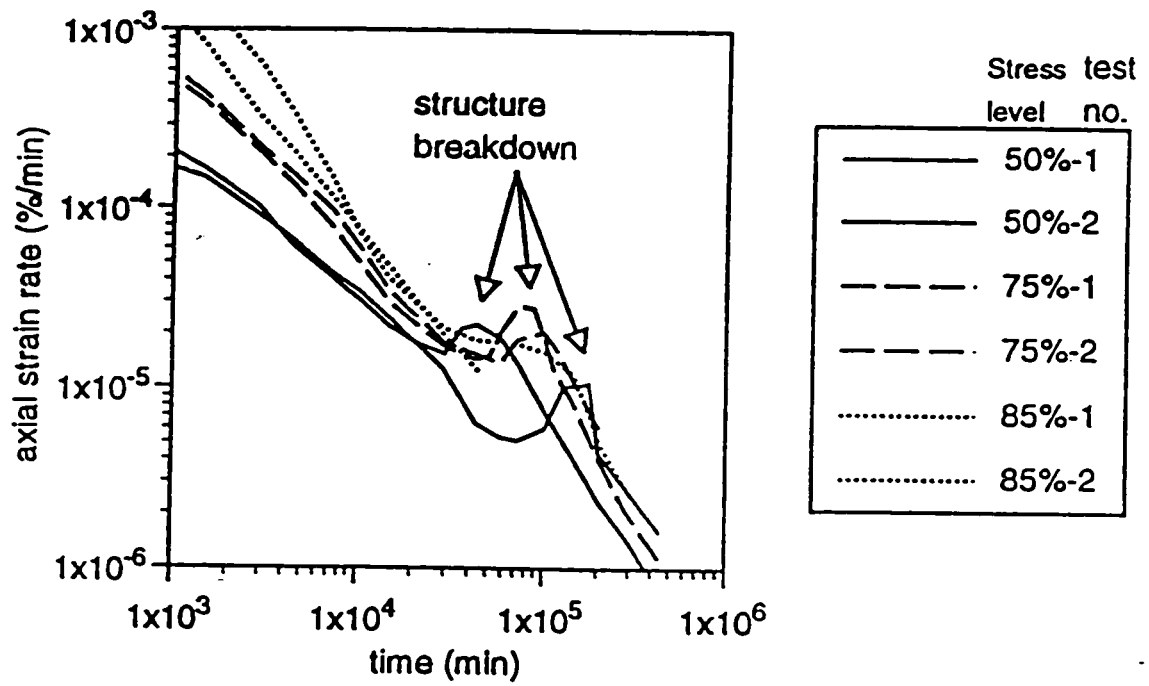


Fig. 3.6 Numerical simulation of triaxial test on PISA clay



(b) magnified
1,000 to 1,000,000 minutes

Fig. 3.7 Axial strain Vs. time for the creep test by Bishop and Lovenbury (1969) (after Mitchell and Soga, 1995)

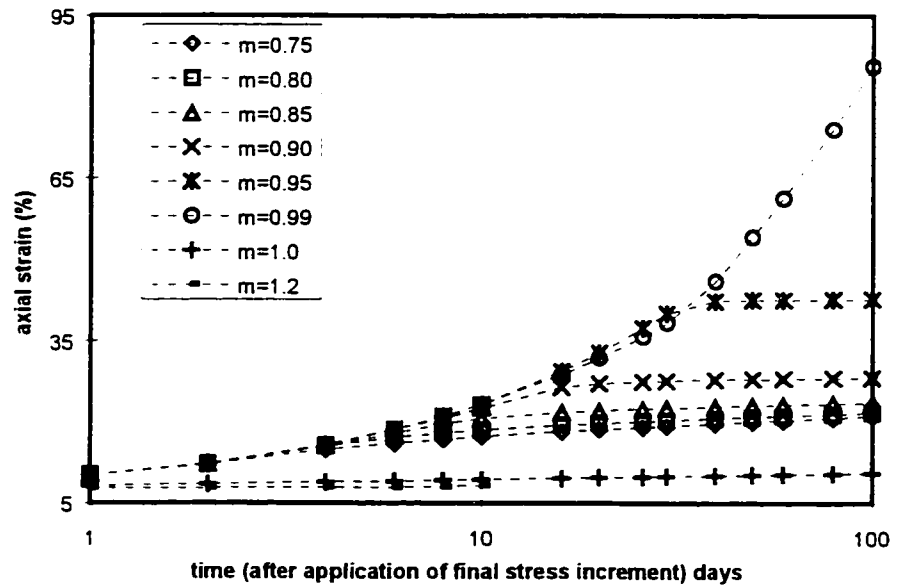


Fig. 3.8 Numerical results of axial strain versus time relationship for 75% loading case (before correction)

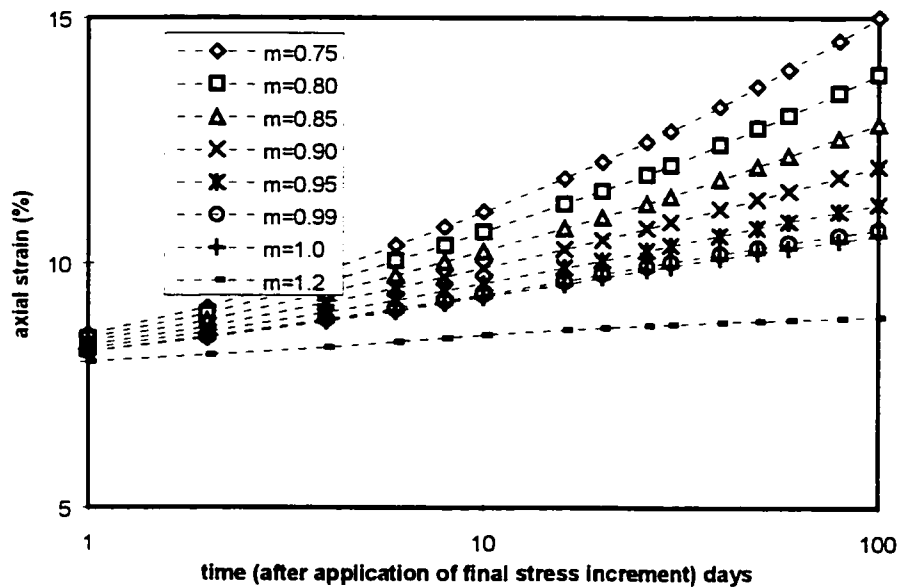


Fig. 3.9 Numerical results of axial strain versus time relationship for 75% loading case (after correction)

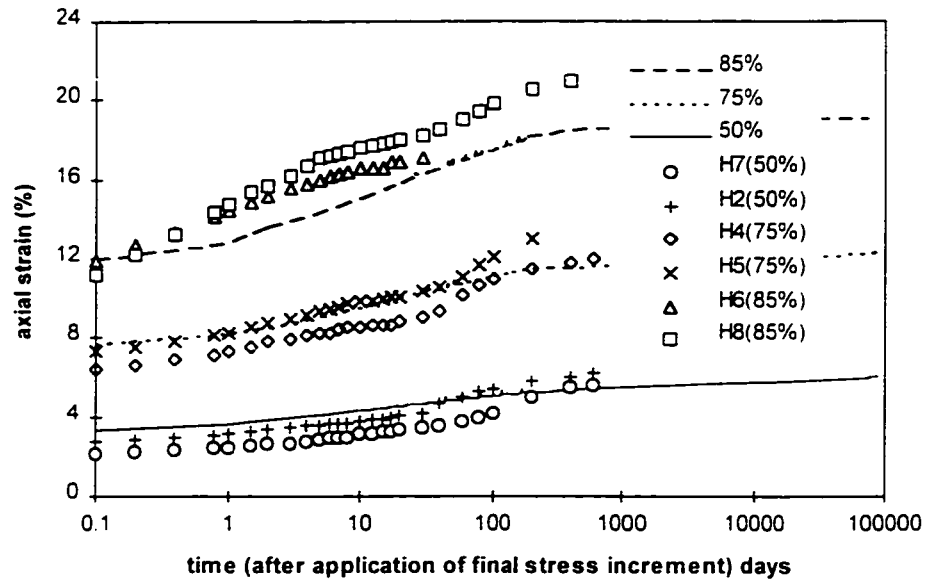


Fig. 3.10 Axial strain versus time relationship

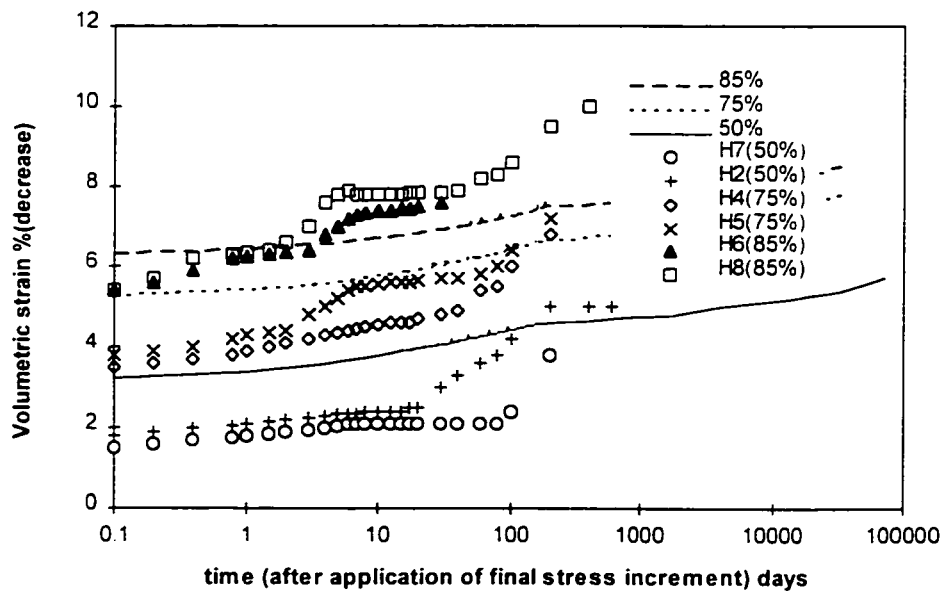


Fig. 3.11 Volumetric strain versus time relationship

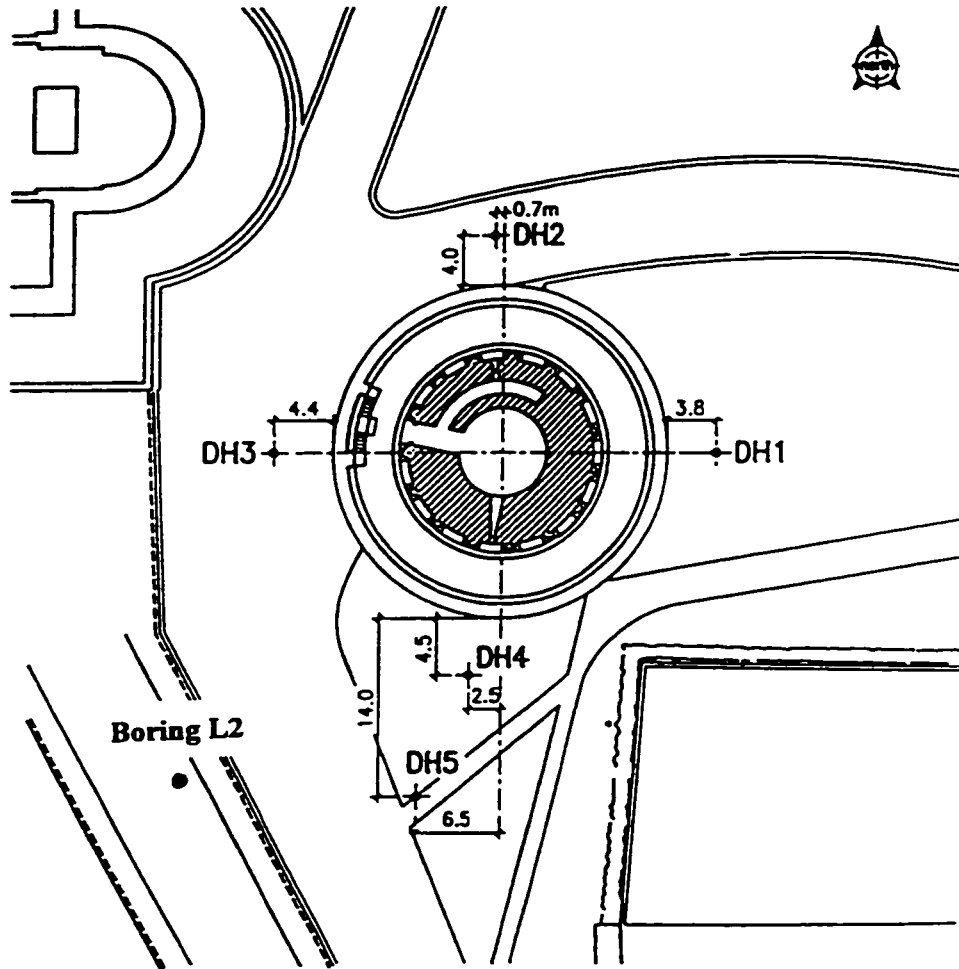


Fig. 3.12 Location of undisturbed sample boring and seismic cone tests

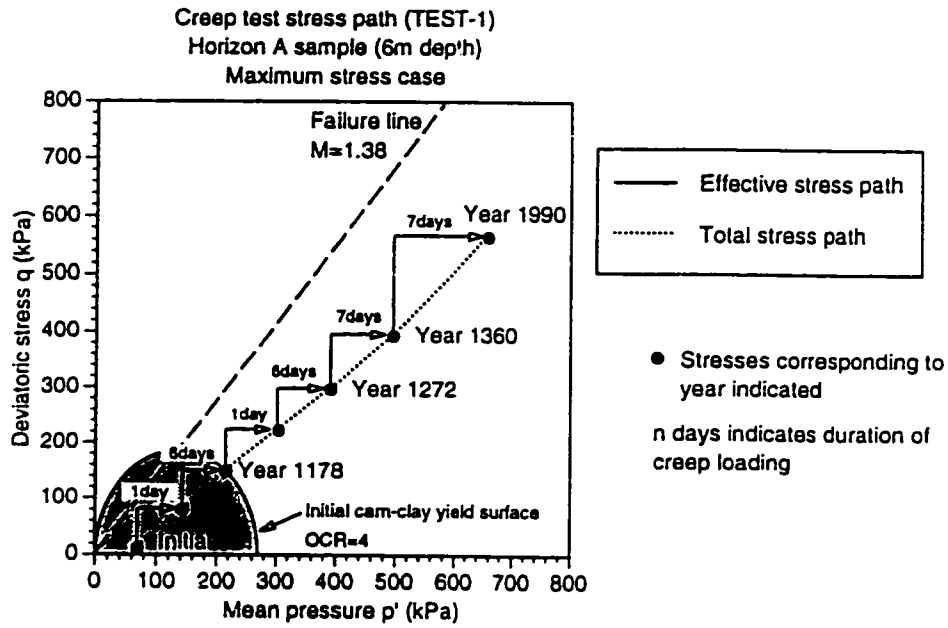


Fig. 3.13 Stress path of Test-1 (after Mitchell and Soga, 1995)

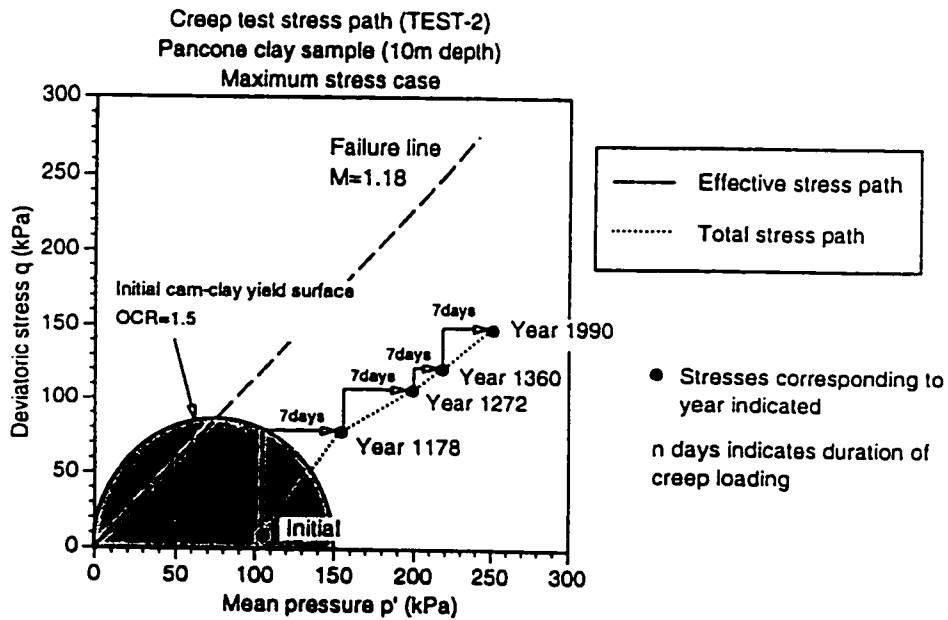


Fig. 3.14 Stress path of Test-2 (after Mitchell and Soga, 1995)

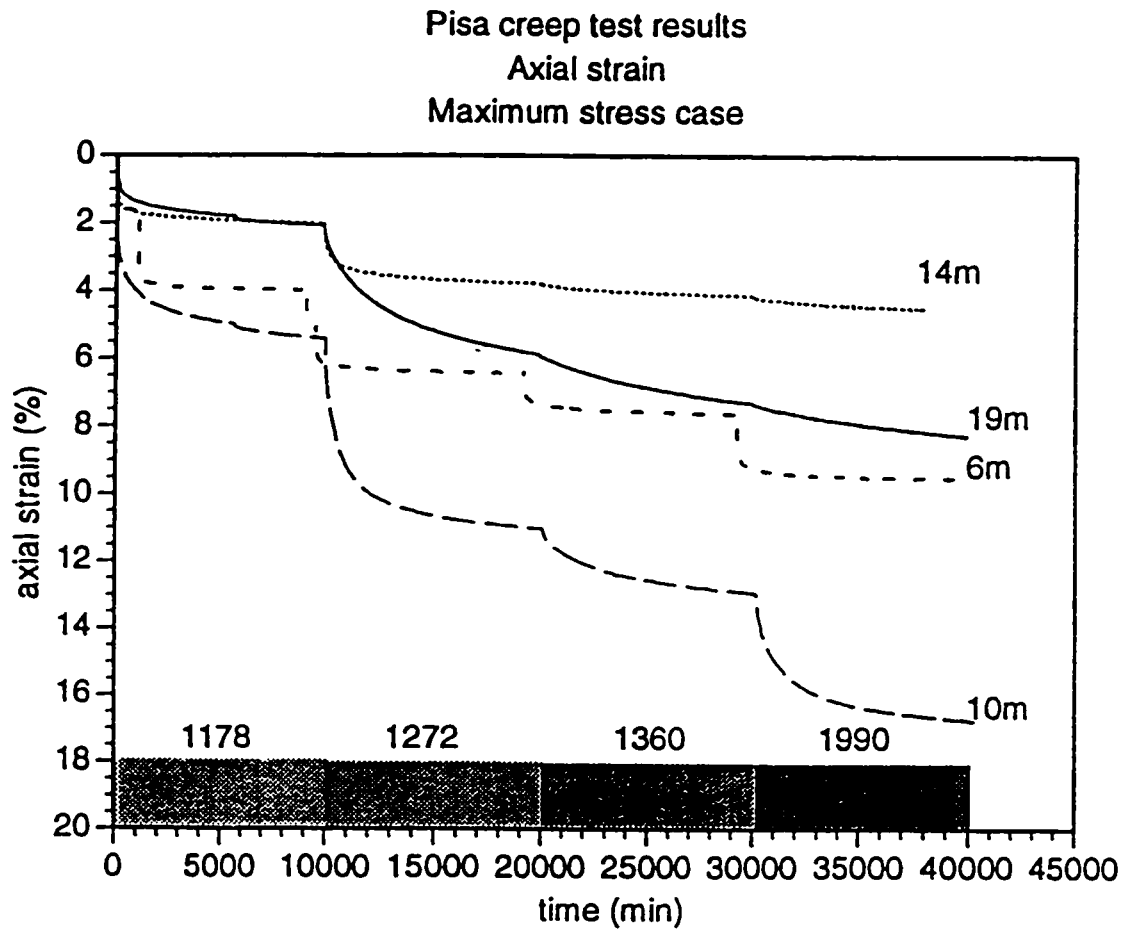


Fig. 3.15 Creep strain curves for maximum stress cases (after Mitchell and Soga, 1995)

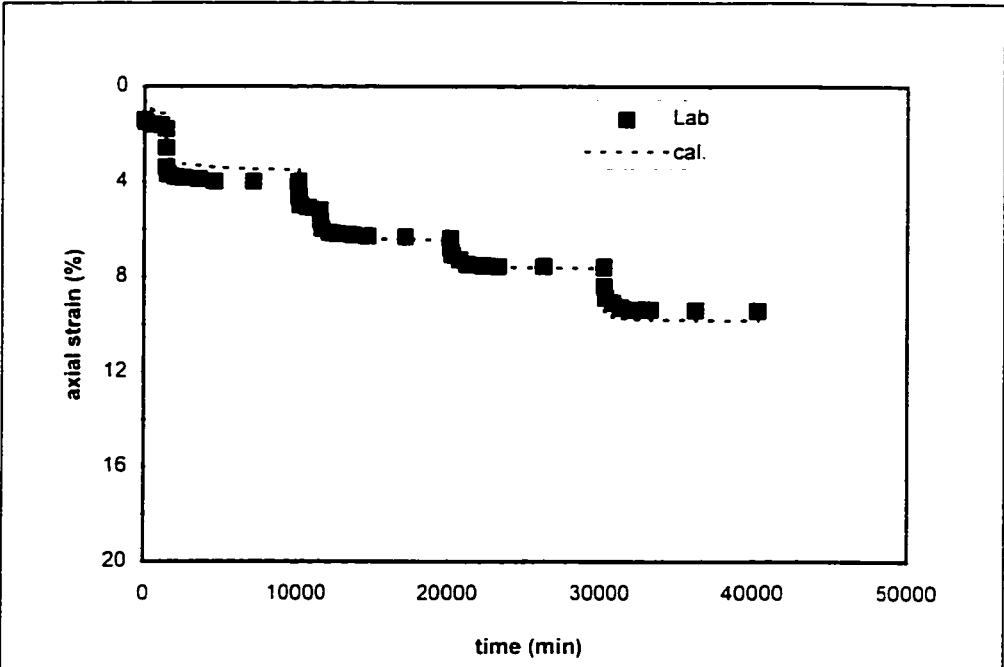


Fig. 3.16 Axial strain versus time curve for Test-1 6m sample, layer A1 (Maximum stress case)

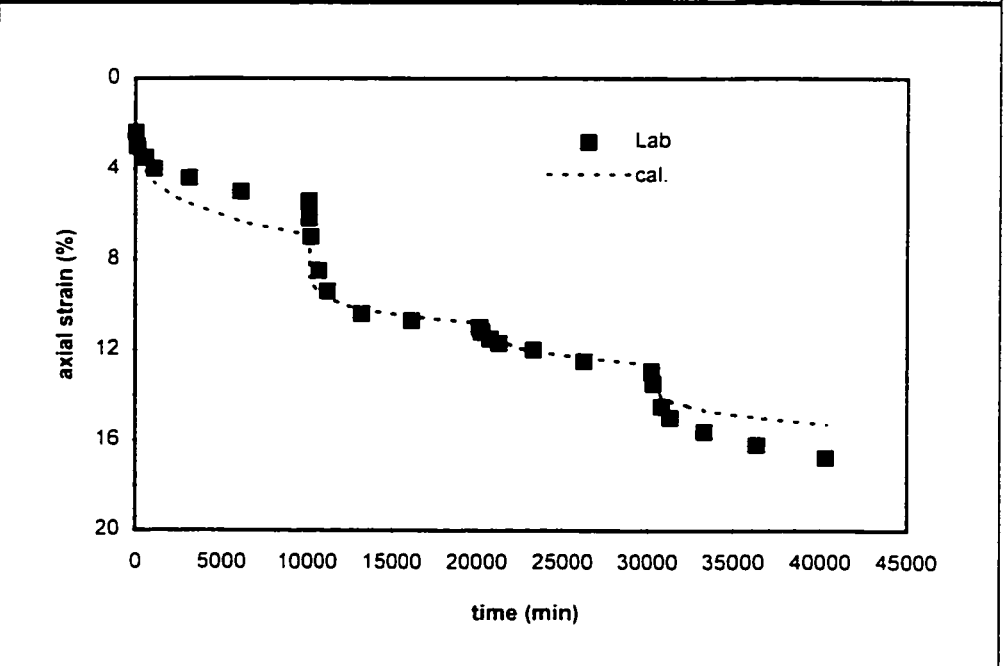


Fig. 3.17 Axial strain versus time curve for Test-2 10m sample, layer B1 (Maximum stress case)

CHAPTER 4

NUMERICAL ANALYSES OF TIME-DEPENDENT BEHAVIOR OF PISA TOWER

4.1 Introduction

The Leaning Tower of Pisa is one of the most fascinating problems that geotechnical engineers have ever faced. During the past 800 years, the south side of the tower has settled more than the north side, which results in about 2 meters differential settlement and 5.5 degrees southward tilting. The seventh cornice presently overhangs the first one by 4.1 meters. The factor of safety against overturning is very close to one. Due to its critical situation, the tower has been closed to tourists since 1990.

In order to find the right solutions to save this world famous landmark, it is very important to understand the deformation mechanisms of the soil underneath its foundation. Numerical modeling is a good way to provide insight to this kind of problem. Previous numerical investigations conducted by both Burland and Potts (1995) and Mitchell and Soga (1995) cannot quantify the amount of creep deformation of the soil beneath the foundation, although the creep tests conducted by Bishop and Lovenbury (1969) and Mitchell and Soga (1995) have concluded the importance of creep effect.

Since creep in soils was first studied five decades ago, various creep models have been developed based on four mechanisms (Buisman 1940 and Barden 1969): (1) the viscous soil skeleton (Murayama and Shibata 1958, Christensen and Wu 1964, and Yoshikuni et al. 1994); (2) jumping of bonds (Eyring 1936, Murayama and Shibata 1961, Mitchell 1964, and Kuhn and Mitchell 1993); (3) structural viscosity (Terzaghi 1941, Barden 1965, Walker 1969); and (4) micropore-macropore structure (De Jong 1968.

Holzer et al. 1973). Various case studies have also been reported (Borja et al. 1990, Brandes et al. 1994, and Morsy et al. 1995).

In this chapter, numerical simulations were conducted to investigate the 800 year tilting history of Pisa Tower. Two-dimensional elastic and elasto-plastic analyses were first carried out to investigate the stress paths and stress levels in each soil layer under the tower. Then a time-dependent plastic model, the double-yield surface Cam-clay plasticity (DYSCP) model developed by Hsieh et al. (1990) and Morsy (1994), was adopted to simulate the creep behavior of the soil beneath the foundation. The results obtained were compared with the ones from non-creep model to quantify the influence of creep effects on the deformation behavior of the tower throughout its history.

4.2 Overview of Pisa Tower

4.2.1 Construction history

The tower was constructed to complete a religious monument complex which includes the Cathedral and the Baptistry. The Cathedral was erected one hundred years earlier and the Baptistry twenty years earlier than the start of the construction on the Pisa Tower. The tower has eight cornices. It is about 60 meters high with a foundation diameter of 20 meters, as shown in Figure 4.1. The construction period of the tower was divided into three stages, as shown in Figure 4.2. The first stage started on August 9, 1173. Six years later, the construction had progressed to the fourth cornice, then it was stopped. This interruption lasted for about 100 years. The second stage began in 1272. Six years later, the tower had been built up to the seventh cornice, then the construction was stopped again. The second interruption lasted for about 80 years. The third stage began in 1360. Ten years later, the eighth cornice (the bell chamber) was completed. The whole construction of the tower lasted about 200 years.

It is interesting that the tower has never really been straight. Not long after the work began in 1173, the foundation began to settle unevenly, which initiated an

inclination of the tower towards the north. Starting from the second construction stage, southward leaning became evident and the movement in this direction has been continuous ever since.

A detailed study shows that if the construction had not been interrupted, the tower would have failed after the first or second construction stages (Jamiolkowski et al. 1993 and Burland and Potts 1995). The interruptions provided the time for the soil to consolidate, thus improving the bearing capacity of the foundation. Even if it was unintentional, the erection of the tower represents an excellent example of staged construction.

4.2.2 Soil profile and soil parameters

Geotechnical explorations of the subsurface condition at the Pisa Tower started in 1913. A large amount of data have been obtained from in situ and laboratory testing programs. The most complete set of data on the subsurface soil was collected by the committee chaired by Polvani since 1965. Calabresi et al. (1992) summarized all of the geotechnical information collected up to 1990 and interpreted it comprehensively. They proposed a set of Cam-clay soil parameters for the soil beneath the foundation. Mitchell and Soga (1995) compared those parameters with other reported values (Tamagnini 1993, Mitchell et al. 1977, Lancelotta and Pepe 1990, MLP 1971, and Calabresi 1992).

4.2.2.1 Soil profile

The soil profile was constructed by the Polvani Committee based on the observed values of the index properties and on the mechanical parameters obtained from laboratory and field (CPT) tests. The initial soil profile beneath the tower's foundation is shown in Figure 4.3. It contains three main formations.

Formation A: about 10m in thickness, clayey silt and silty sand. It can be subdivided into three layers: (1) MG, top soil and made ground, about 3.0m thick; (2) layer A₁, loose to very loose yellow sandy silt to clayey silt without stratification. It is

formed by a first layer of clayey silts A_1' , 1.4m thick, overlying the silty sands A_1'' , 4.0m thick. The second clayey silts layer A_1' is included in the silty sands layer A_1'' , its thickness increase linearly from 0.0m at 60m north of the tower axis, to 3.0m at 35m south of the tower axis; and (3) layer A_2 , uniform gray sand with inter-bedded clay layers and broken fossils, 2.0m thick. Figure 4.4 presents the results of CPT tests at a radius of about 30m from the north and south of the axis of the tower. It shows that the inhomogeneity of Formation A is significant, which is believed to be of major significance with regards to the lean of the tower (Mitchell et al. 1977).

Formation B: about 30m in thickness, predominantly clay, can be subdivided into four layers: (1) upper clay or Pancone clay (B_1 to B_3), about 11m thick, high plasticity, normal consolidated or slightly overconsolidated clay; (2) intermediate clay (B_4 and B_5), dark gray to yellow, low plasticity clayey silts, overconsolidated with OCR of 1.8; (3) intermediate sand (B_6), about 2.5m thick, gray, sometimes yellow; and (4) lower clay (B_7 to B_{10}), about 13m thick, clays and silts, blue gray to gray with yellow zones, medium plasticity, normal consolidated clay. Formation B is laterally very uniform, and is believed to be the major seat of the tower settlement.

Formation C: slightly silty sand, encountered at a depth of 40m. It extends to a depth greater than the deepest boring.

The bore-hole profiles and the cone penetration diagrams along the N-S cross section show that apart from the apparent depression in the upper face of layer B_1 (caused by the weight of the tower), the separation surfaces are flat and the thickness of each layer is almost constant, as shown in Figure 4.5.

4.2.2.2 Soil parameters

Mitchell and Soga (1995) studied soil parameters necessary for a Cam-clay model-based analysis. They compared the values of these parameters to those proposed by other investigators (Tamagnini 1993, Mitchell et al. 1977, Lancelotta and Pepe 1990,

Ministero dei Lavori Pubblici (MLP) 1971, and Calabresi 1992). Their study shows a reasonable consistency among these values. However, a certain level of variations exists in parameters such as the compression index in the upper Pancone clay layers.

4.2.3 Stabilization measures

Throughout the tower history, architects and engineers have attempted to halt the lean, but regular monitoring showed that the rate of inclination of the tower in 1990 had doubled since the 1930's and was about 6" per year. When a similarly constructed bell tower at the Cathedral of Pavia collapsed suddenly in 1989, fears about the safety of the landmark became acute. In 1990, a special commission, composed of Italian and foreign experts, was brought together by the Italian government to determine new ways to save the tower. The commission's ultimate goal is not to straighten the tower, since the tower curves like a banana shape and will never stand truly upright; instead, it aims to reduce the lean by half a degree to secure this landmark for another century, by which time our followers will have developed new techniques we cannot dream of (Wheeler 1995, Heiniger 1995).

To achieve the ultimate goal, the entire stabilization work was divided into two stages involving temporary and permanent measures, respectively. Short term temporary and fully reversible measures were implemented first, because the selection, design and implementation of permanent measures would take a long time. The following temporary measures have been implemented: (1) the installation of the temporary local reinforcement (post-tensioned cables) at the first cornice to prevent local buckling; (2) the implementation of 6MN lead counterweight at the north rim of the tower base to improve the foundation stability against overturning, which caused tilt towards the north by about 50 seconds of arc; and (3) the closing of a number of water wells in the area within 1km of the tower to mitigate the possible influence of the subsidence of the whole Pisa plain. These actions slightly improved the safety of the tower.

Following the temporary solutions, some permanent solutions had been studied. Among various possible approaches, the one inducing controlled settlement below the north side of the tower was highly recommended with two alternatives: the electro-osmotic consolidation treatment and the underground excavation technique. The first alternative, proposed by Mitchell (1991), would induce the settlement of the tower at the north side by causing the reduction of the volume in the top most part of the Pancone clay. The second one, first postulated by Terracina (1962), would obtain a similar effect by drilling into the clay at an angle and removing small volumes with a sampling tool. However, detailed investigations showed that both alternatives were less than convincing. The final adopted measure, named the “last option” started on April 20, 1995. It includes three phases: (1) freezing the ground using liquid nitrogen and excavating the ground; (2) casting a post tensioned concrete ring beam to embrace the tower’s foundation and applying ground anchors on the north side of the beam; and (3) excavating bore-holes. The anchored ring beam will replace the function of the temporary measure of 6MN lead weight placed on the towers’ up-tilt side. Then the controlled subsidence to the north of the tower will be achieved by excavating bore-holes. In early September 1995, the installation of the concrete ring beam was temporarily suspended because excavation unearthed a 1m thick mass of boulders, rocks and bricks bound together by a lime mortar. It also discovered undocumented old steel grout tubes tying the tower’s foundation to a surrounding walkway. The tower did not react as expected. The stabilization work caused the tower to move back to the south side by 3.5 arc seconds. The commissioners have to decide whether to continue with the current process or directly move to the last phase of bore-hole excavation beneath the tower’s foundation (Oliver 1995, Parker 1995).

4.2.4 Previous numerical investigation

Numerical analyses have been conducted for the soil under the Pisa Tower. The most recent work includes Burland’s (1995) and Mitchell’s (1995).

Burland and Potts (1995) developed a numerical model for Pisa Tower. The model was intended to match the history of inclination of the tower during and

subsequent to its construction. The Modified Cam-clay model was used for the clay layers and the Mohr-Coulomb model was used for the sandy layers. Fully coupled consolidation was incorporated into the analysis. The time-dependent deformation behavior was excluded. The overturning moment was self-generated in response to any change of the inclination of the foundation. Large strain formulation was attempted in the initial studies, but the results did not differ significantly from a traditional infinitesimal strain analysis. The traditional small strain two-dimensional plane strain approach was adopted. By gradually adjusting the applied overturning moments, the model predicts final tilting of 5.44 degrees, which is very close to the observed value of 5.5 degrees, but the calculated inclination history is different from the observed one. The calculated final settlement is 3.8m, which is larger than the actual value of 3.0m.

Burland and Potts (1995) attributed the tilting of the tower to a mechanism known as "leaning instability", which results from the high compressibility of the underlying Pancone clay and is not related to its strength. The tapered layer A1' only determines the direction of the lean, not its magnitude.

Mitchell and Soga (1995) explored both two-dimensional plane strain and three-dimensional elastic models. It was found that the stresses beneath the south and north sides obtained from the three-dimensional model were greater than those obtained from the two-dimensional model. The two-dimensional model gave larger settlement but smaller tilting. Then, Mitchell and Soga (1995) attempted a three-dimensional elastoplastic analysis using the Cam-clay model for clay as well as for the sandy layers. Results showed a larger increase in mean stress in the upper Pancone clay (B₁ and B₃). Thus, large volumetric strain was expected in these layers which are the main seat of settlement. A large increase in deviatoric stress was developed in the sandy layers (A₂ and B₆) due to their high stiffness. The tapered clayey silt layer A₁' was believed to contribute to the initial leaning of the tower. The results also showed that the normal consolidation zone spreads downward as time progresses. Part of the soil in Formation A was at a state of failure. Stress levels of 50% to 80% were observed in the upper clay layers. The

calculated final rotation was 3.5 degrees and the final average settlement was 1.6m. These values were smaller than measured. Mitchell and Soga (1995) believed that one of the major reasons was the creep deformation which could not be incorporated into the time-independent Cam-clay model.

In summary, the time-dependent deformation behavior has not been incorporated so far into the numerical models to study the deformation mechanism of the soil beneath the foundation, although it might be a very important factor as concluded by a number of researchers.

4.3 Time-dependent constitutive model

The time-dependent constitutive model employed here belongs to the phenomenological approach, as shown in Figure 4.6. This approach can be subdivided into three groups: (a) the volumetric scaling; (b) the deviatoric scaling; and (c) the coupling of volumetric and deviatoric scaling. The volumetric scaling procedure is based on Taylor's (1948) secondary creep law. The increments of volumetric creep deformation are calculated using this secondary creep law. The deviatoric components of viscous deformation are computed by the normality rule. In this way, the deviatoric creep strain increments will be overestimated, especially at high values of the stress ratio η . For $\eta=M$, the deviatoric creep strain increments are infinite. This procedure can only be used at low values of η (Kavazanjian and Mitchell 1977, Borja and Kavazanjian 1985, Yin and Graham 1991, and Burghignoli et al. 1994). The deviatoric scaling procedure is based on Singh and Mitchell's (1968) creep equation. The deviatoric viscous deformation is computed as a function of time using Singh and Mitchell's equation. The volumetric component is obtained by introducing normality. In this procedure, the volumetric creep strain increments will be overestimated at low values of the stress ratio η . For isotropic stress states, the volumetric creep strain increments will be infinite. This procedure can only be used at high values of η (Chang et al. 1974, Burke 1983, and Borja and Kavazanjian 1985). The volumetric and deviatoric coupled scaling procedure (Borja et al.

1990 and Hsieh et al. 1990) combines both Taylor's secondary creep law and Singh and Mitchell's (1968) creep equation by satisfying them simultaneously. It overcomes the limitations of the volumetric scaling procedure for high η value and deviatoric scaling for low η value cases. This procedure is used in this study.

General phenomenological representations for volumetric and deviatoric soil deformations, including the effect of time, were first attempted by Kavazanjian and Mitchell (1977). They postulated that strain tensors can be decomposed into volumetric and deviatoric components, which can be further decomposed into immediate and delayed components based on Bjerrum's (1967) concept, as shown in Figure 4.7. The general theory within the theoretical framework of pseudo-linear elasticity was developed by Kavazanjian and Mitchell (1980). Borja and Kavazanjian (1985) extended the general phenomenological theory within the classical theory of plasticity by proposing a consistency law based on Taylor's (1948) secondary creep law (volumetric scaling) at low values of the stress ratio η and the Singh and Mitchell (1968) creep equation (deviatoric scaling) at high values of η . The time-independent plastic strain and time-dependent total strain (creep) are obtained by the normality condition and the consistency requirement on the ellipsoidal yield surface of the modified Cam-clay model (Roscoe and Burland 1968).

Borja (1984) proposed the concept of a horizontal deviatoric yield surface represented by the Von-Mises model within the ellipsoid of the modified Cam-clay model to account for plastic shear distortion that occurs without volume change below the state boundary surface. Hsieh et al. (1990) introduced this cylindrical yield surface into Borja and Kavazanjian's general stress-strain-time model. A scaling procedure that can simultaneously satisfy both the volumetric and deviatoric creep experimental relationships was proposed. The increments of volumetric viscous deformation are calculated based on Taylor's secondary creep law, while the deviatoric creep deformation is computed as a function of time using Singh and Mitchell's creep equation. Thus a new model named the double-yield surface Cam-clay plasticity (DYSCP) model was postulated (see Figure 4.8).

The double-yield criteria are defined by the ellipsoid MCCM and the Von-Mises cylinder inscribed in this ellipsoid (Hsieh et al. 1990, Morsy 1994):

$$[4.1] \quad F = F(\sigma'_{ij}, p_c) = \frac{q^2}{M^2} + p(p - p_c) = 0$$

$$[4.2] \quad G = G(\sigma'_{ij}, q_c) = q - q_c = 0$$

where σ'_{ij} are the effective stress components; M is the slope of the critical state line in the p - q plane; p is the mean stress ($p = \frac{\sigma'_1 + \sigma'_2 + \sigma'_3}{3}$); q is the deviatoric stress ($q = \frac{1}{\sqrt{2}} \sqrt{(\sigma'_1 - \sigma'_2)^2 + (\sigma'_2 - \sigma'_3)^2 + (\sigma'_3 - \sigma'_1)^2}$); p_c is the isotropic preconsolidation pressure which controls the size of the F surface; and q_c is the shear yield stress based on the Von-Mises yield criterion. q_c value controls the size of G surface.

The total strain-rate tensor can be decomposed into four components (Borja and Kavazanjian 1985, Hsieh et al. 1990, and Morsy 1994):

$$[4.3] \quad \underline{\dot{\epsilon}} = \underline{\dot{\epsilon}}^e + \underline{\dot{\epsilon}}^p_f + \underline{\dot{\epsilon}}^p_g + \underline{\dot{\epsilon}}^t$$

where subscripts F and G denote the Modified Cam-clay model (MCCM) and the Von-Mises cylinder yield surfaces, respectively; superscripts e and p denote the immediate elastic and plastic parts, respectively; and superscript t denotes the delayed or creep part.

The time-dependent strain rate tensor can be further divided into distinct but interdependent volumetric and deviatoric parts (Kavazanjian and Mitchell 1980)

$$[4.4] \quad \underline{\dot{\epsilon}}^t = \underline{\dot{\epsilon}}^t_v + \underline{\dot{\epsilon}}^t_d$$

where subscripts v and d denote volumetric and deviatoric creep components, respectively.

The above mentioned strain rate components can be evaluated as follows: (1) the elastic part of time-independent components can be evaluated by the generalized Hooke's law; (2) the immediate plastic deformation can be evaluated based on the current stress state with respect to the double-yield surface, in three different cases: (a) semi-plastic process on F surface, where F is the only surface involved in the deformation process; the soil is to be considered normally consolidated with respect to F but overconsolidated with respect to G; (b) semi-plastic process on G surface, where G is the only surface involved in the deformation process; the soil is to be considered normally consolidated with respect to G but overconsolidated with respect to F; (c) fully plastic process: the F and G surfaces are both involved in the deformation process; and (3) the total creep strain rate can be evaluated by employing a flow rule to both F and G surfaces and by forcing the resulting creep strain rate tensor to satisfy the secondary creep law for volumetric creep and the Singh and Mitchell creep equation for the deviatoric creep simultaneously.

The DYSCP model has been successfully applied to two field cases to study the time-dependent deformation behavior (Borja et al. 1990 and Morsy 1994). This model is employed in this study to investigate the time-dependent deformation behavior of the soil beneath the foundation

4.4 Plane strain elastic and elasto-plastic analysis

As a beginning, two-dimensional elastic and elasto-plastic analyses were carried out using the finite element program named PISA-FORTRAN developed by Chan and Morgenstern (1992), and Morsy (1994). The stress paths as well as the stress levels for each layer were investigated. The obtained results provided the basis for studying the effect of soil creep.

The observed piezometer results showed that water table in the soil beneath the foundation was between 1m to 2m below ground surface and quite stable. In this study, the water table was assumed to be at the surface of the ground and in a hydrostatic

equilibrium state. A drained condition held if neglecting the consolidation process during the early construction stage.

4.4.1 Finite element

The two-dimensional plane strain finite element model consisting of 425 eight-node quadrilateral isoparametric elements has been constructed, as shown in Figure 4.9. The mesh represents a vertical plane through the center of the tower along the N-S direction. It extends horizontally to 60m on either side of the axis of the tower, and vertically to 40m (up to the top of Formation C). The boundaries of the FEA mesh are determined based on Mitchell and Soga's (1995) results about the influence range of the tower weight.

In plane strain analysis, the actual three-dimensional rigid annular plate with 19.6m outer and 4.5m inner diameters needs to be transformed to two rigid plates of infinite length. Those two rigid plates must be connected to prevent them from acting separately (see Figure 4.10). The actual applied loads must be converted to loads of unit length using a correction factor of CF, as introduced by Mitchell and Soga (1995).

$$[4.5] \quad \text{Load (plane strain)} = \frac{\text{Load(3D)}}{\text{CF}}$$

Mitchell and Soga's (1995) results showed that a better agreement for the stress distribution at shallow depths could be obtained when CF took a value of 24.

Another correction factor I_c , is applied to adjust the secondary moments to account for the difference between a rectangular and a circular foundation.

$$[4.6] \quad \text{Load(plane strain)}_{\text{South, North}} = \frac{1}{\text{CF}} \cdot \left[\frac{\text{Weight}}{2} \pm \frac{\text{Moment} * I_c}{L} \right]$$

where L is the distance between the center of the two strip footings.

For a rectangular foundation with a width of 19.6m and the same area as the foundation of the tower, Burland and Potts (1995) suggested that the value of I_c was 1.27. In this study, CF value of 24 and I_c value of 1.27 were used initially.

The tower weight and overturning moment are shown in Table 4.1. The actual loads applied to the foundation were obtained by subtracting an amount of 11.589 kN from the weights of the tower to account for the weight of the soil excavated for the tower's foundation. Each applied load was converted into two loads using Equation [4.6] with the adopted values of the correction factors. The two loads were applied at 6.02m south and north from the footing center, respectively. The obtained loading conditions relative to different construction stages are listed in Table 4.2.

The soil parameters used in the elastic analysis are detailed in Table 4.3. Young's modulus for the rigid footing is chosen as 10^{10} kPa, based on Mitchell and Soga's (1995) study. A Poisson's ratio of 0.12 was initially attempted, but results showed that very high shear stresses were generated due to the extremely low horizontal stress. To compensate, the value of Poisson's ratio was increased to 0.3 in the elastic analysis.

In the elasto-plastic analysis, the elastic model was still used for the sand and silty sand layers because these layers were not the main focus in this study. The DYSCP model was employed to simulate the creep behavior of the clay and clayey silt layers because this model has been proven to be able to represent normal to slightly overconsolidated soils. If the influence induced by the tower is taken into consideration, all layers beneath the tower's foundation including Formation A are mainly normal consolidated to slightly overconsolidated soils (Mitchell and Soga' 1995). The input data used in the elasto-plastic analysis are shown in Tables 4.4 and 4.5. They are mainly based on Tamagnini's (1993) recommendation and Mitchell and Soga's (1995) study.

4.4.2 Stress distributions in the soil beneath the foundation

In order to obtain reasonable results, a realistic loading sequence needs to be carefully followed. In this analysis, the loading sequence comprised a switch-on gravity process to get the pre-existing stress field before the construction of the tower and the subsequent loads due to the construction of the tower. The initial in-situ stress conditions were obtained by applying gravity load. In order to get more accurate initial stress states, the switch-on gravity process was repeated ten times by applying 10% gravity load each time. Then, the displacements and strains were both set to zero to give the initial configuration of the soil beneath the foundation the same as the field. Figure 4.11 presents the comparison between the computed and the estimated initial in-situ vertical and horizontal stress distributions. The computed horizontal stresses are reasonably close to the estimated values, but the computed vertical stresses are smaller than the estimated values. The maximum difference is 10%.

The tower loads corresponding to different construction stages were applied to the initial in-situ stress conditions through four distinct individual loading cases corresponding to the years 1173, 1272, 1360, and 1990, respectively. The stress distributions of the vertical effective stress (σ_v'), the mean effective stress (p'), and the deviatoric stress (q) from the elasto-plastic analysis are shown in Figures 4.12 to 4.14. Here only the stress distributions corresponding to the years 1173 and 1990 are shown. It can be seen that as loading increase, stresses concentrate more toward the south side. The upper clay layers carry more mean effective stresses while the sandy layers carry more deviatoric stresses.

Figures 4.15 and 4.16 show the computed mean effective and deviatoric stresses along horizontal planes at various depths for plastic analysis. The stress difference between the south and north sides increases as time progresses. The difference is more significant at the shallow depth. At greater depth, the maximum values of p' and q are not located at the same location. The maximum p' value is located around the center of the

footing while maximum q remains on the south side. This phenomenon was also observed by Mitchell and Soga (1995). The stress ratio (q/p') distributions along horizontal planes are plotted against depth, as shown in Figure 4.17, which also shows the values of the critical stress ratio M . Stress concentrations are observed around both the north and south sides of the footing. Starting from the year 1360, stress ratios near the edges of the footing are greater than the critical stress ratio in the clayey silt layers (3.7m deep and 6.5m deep). This suggests the a local failure in those elements may occur. Because the failure is localized in a small area the whole tower still remains stable. Stress states of 50% to 60% failure strength are observed in the upper clay layers and intermediate clay layers. This suggests that the impending instability of the footing could not be due to the onset of a bearing capacity failure within the upper Pancone clay. As time progresses, the stress ratio curves shift to the south side of the tower. Increase in stress ratio due to the tower weight can only be observed in the radius of 30m north and south of the footing axis. Close to the footing, the largest stress ratio concentration can be found at the north side of the footing. However, apart from the footing (see the upper and intermediate clay layers), the largest stress ratio concentration is located at the south side of the footing. This was also observed by Mitchell and Soga (1995). Due to the south side eccentricity of the tower, more stress concentrating on the south is expected. The simulated stress concentrating more on the north side at the shallow depth is probably due to the influence of the inclined layer A_1 (silty sand).

4.4.3 Displacements of the footing

Figure 4.18 shows the observed vertical displacements of the footing in the year 1990, and the calculated vertical displacements corresponding to different years. The major vertical displacements are generated after the first construction stage (in 1178) due to the fact that the major weight of the tower is applied at this stage. The tilting angle in this stage is negligible, but it increases as time progresses. The calculated final average settlement of the footing is 2.4m. The final tilting angle is 1.7 degrees. The estimated final average settlement is about 3.0m according to Burland and Potts (1995). The

observed tilt of the tower is 5.5 degrees. Both the calculated settlement and the tilting angle are smaller than the observed values.

4.4.4 Sensitivity analysis of correction factors

The values of correction factor CF of 24 and I_c of 1.27 were initially determined based on the previous studies. The sensitivity of these factors is studied in the following sections.

4.4.4.1 Correction factor CF

The settlement of the tower's foundation is mainly influenced by the vertical pressure acting on the soil underneath the footing. If the total load is kept constant, the vertical pressure is inversely proportional to the correction factor CF. By varying the value of CF at 19.6, 24, and 32, respectively, the deformations of the footing in 1990 are plotted in Figure 4.19. A higher value of CF results in a lower value of settlement. However, CF has very little influence on the tilting angle.

4.4.4.2 Correction factor I_c

The rotation angle of the tower is mainly influenced by overturning moments. By varying the value of correction factor I_c at 1.27, 2.4, and 3.0 respectively, while keeping CF at 24, the final settlement of the footing is plotted in Figure 4.20. A higher value of I_c results in higher tilting angles and larger settlements. When I_c takes the value of 2.4, the load at the north side of the footing equals 0.2 MPa, and the footing develops a tilting angle of 3.4 degrees and settlement of 2.6m. When I_c takes the value of 3.0, a negative load of 16.4MPa at the north side is obtained, although a tilting angle of 4.5 degrees can be achieved. Obviously, a negative load at the north side is not possible. Hence, the value of I_c cannot be greater than 3.0.

Although the simulation results can be improved more or less by varying the values of the two correction factors, the improvement is limited and the expected tilting

angle of 5.5 degrees still cannot be achieved. To keep consistent with the previous work. CF of 24 and I_c of 1.27 are still used.

4.5 Plane strain visco-plastic analysis

The DYSCP model is employed to investigate the creep effect on the clayey layers underneath the tower. The elastic model is still used for the sandy layers. The geometry and the loading conditions of the soil and the foundation are kept the same as those in the elasto-plastic analysis case.

4.5.1 Input parameters

The input parameters are the same as those in the elasto-plastic analysis, as detailed in Tables 4.4 and 4.5.

Elasto-plastic analysis showed that the stress in the upper and intermediate clay layers were on the range of 50% to 60% of their strength. On the other hand, stress levels in Formation A were very high. Some areas were already in a state of failure. Moreover, these layers were believed to have a major influence on the tilt of the tower. In the creep analysis, the Singh and Mitchell creep equation was used for the upper and intermediate clay layers. Although this equation might under-predict creep strains in the sandy layers, it was still employed in these layers because no other alternative was available.

Drained creep tests on the upper clay layer B_3 were first conducted by Lovenbury (1969), but creep parameters from this layer might not be a good representation for the rest of the clay layers due to its highly structural characteristics. Therefore, creep parameters obtained from Mitchell and Soga's (1995) strain rate controlled undrained triaxial tests are therefore selected, as shown in Table 4.6.

The loading history of the tower is detailed in Figure 4.21.

4.5.2 Stress distributions in the soil beneath foundation

Stress contours of σ_v' , p' , and q corresponding to the years 1178 and 1990 are plotted in Figures 4.22 to 4.24. Comparing the stress contours with those of elasto-plastic analysis (Figures 4.12 to 4.14), it is obvious that the vertical stress level is increased directly underneath the footing and extends below the footing because of the creep effect. Vertical stresses concentrate more at the edge of the footing. Mean effective stresses concentrate more in the clay layers. They are increased by 20% in the upper clay layers. Thus, substantial settlement can be expected. Creep also has a significant effect on the deviatoric stresses. Generally speaking, deviatoric stresses decrease significantly in the areas horizontally far away from the footing, and increase significantly underneath the footing. The creep effect causes the clay layers to bear less deviatoric stress and the sandy layers to carry more. Thus the deviatoric stresses concentrate more in the sandy layers. The high deviatoric stresses may have driven the sandy soil into a state of failure, if a more realistic Mohr-Coulomb model was used for these layers.

The stress paths in the p' versus q plots are plotted along the two edges of the south and north of the footing, as shown in Figure 4.25. The results from elastic, elasto-plastic, and creep analyses are given. Stress ratios from elastic analysis are greater than the failure ratio, which means that some soils are no longer in an elastic state. At elasto-plastic conditions, mean effective stresses develop more and the shear stresses are more constrained underneath the critical state line than those under elastic conditions. Figure 4.25 (a) clearly indicates the increase of the mean effective stresses and decrease of the deviatoric stresses due to the creep effect. Thus the stress states in the clay layers move away from the critical state line. This phenomenon has also been observed by Morsy et al. (1995). Unloading can be found on the north side of the footing, as shown in Figure 4.25 (b).

Figures 4.26 to 4.28 show the mean effective stress, the deviatoric stress, and the stress ratio (q/p') distributions respectively along horizontal planes at different depths.

Comparing the creep results with those from the elasto-plastic analysis (Figures 4.15 to 4.17), the same phenomenon of the creep effects on the values of p' and q can be observed. Stress ratios decrease in the area away from the footing. Below the depth of 12m, stress ratios decrease as time progresses, and stress ratio curves move downward. Close to the footing, stress ratios are highly concentrated. Failures can be observed at the depth of 3.7 m at the south edge, and at the depth of 6.5 m around both the south and north edges of the footing.

4.5.3 Displacements of the footing

The calculated vertical displacements of the footing are plotted in Figure 4.29. A total settlement of 3.3m and a tilting angle of 3.4 degrees are obtained after taking the effect of creep into consideration. The total vertical displacements of the footing under both non-creep and creep cases are compared in Figure 4.30. Creep has caused one meter additional settlement and 1.7 degrees additional tilting. In other words, the settlement is increased by 37%, and the tilting angle by 100%. However, the calculated settlement is slightly larger than the estimated value and the tilting angle is smaller than the observed one. These discrepancies may be caused by the limitations of the two-dimensional plane strain analyses. The influence depth of the real circular footing should be less than the strip footing used in these analyses.

The calculated tilting angle is plotted against time in Figure 4.31 (a) in comparison with the observed tilting history given by Jamiolkowski et al. (1993). The calculated settlement is plotted in Figure 4.31 (b). However, no settlement history is available for comparison. The calculated results show that the settlement is mainly accumulated during the construction period, especially in the first stage. Both observed and calculated results show that the tilting angle is mainly accumulated after the third construction stage. The calculated tilting can match the history during the construction period, but the northward lean cannot be simulated although it was reported to have

occurred during the first construction stage. After the year 1550, the southward lean is under-predicted.

The deformation process of the tower can be generally divided into three stages: (1) consolidation; (2) steady-state creep; and (3) post creep. Since the consolidation for the sandy layers has not been taken into consideration, the model cannot predict the northward lean during the early construction stage. During and right after the construction stage, the tower is mainly at the creep state, thus the creep model can predict the tilting history relatively well. As time progresses, the creep strain rate decreases and finally reduces to zero since the tower is mainly under drained conditions in which creep rupture is not possible for normally consolidated soil. On the other hand, leaning instability mechanism might exist after the tower reached its full height. The pure rotation caused by this mechanism would result in larger tilting angle. This may help explain why after the construction finished, there is an abrupt increase in tilting angle, as shown in Figure 4.31 (a). Since the tower has been driven to a very critical situation, it becomes very sensitive to even very small perturbations, such as solar energy or the daily temperature change. These perturbations may have become the major driving mechanism for the continuous deformation of the tower. Because the numerical model cannot quantify the effects of these factors, relatively larger errors of the calculated values have been obtained in the last couple of centuries.

4.6 Summary and conclusion

This chapter summarizes the information related to the Leaning Tower of Pisa up to the late 1995. The numerical analyses conducted under both non-creep and creep conditions have concluded that creep is one of the major important factors which cause the tilting of the tower.

A time-dependent constitutive model has been adopted. In this model, strain tensors are decomposed into volumetric and deviatoric components, which are further decomposed into immediate and delayed components. The double-yield criteria defined

by the ellipsoid MCCM and the Von-Mises cylinder inscribed in the ellipsoid is incorporated to evaluate both the time-independent and time-dependent strain components.

Because of the influence of creep, the vertical effective stresses increase in the area right below the footing, and mean effective stress increases by 20% in the upper clay layers. Deviatoric stresses are more concentrated in the sandy layers and directly below the footing. The stress states in the clay layers move away from the critical state.

Comparison between the non-creep and creep results indicates that creep causes one meter additional settlement and 1.7 degrees additional tilting. The calculated settlement is larger than the estimated value and the calculated tilting angle is smaller than the measured one.

Comparing the calculated tilting history with the measured one, one can see that creep may be an important factor during and right after the construction period. Apart from that, many other factors may have accounted to the tilting of the tower, such as leaning instability, solar energy, and other perturbations, but they cannot be quantified in the current creep model.

The two-dimensional model has certain limitations compared with a three-dimensional one in representing the complicated conditions of the tower. A fully three-dimensional visco-plastic model may improve the accuracy of the prediction.

Table 4.1 Weight, overturning moment and rigid tilt versus time

Year	Weight (MN)	Moment (MNm)	Tilt (degree)
1178	94.80	-	-
1272	137.28	5.51	0.103
1360	144.53	97.7	1.611
1990	144.53	332.56	5.469

Table 4.2 Loading conditions for elastic and elasto-plastic analyses (CF=24, $I_c = 1.27$)

Year	Δp (kPa)		$\Delta p / CF$ (kPa)	
	North	South	North	South
1178	41605.5	41605.5	1733.6	1733.6
1272	20658.8	21821.2	860.8	909.2
1360	-6100.8	13351.2	-254.2	556.3
1990	-24775.2	24775.2	-1032.3	1032.3

Table 4.3 Soil parameters for elastic analysis

layer	elevation (m)	G* (MPa)	E** (MPa)	v
made ground MG	+3 to +0.7	13.44	22.0	0.30
clayey silts A ₁ and A ₁ '	variable	13.44	11.0	0.30
upper Pancone clay B ₁ -B ₃	-7.4 to -17.8	10.27	23.0	0.30
intermediate clays B ₃ -B ₅	-17.8 to -22.0	15.18	34.0	0.30
lower clays B ₅ -B ₁₀	-24.4 to -37.0	22.32	50.0	0.30
layer	elevation (m)	E (MPa)		v
upper gray sands A ₁ ''-A ₂	variable	13.0		0.30
intermediate sands B ₆	-22.0 to -24.4	18.0		0.30

*-- average value from Calabresi et al. (1992) TAB 5.XIV:

**-- $E=2(1+\nu)*G$.

Table 4.4 Cam-clay parameters for the clay layers

material No.	layer	γ (kN/m ³)	C_c	C_i	Φ' (degree)	e_h	a	b	R_f	C_u
1	made ground MG	9.09	0.205	0.021	33.67	1.290	0.0046	1.220	0.89	0.0051
2	clayey silts A ₁ and A ₁ '	9.09	0.205	0.021	33.67	1.290	0.0046	1.220	0.89	0.0051
5	upper Pancone clay B ₁	7.32	0.615	0.081	26.54	2.730	0.0063	1.548	0.89	0.0154
6	upper Pancone clay B ₂	7.32	0.615	0.081	26.54	2.730	0.0038	1.548	0.89	0.0154
7	upper Pancone clay B ₃	7.32	0.615	0.081	26.54	2.730	0.0057	1.548	0.89	0.0154
8	intermediate clays B ₄	10.21	0.297	0.062	28.62	1.524	0.0095	1.351	0.89	0.0059
9	intermediate clays B ₅	10.21	0.297	0.062	28.62	1.524	0.0055	1.351	0.89	0.0059
11	lower clay B ₇	9.21	0.421	0.053	25.84	2.053	0.0051	1.538	0.89	0.0098
12	lower clays B ₈	9.21	0.421	0.053	25.84	2.053	0.0039	1.650	0.89	0.0098
13	lower clays B ₉	9.21	0.421	0.053	25.84	2.053	0.0039	1.650	0.89	0.0098
14	lower clays B ₁₀	9.21	0.421	0.053	25.84	2.053	0.0039	1.650	0.89	0.0098

Note: Material No. 3, 4, and 10 are the sandy layers, they are tabulated in the next table.

Table 4.5 Soil parameters for the sandy layers

material No.	layer	γ (kN/m ³)	E * (MPa)	ν *	ϕ'
3	Silty sand A ₁ ''	8.39	13.0	0.12	34
4	upper gray sand A ₂	8.39	13.0	0.12	34
10	intermediate sand B ₆	9.29	18.0	0.12	34.3
15	rigid footing	9.09	1*10 ⁷	0.12	-

Note: All the rest of materials are clay and clayey silt, they are tabulated in the previous table.

*--from Calabresi et al. (1992) TAB5.XV.

Table 4.6 Singh and Mitchell parameters (from Mitchell and Soga 1995)

Sample	layer	$\bar{\alpha}$	m	A' (%/min.)	A (%/year)
4m	clayey silt A ₁	5.81	0.89	2.12*10 ⁻²	9.03*10 ⁻²
6m	clayey silt A ₁ '	5.86	0.95	2.19*10 ⁻²	4.23*10 ⁻²
10m	upper clay B ₁	6.33	0.83	1.62*10 ⁻²	15.21*10 ⁻²
14m	upper clay B ₂	6.39	0.86	8.35*10 ⁻³	5.279*10 ⁻²
19m	upper clay B ₃	8.82	0.75	2.15*10 ⁻³	5.789*10 ⁻²

Note: $A = A' * (365*24*60)^{(1-m)}$

Due to the lack of creep test data, and the fact that layer B₃ is highly structured soil, creep parameters from layer B₂ were assumed to represent those of B₄ to B₁₀.

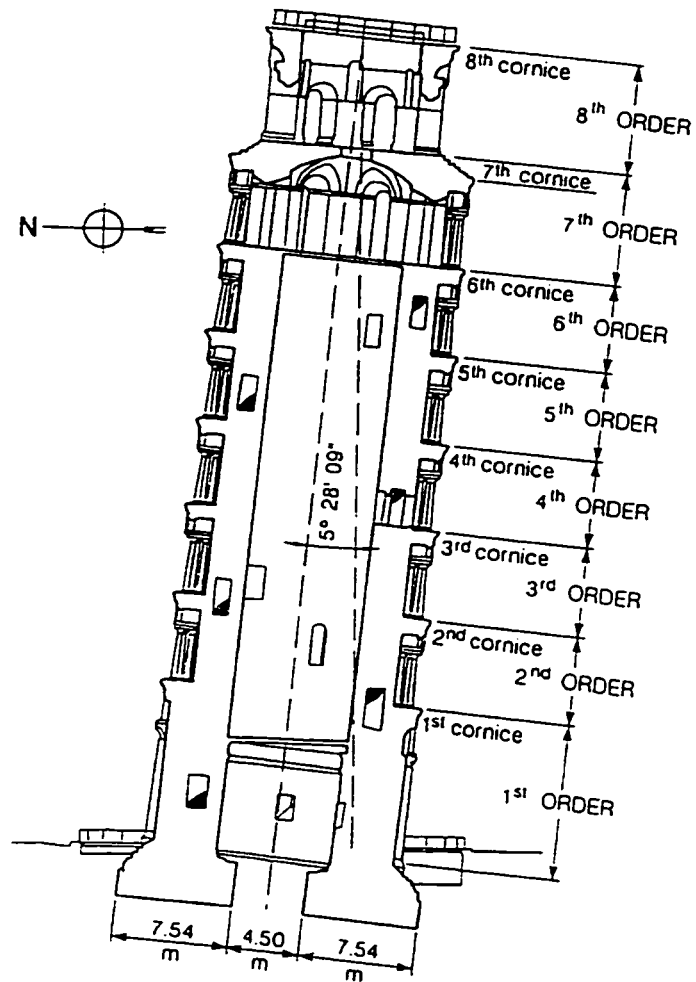


Fig. 4.1 Geometrical characteristics of Pisa Tower
 (after Jamiolkowski et al., 1993)

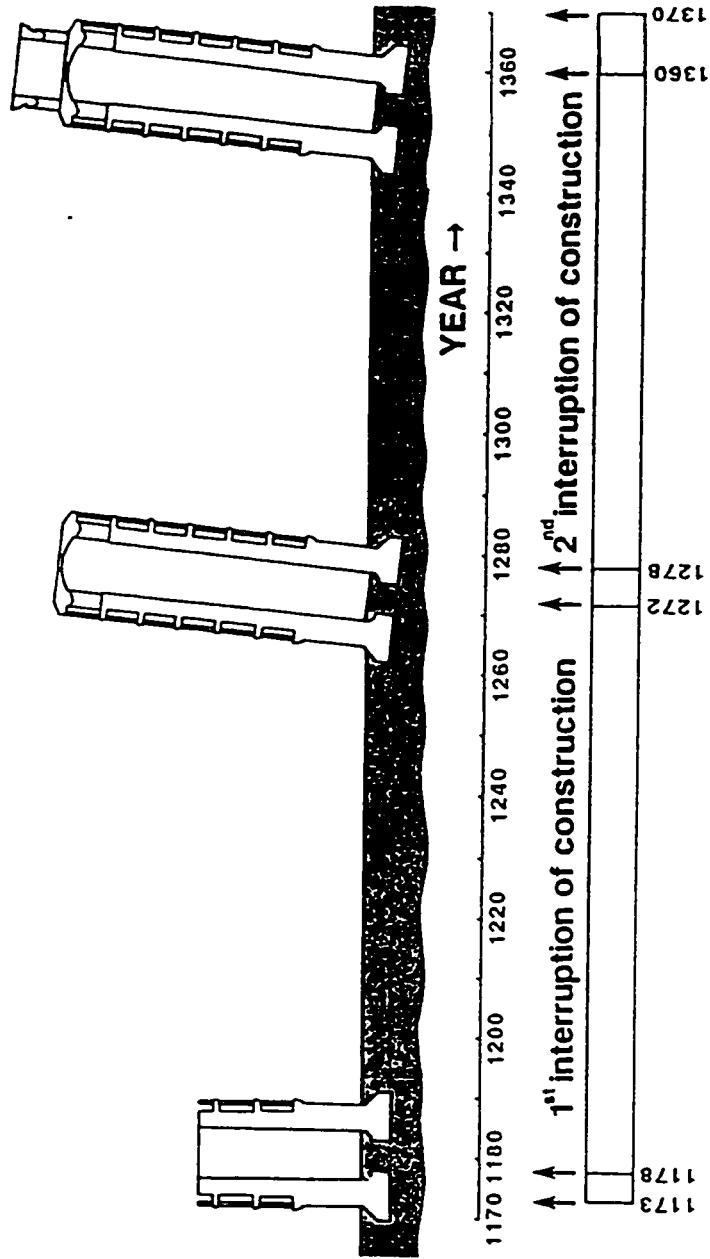


Fig. 4.2 Construction history (after Jamiolkowski et al., 1993)

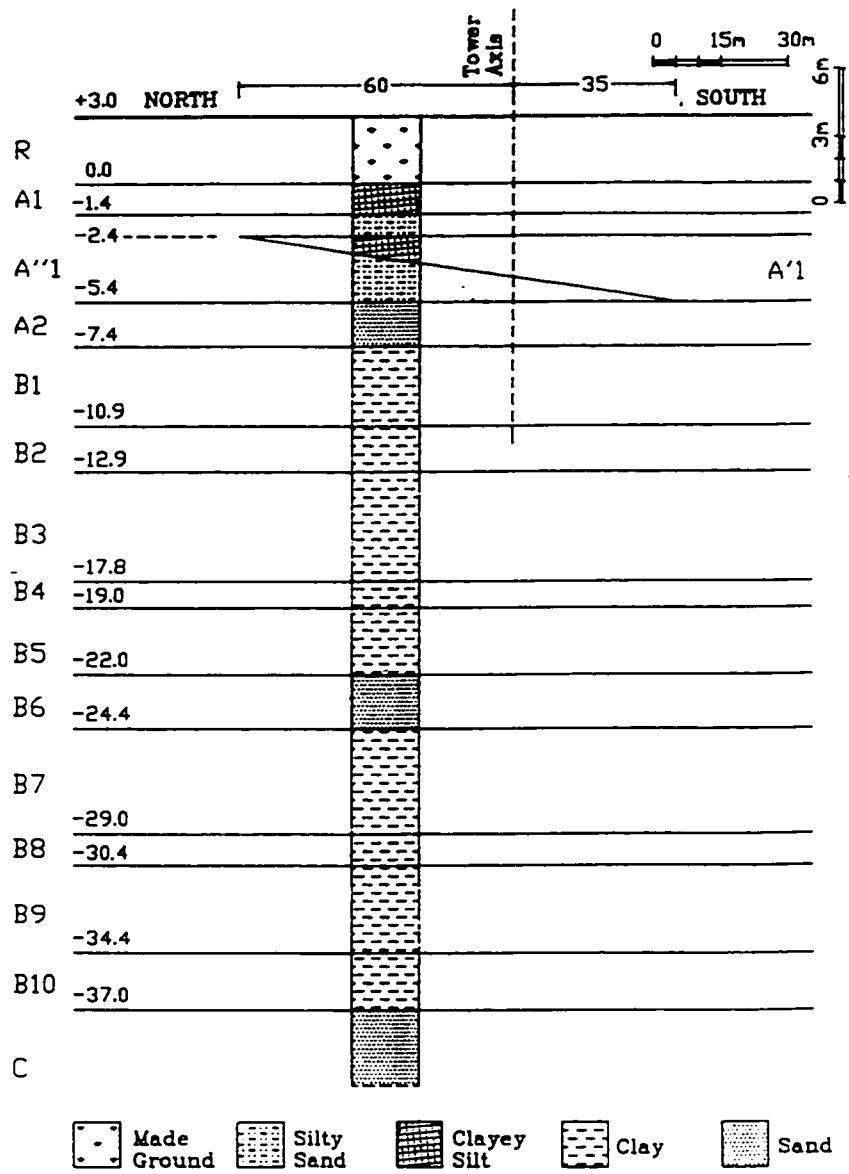


Fig. 4.3 Probable initial soil profile at the site of Pisa Tower (Calabresi et al., 1992)

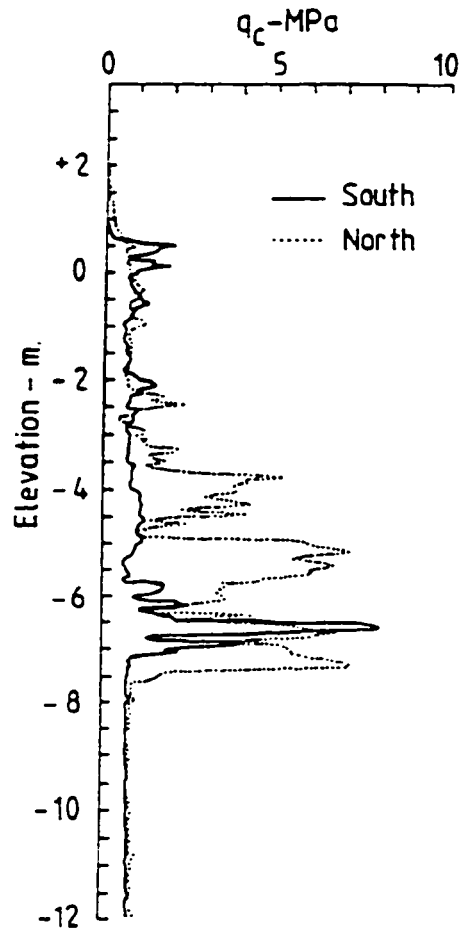


Fig. 4.4 Comparison of cone resistance profiles (Burland and Potts, 1994)

Pisa Tower (1990) Present condition

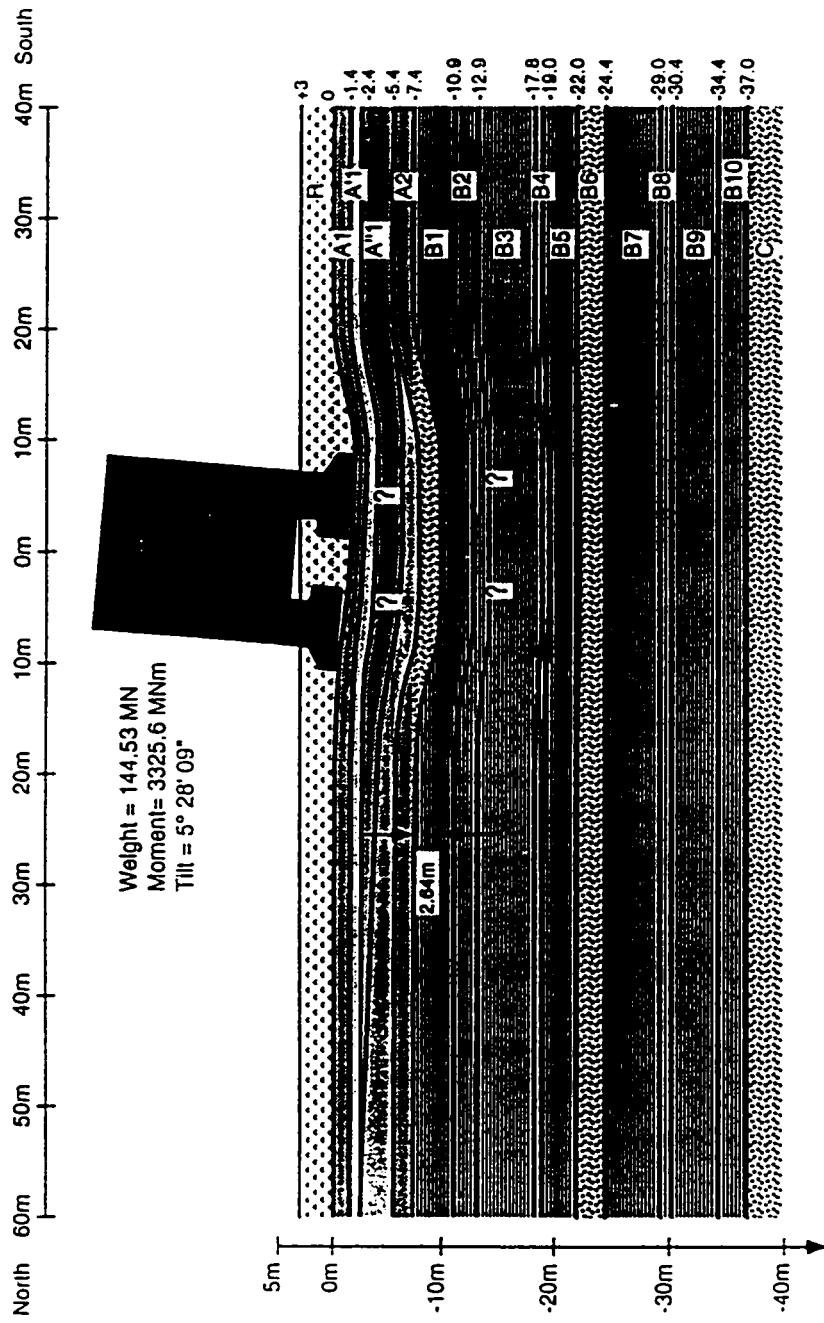


Fig. 4.5 Current soil condition at the tower (after Mitchell and Soga, 1995)

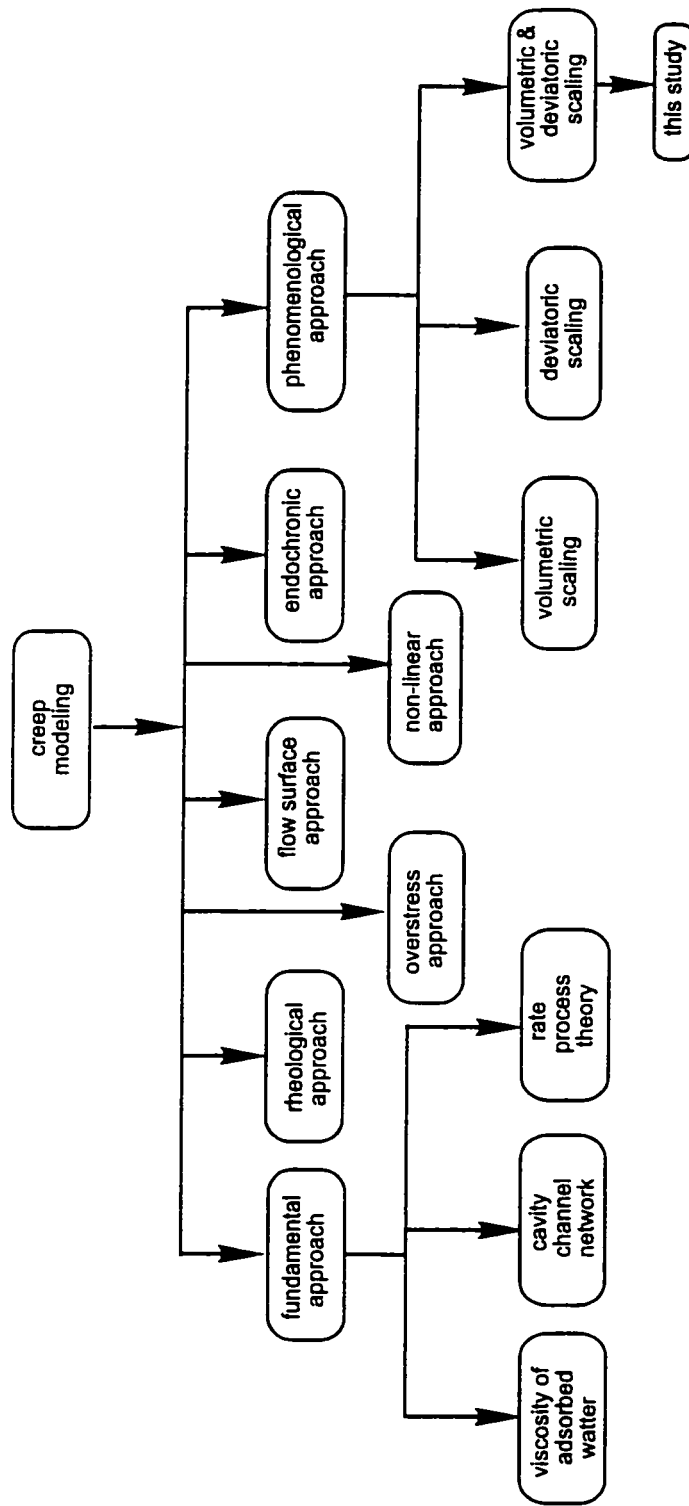


Fig. 4.6 Schematic show of existing approaches of creep modelling

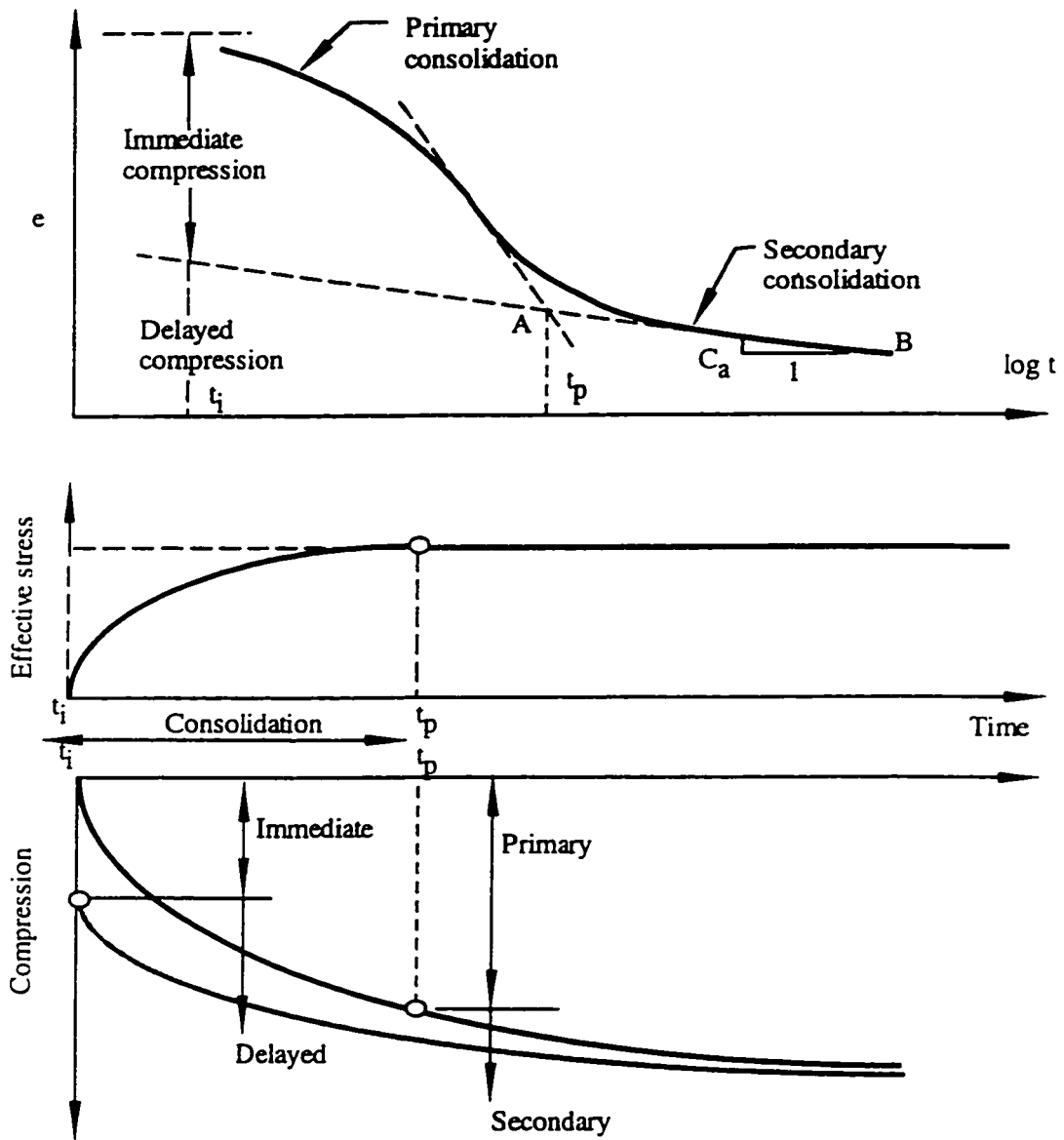


Fig. 4.7 Definition of primary and secondary consolidation and immediate and delayed compression (modified after Borja and Kavazanjian, 1995)

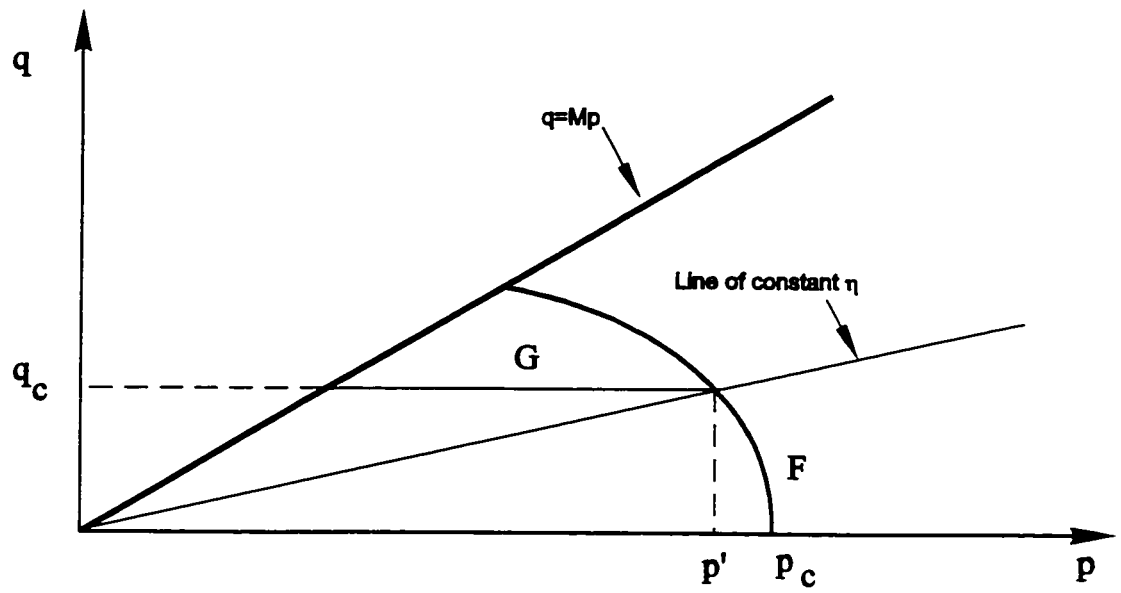


Fig. 4.8. Projection of double yield surface on p-q plane

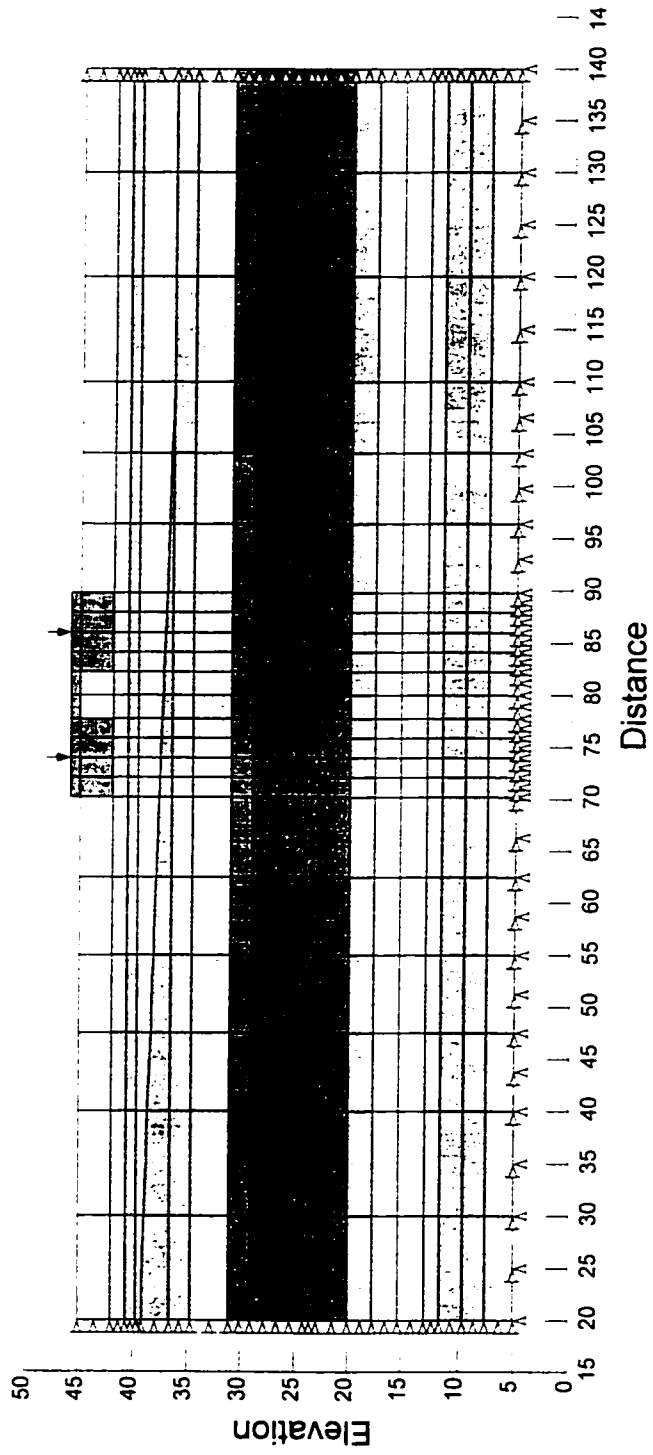


Fig. 4.9 Finite element mesh for two-dimensional analysis

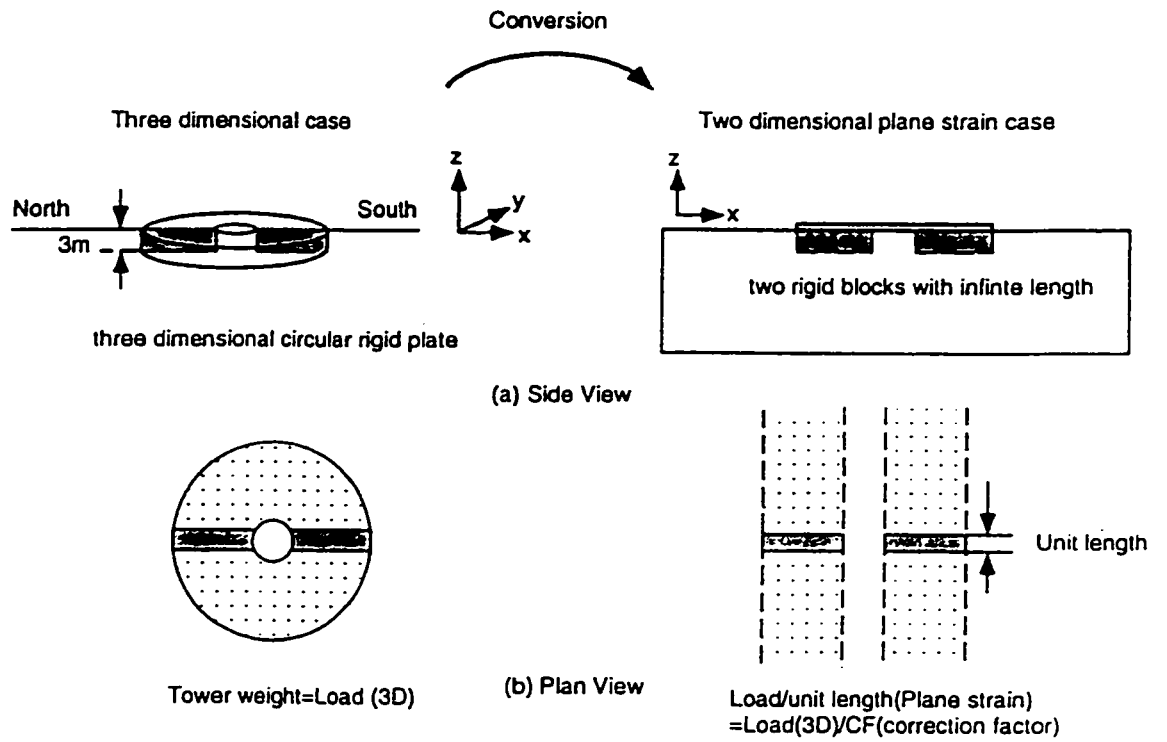


Fig. 4.10 Conversion of three dimensional condition to plane strain condition
(after Mitchell and Soga, 1995)

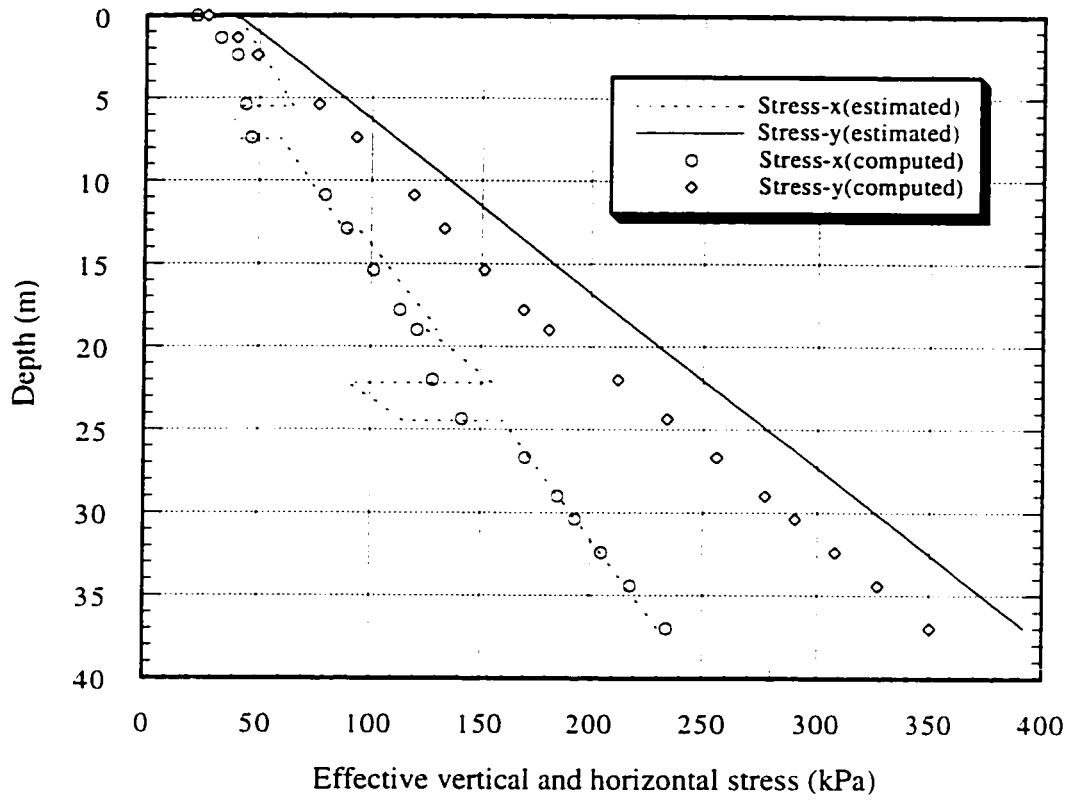


Fig. 4.11 Calculated and observed in-situ stress versus depth

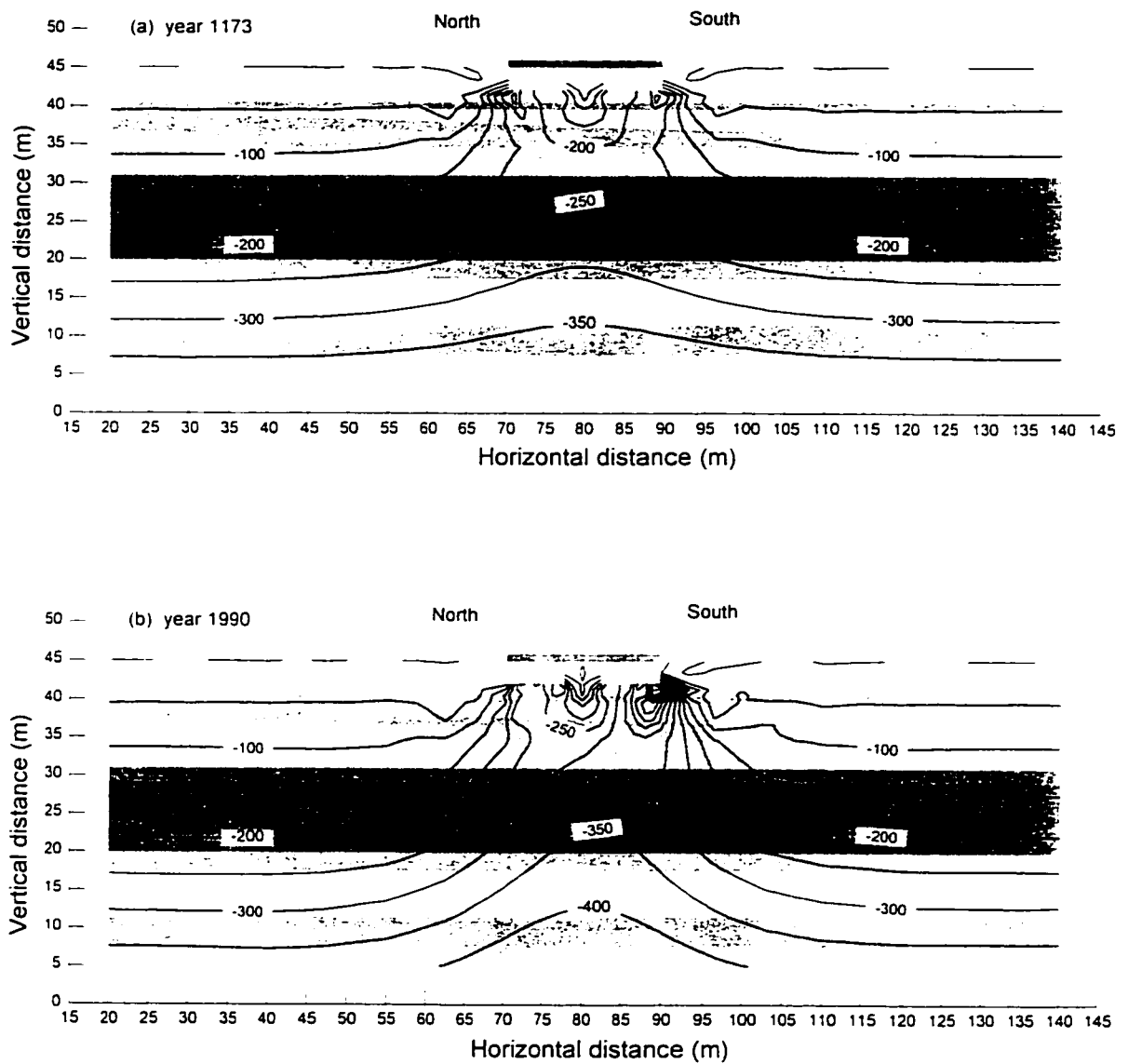


Fig. 4.12 Vertical stress contours (elasto-plastic analysis)

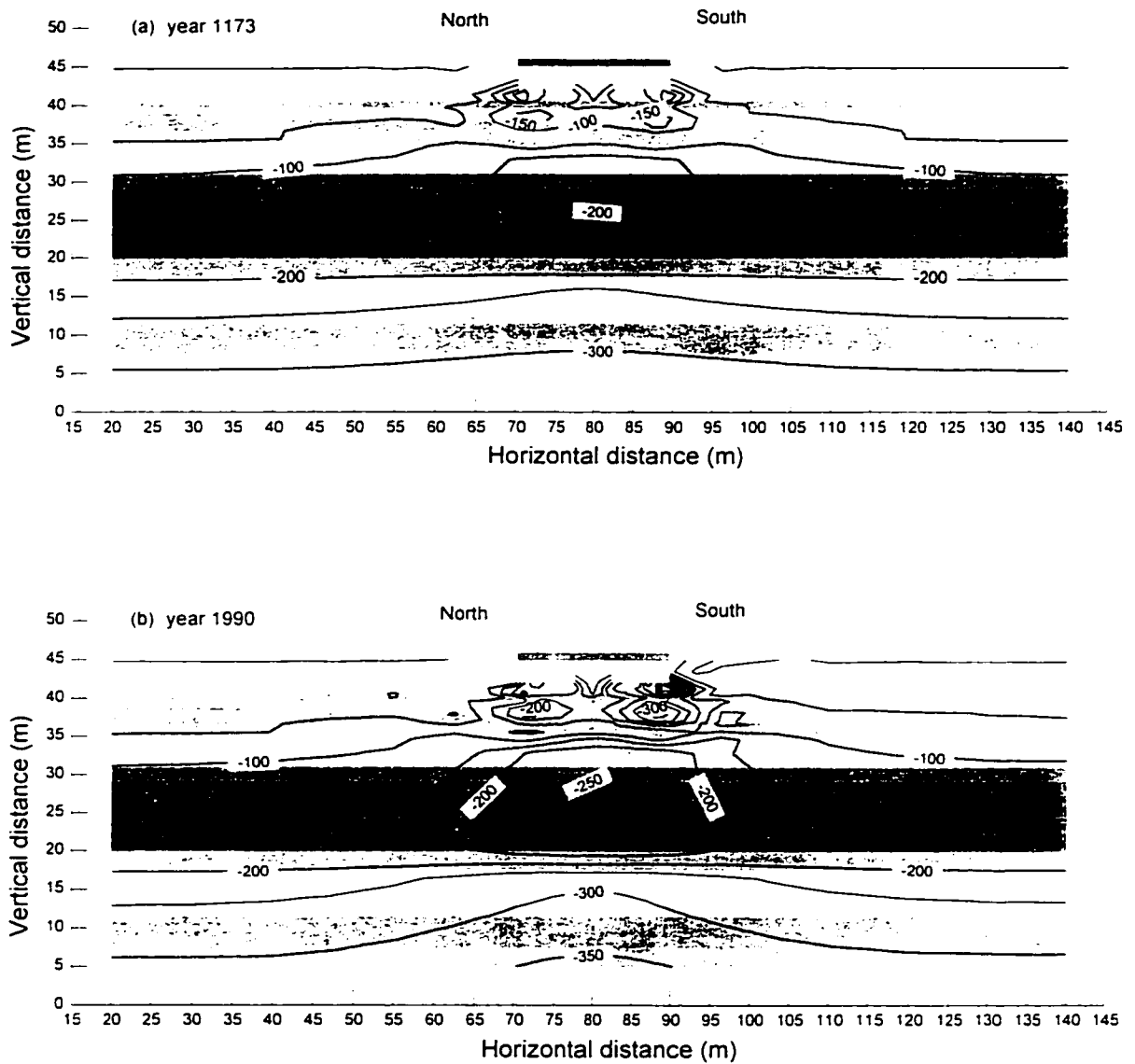


Fig. 4.13 Mean stress contours (elasto-plastic analysis)

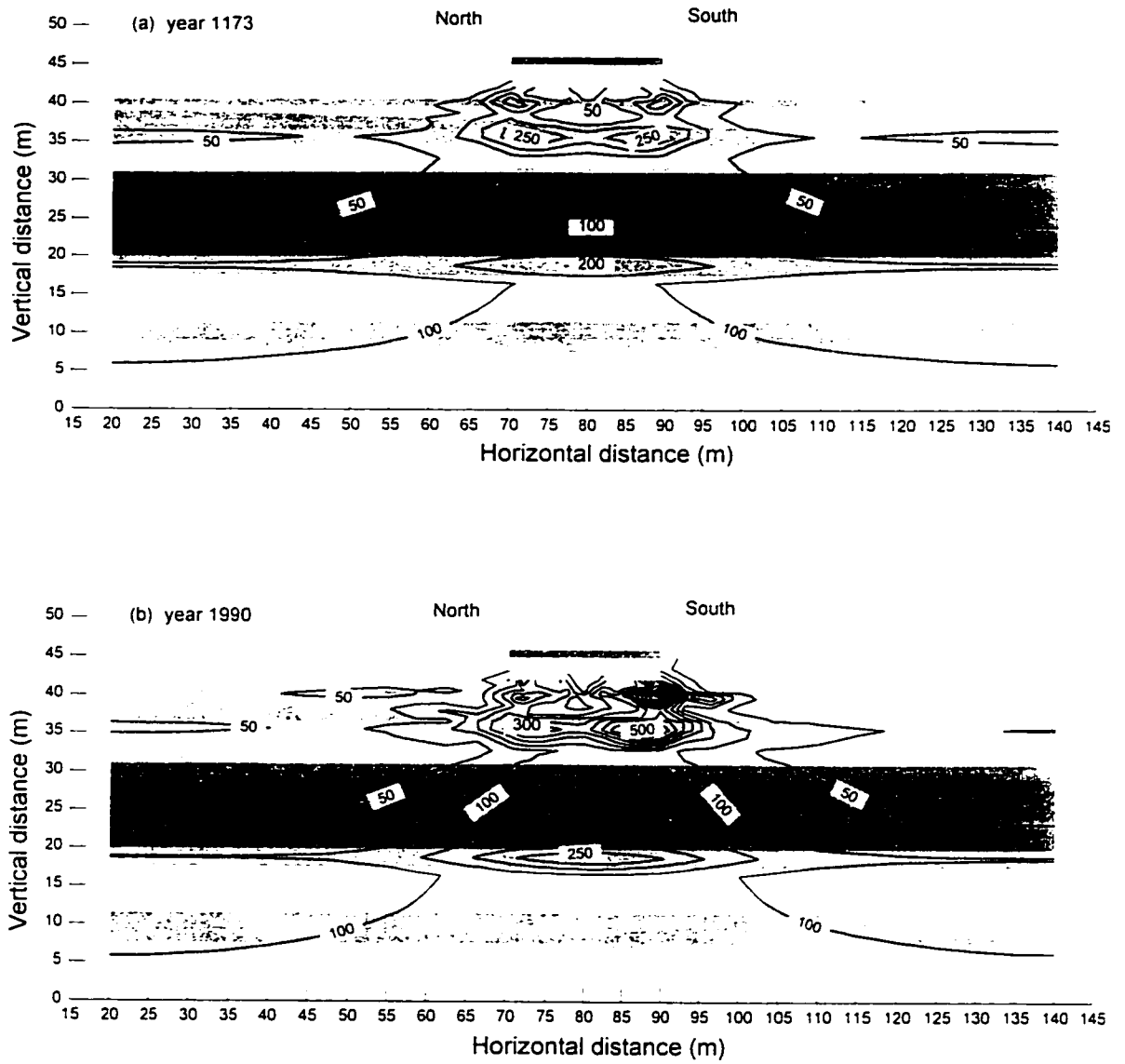


Fig. 4.14 Deviatoric stress contours (elasto-plastic analysis)

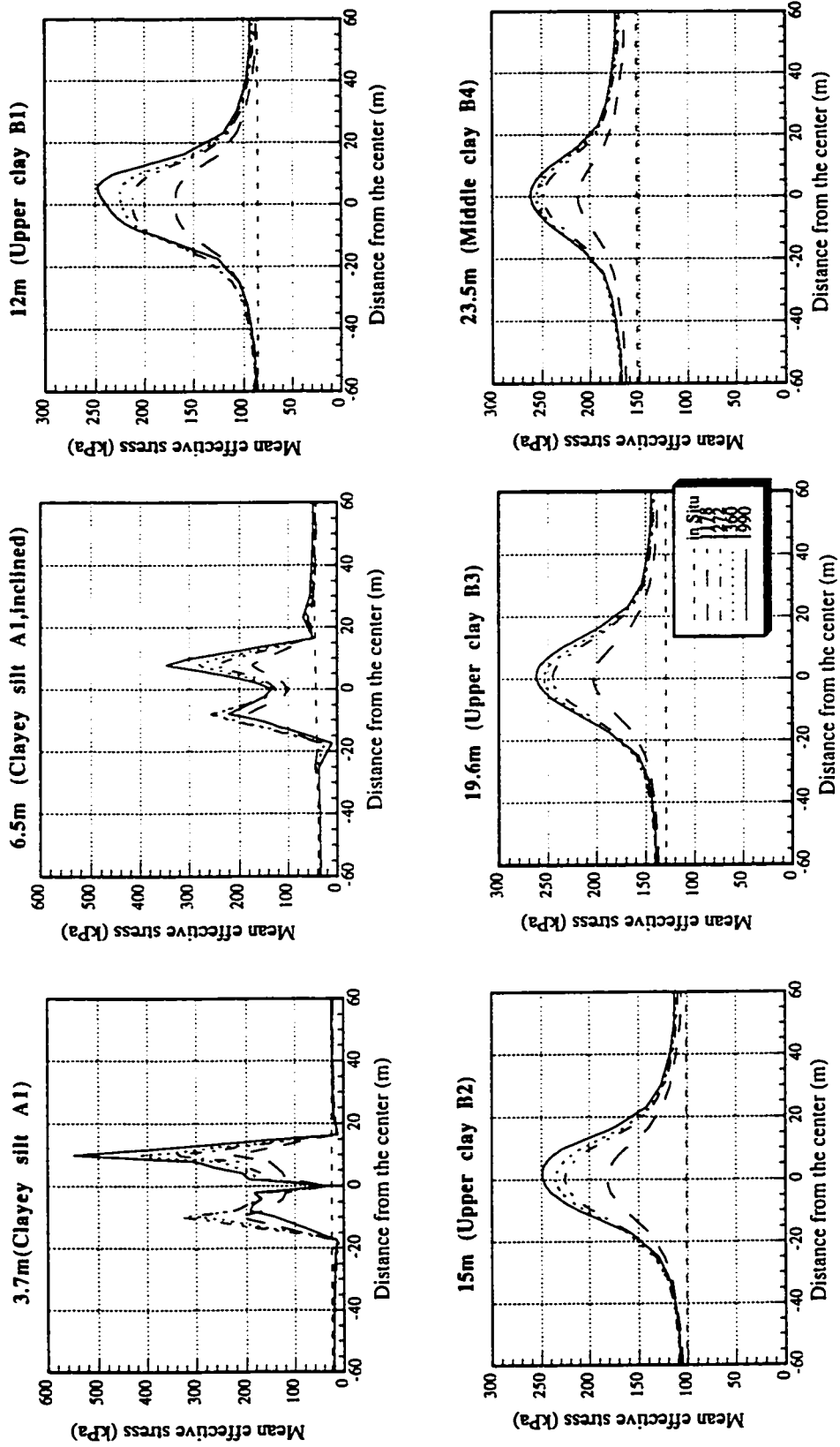


Fig. 4.15 Mean stress distributions at various depths (elasto-plastic analyses)

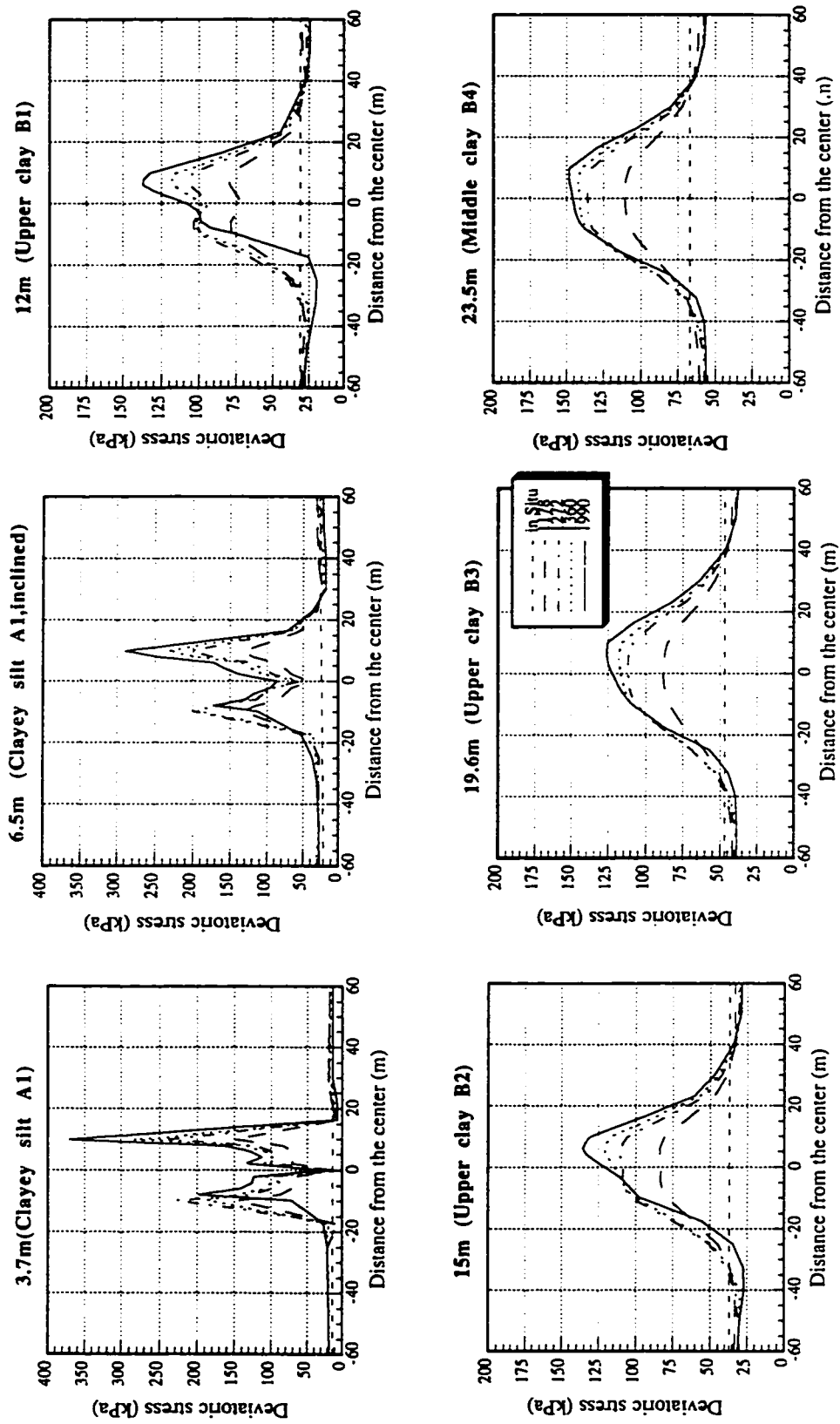


Fig. 4.16 Deviatoric stress distributions at various depths (elasto-plastic analyses)

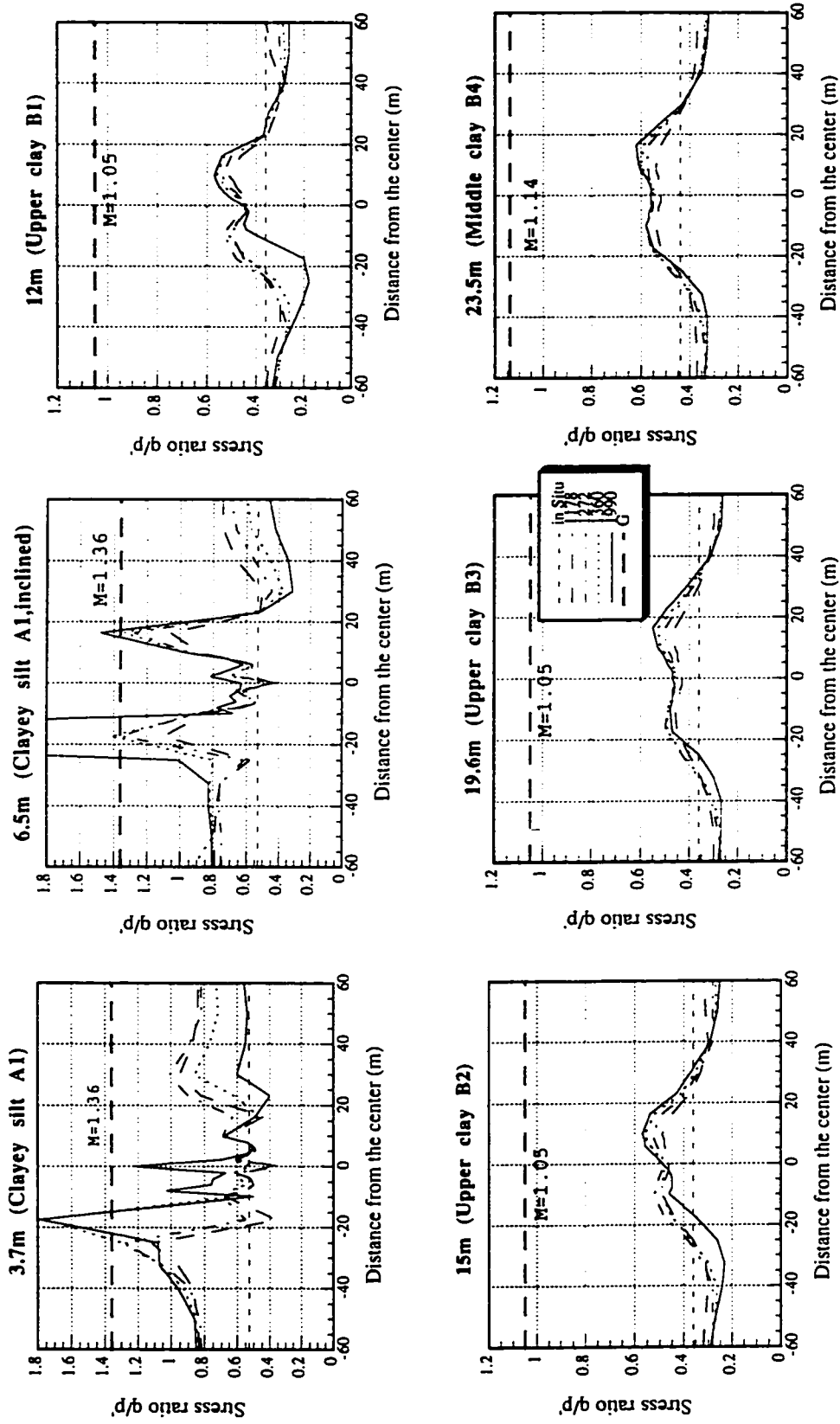


Fig. 4.17 Stress ratio distributions at various depths (elasto-plastic analyses)

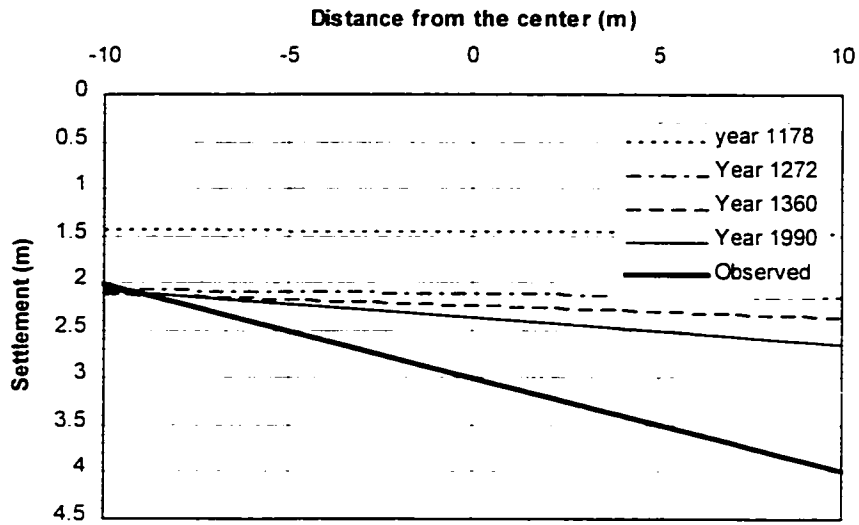


Fig. 4.18 Settlement of the footing ($CF=24$, $I_c=1.27$, elasto-plastic analyses)

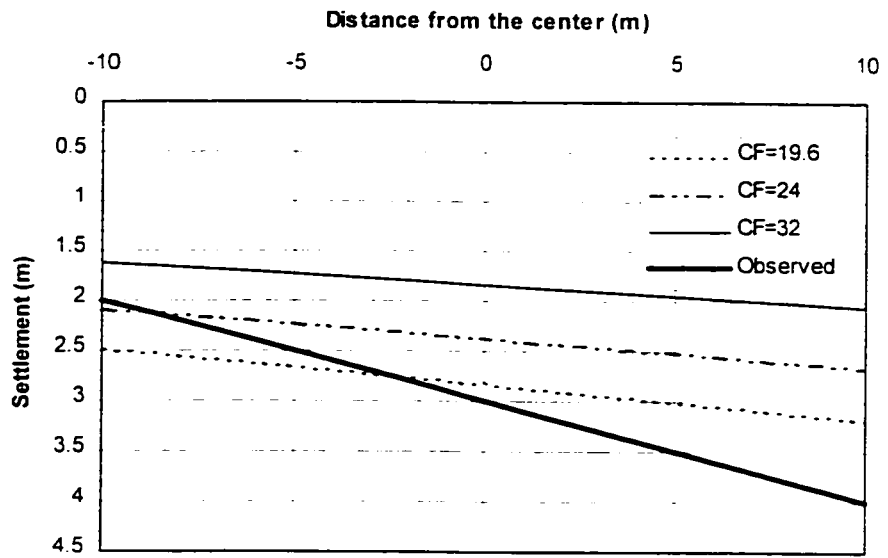


Fig. 4.19 Influence of CF on the final settlement of the footing ($I_c=1.27$)

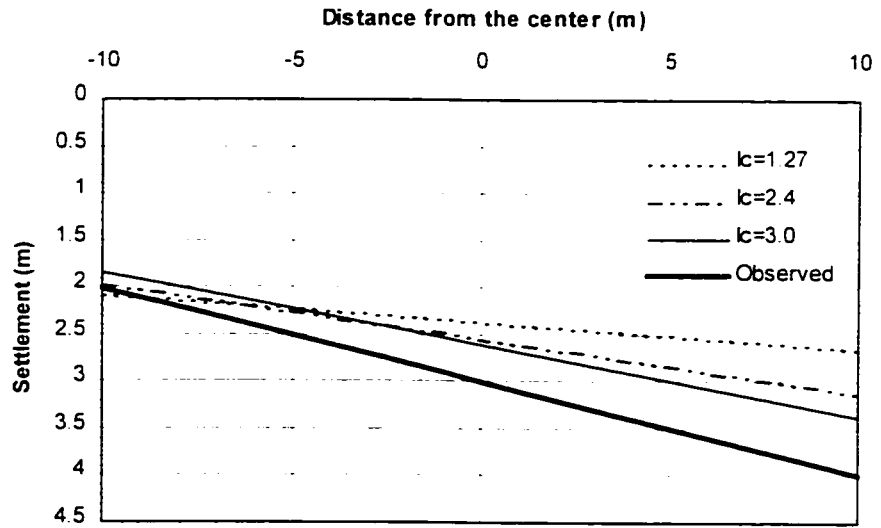


Fig. 4.20 Influence of I_c on the final settlement of the footing (CF=24)

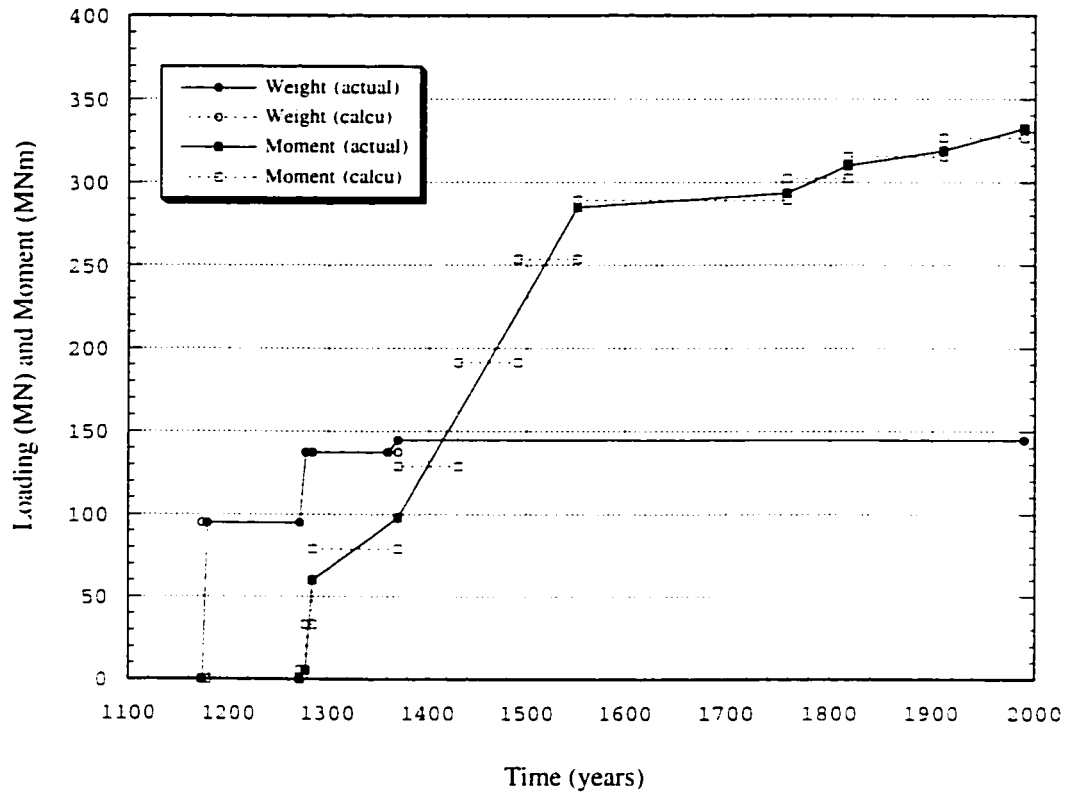


Fig. 4.21 Pisa Tower weight and overturning moment versus time

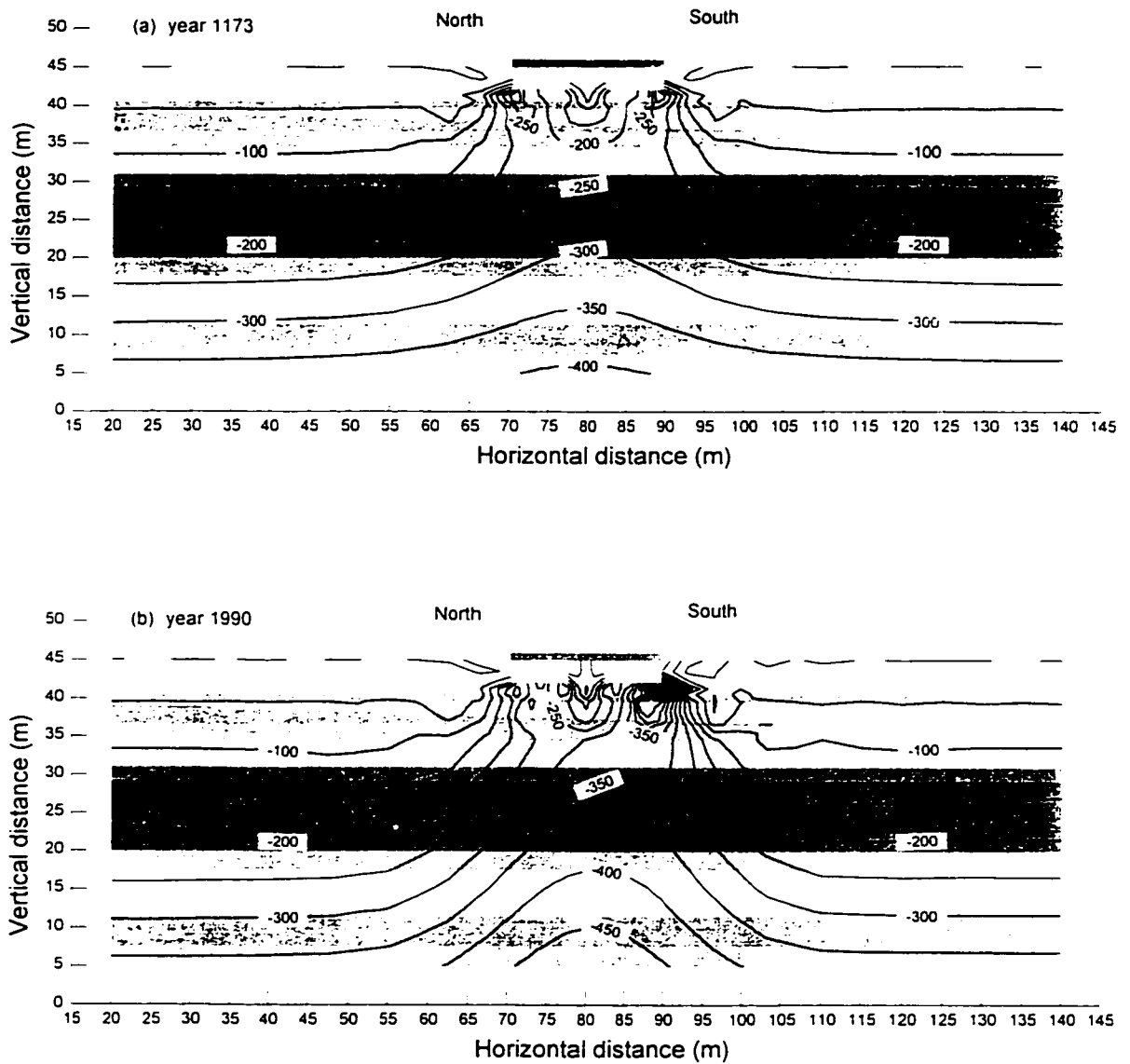


Fig. 4.22 Vertical stress contours (visco-plastic analysis)

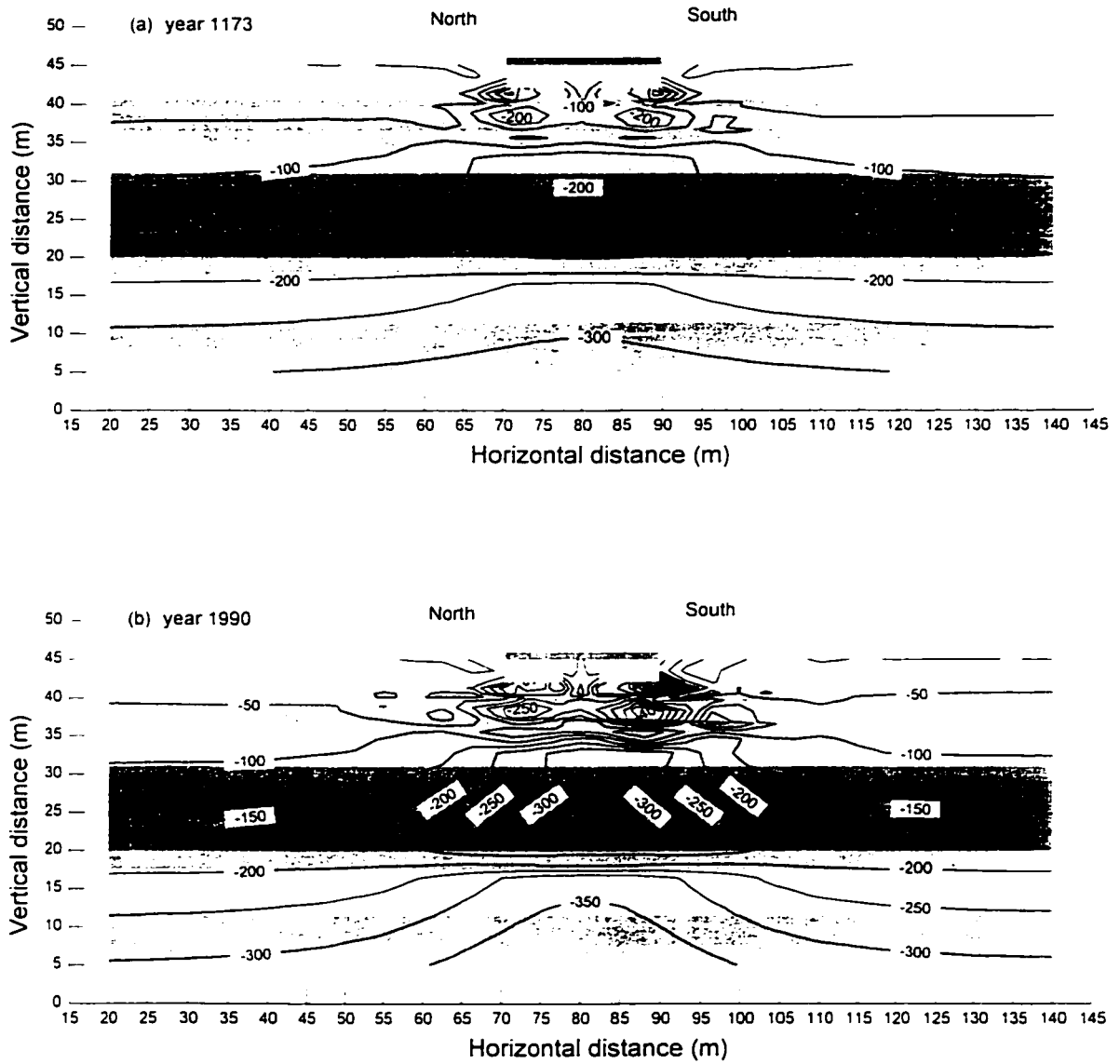


Fig. 4.23 Mean stress contours (visco-plastic analysis)

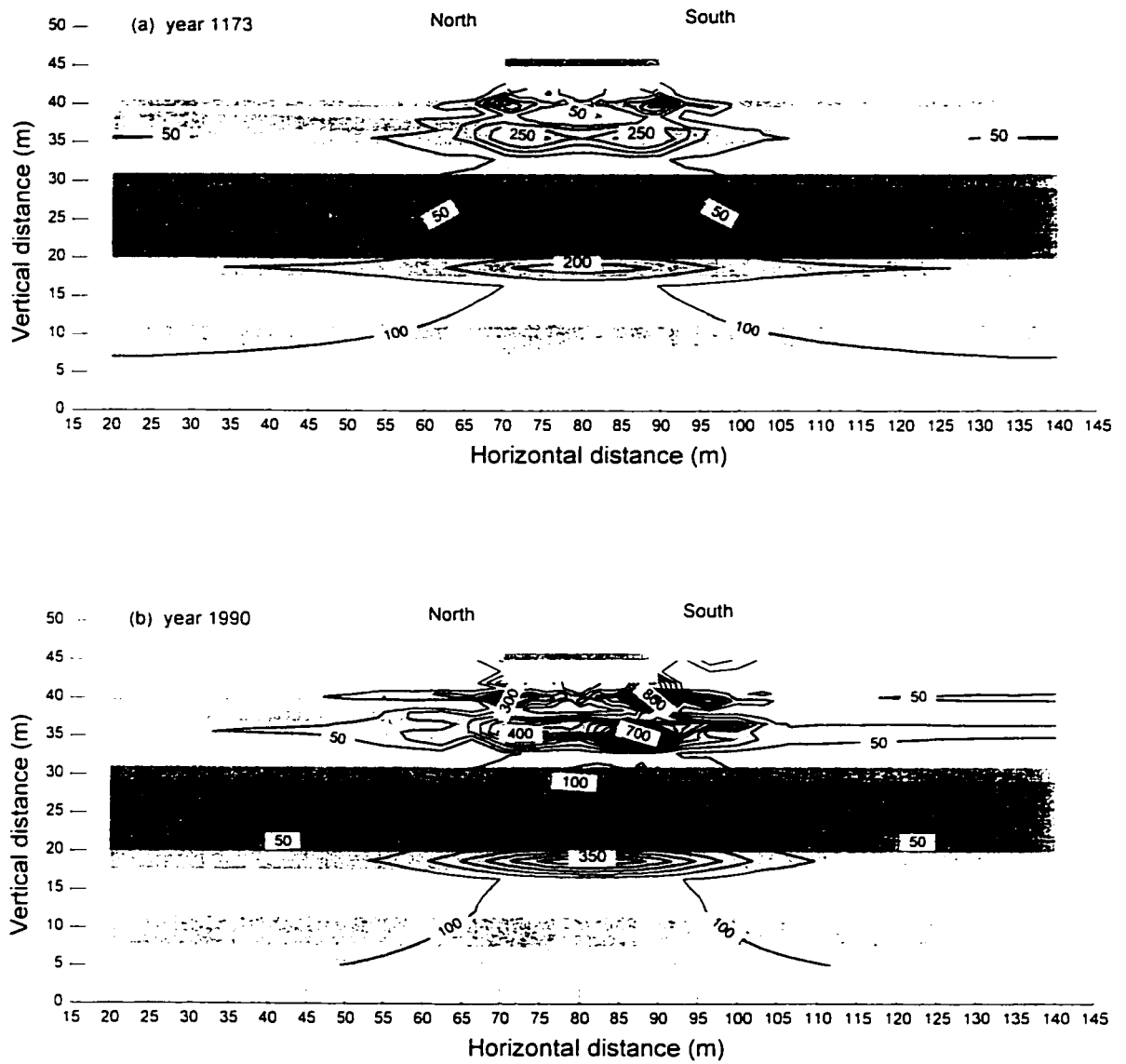


Fig. 4.24 Deviatoric stress contours (visco-plastic analysis)

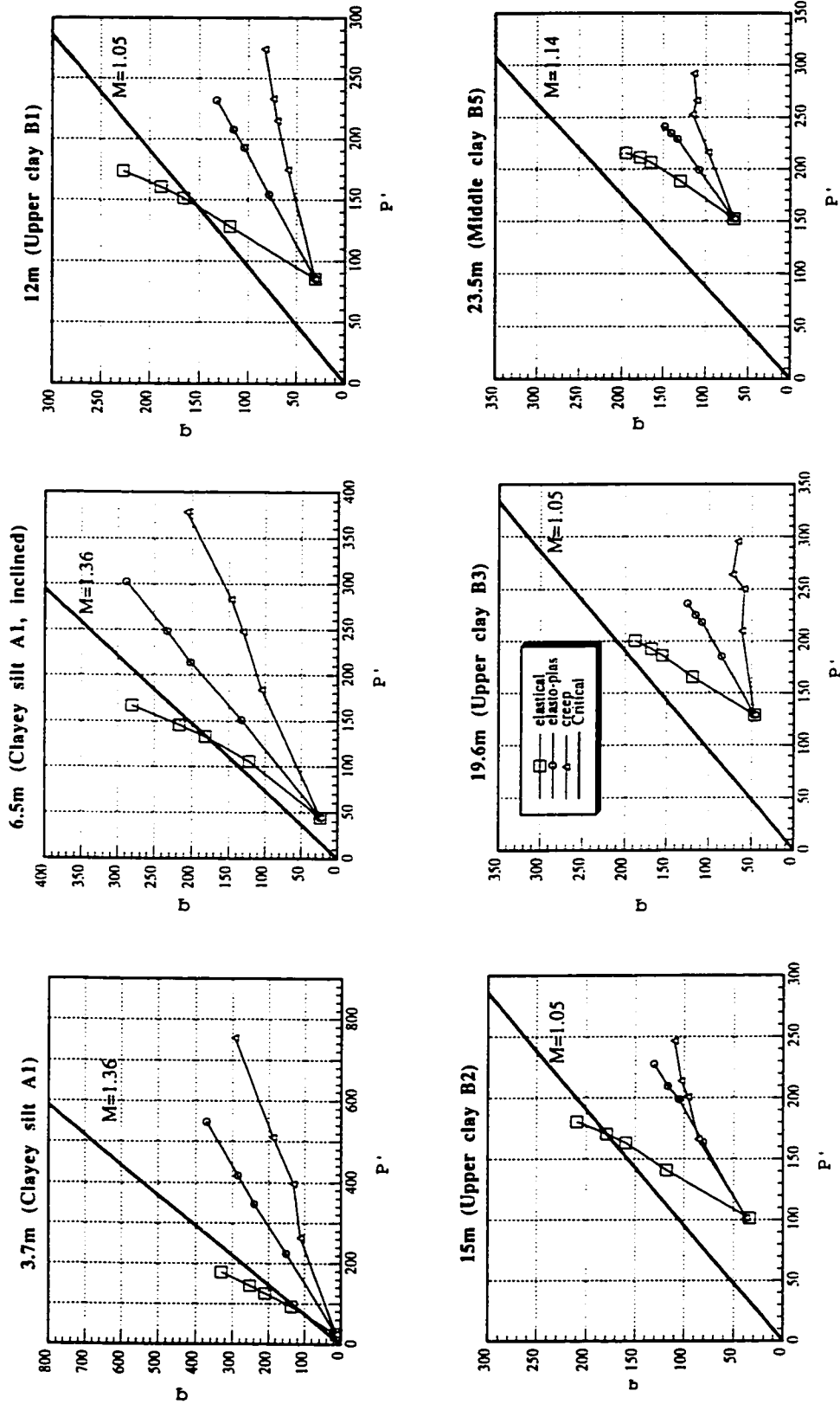


Fig. 4.25 (a) Stress path at 9.8m south

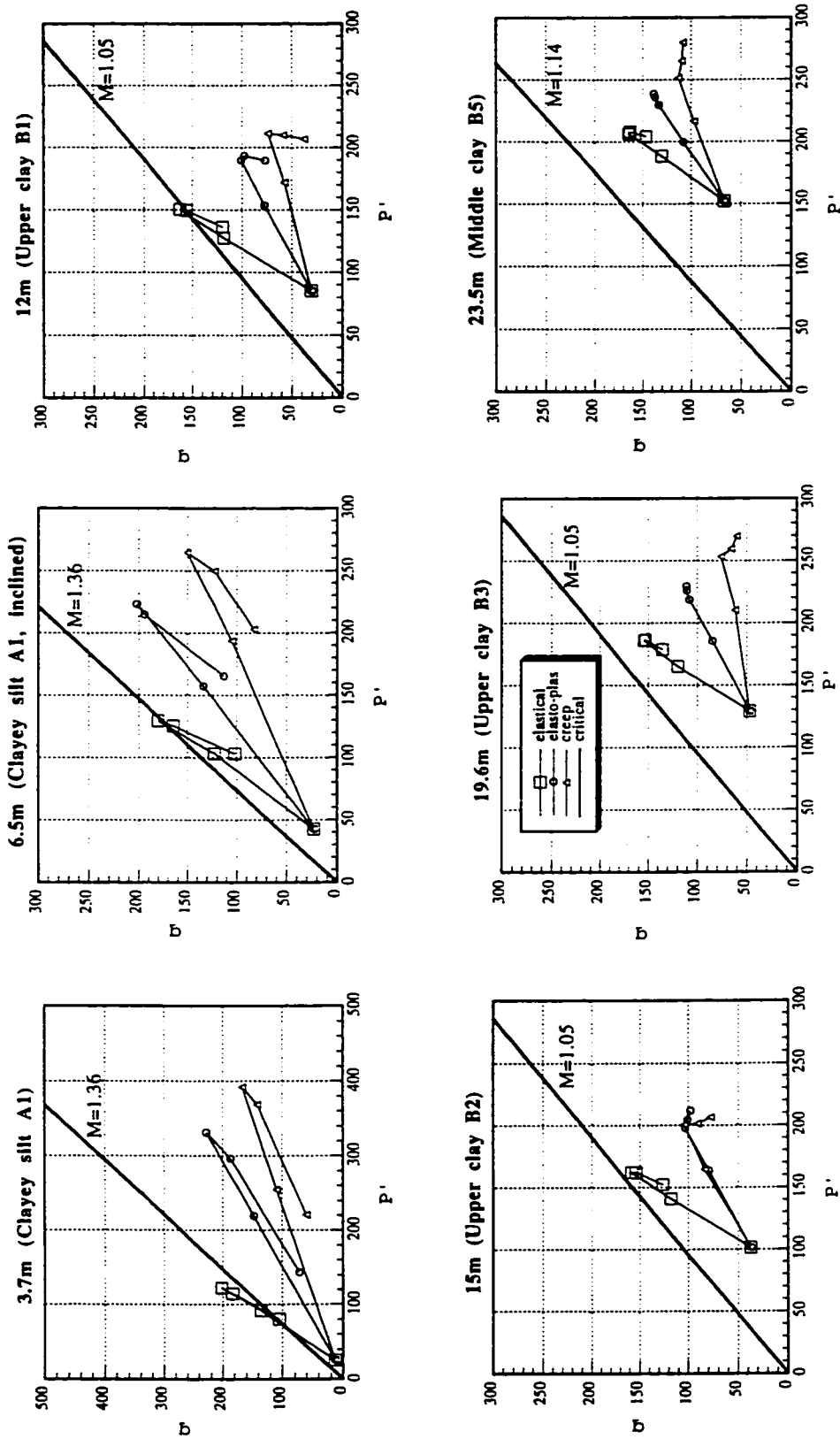


Fig. 4.25 (b) Stress path at 9.8m north

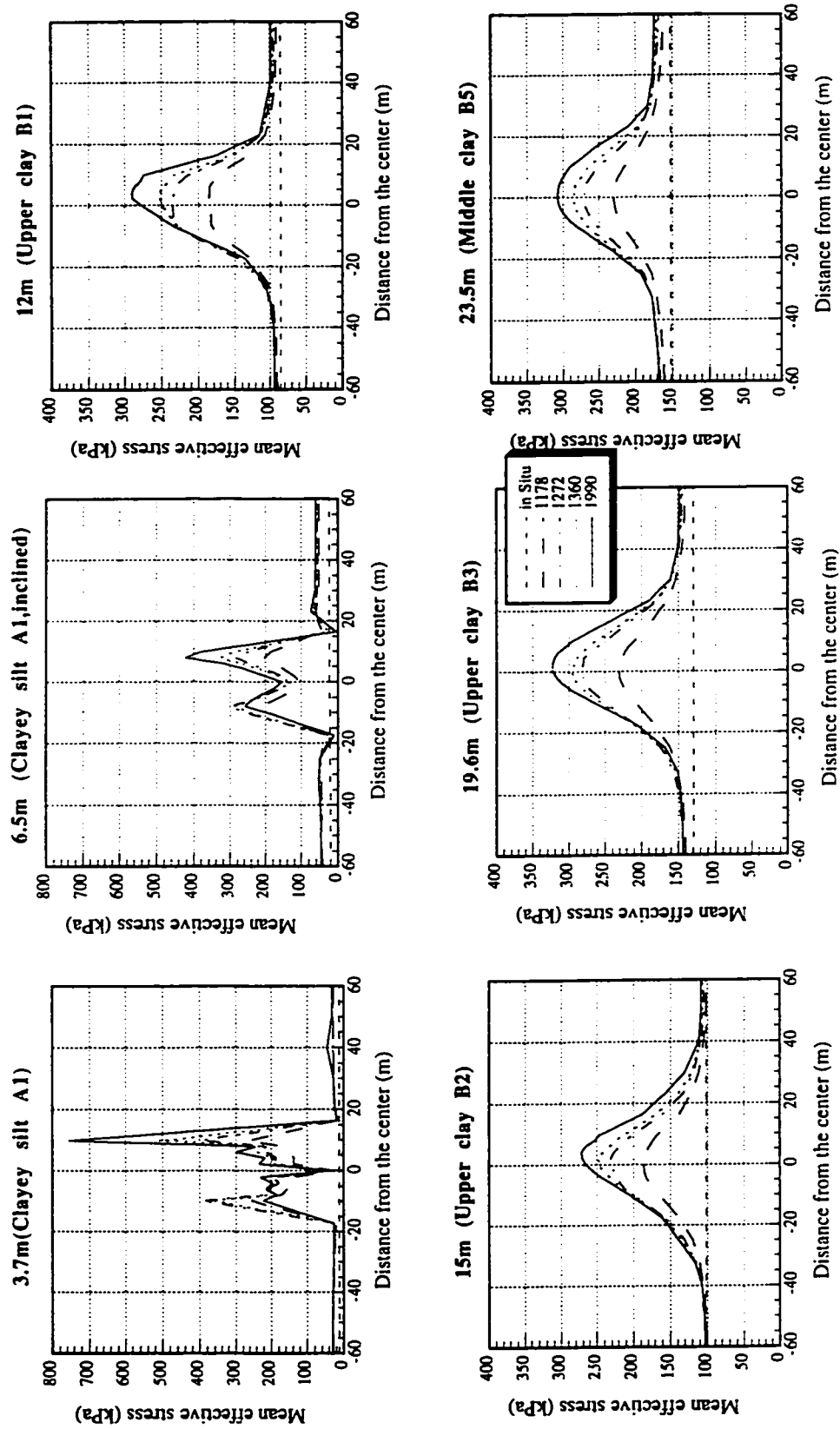


Fig. 4.26 Mean stress distributions at various depths (visco-plastic analyses)

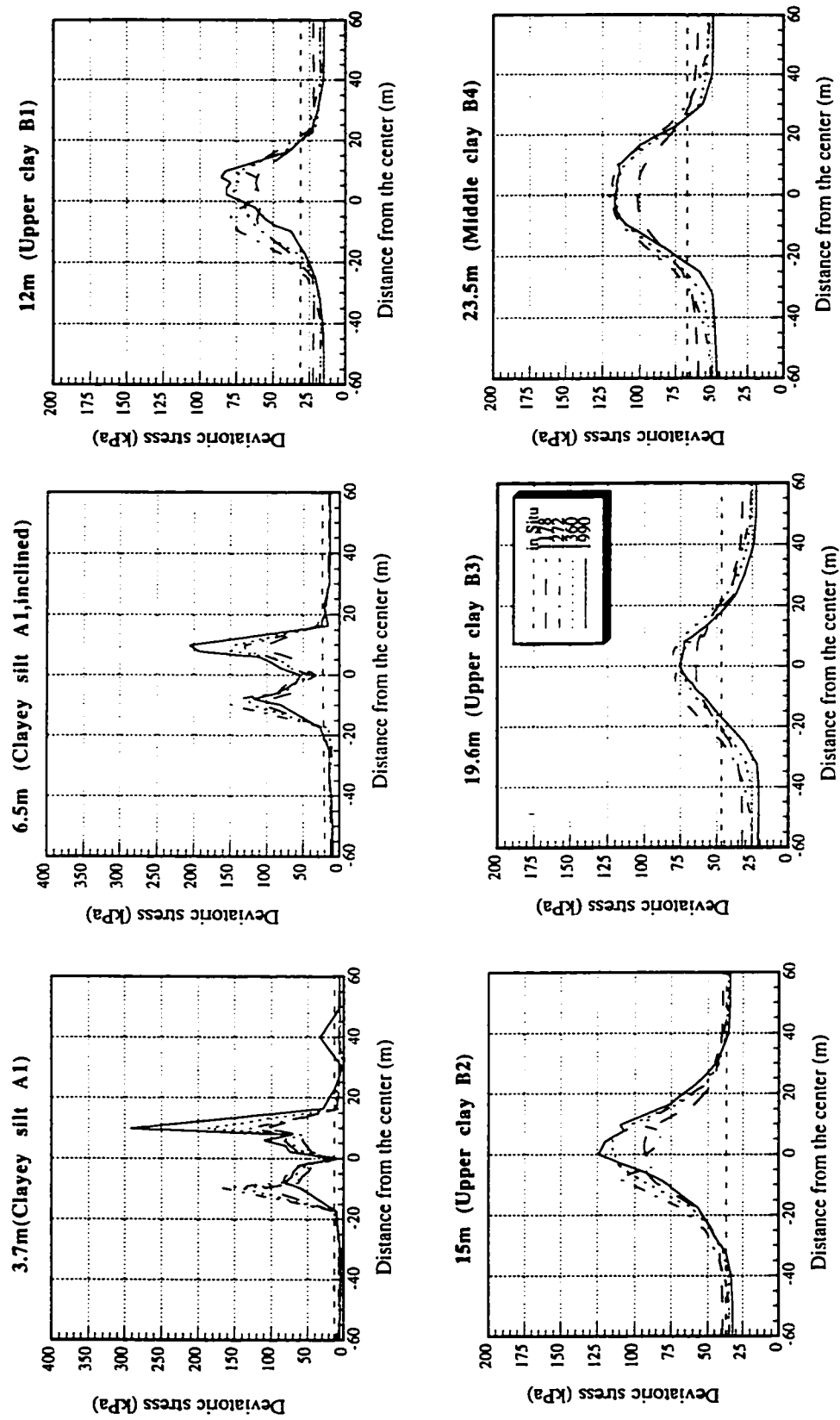


Fig. 4.27 Deviatoric stress distributions at various depths (visco-plastic analyses)

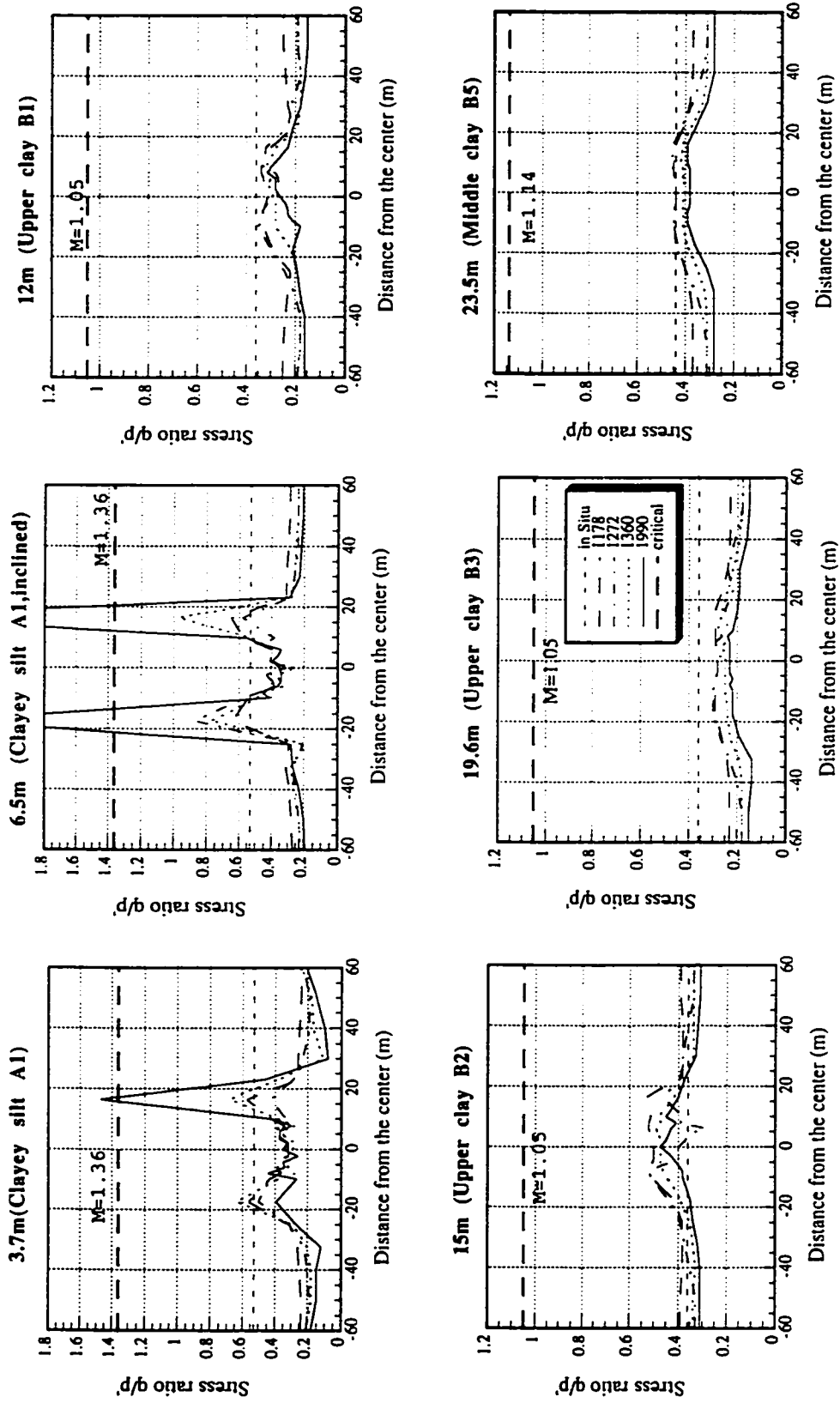


Fig. 4.28 Stress ratio distributions at various depths (visco-plastic analyses)

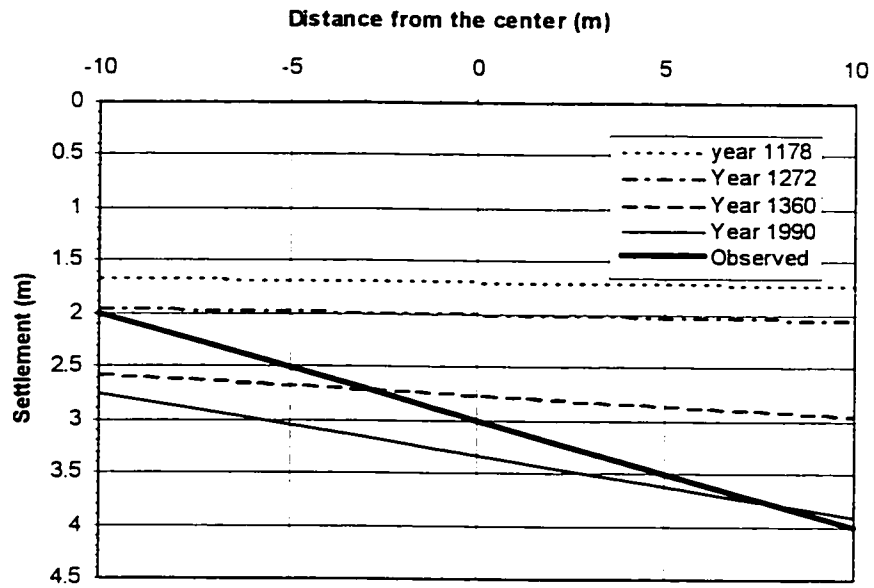


Fig 4.29 Settlement of the footing ($CF=24$, $I_c=1.27$, visco-plastic analyses)

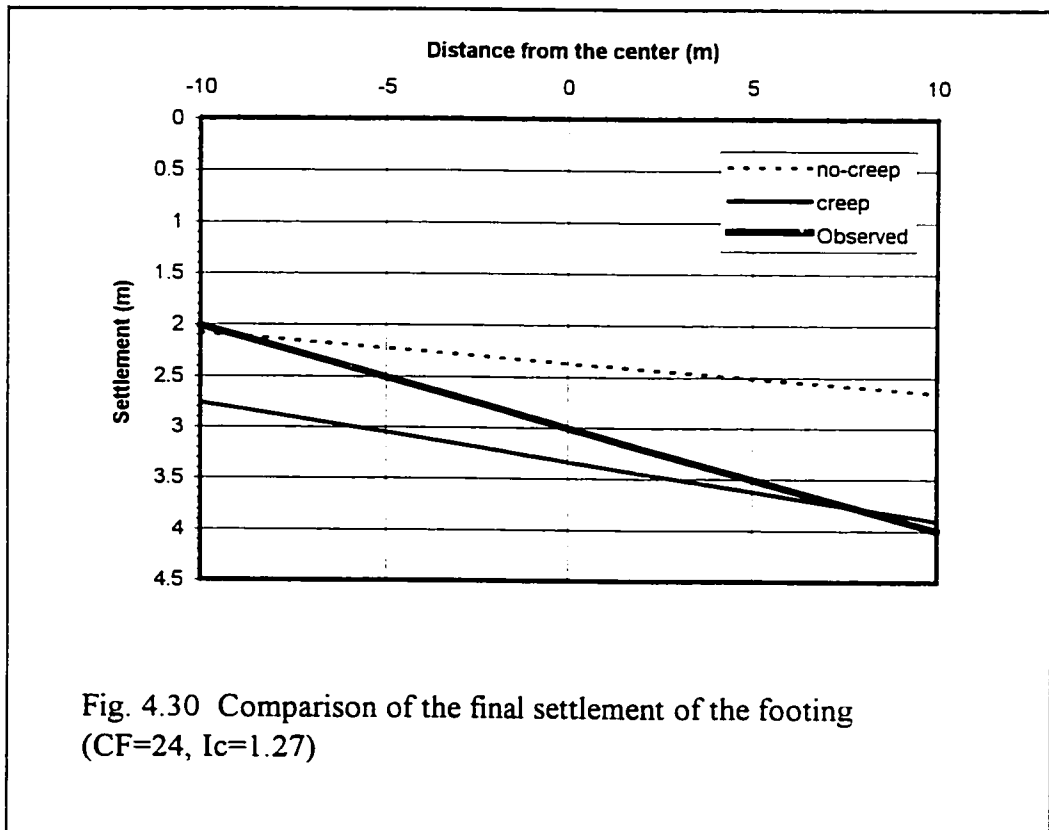


Fig. 4.30 Comparison of the final settlement of the footing ($CF=24$, $I_c=1.27$)

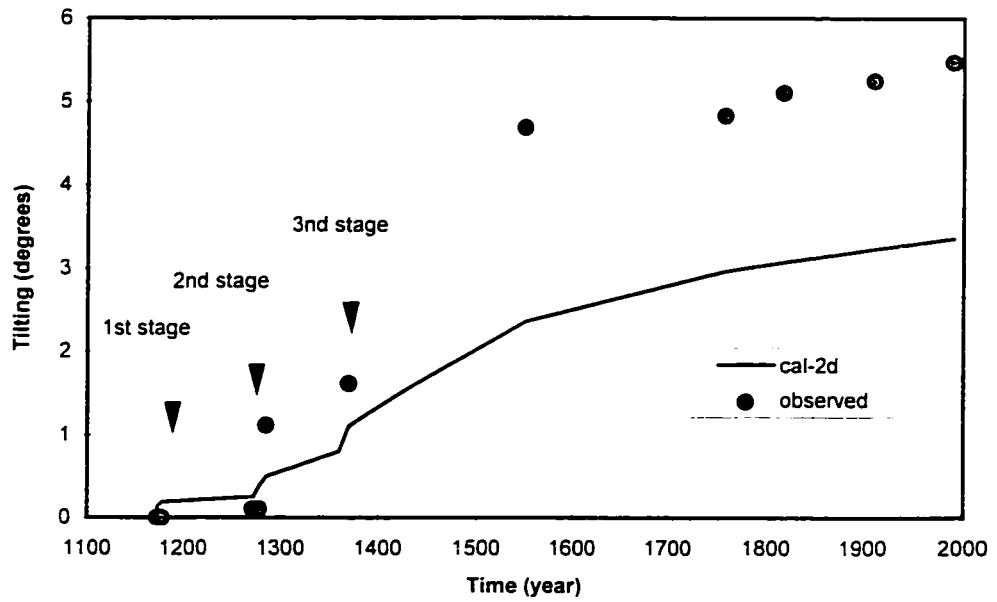


Fig. 4.31 (a) Tilting history of the tower

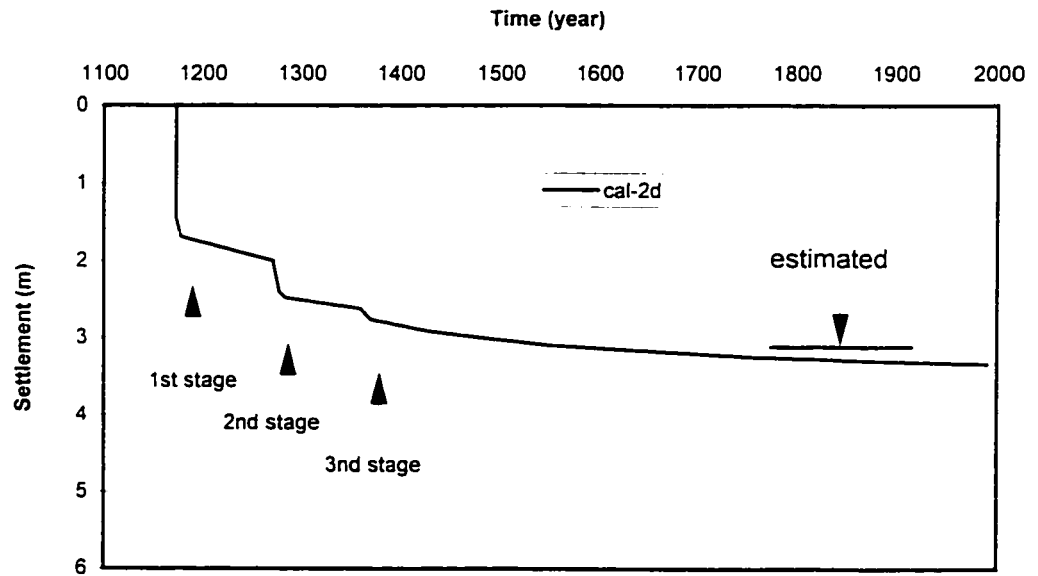


Fig. 4.31 (b) Settlement versus time relationship

CHAPTER 5

DEFORMATION BEHAVIOR OF PISA TOWER

--PARAMETER SENSITIVITY STUDIES

5.1 Introduction

It is a recognized fact that soft soils exhibit a property of continuing settlement under constant effective stress. This phenomenon is usually known as secondary consolidation. It is a special case of creep (volumetric creep). Creep phenomena include both volumetric creep and deviatoric creep. Time-dependent shear deformations are usually referred to as deviatoric creep. After many decades, creep still remains a secondary issue in the long term design of geotechnical projects. Creep is usually treated as a theoretical exercise. There are only a few cases where researchers have tried to study the problem of creep in the field situations. Wu et al. (1969) analyzed the time-dependent ground movement of an excavation near Cleveland, but they found that this excavation was far from an ideal case to check the creep prediction. Borja et al. (1990) investigated the time-dependent deformation of the I-95 embankment near Boston. They found that creep was present but the results of the analysis underscored the importance of creep deformation. Morsy (1994) analyzed the time-dependent deformation of the clay foundation underneath Tar Island Dyke (TID). He also carried out a sensitivity study for deviatoric creep parameters A and $\bar{\alpha}$ to look at their effects on the deformation behavior of the TID clay. The satisfactory agreement between the calculated and the measured values emphasized the need to include creep effects to account for all the observed deformations. Desai and Samtani (1995) analyzed a creeping slope at Villarbeney, Switzerland through a Hierarchical Single Surface (HISS) model. Typical comparisons

between finite-element predictions and field data showed that the proposed modeling procedure provided a highly satisfactory correlation for the field situations.

In the present study, a time-dependent plastic model (DYSCP model) was used in analyzing the deformation behavior of the soil beneath the Pisa Tower. This model has been used efficiently in time-dependent analysis of the I-95 embankment by Borja et al. (1990) and the TID by Morsy (1994). Pisa Tower's well-documented data and its more than 800 years of history provide an excellent time-dependent deformation case study. This tower started to lean southward during the second construction stage. The movement in this direction has been continuous for several centuries.

Time-dependent analysis carried out in Chapter Four has shown that creep effects are significant in the soil beneath the tower's foundation. Since it was performed mainly based on the mean values of the model parameters, it is of interest to know to what degree these parameters affect the predictions. In this chapter, the sensitivity study was conducted to investigate all the major parameters which might influence the deformation behavior of the soil underneath the tower's foundation. On the other hand, as mentioned by Brandes et al. (1996), it should be kept in mind that the model parameters do not act independently. The sensitivity of these parameters could be less significant than the results shown in this study if the dependence of these parameters on each other were considered.

5.2 The Leaning Tower of Pisa

At the beginning of 1990, Pisa Tower was closed to the general public due to its critical situation. The nearly 60m high tower with a 19.6m footing diameter started to lean southward in the thirteenth century. At present, its inclination is about 5.5 degrees. Pepe et al. (1995) predicted that the safety factor will approach 1.0 when the tilt approaches 7.0 degrees. In order to save the tower, different stabilization measures have been proposed. The temporary application of a 6 MN lead counterweight at the north rim

of the tower base has brought the tower back 50 seconds of arc. Additional measures are being considered to provide a more permanent solution.

5.2.1 History of construction

The construction of the tower lasted nearly 200 years. It was divided into three stages, as shown in Figure 5.1. The first stage started in 1173. By 1178, it reached the fourth storey, and then the work stopped. This interruption lasted 94 years. The second construction stage started in 1272 and ended in 1278. It brought the tower to the seventh storey, and then work stopped again. The second interruption lasted 82 years. The third construction stage started in 1360 and in 1370 the bell tower was finished. It was clear that if the construction continued without any interruption, the foundation soil would have experienced an undrained bearing capacity failure. The erection of the tower represents an excellent example of staged construction, even if it was unintentional.

5.2.2 Subsurface conditions

Figure 5.2 shows the ground profile underlying the tower. There are three distinct formations. Formation A is about 10m thick and consists of rather variable sandy and clayey silts. Sample descriptions and piezocone tests show that the material in the south side of the tower appears to be more silty and clayey than in the north. This is believed to be the major factor in causing the tower to lean to the south. The bottom layer of Formation A is a 2m thick medium dense sand known as the upper sand (A_2). Formation B is about 30m thick and consists of marine clay. It is subdivided into four distinct layers. The upper layer (B_1 - B_3) is a soft sensitive clay known as the Pancone clay. It is underlain by an overconsolidated clay (B_4 - B_5) known as intermediate clay which in turn overlies by a sand layer (B_6). Underneath the sand layer is a normally consolidated clay known as the lower clay (B_7 - B_{10}) which in turn overlies Formation C (dense sand known as the lower sand). Formation C extends to a considerable depth. Both Formation B and Formation C are laterally very uniform in the vicinity of the tower.

5.3 The constitutive model

The constitutive model presented here is called the double-yielding surface cam-clay plasticity (DYSCP) model. It is based on the concept of decomposition of total strain into an immediate part and a delayed part in a generalized three-dimensional frame work (Bjerrum 1967, Borja and Kavazanjian 1985, and Hsieh et al. 1990). To fully define the model, only thirteen material parameters are required. Seven of them are needed in the absence of creep; six more are required for in the presence of creep. All these parameters can be easily determined through isotropic triaxial tests, consolidation tests, and triaxial creep tests.

In the DYSCP model, the total strain-rate tensor can be decomposed into four components based on phenomenological creep models (Bjerrum 1967, Borja and Kavazanjian 1985, and Hsieh et al. 1990):

$$[5.1] \quad \dot{\underline{\underline{\epsilon}}} = \dot{\underline{\underline{\epsilon}}}^e + \dot{\underline{\underline{\epsilon}}}^p_F + \dot{\underline{\underline{\epsilon}}}^p_G + \dot{\underline{\underline{\epsilon}}}^t$$

where subscripts F and G refer to the appropriate ellipsoidal and interdependent cylindrical yield surfaces, respectively; superscripts e and p denote the time-independent elastic and plastic components, respectively; and superscript t denotes the time-dependent (creep) components.

$\dot{\underline{\underline{\epsilon}}}^e$ is evaluated by applying the generalized Hooke's law. $\dot{\underline{\underline{\epsilon}}}^p_F$ and $\dot{\underline{\underline{\epsilon}}}^p_G$ are evaluated according to the yielding surface F and G, as shown in Figure 5.3. The soil is normally consolidated with respect to F but overconsolidated with respect to G if the deformation process only involves F. The soil is normally consolidated with respect to G but overconsolidated with respect to F if the deformation process only involves G. It is a fully plastic process if the deformation process involves both F and G. $\dot{\underline{\underline{\epsilon}}}^t$ is evaluated by applying a flow rule for both volumetric and deviatoric yield surfaces and by

simultaneously forcing it to satisfy Taylor's (1948) secondary compression law for volumetric creep and Singh and Mitchell's (1968) equation for deviatoric creep.

5.4 Sensitivity analyses of time-independent parameters

The constitutive model used in this study requires seven parameters for complete material definition in the absence of creep. They are: the virgin compression index C_c ; the recompression index C_r ; the angle of internal friction ϕ' ; the void ratio e_a at unit preconsolidation pressure; and the hyperbolic stress-strain parameters a and b , and R_f . In this study, the parameters from the clayey silt layer A_1 and the upper clay layer B_1 (see Figure 5.2) are focused in a sensitivity investigation, due to the significance of these layers in the deformation behavior of the foundation soil and the scatter characterization of their material parameters.

The possible ranges of the model parameters in layers A_1 and B_1 are shown in Table 5.1. It is mainly based on Mitchell and Soga's (1995) investigation, as shown in Figures 5.4 to 5.7. For layer A_1 , the maximum value of C_c (0.299) was given by MLP (1971), while the minimum value (0.161) was given in Report 2.2 by Lancellotta and Pepe (1990), as shown in Figure 5.4. Both the maximum and minimum values of C_r (0.028 and 0.007) were proposed in Report 2.2 by Lancellotta and Pepe (1990), as shown in Figure 5.5. The minimum ϕ' value (30.92) was proposed by MLP (1971), as shown in Figure 5.6. The minimum e_a value (0.71) was proposed by Tamagnini (1993), as shown in Figure 5.7. For layer B_1 , the maximum value of C_c (1.0) was given by Burland and Potts (1994) to account for sample disturbance. This value is beyond the upper limits of the experimental values. The minimum value of C_c (0.507) was given in Report 2.2 by Lancellotta and Pepe (1990), as shown in Figure 5.4. The maximum value of C_r (0.147) was proposed by Calabresi (1992), while the minimum value of C_r (0.053) was given in Report 2.2 by Lancellotta and Pepe (1990), as shown in Figure 5.5. The minimum value of ϕ' (24.44^o) was given by MLP (1971), as shown in Figure 5.6. The minimum value of

e_a (2.67) was proposed by Calabresi (1992) (see Figure 5.7). The possible range of R_f for both layers A_1 and B_1 is 0.7 to 1.0.

Since Pisa subsoils are mainly in a loading state, the influence of recompression index C_r is not expected to be significant. Parameter a is the reciprocal of the initial tangent modulus, expressed as follows:

$$[5.2] \quad a = \frac{p_c R_f}{3\mu_e}$$

where p_c is the preconsolidation pressure; and μ_e is the elastic shear modulus. Parameter a is not sensitive in the stress strain relationship (as shown in Figure 5.13 and will be discussed later on).

Hyperbolic parameter b is not an independent parameter, it depends on C_r , C_c , M , and R_f through the following relationship (Borja and Kavazanjian, 1985):

$$[5.3] \quad b = R_f \frac{2^{(1-\frac{C_r}{C_c})}}{M}$$

Thus only four parameters, C_c , ϕ' , R_f , and e_a , are selected for the sensitivity study.

As a reference case in this discussion, the parameters used in the previous study conducted in Chapter Four are shown in Tables 5.2 to 5.4. The sensitivity analyses are done by taking a 10% change of the reference values of parameters C_c , ϕ' , R_f , and e_a individually, as shown in Table 5.5. They are investigated at two different locations, at element 267, which is at a depth of 12m in layer B_1 and at element 321, which is at the depth of 6.5m in layer A_1 . Both elements are located at about 10m south of the tower center, as shown in Figure 5.8.

5.4.1 Virgin compression index C_c

Traditionally, it is believed that the compressibility of the underlying soils plays an important role in the deformation behavior of the soil beneath the tower's foundation. Parameter C_c represents the slope in the void ratio and mean effective stress in log scale plots, as shown in Figure 5.9, where $C_c = \lambda \ln 10$. For the same amount of stress increase, a higher value of C_c will result in a bigger strain. Previous analysis in Chapter Four showed that the tower load increments caused the mean effective stresses to increase one order of magnitude from their initial values.

Two values of C_c were used in the analyses, 0.226 for layer A_1 and 0.678 for layer B_1 (a 10% increase of their reference values). The results of the analyses are summarized in Figure 5.10 and Table 5.6. The increase of the C_c value in layer A_1 results in an increase in vertical strain by an average of 9% in element 321 before the year of 1370, which marks the end of the construction stage. After that year, the vertical strain increases by 7% on average. C_c of layer B_1 is even more sensitive in terms of strain. The increase of the C_c value in layer B_1 results in an increase in vertical strain by an average of 14.2% in element 267 before the year 1370. After that year, the vertical strain increases by 11.3% on average. Figure 5.10 also shows that increasing C_c causes both settlement and inclination to increase. C_c of layer A_1 is more sensitive than C_c of layer B_1 . A 10% change in C_c of layer A_1 causes a 3.8% increase in tilting and a 2.7% increase in settlement. In general, parameter C_c of layer A_1 is sensitive in terms of strain, but not very sensitive in terms of total settlement and tilting angle. The mean values of C_c , 0.205 for layer A_1 and 0.615 for layer B_1 , are believed to be reasonable.

5.4.2 The angle of internal friction ϕ'

The model parameter ϕ' is usually evaluated from isotropically consolidated undrained or drained triaxial tests. In the constitutive model, it determines the shape of

the Cam-clay yielding locus as well as the slope of the critical state line M in the p'-q plane through the following relationship:

$$[5.4] \quad M = \frac{6 \sin \phi'}{3 - \sin \phi'}$$

Figure 5.11 shows the initial yielding locus in the absence of the G surface for layers A₁ and B₁. It also shows the yielding locus under the cases with ϕ' values of 10% increase and decrease. A lower value of ϕ' predicts a smaller yielding locus. The ϕ' value significantly influences the yielding surface under high stress ratio η . For the Pisa soil, the η value could not be too high due to the fact that shear stresses develop much slower than mean stresses under creep conditions. Thus the influence of ϕ' cannot be too big.

Two analyses were carried out by using different values of ϕ' , 30.3 for layer A₁ and 23.89 for layer B₁. The results are shown in Figure 5.12 and Table 5.6. The decrease of the ϕ' value in layer A₁ results in an increase in vertical strain by an average of 3% in element 321 and 0.1% in element 267 before the year 1370. After that year, the vertical strain increases by an average of 3% in element 321 and 2% in element 267. A 10% decrease in the ϕ' value of layer A₁ causes the settlement to increase by 0.9% and the tilting angle to increase by 6.5%. A 10% decrease in ϕ' value of layer B₁ causes the settlement to decrease by 0.7% and the tilting angle to increase by 1.2%. Although the parameter ϕ' of layer A₁ is relatively sensitive in terms of the tilting angle, it is not necessary to worry about it since the actual possible decrease range of ϕ' is only 8% for this layer.

5.4.3 Failure ratio R_f

In DYSCP model, the time-independent elastic component is evaluated by assuming the trace of the modified Cam-clay yield surface on the q- γ plane (the deviatoric stress versus strain plane under triaxial stress condition) is a hyperbola of the form:

$$[5.5] \quad q = \frac{\gamma \cdot p_c'}{a + b \cdot \gamma} \cdot R_f$$

where γ is the deviatoric strain, $\gamma = \frac{\sqrt{2}}{3} \sqrt{(\epsilon_1 - \epsilon_2)^2 + (\epsilon_2 - \epsilon_3)^2 + (\epsilon_3 - \epsilon_1)^2}$; a and b are the normalized hyperbolic stress-strain parameters; R_f is the failure ratio. $R_f = \frac{(\sigma_1 - \sigma_3)_{failure}}{(\sigma_1 - \sigma_3)_{ultimate}}$; p_c' is the preconsolidation pressure; and q is the deviatoric stress.

$$q = \frac{1}{\sqrt{2}} \sqrt{(\sigma_1' - \sigma_2')^2 + (\sigma_2' - \sigma_3')^2 + (\sigma_3' - \sigma_1')^2} .$$

The R_f value is introduced because of the fact that the asymptotic value of q is usually larger than the compressive strength of the soil. The failure ratio of R_f will force the hyperbolic curve to pass through the observed failure point. Usually R_f value is between 0.7 to 1.0. The stress-strain curves of layers A_1 and B_1 from the hyperbolic model are shown in Figure 5.13 (a) and (b). They also show the stress-strain curves under a 10% increase or decrease of the parameters a , b , and R_f . It can be seen that the lower value of R_f will predict higher strain. The influence of R_f becomes significant as shear stresses increase. Previous results presented in Chapter Four showed that creep restricts shear stress development, thus decreasing the influence of R_f . Thus, the parameter R_f will not be so sensitive in creep analyses. Parameter a is not sensitive under any circumstances. Parameter b is sensitive but it is not independent. Therefore, among the three hyperbolic parameters, a , b , and R_f , only R_f is selected in the sensitivity analysis.

There are no recommended R_f values for the Pisa soil. An R_f value of 0.89 has been chosen as a reference value. Two more analyses were conducted with R_f values of 0.80 (a 10% decrease from its reference value) for layers A_1 and B_1 respectively. Results show that a decrease of R_f in layer A_1 results in the total settlement increasing by 0.8% and the tilting angle increasing by 4.0%, as shown in Table 5.6 and Figure 5.14. The decrease of the R_f value in layer A_1 has a slight effect on the vertical strain. It only causes vertical strain to increase by about 2% in element 321 and 1% in element 267 after the

year 1370. The total settlement increases 0.3% and the tilting angle increases 1.7% under a 10% decrease of R_f value in layer B_1 . Thus the R_f value is not very sensitive in terms of strain, the total settlement and tilting angle, so the mean value of 0.89 appears to be acceptable.

5.4.4 Reference void ratio e_a

Parameter e_a determines the position of the VCL and CSL lines in the e -log p plots, as shown in Figure 5.9. Two analyses were conducted using different values of e_a , 1.419 for layer A_1 and 3.003 for layer B_1 . The results are shown in Figure 5.15 and Table 5.6. It can be seen that the increase of the e_a value in layer A_1 causes the vertical strain to decrease by about 3% in element 321 with no change in element 267. Increasing the e_a value causes a decrease in both the settlement and tilting. The total settlement decreases by 0.8% and the tilting angle decreases by 1.9% under a 10% increase in e_a of layer A_1 . The total settlement decreases by 1.6% and tilting angle decreases by 1.4% for a 10% increase in e_a of layer B_1 . Over all, the parameter e_a is relatively non-sensitive. A mean value of e_a is believed acceptable.

5.5 Sensitivity analyses of time-dependent parameters

In the time-dependent constitutive model, the creep strain tensor is divided into distinct but interdependent volumetric and deviatoric components (Hsieh et al. 1990 and Morsy 1994). The creep component is represented by six input parameters: the secondary compression coefficient C_α ; the Singh and Mitchell creep parameters A , m and $\bar{\alpha}$; and the reference times $(t_v)_i$ and $(t_d)_i$. Both $(t_v)_i$ and $(t_d)_i$ are usually taken as unity. The secondary compression coefficient C_α mainly controls the volumetric creep component through the following equation (Taylor 1948):

$$[5.6] \quad \dot{\epsilon}_v = \frac{\Psi}{(1 + e)t_v}$$

where $\dot{\epsilon}_v$ is the volumetric creep strain rate; ψ is the secondary compression coefficient in natural log scale ($C_\alpha = \ln 10 * \psi$); e is the current void ratio; and t_v is the volumetric age relative to an initial reference time $(t_v)_i$.

The Singh and Mitchell creep parameters A , m , and $\bar{\alpha}$ mainly control the deviatoric creep component through the following equation (Singh and Mitchell 1968):

$$[5.7] \quad \dot{\epsilon}_a = A \exp(\bar{\alpha} \bar{D}) \left(\frac{(t_d)_i}{t_d} \right)^m$$

where $\dot{\epsilon}_a$ is the axial strain rate in a triaxial creep test; A , m , and $\bar{\alpha}$ are the Singh and Mitchell parameters; \bar{D} is the deviatoric stress level; $(t_d)_i$ is the reference time after loading at which creep is assumed to commence; and t_d is the deviatoric age relative to $(t_d)_i$.

Due to the fact that there is limited experience in transforming creep parameters into field behavior, sensitivity analyses of creep parameters are necessary. At 9.8m south of the footing center, the tower load causes both mean effective stresses and deviatoric stresses to increase by one order of magnitude from their initial values, as shown by previous analyses in Chapter Four. Thus, both volumetric and deviatoric creep components may be important in the Pisa soil. In this study, the sensitivity of the secondary compression coefficient C_α and the Singh and Mitchell creep parameters A , m and $\bar{\alpha}$ is investigated to give a better understanding of the time-dependent deformation behavior of the Pisa soil.

Creep tests on the Pisa soil are all restricted to clayey silt layer A_1 and the upper clay layers B_1 - B_3 (Bishop and Lovenbury 1969, and Mitchell and Soga 1995). Figure 5.16 shows the triaxial drained creep test results from Mitchell and Soga (1995). It includes samples from the depths of 6m (layer A_1), the 10m (layer B_1), the 14m (layer B_2), and the 19m (layer B_3). It can be seen that creep effect in layer B_1 is very significant compared

with the rest of the layers. Creep effect in the clayey silt layer A_1 is also important. Moreover, the stress level in this layer is very high. Thus sensitivity analyses of the time-dependent parameters C_α , A , m , and $\bar{\alpha}$ will also be limited to the layers A_1 and B_1 .

5.5.1 Volumetric creep parameter C_α

Parameter C_α plays an important role in the volumetric creep behavior. For the soil underneath the tower's foundation, it is one of the most uncertain values in the time-dependent analyses.

Layer A_1

Mitchell and Soga's (1995) triaxial drained creep tests gave $C_{\alpha c}$ of 0.00229. Calabresi's (1992) study provided $C_{\alpha c}$ of 0.00451 to 0.00738 by considering C_c of 0.205 (see Figure 5.17). If considering the mean value of initial void ratio to be 0.85 (see Figure 5.18), the possible range of C_α would be 0.0041 to 0.0137. A C_α value of 0.0051 has been chosen as a reference value (see Table 5.7).

Layer B_1

Mesri and Goldewski (1977) postulated that the ratio of C_α/C_c is constant for fine-grained soils that lie within a range of 0.025 to 0.10. By considering C_α/C_c of 0.10 and C_c of 0.615, the maximum value of C_α will be 0.0615. The minimum value of 0.0075 comes from Nathan's (1978) study. The mean value of 0.0154 has been chosen as a reference value (see Table 5.7).

The results of taking a C_α value of 0.0056 for layer A_1 and 0.0169 for layer B_1 (a 10% increase of their reference values, see Table 5.8), are shown in Table 5.9 and Figure 5.19. It can be seen that parameter C_α is relatively non-sensitive. The increase in C_α value for layer A_1 has only a slight effect on vertical strain in both elements 267 and 321. The increase in the C_α value in layer B_1 causes the vertical strain to increase by 1% in element

267. A 10% increase of the C_α value in layer A_1 causes no change in the total settlement and only 0.8% increase in the total tilting angle. A 10% increase in the value of C_α in layer B_1 only cause a 0.5% increase in the tilting angle and a 0.1% in the total settlement. Thus, mean values of C_α should be acceptable.

5.5.2 Singh and Mitchell creep parameter A

The parameter A represents the value of shear strain rate at the reference time and the zero deviatoric stress level, as shown in Figure 5.20 (a). It reflects the soil composition, structure, and stress history. The value of parameter A, used in this study was back calculated from the stress-strain curves of strain rate controlled undrained triaxial tests conducted by Mitchell and Soga (1995). They recommended an A value of $2.12 \cdot 10^{-4}/\text{min}$ ($9.03 \cdot 10^{-4}/\text{year}$) for layer A_1 and $1.62 \cdot 10^{-4}/\text{min}$ ($15.21 \cdot 10^{-4}/\text{year}$) for layer B_1 . These values have been chosen as reference values.

In this study, two analyses were carried out using different A values, $9.93 \cdot 10^{-4}/\text{year}$ for A_1 and $16.7 \cdot 10^{-4}/\text{year}$ for B_1 (a 10% increase of their reference values, see Table 5.8). The results of the analyses are summarized in Table 5.9 and Figure 5.21. Parameter A is relatively non-sensitive. For element 267, the increase in the A value for both layers A_1 and B_1 causes the vertical strain to increase by 1% after the year 1370. For element 321, the increase in the A value of layer A_1 causes the vertical strain to increase by 2%, while the increase in the A value of layer B_1 causes the vertical strain to increase by only 0.6%. A 10% increase of the A value in layer A_1 causes the total settlement to increase by only 0.3% and the total tilting angle to increase by 1.3%. A 10% increase of the A value in layer B_1 causes the total settlement to increase by 0.1% and tilting angle to increase by 0.2%. Thus, the mean value of parameter A is considered acceptable.

5.5.3 Singh and Mitchell creep parameter m

The Singh and Mitchell creep parameter m controls the rate at which the strain rate decreases with time, as shown in Figure 5.20 (b). Mitchell (1968) found that for most

soils the m value lay between 0.75 and 1.0. On the other hand, he found that m was not unique for a given soil type. Consolidation and overconsolidation appeared to cause variations in m values. Mesri et al. (1981) found that m was rarely independent of time or shear stress level.

Mitchell and Soga's (1995) strain rate controlled undrained triaxial tests gave m values of 0.77 to 0.96 with a mean value of 0.89 for layer A_1 , and m values of 0.78 to 0.86 with a mean value of 0.83 for layer B_1 . In this study, two analyses were carried out using m values of 0.80 for A_1 and 0.75 for B_1 (a 10% increase of their reference values: see Table 5.8). The results are shown in Table 5.9 and Figure 5.22. It can be seen that parameter m has a slight effect on the deformation behavior of the Pisa soil before the year 1370. After that year, the decrease in the m value of layer A_1 results in an increase in vertical strain by 1% for element 267 and 4% for element 321. On the other hand, the decrease in the m value of layer B_1 results in an increase in vertical strain by 2% for element 267 and 1% for element 321. Parameter m is relatively sensitive in terms of the tilting angle. The total tilting angle increases by 7.6% and the settlement increases by 2.2% under a 10% change of m value in layer A_1 . On the other hand, parameter m of layer B_1 is not so sensitive. A 10% change of the m value only causes the total settlement to increase by 0.9% and the tilting angle to increase by 3.0%. Thus no further investigation is thought necessary.

5.5.4 Singh and Mitchell creep parameter $\bar{\alpha}$

The Singh and Mitchell creep parameter $\bar{\alpha}$ indicates the stress-intensity effect on creep rate, as shown in Figure 5.20 (a). Mitchell and Soga's (1995) strain rate controlled undrained triaxial tests gave $\bar{\alpha}$ values of 5.07 to 6.29 with a mean value of 5.81 for layer A_1 and $\bar{\alpha}$ values of 5.50 to 9.00 with a mean value of 6.33 for layer B_1 . These two mean values are used as reference values in this discussion. Two more analyses were conducted based on $\bar{\alpha}$ values of 6.39 for A_1 and 6.96 for B_1 (a 10% increase of their reference

values: see Table 5.8). The results are shown in Table 5.9 and Figure 5.23. It can be seen that the change in $\bar{\alpha}$ value has some effect during the construction period of the tower as well as after that. For element 321, the increase of the $\bar{\alpha}$ value in layer A_1 causes vertical strain to increase by 2% before the year 1370 and 6% after then. The change in $\bar{\alpha}$ value in layer B_1 has a slight effect on this element. For element 267, the change in the $\bar{\alpha}$ value in layer A_1 as well as in layer B_1 results in a vertical strain increase by 2% in average after the year 1370. It has only a slight influence in the vertical strain before that year. Parameter $\bar{\alpha}$ of layer A_1 is relatively sensitive in terms of the total settlement and the tilting angle. A 10% increase in this value causes a 1.8% increase in the total settlement and a 6.1% increase in the tilting angle. However, there is reasonable confidence in the value of $\bar{\alpha}$ since the possible maximum value of $\bar{\alpha}$ is only 6.29 for this layer, which is within the 10% range. Parameter $\bar{\alpha}$ of layer B_1 is not sensitive in terms of the total settlement and the tilting angle. A 10% increase in this value only causes a 0.5% increase in the settlement and a 0.8% decrease in the tilting angle. No further investigation is thought necessary for layer B_1 , even if the possible increase range of $\bar{\alpha}$ is 42%. The mean value of $\bar{\alpha}$ is considered acceptable.

5.6 Summary and conclusions

In this study, the sensitivity of time-independent as well as time-dependent parameters required in the DYSCP model have been studied through total of sixteen visco-plastic analyses. Figures 5.24 and 5.25 summarize the results in terms of the total inclination and settlement under the changes of model parameters of layer A_1 , respectively. The difference in the total settlement is within 2.7% and the tilting angle is within 7.6% under a 10% change of both time-independent and time-dependent parameters. The difference could be even lower if the dependence of these parameters on each other is considered. This suggests that the deformation behavior of the soil beneath

the tower's foundation is not controlled by any specific parameter. It is the combination of all the time-independent as well as time-dependent parameters in the model.

The time-independent as well as time-dependent parameters of layer A_1 are more sensitive than those of layer B_1 in the deformation behavior of the Pisa soil, although creep in layer B_1 is more significant compared with the rest of the layers. This indicates that the stress level has more effect on the final results when compared with the creep effect of the material itself. The time-independent as well as time-dependent parameters become more sensitive under high stress levels. Increasing the accuracy of the parameters of layer A_1 could improve the accuracy of the FEA results.

Among the time-independent parameters, the angle of internal friction ϕ is relatively sensitive in terms of the total tilting angle. A 10% decrease of this value causes a 6.5% increase in the total tilting angle. Time-independent parameters C_c , R_f , and e_a are non-sensitive in terms of the total settlement and tilting angle. C_c of layers A_1 and B_1 are both sensitive in terms of vertical strains. A 10% increase in the C_c value of layer A_1 results in a vertical strains increase by 9% during the construction period and 7% after that. A 10% increase in the C_c value of layer B_1 results in a vertical strain increase of 14.2% during the construction period and 11.3% after that.

Among the time-dependent parameters, the Singh and Mitchell parameters m and $\bar{\alpha}$ of layer A_1 are relatively sensitive in terms of the total tilting angle. A 10% decrease of m value results in a 7.6% increase in tilting, while a 10% increase of $\bar{\alpha}$ results in a 6.1% increase in tilting. The parameter $\bar{\alpha}$ of layer A_1 is also relatively sensitive in terms of vertical strains. A 10% increase of that value causes a 6% increase in the vertical strains after the construction period.

Overall, the mean values used in the previous visco-plastic study carried out in Chapter Four are still acceptable.

Table 5.1 Possible range of time-independent parameters

(a) Layer A₁

Param.	C _c		C _r		φ (degree)		e _n		a		b		R _r	
	value	Δ	value	Δ	value	Δ	value	Δ	value	Δ	value	Δ	value	Δ
min	0.161	-21%	0.007	-67%	30.92	-8%	0.71	-45%					0.7	-21%
mean	0.205	*	0.021	*					0.0046	*	1.220	*	0.89	*
max.	0.299	+46%	0.028	+33%	33.67	*	1.290	*					1.0	+12%

(b) Layer B1

Param.	C _c		C _r		φ (degree)		e _n		a		b		R _r	
	value	Δ	value	Δ	value	Δ	value	Δ	value	Δ	value	Δ	value	Δ
min	0.507	-18%	0.053	-35%	24.44	-8%	2.67	-2%					0.7	-21%
mean	0.615	*	0.081	*					0.0063	*	1.548	*	0.89	*
max	1.0	+63%	0.147	+81%	26.54	*	2.73	*					1.0	+12%

Table 5.2 Cam-clay parameters for the clay layers

material No.	layer	γ (kN/m ³)	C_c	C_r	Φ' (degree)	e_n	a	b	R_f	C_u
1	made ground MG	9.09	0.205	0.021	33.67	1.290	0.0046	1.220	0.89	0.0051
2	clayey silts A ₁ and A ₁ '	9.09	0.205	0.021	33.67	1.290	0.0046	1.220	0.89	0.0051
5	upper Pancone clay B ₁	7.32	0.615	0.081	26.54	2.730	0.0063	1.548	0.89	0.0154
6	upper Pancone clay B ₂	7.32	0.615	0.081	26.54	2.730	0.0038	1.548	0.89	0.0154
7	upper Pancone clay B ₃	7.32	0.615	0.081	26.54	2.730	0.0057	1.548	0.89	0.0154
8	intermediate clays B ₄	10.21	0.297	0.062	28.62	1.524	0.0095	1.351	0.89	0.0059
9	intermediate clays B ₅	10.21	0.297	0.062	28.62	1.524	0.0055	1.351	0.89	0.0059
11	lower clay B ₇	9.21	0.421	0.053	25.84	2.053	0.0051	1.538	0.89	0.0098
12	lower clays B ₈	9.21	0.421	0.053	25.84	2.053	0.0039	1.650	0.89	0.0098
13	lower clays B ₉	9.21	0.421	0.053	25.84	2.053	0.0039	1.650	0.89	0.0098
14	lower clays B ₁₀	9.21	0.421	0.053	25.84	2.053	0.0039	1.650	0.89	0.0098

Note: Material No. 3, 4, and 10 are sand layers, they are tabulated in the next table.

Table 5.3 Soil parameters for the sandy layers

material No.	layer	γ (kN/m ³)	E * (MPa)	ν *	ϕ'
3	Silty sand A ₁ "	8.39	13.0	0.12	34
4	upper gray sand A ₂	8.39	13.0	0.12	34
10	intermediate sand B ₆	9.29	18.0	0.12	34.3
15	rigid footing	9.09	1*10 ⁷	0.12	-

Note: All the rest of materials are clay and clayey silt, they are tabulated in the previous table.

*--from Calabresi et al. (1992) TAB5.XV.

Table 5.4 Singh and Mitchell parameters (from Mitchell and Soga 1995)

Sample	layer	$\bar{\alpha}$	m	A' (%/min.)	A (%/year)
4m	clayey silt A ₁	5.81	0.89	2.12*10 ⁻²	9.03*10 ⁻²
6m	clayey silt A ₁ '	5.86	0.95	2.19*10 ⁻²	4.23*10 ⁻²
10m	upper clay B ₁	6.33	0.83	1.62*10 ⁻²	15.21*10 ⁻²
14m	upper clay B ₂	6.39	0.86	8.35*10 ⁻³	5.279*10 ⁻²
19m	upper clay B ₃	8.82	0.75	2.15*10 ⁻³	5.789*10 ⁻²

Note: $A = A' * (365*24*60)^{(1-m)}$

Due to the lack of creep test data, and the fact that layer B₃ is highly structured soil, creep parameters from layer B₂ were assumed to represent those of B₄ to B₁₀.

Table 5.5 Time-independent parameters used in FEA analyses

Layer	A ₁				B ₁			
	C _c	φ (degree)	R _f	e _a	C _c	φ (degree)	R _f	e _a
used	0.205	33.67	0.89	1.29	0.615	26.54	0.89	2.730
10% change	0.226	30.30	0.80	1.419	0.678	23.89	0.80	3.003

Table 5.6 Sensitivity analyses results of time-independent parameters

Layer	A ₁				B ₁			
	Settlement (m)		Tilting angle (degree)		Settlement (m)		Tilting angle (degree)	
Items	FEA result	change (%)	FEA result	change (%)	FEA result	change (%)	FEA result	change (%)
Reference	3.34	-	3.35	-	3.34	-	3.35	-
C _c (+10%)	3.43	+2.7	3.48	+3.8	3.40	+1.9	3.37	+0.6
φ (-10%)	3.37	+0.9	3.57	+6.5	3.36	+0.7	3.39	+1.2
R _f (-10%)	3.36	+0.8	3.48	+4.0	3.35	+0.3	3.41	+1.7
e _a (+10%)	3.31	-0.8	3.29	-1.9	3.29	-1.6	3.31	-1.4

Table 5.7 Possible range of time-dependent parameters

(a) Layer A₁

Param	C _α		A (/year)		m		α	
	value	Δ	value	Δ	value	Δ	value	Δ
min	0.0041	-20%	0.000423	-53%	0.77	-13%	5.07	12.7%
mean	0.0051	*	0.000903	*	0.89	*	5.81	*
max	0.0137	+169%			0.96	+8%	6.29	+8%

(b) Layer B₁

Param	C _α		A (/year)		m		α	
	value	Δ	value	Δ	value	Δ	value	Δ
min	0.0075	-51%			0.78	-6%	5.50	-13%
mean	0.0154	*	0.001521	*	0.83	*	6.33	*
max	0.0615	+299%			0.86	+4%	9.00	+42%

Table 5.8 Time-dependent parameters used in FEA analyses

Layer	A ₁				B ₁			
	C _α	A(/year)	m	α	C _α	A(/year)	m	α
used	0.0051	0.000903	0.89	5.81	0.0154	0.001521	0.83	6.33
10% change	0.0056	0.000993	0.80	6.39	0.0169	0.00167	0.747	6.96

Table 5.9 Sensitivity analyses results of time-dependent parameters

Layer	A ₁				B ₁			
	Settlement (m)		Tilting angle (degree)		Settlement (m)		Tilting angle (degree)	
Items	FEA result	change (%)	FEA result	chang e (%)	FEA results	change (%)	FEA results	change (%)
Reference	3.34	-	3.35	-	3.34	-	3.35	-
C _α (+10%)	3.34	0	3.38	+0.8	3.34	+0.1	3.37	+0.5
A (+10%)	3.35	+0.3	3.40	+1.3	3.34	+0.1	3.36	+0.2
m (-10%)	3.41	+2.2	3.61	+7.6	3.37	+0.9	3.45	+3.0
α (+10%)	3.40	+1.8	3.56	+6.1	3.35	+0.5	3.33	-0.8

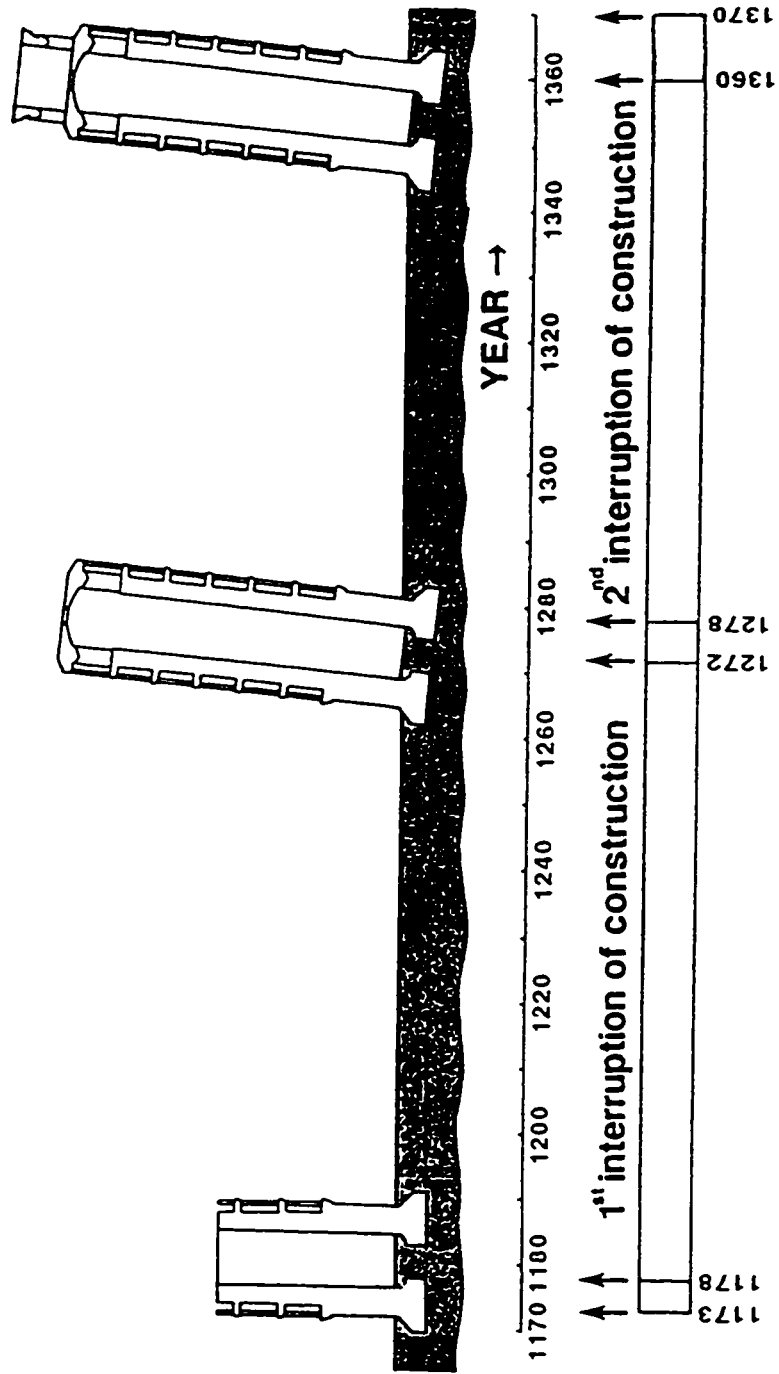


Fig. 5.1 Construction history (Jamiolkowski, et al. 1993)

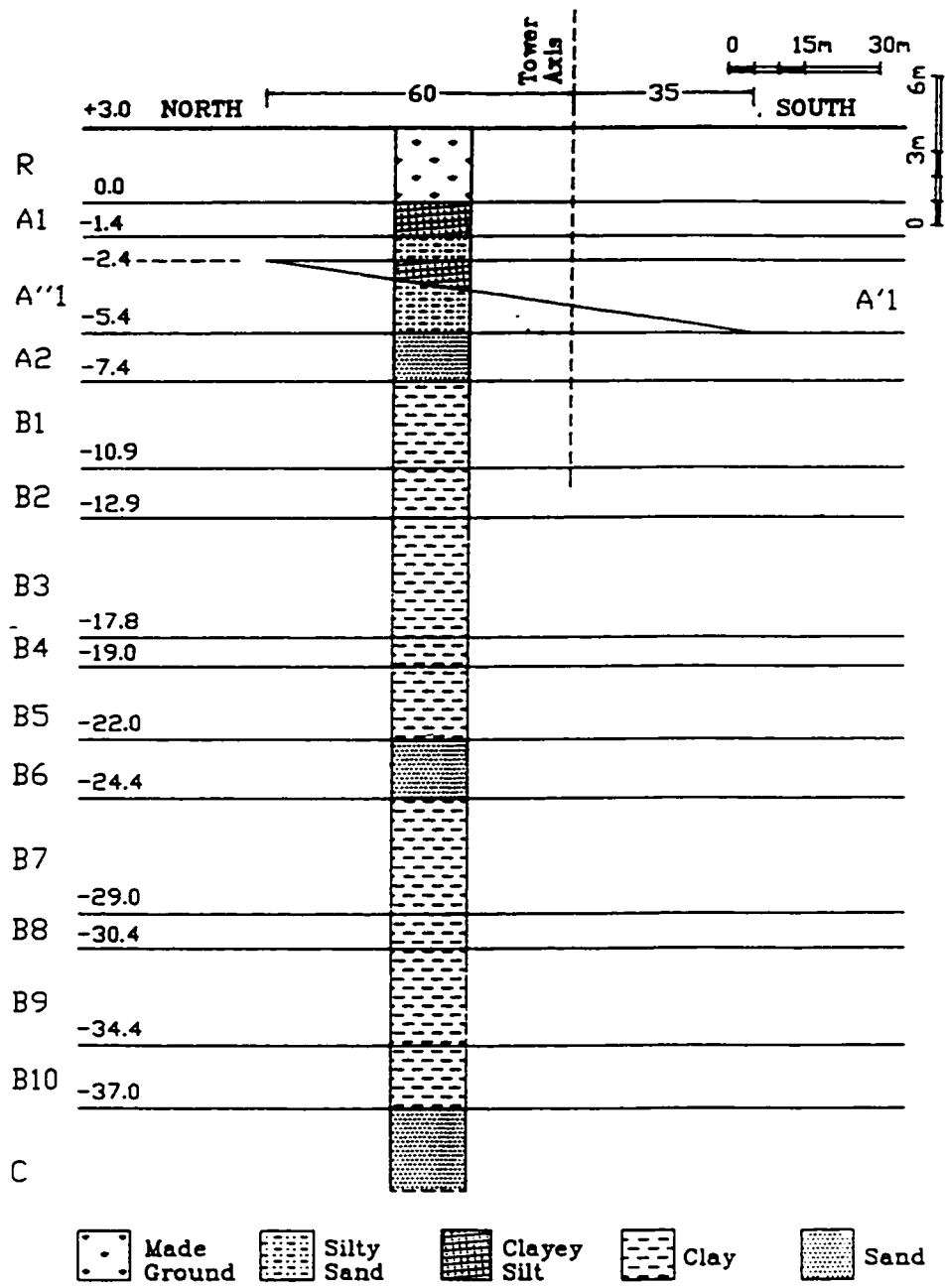


Fig. 5.2 Probable initial soil profile at the site of Pisa Tower (Calabresi, et al. 1992)

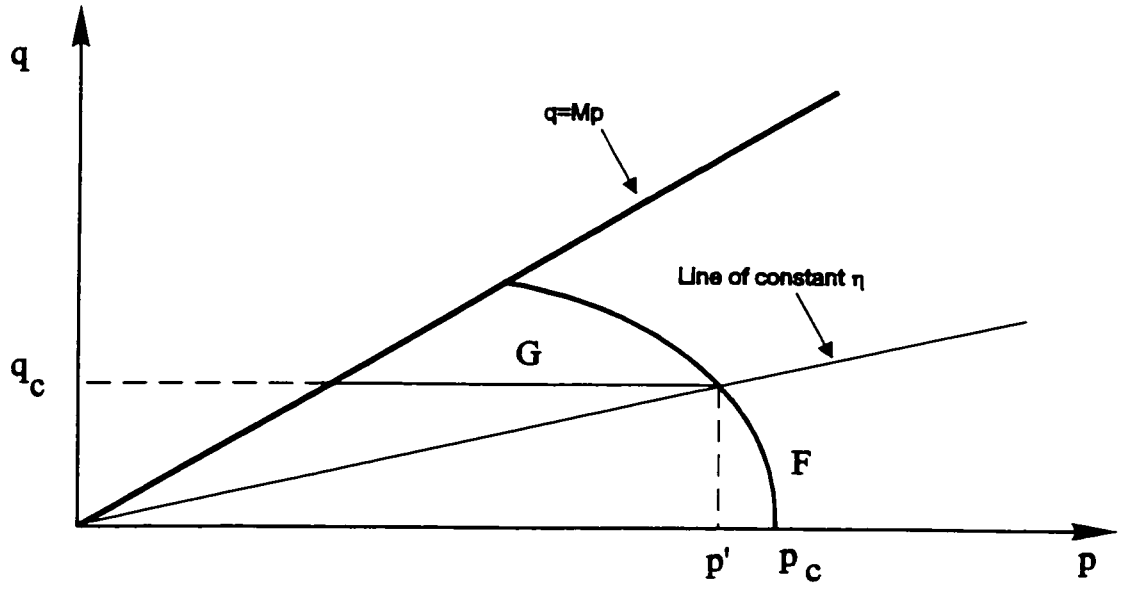


Fig. 5.3. Projection of double yield surface on p-q plane

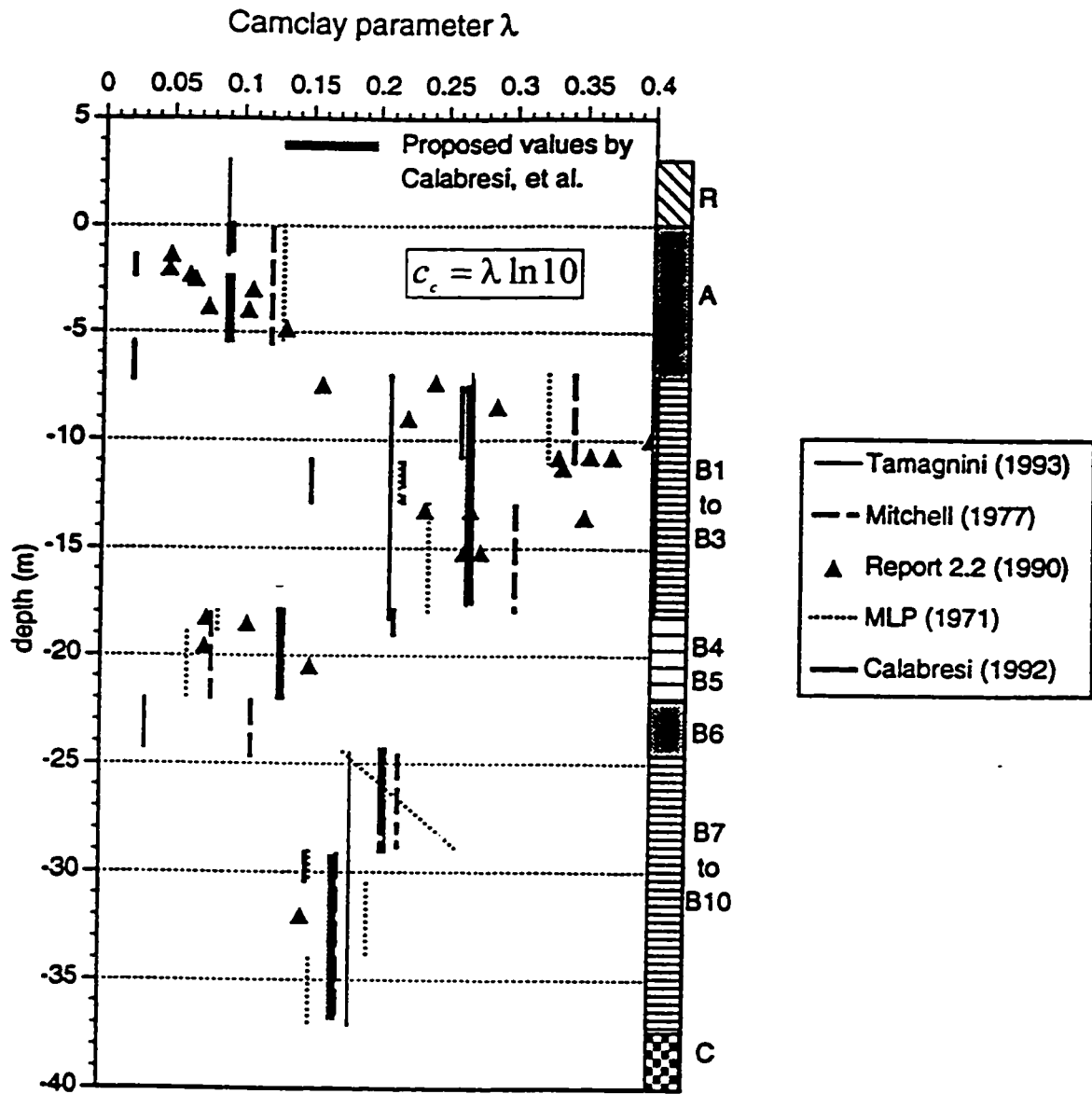


Fig. 5.4 Cam-clay compression index λ vs depth
(Mitchell and Soga, 1995)

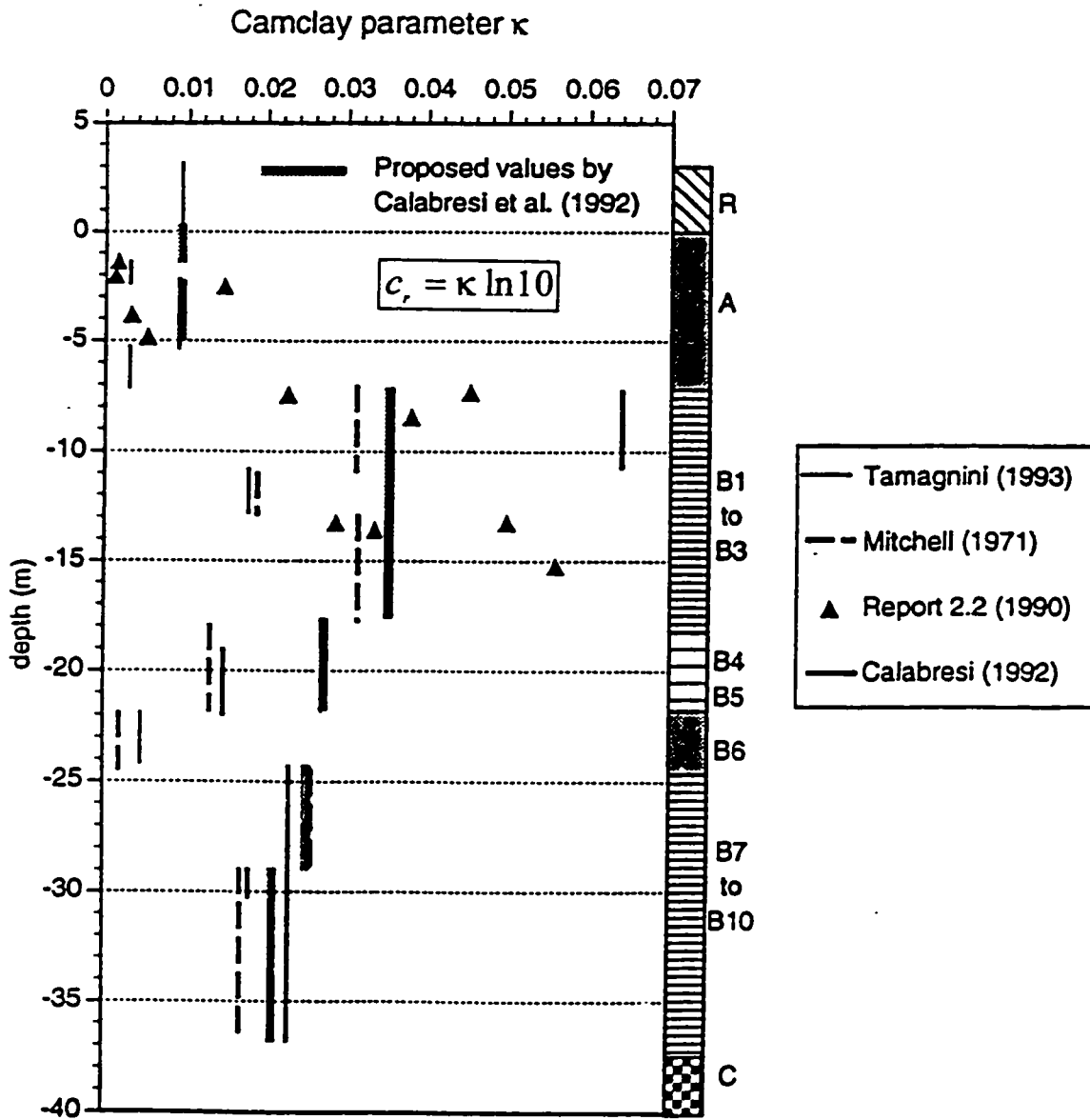


Fig. 5.5 Cam-clay compression index κ vs depth
(Mitchell and Soga, 1995)

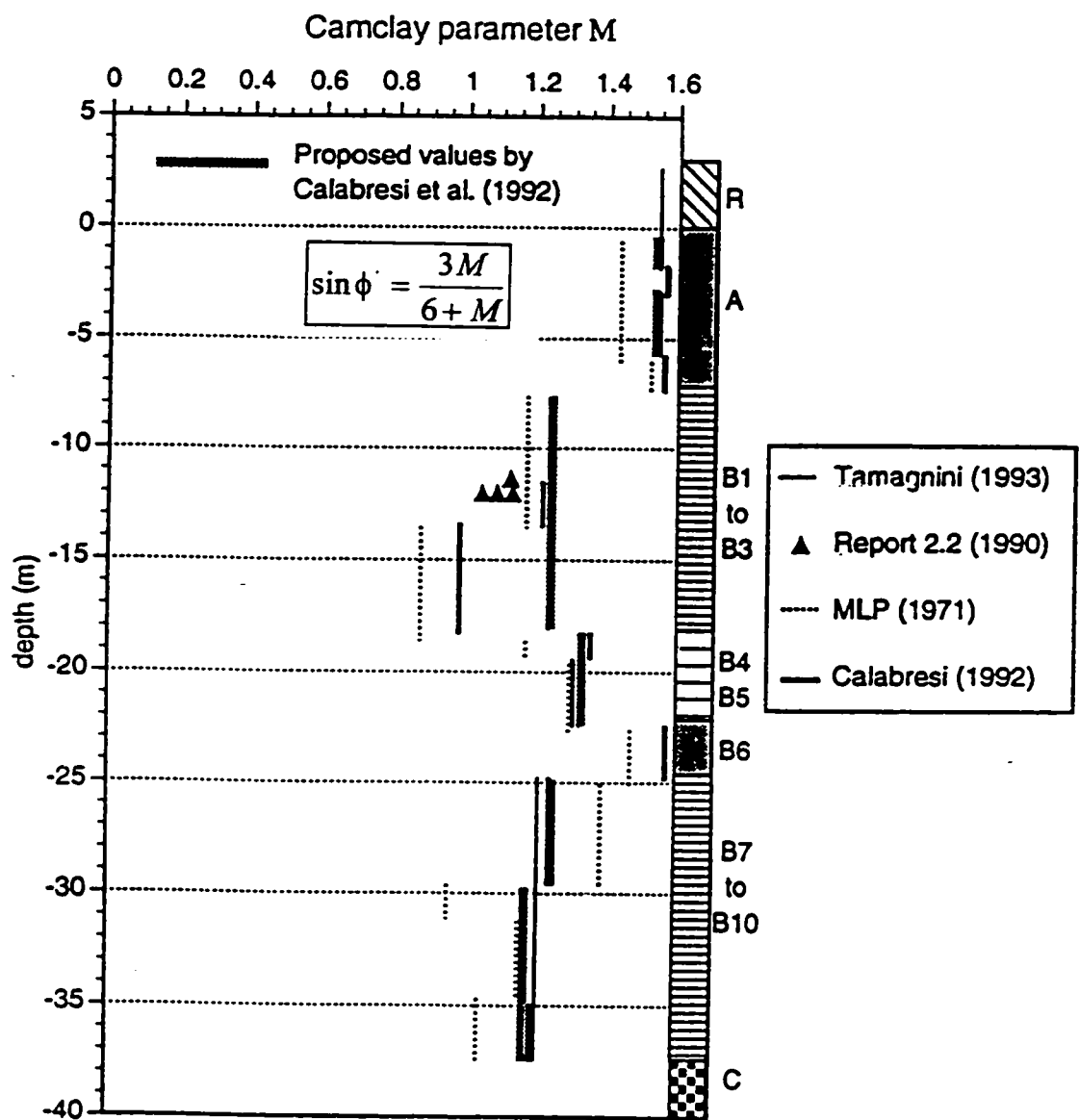


Fig. 5.6 Cam-clay compression index M vs depth
(Mitchell and Soga, 1995)

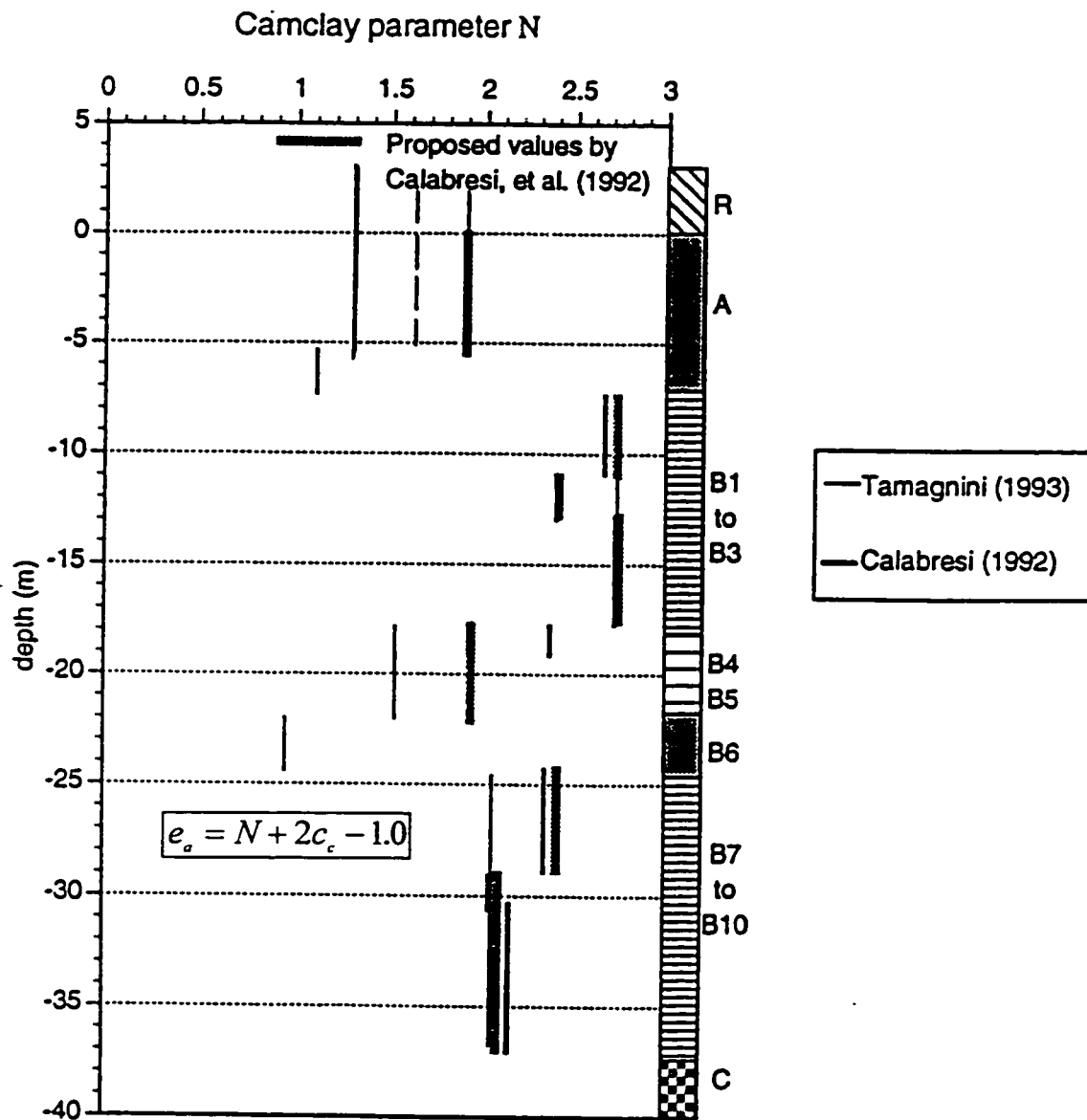


Fig. 5.7 Cam-clay compression index N vs depth
(Mitchell and Soga, 1995)

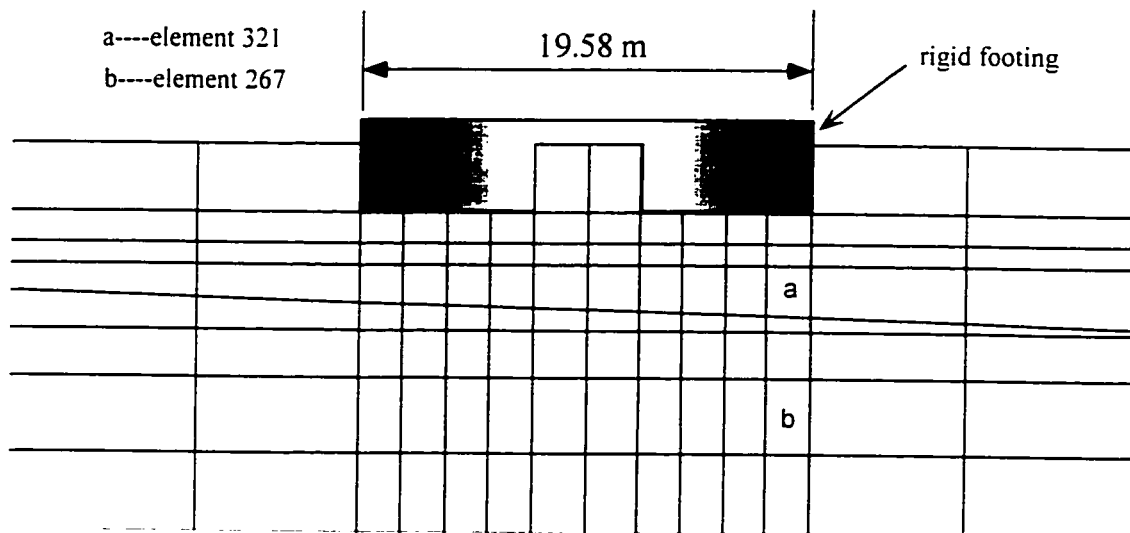


Fig. 5.8 Finite element idealization of Pisa foundation (part)

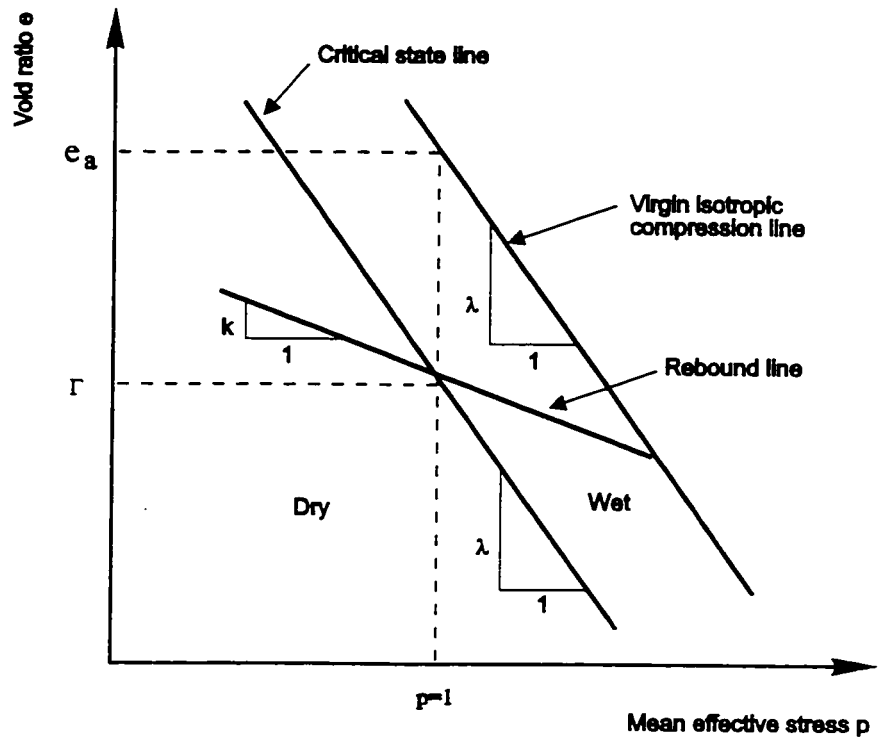
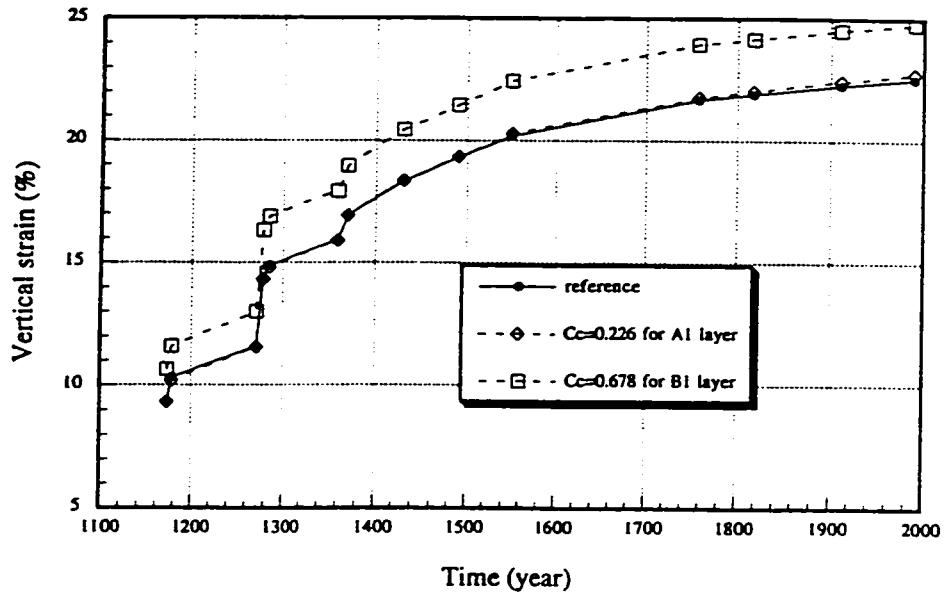
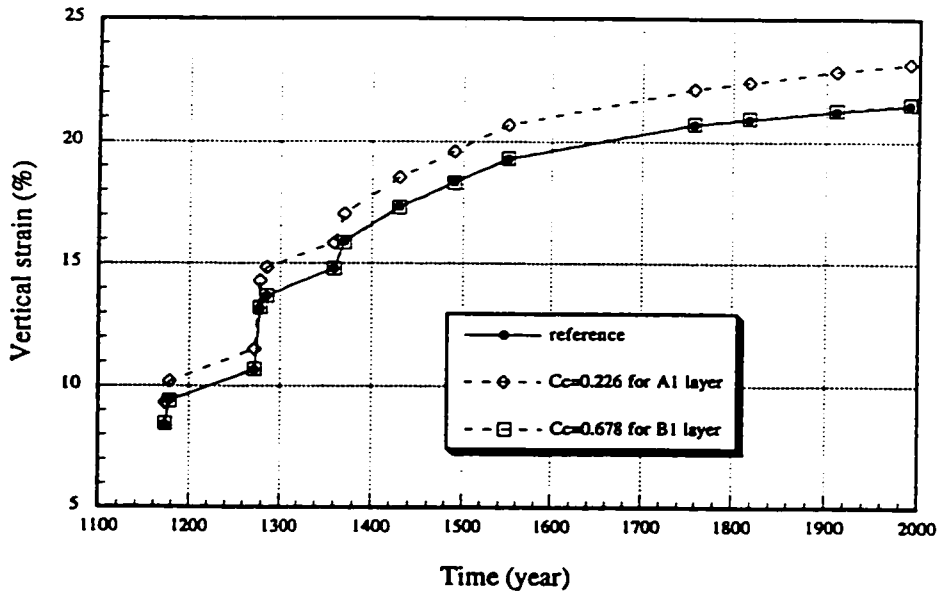


Fig. 5.9 Consolidation curves on e - $\ln p$ space

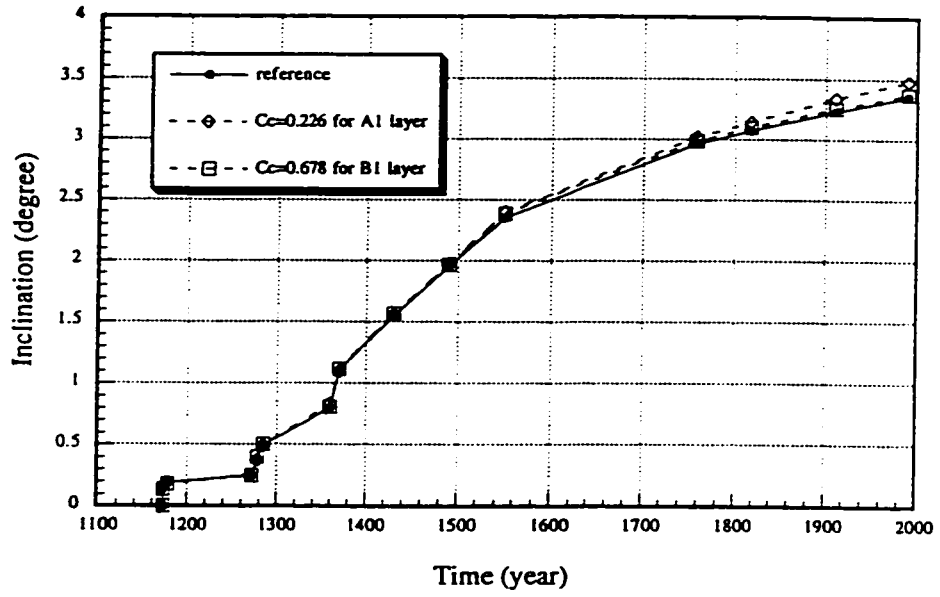


(a). Vertical strain Vs time curve (element 267, gauss point 22)

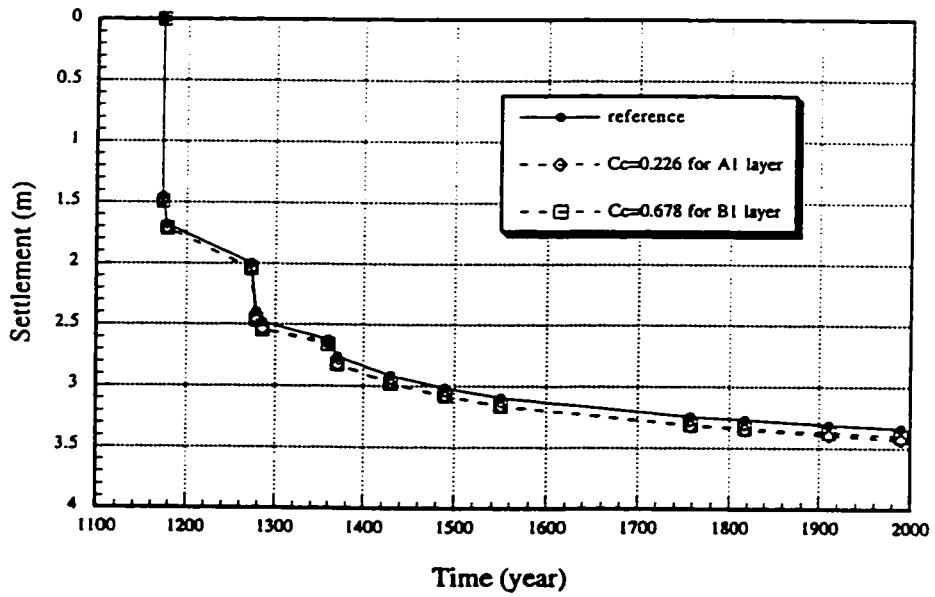


(b). Vertical strain Vs time curve (element 321, gauss point 22)

Fig. 5.10 FEA results for different values of C_c at layers A_1 and B_1



(c). Inclination Vs time curve



(d). Settlement Vs time curve

Fig. 5.10 FEA results for different values of C_c at layers A_1 and B_1 (continued)

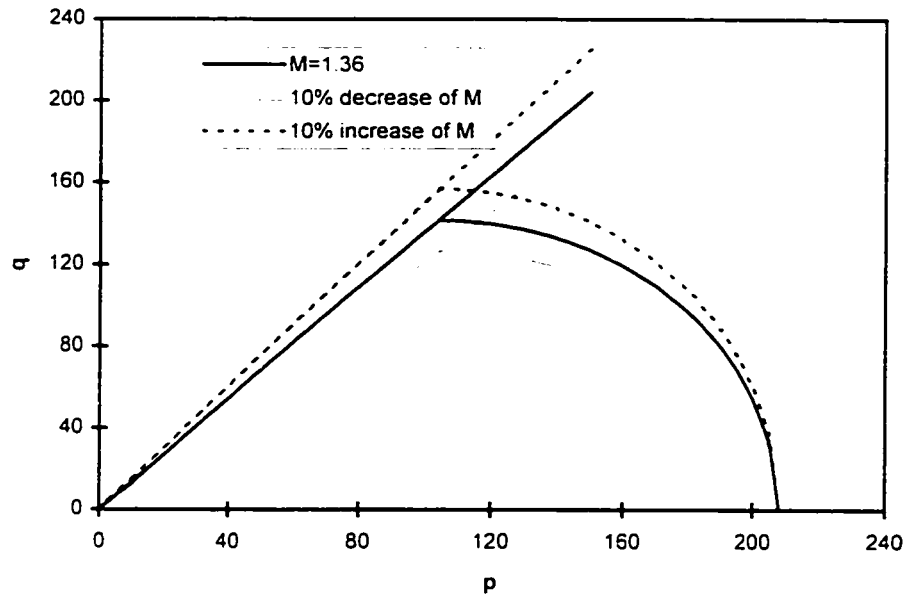


Fig. 5.11 (a) MCCM yielding surface for A1 layer

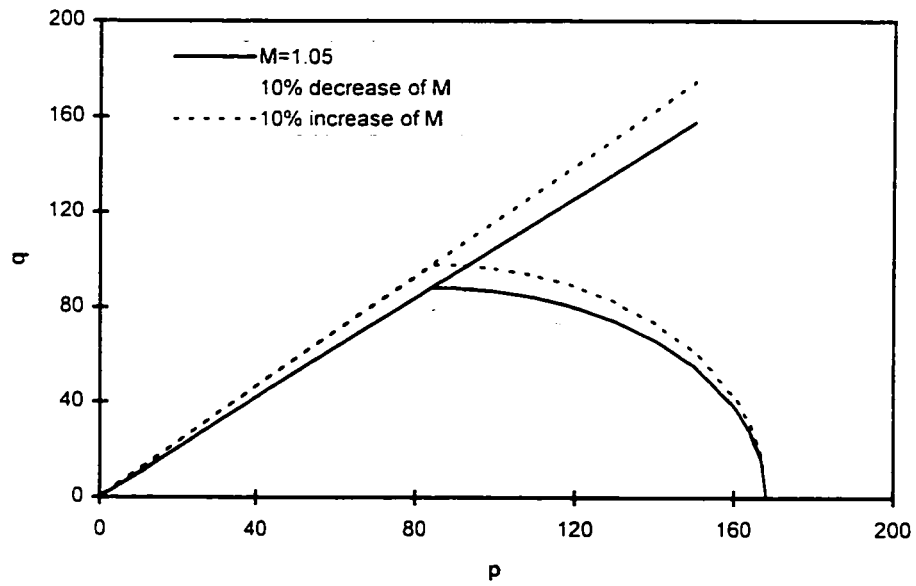
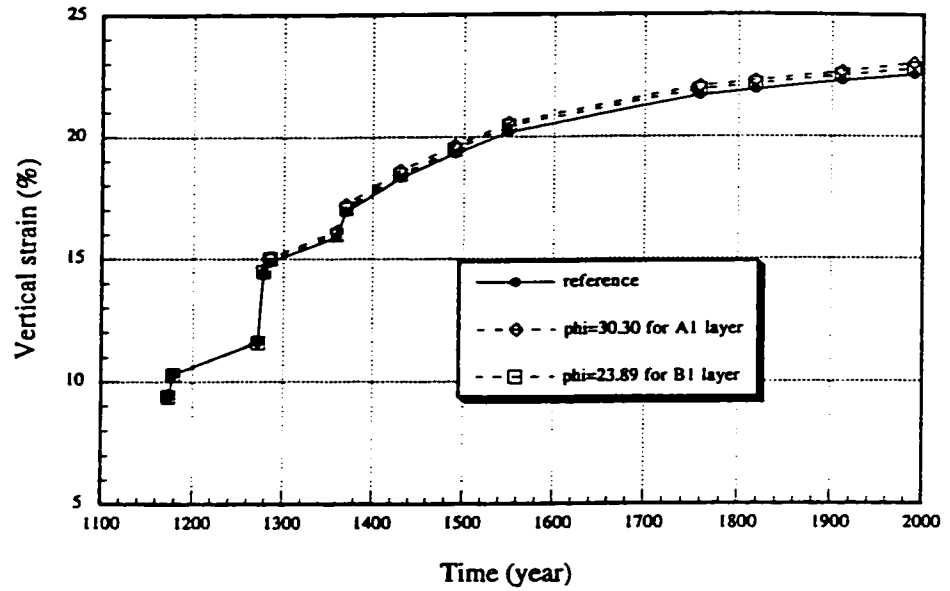
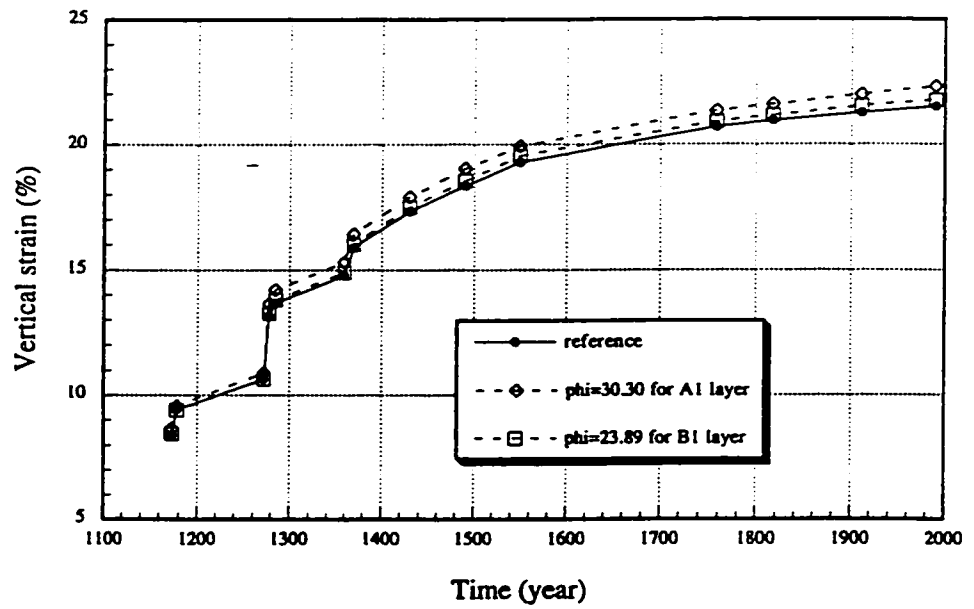


Fig. 5.11 (b) MCCM yielding surface for B1 layer

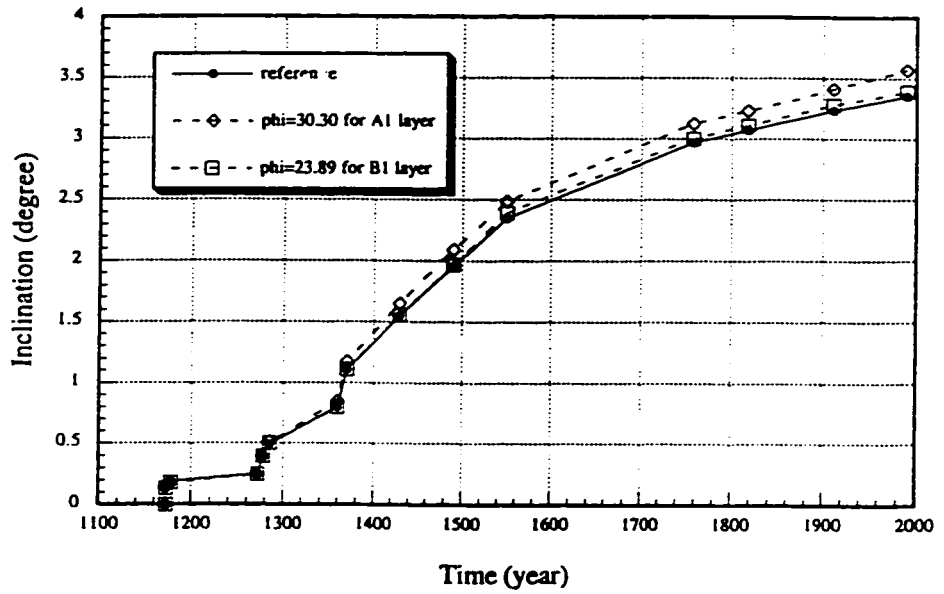


(a). Vertical strain Vs time curve (element 267, gauss point 22)

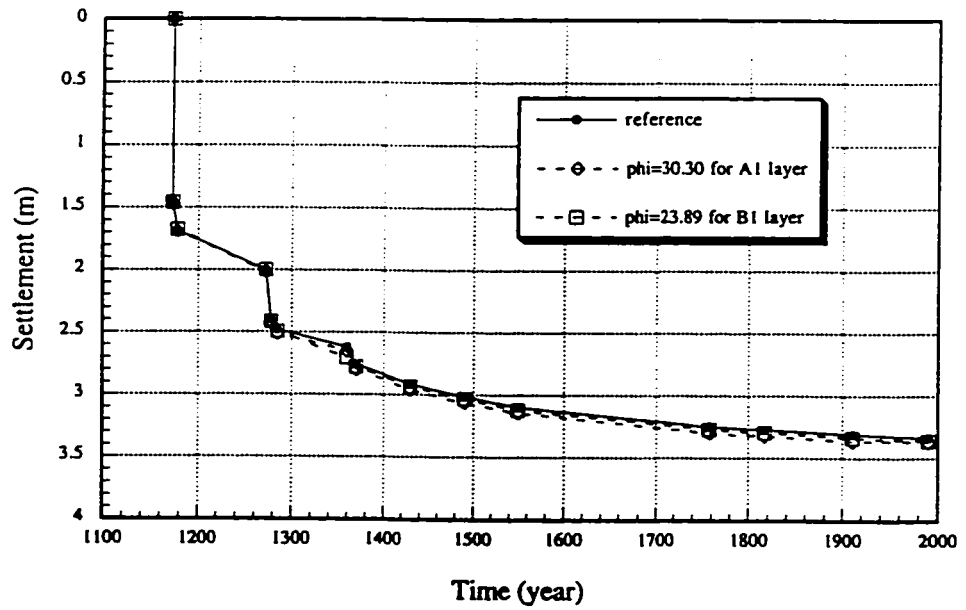


(b). Vertical strain Vs time curve (element 321, gauss point 22)

Fig. 5.12 FEA results for different values of ϕ' at layers A_1 and B_1



(c). Inclination Vs time curve



(d). Settlement Vs time curve

Fig. 5.12 FEA results for different values of ϕ' at layers A_1 and B_1 (continued)

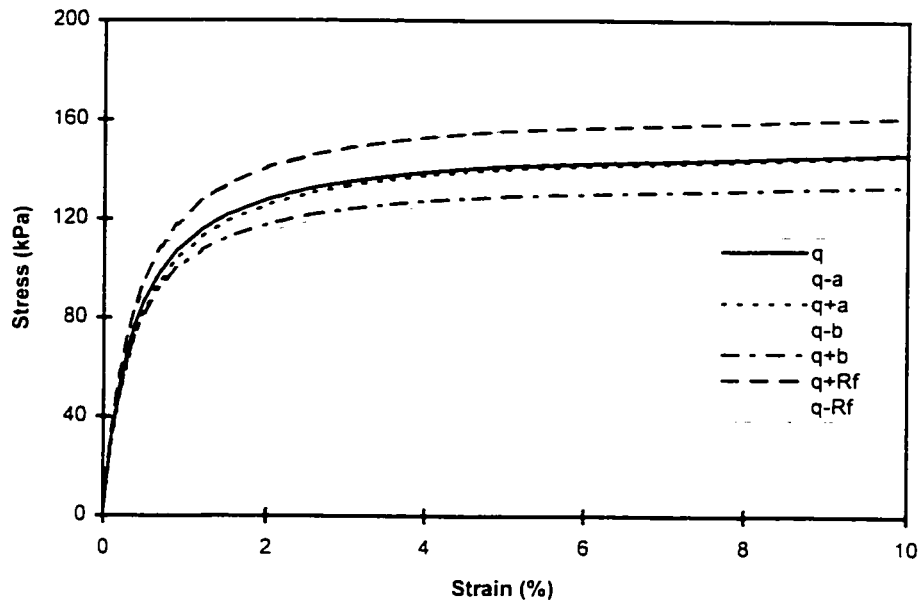


Fig. 5.13 (a) Stress-strain curves from Hyperbolic model for Al layer

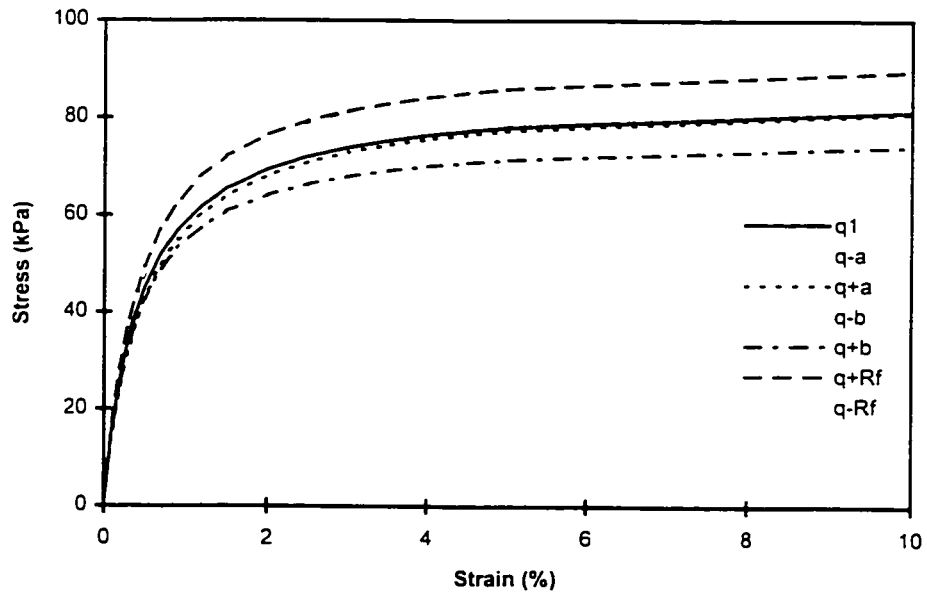
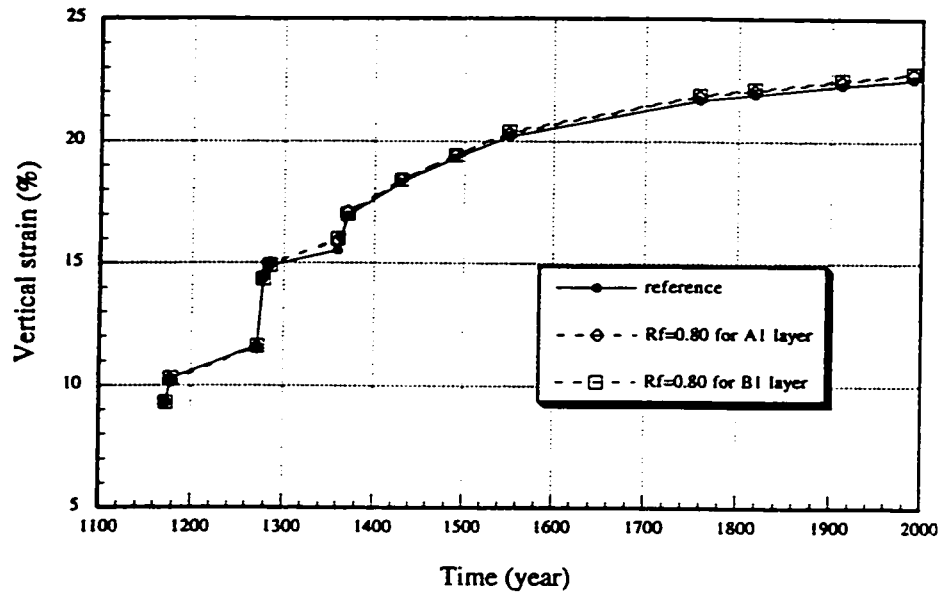
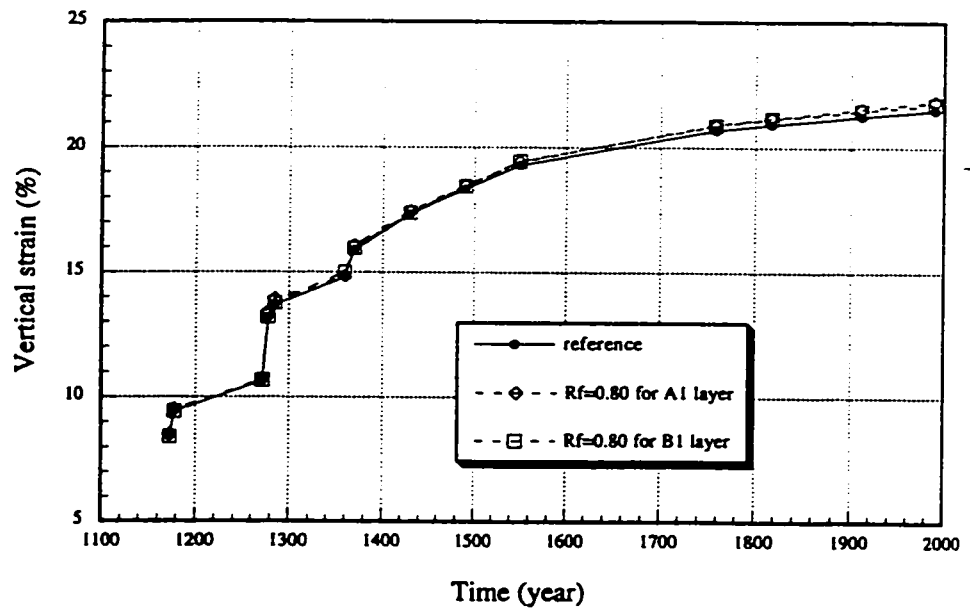


Fig. 5.13 (b) Stress-strain curves from Hyperbolic model for B1 layer

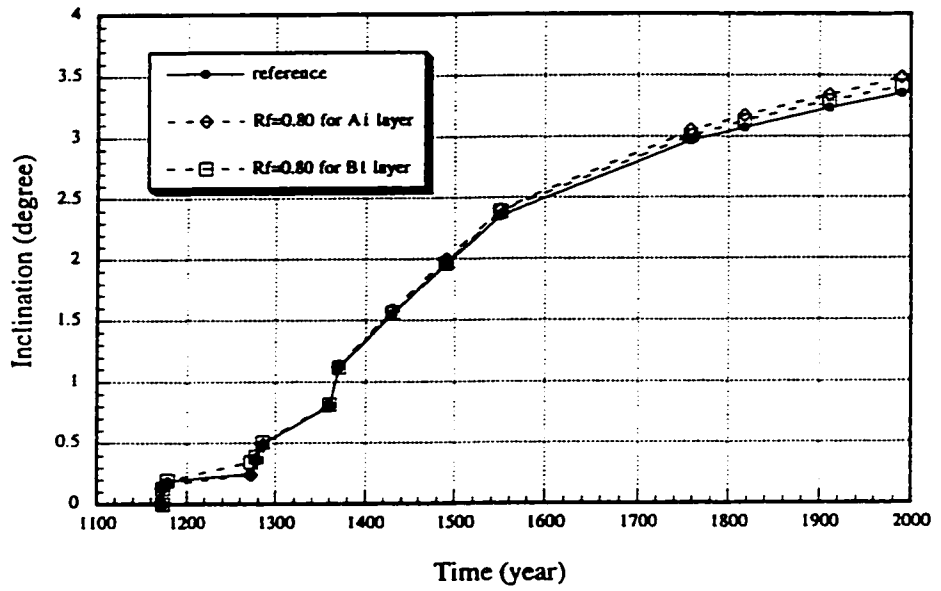


(a). Vertical strain Vs time curve (element 267, gauss point 22)

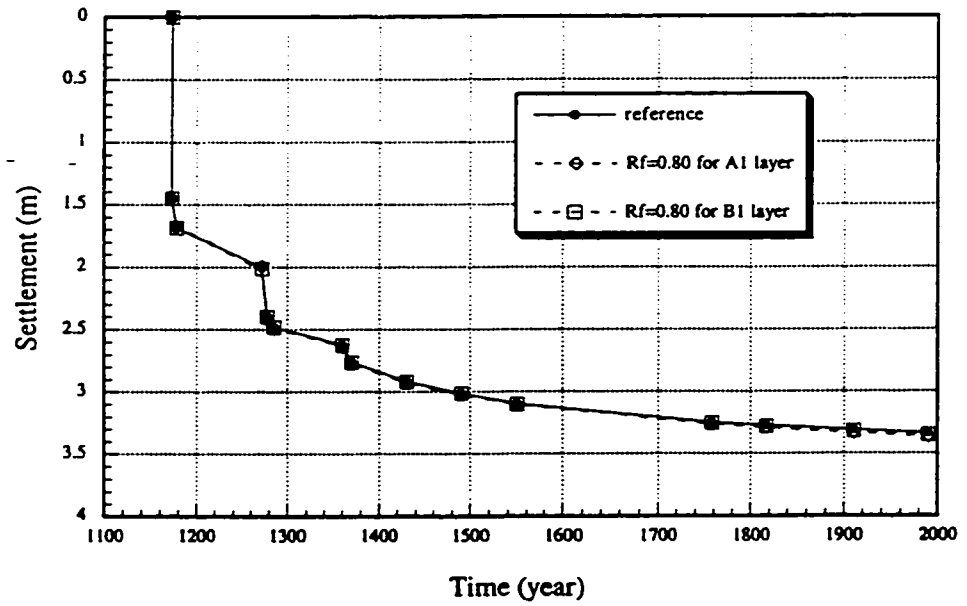


(b). Vertical strain Vs time curve (element 321, gauss point 22)

Fig. 5.14 FEA results for different values of R_f at layers A_1 and B_1

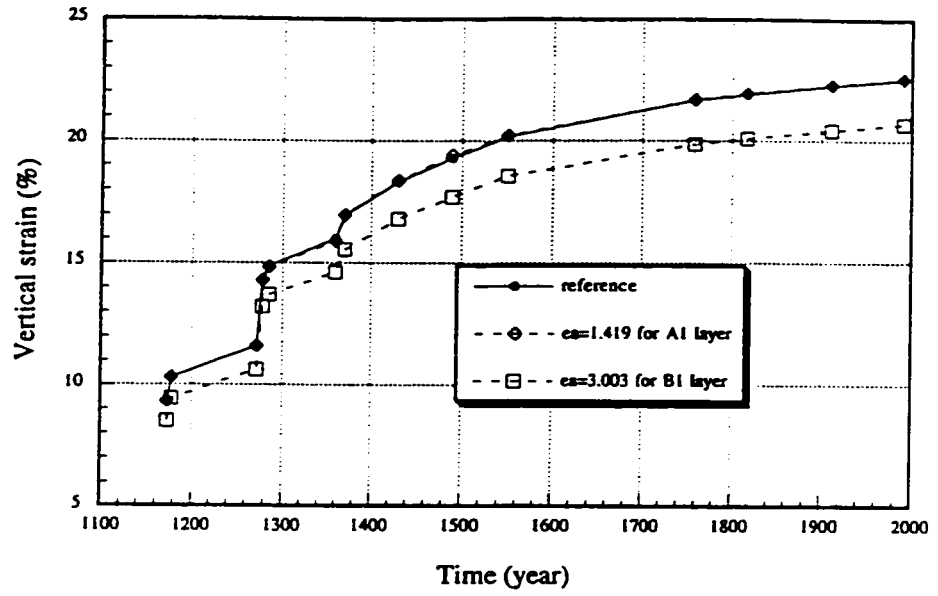


(c). Inclination Vs time curve

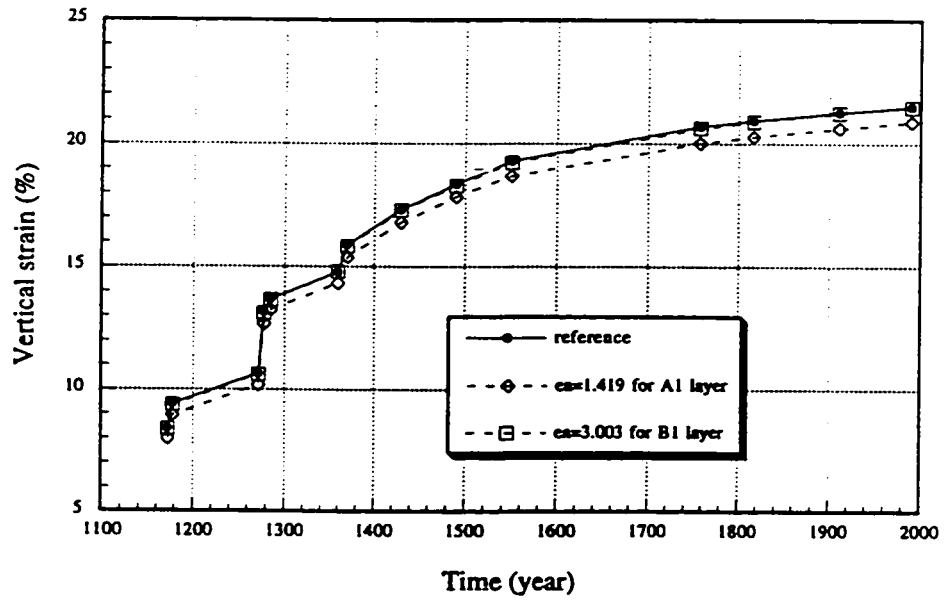


(d). Settlement Vs time curve

Fig. 5.14 FEA results for different values of R_f at layers A_1 and B_1 (continued)

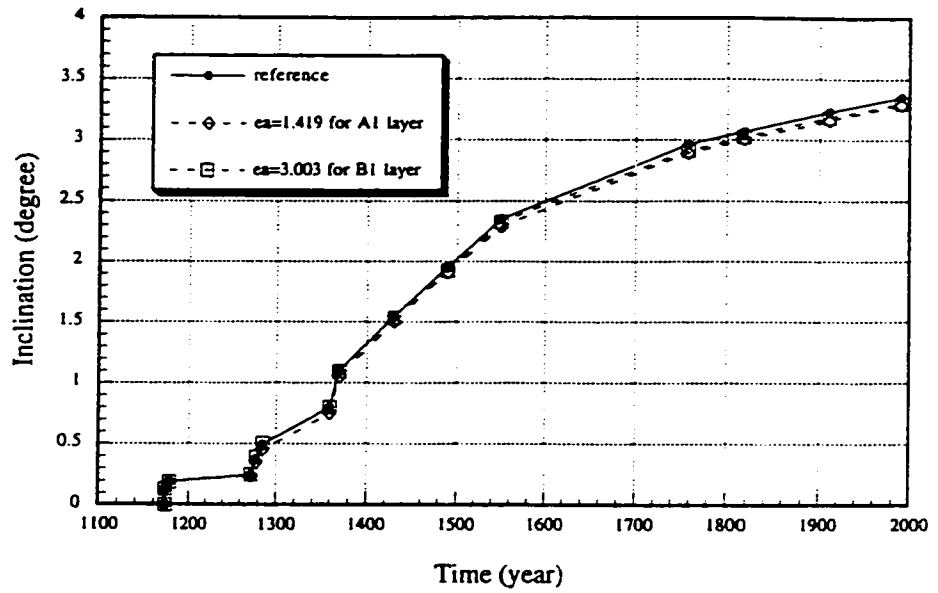


(a). Vertical strain Vs time curve (element 267, gauss point 22)

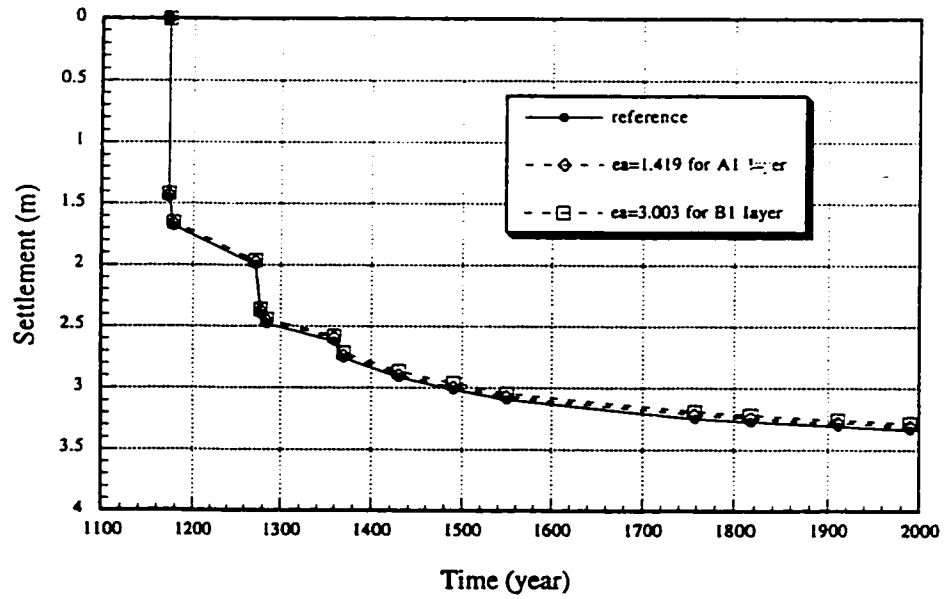


(b). Vertical strain Vs time curve (element 321, gauss point 22)

Fig. 5.15 FEA results for different values of ea at layers A_1 and B_1



(c). Inclination Vs time curve



(d). Settlement Vs time curve

Fig. 5.15 FEA results for different values of e_a at layers A_1 and B_1 (continued)

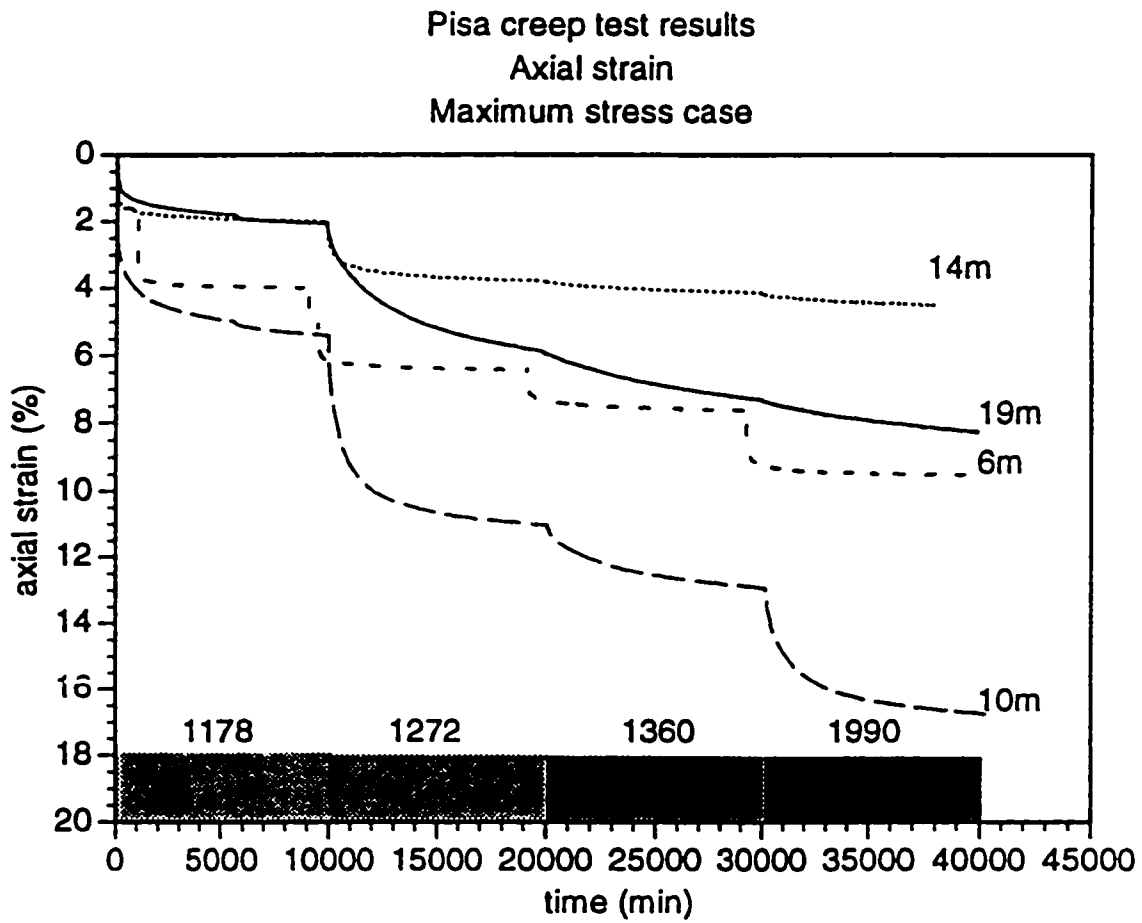


Fig. 5.16 Creep strain curves for maximum stress cases (Mitchell and Soga, 1995)

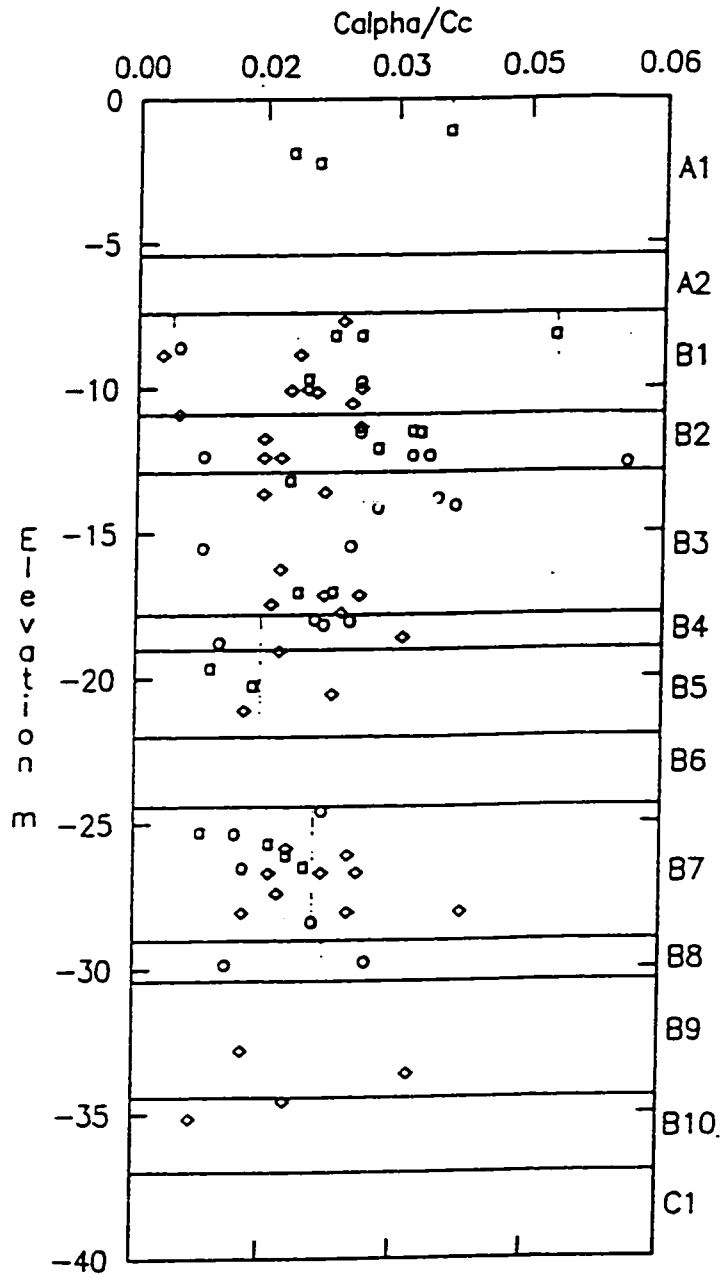


Fig. 5.17 C_α/C_c vs. depth (Calabresi, et al. 1992)

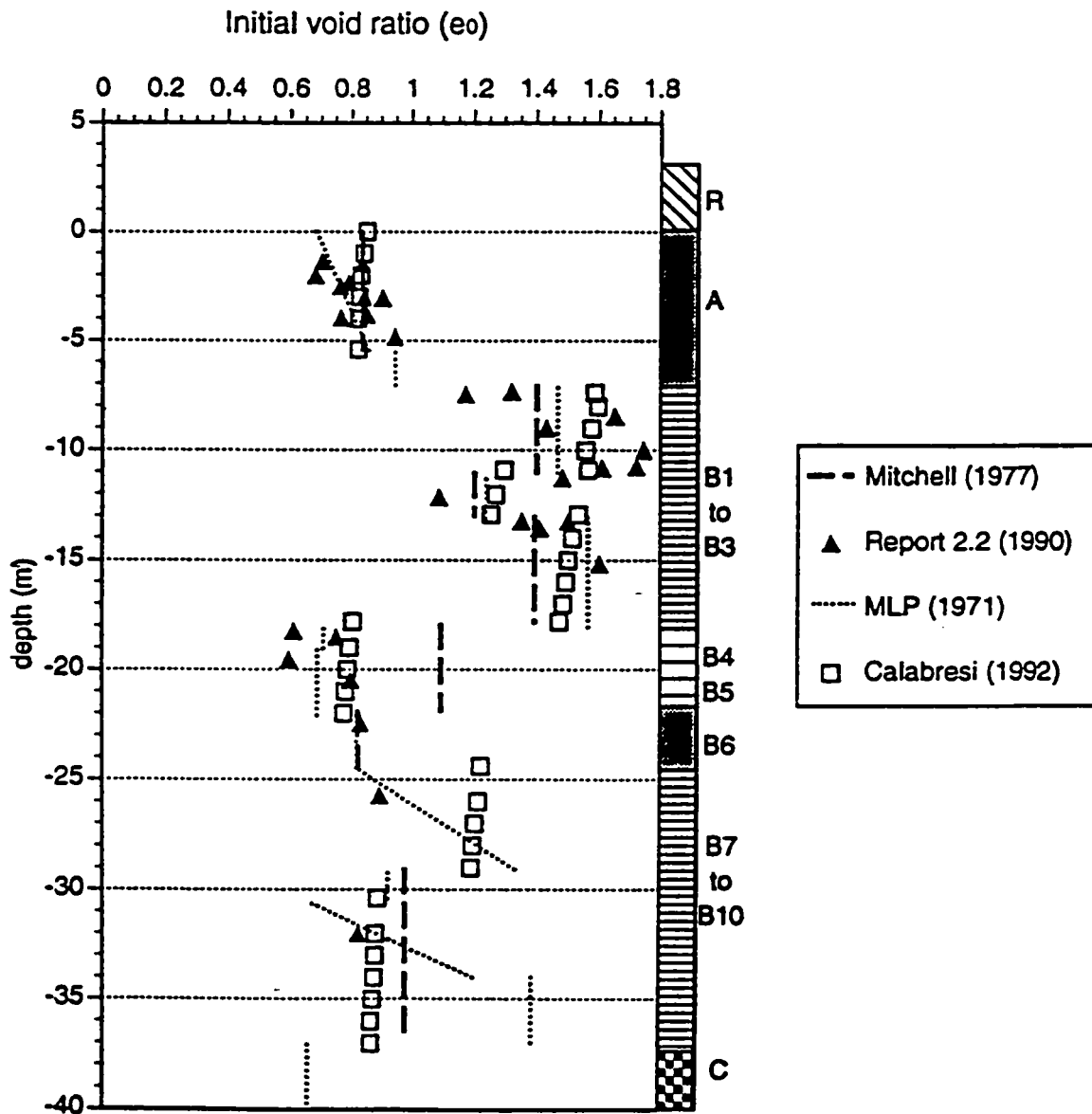
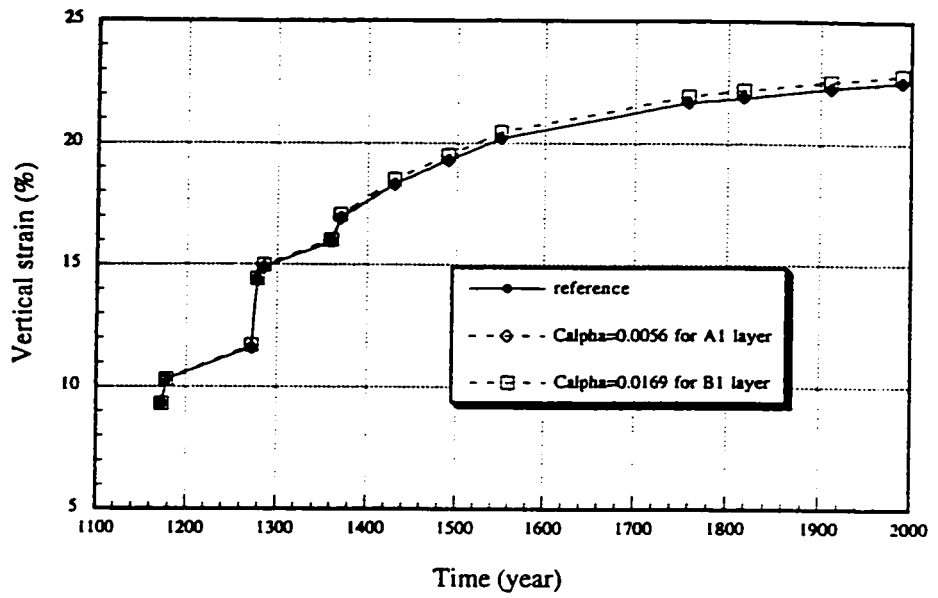
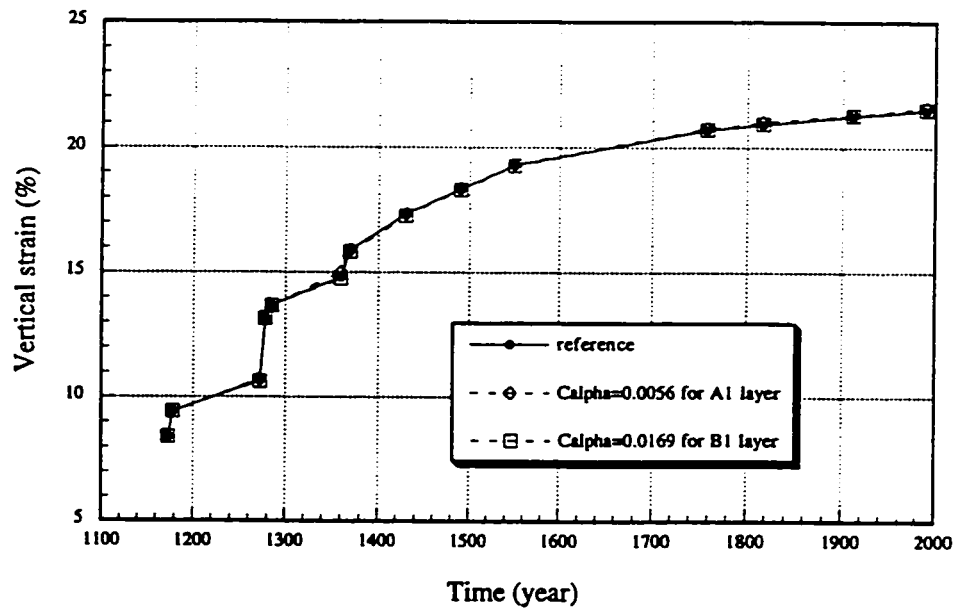


Fig. 5.18 Initial void ratio vs. depth
(Mitchell and Soga, 1995)

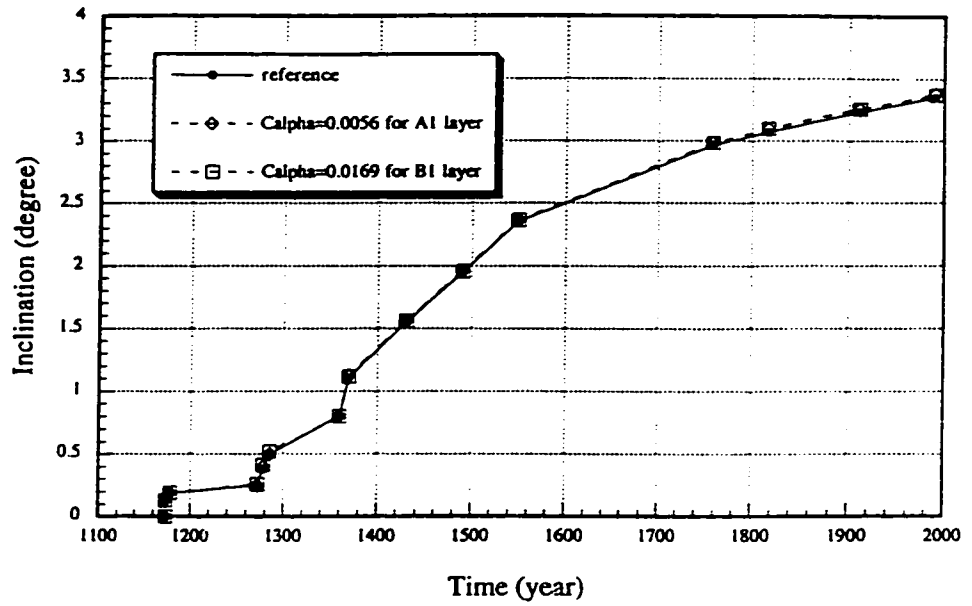


(a). Vertical strain Vs time curve (element 267, gauss point 22)

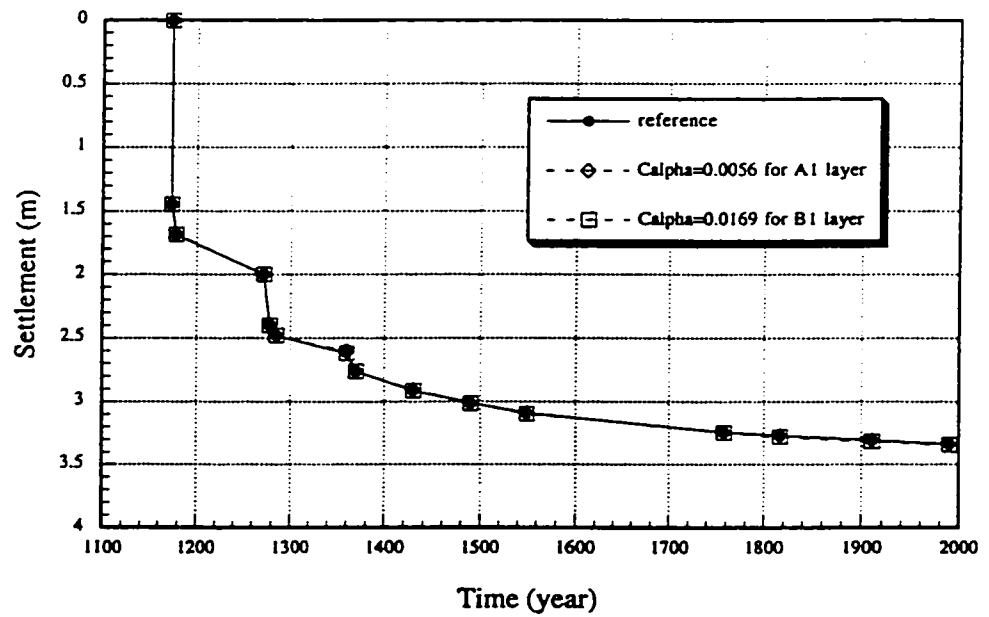


(b). Vertical strain Vs time curve (element 321, gauss point 22)

Fig. 5.19 FEA results for different values of C_a at layers A_1 and B_1



(c). Inclination Vs time curve



(d). Settlement Vs time curve

Fig. 5.19 FEA results for different values of C_a at layers A_1 and B_1 (continued)

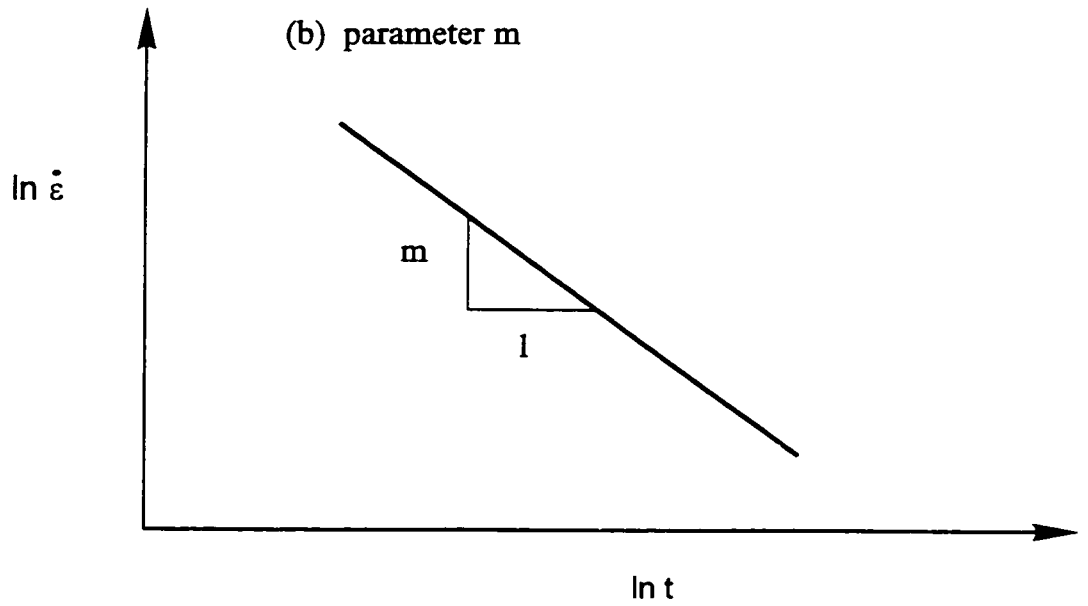
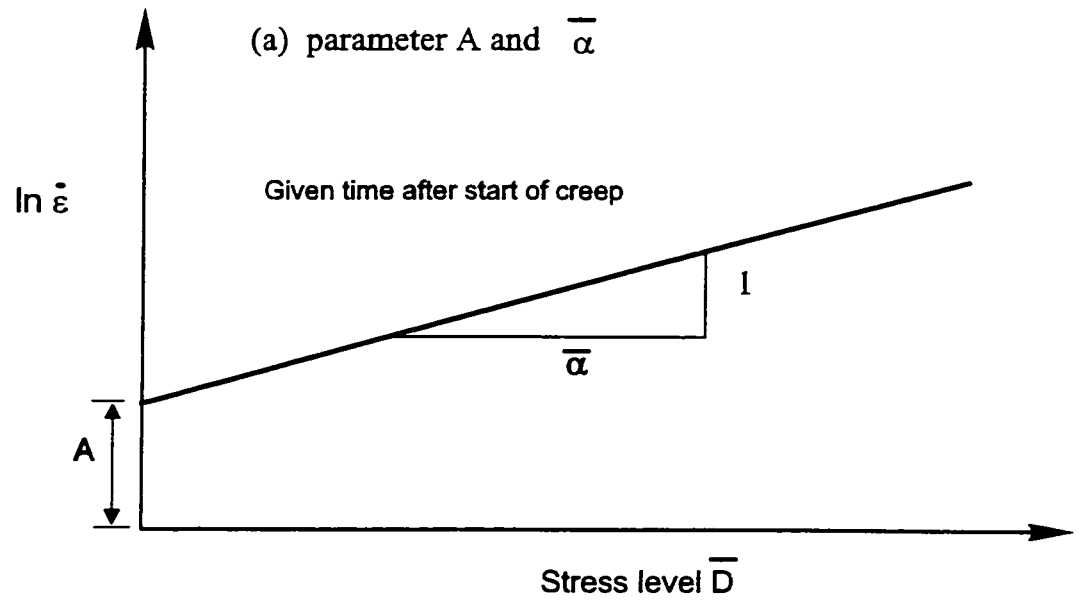
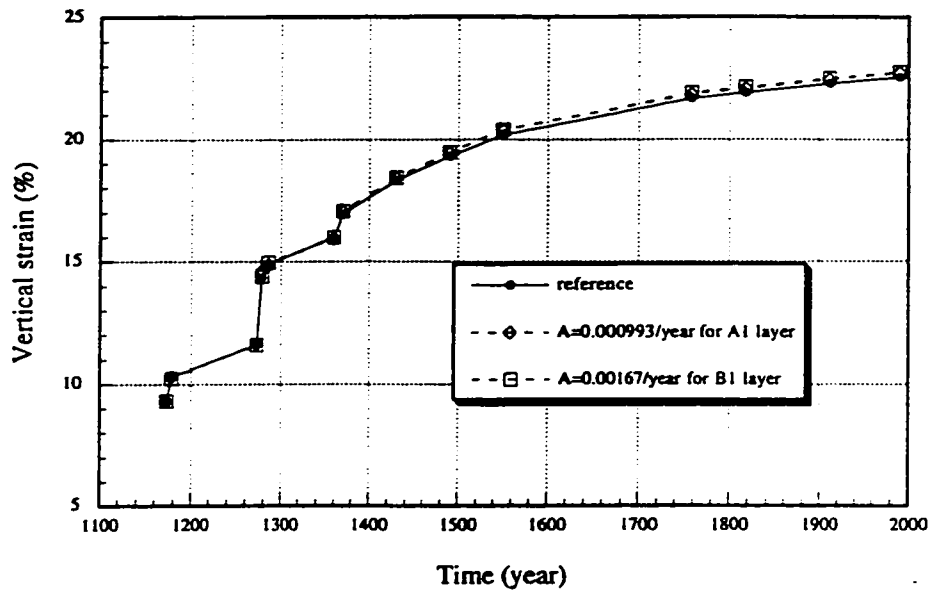
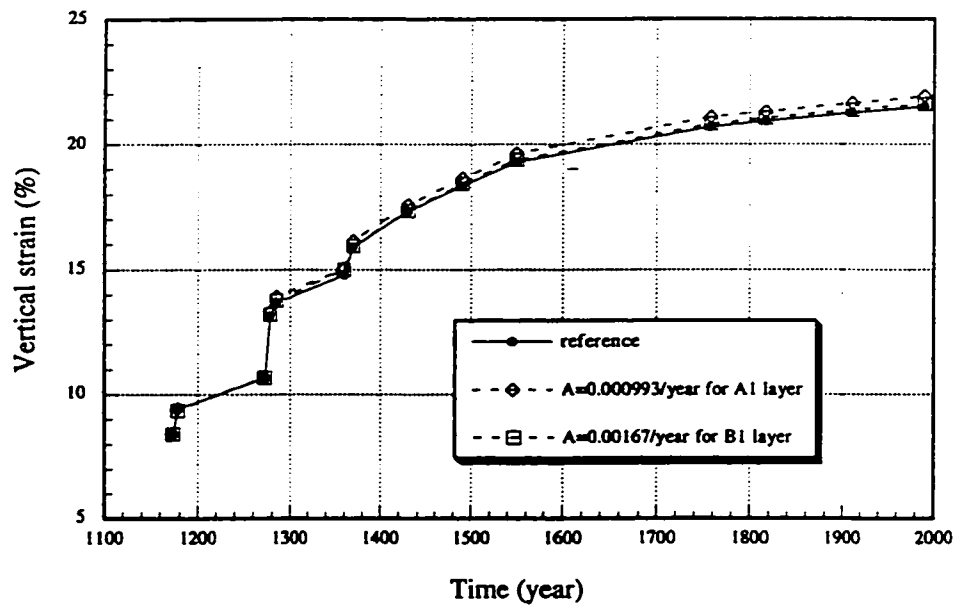


Fig. 5.20 Singh Mitchell creep parameters

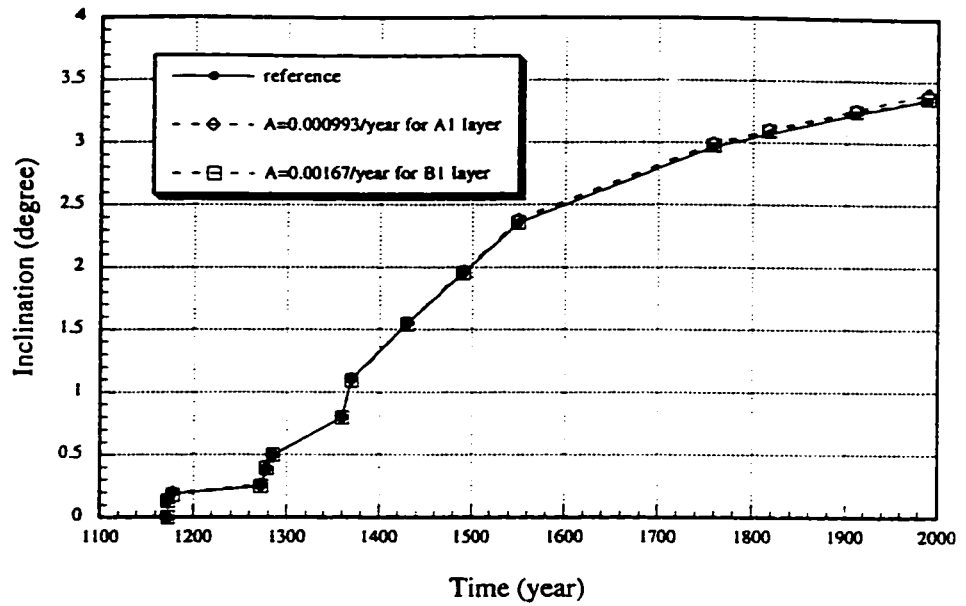


(a). Vertical strain Vs time curve (element 267, gauss point 22)

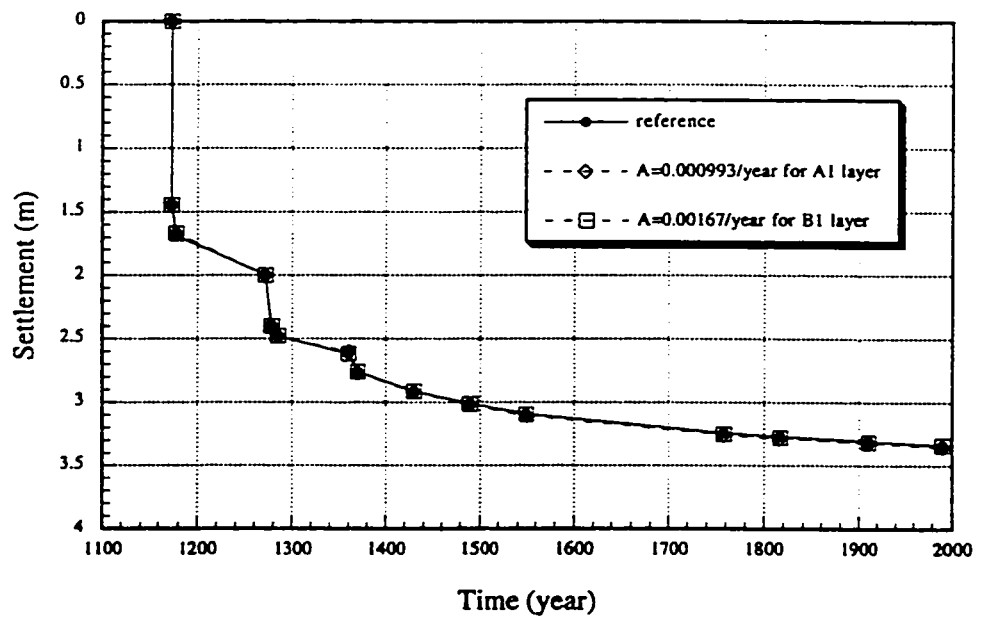


(b). Vertical strain Vs time curve (element 321, gauss point 22)

Fig. 5.21 FEA results for different values of A at layers A_1 and B_1

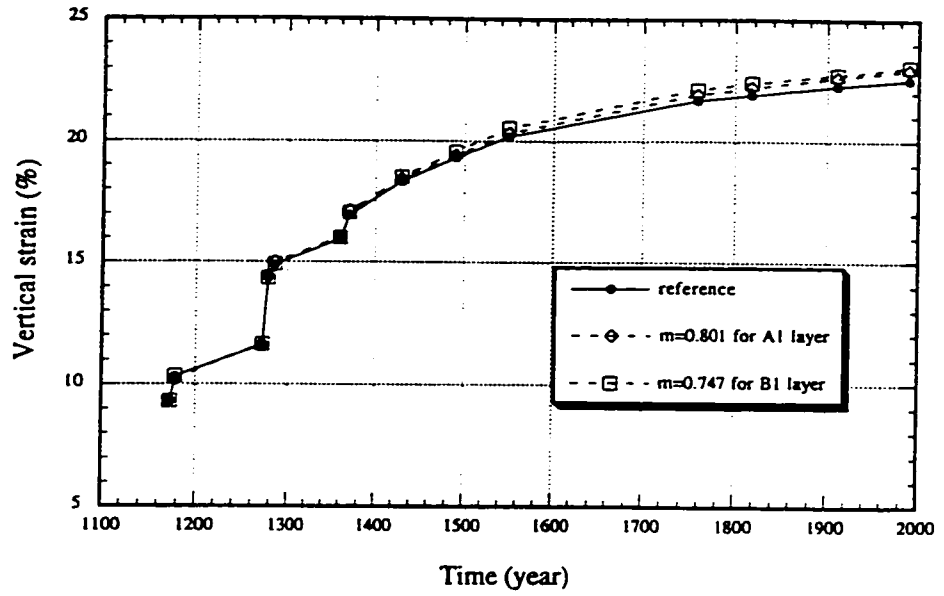


(c). Inclination Vs time curve

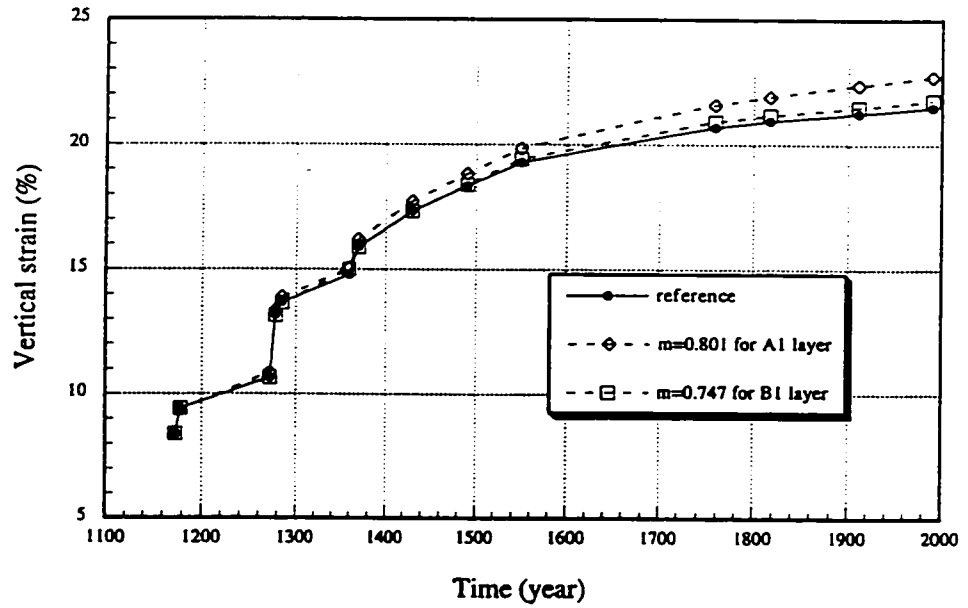


(d). Settlement Vs time curve

Fig. 5.21 FEA results for different values of A at layers A₁ and B₁ (continued)

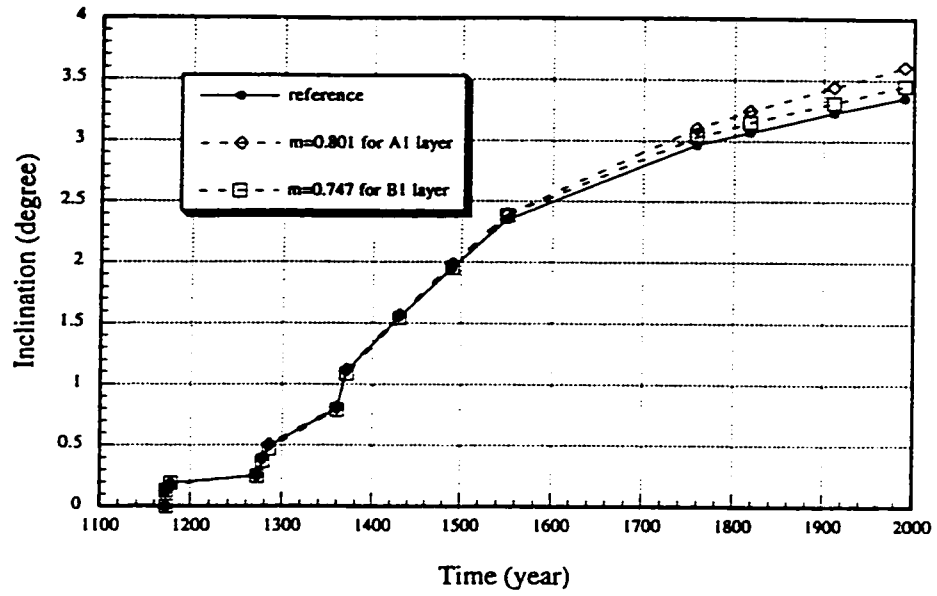


(a). Vertical strain Vs time curve (element 267, gauss point 22)

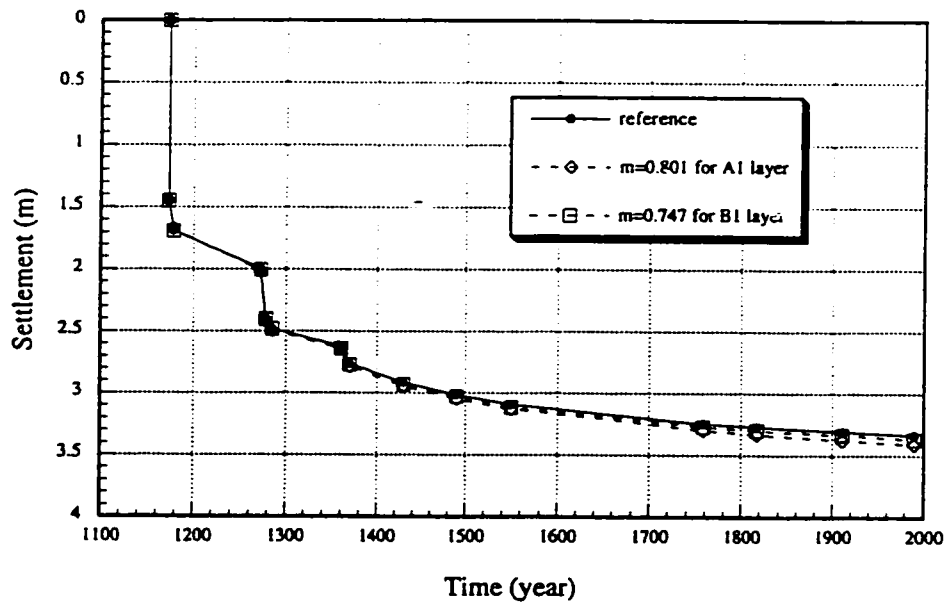


(b). Vertical strain Vs time curve (element 321, gauss point 22)

Fig. 5.22 FEA results for different values of m at layers A_1 and B_1

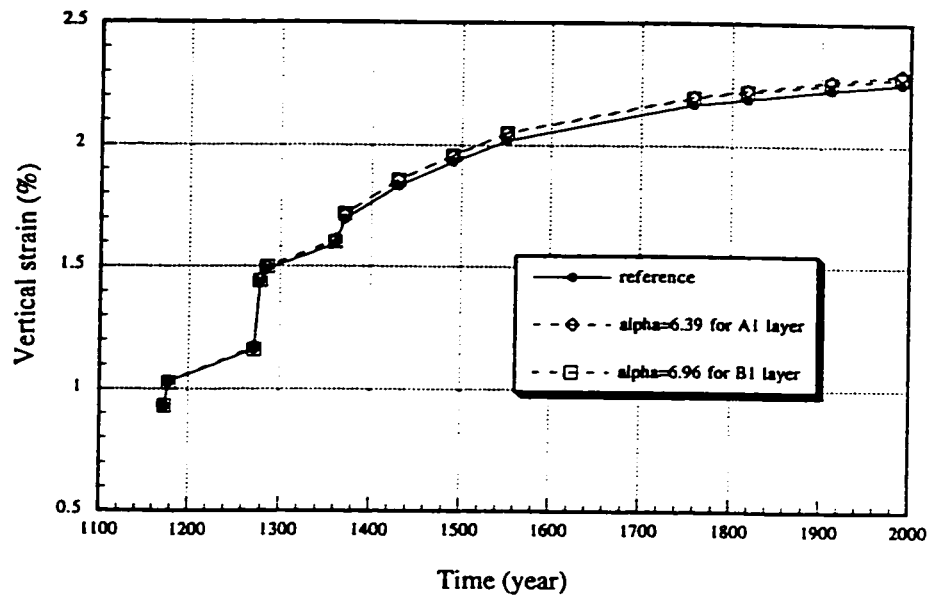


(C). Inclination Vs time curve

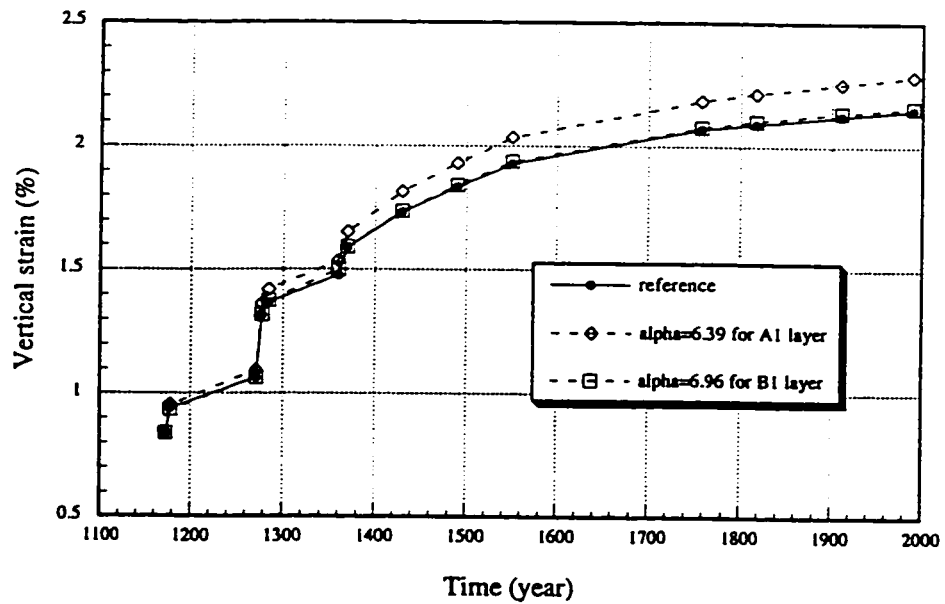


(d). Settlement Vs time curve

Fig. 5.22 FEA results for different values of m at layers A_1 and B_1 (continued)

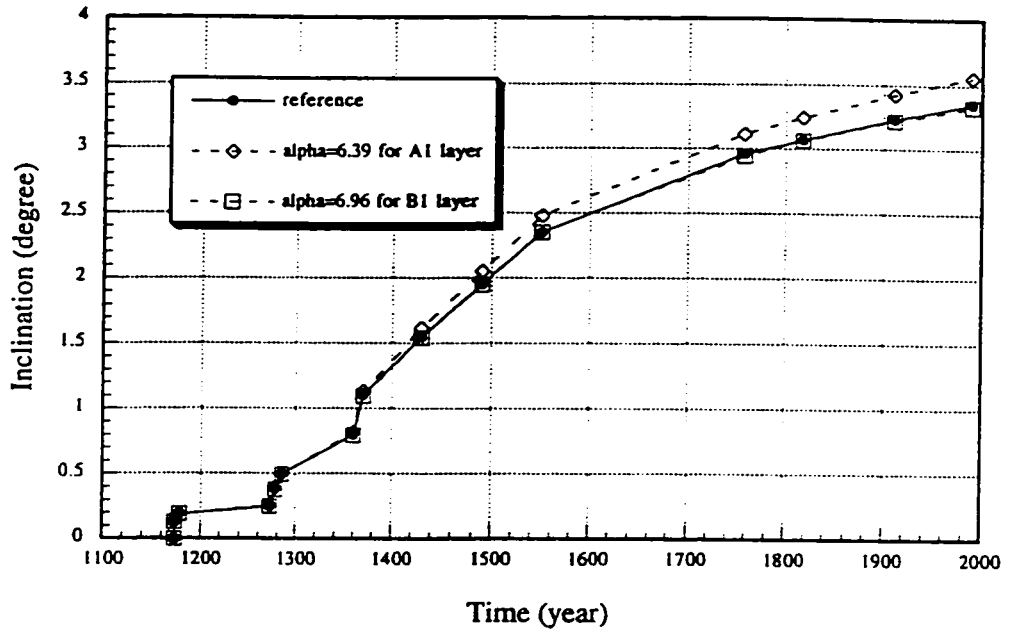


(a). Vertical strain Vs time curve (element 267, gauss point 22)

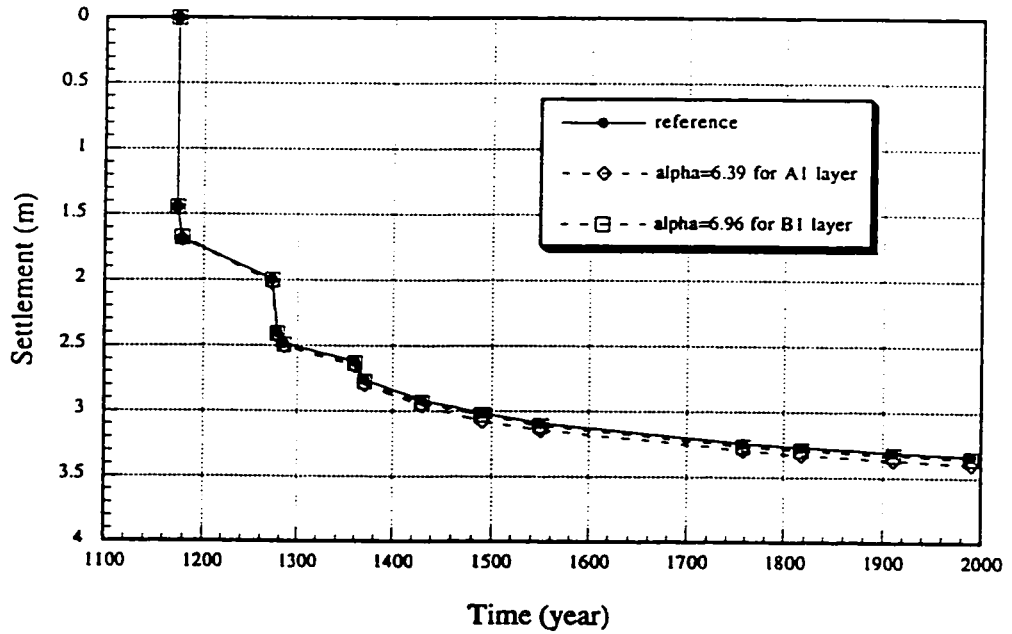


(b). Vertical strain Vs time curve (element 321, gauss point 22)

Fig. 5.23 FEA results for different values of $\bar{\alpha}$ at layers A₁ and B₁



(c). Inclination Vs time curve



(d). Settlement Vs time curve

Fig. 5.23 FEA results for different values of $\bar{\alpha}$ at layers A₁ and B₁ (continued)

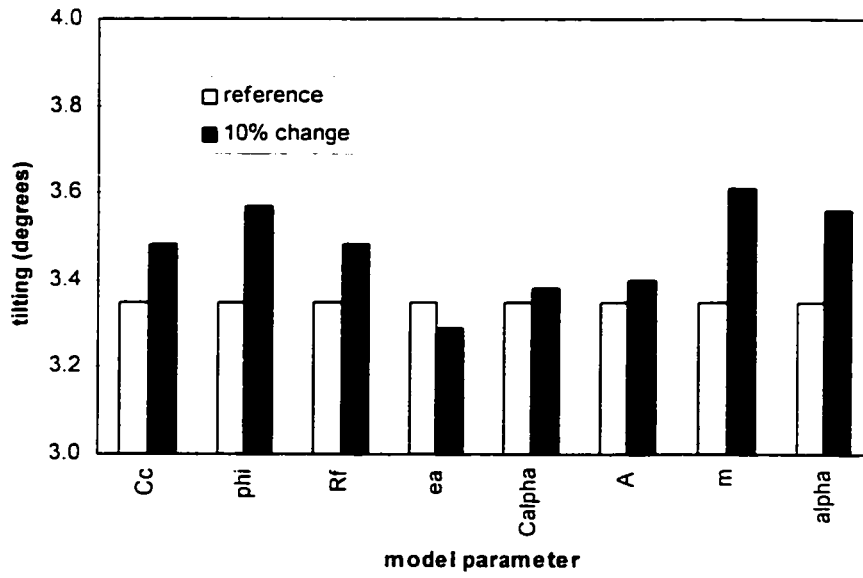


Fig. 5.24 Sensitivity of model parameters in terms of final inclination

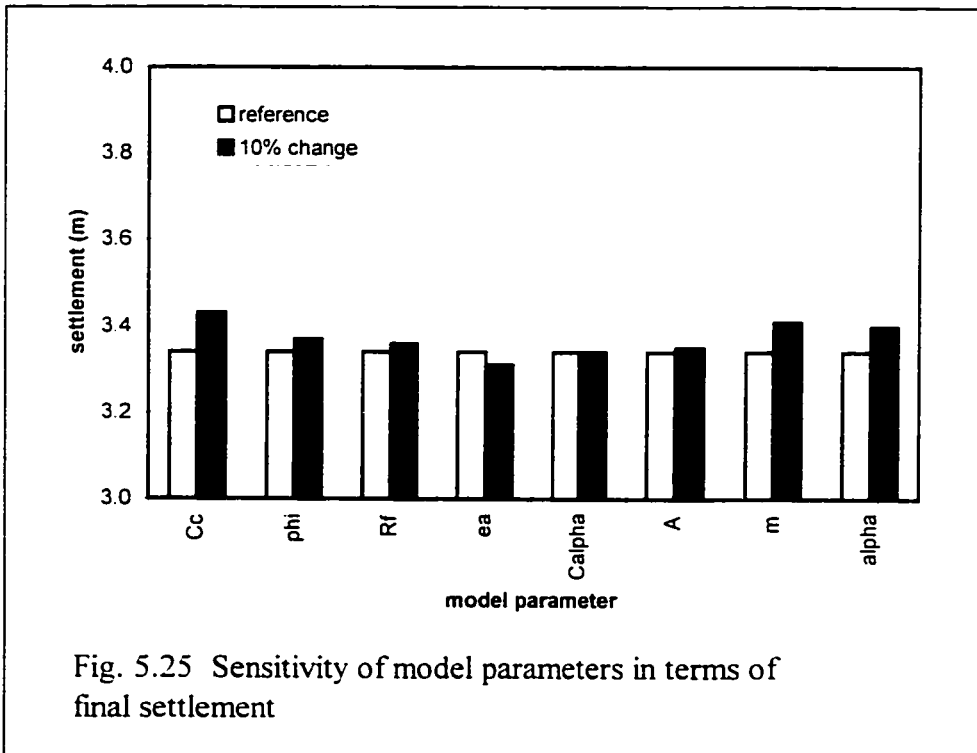


Fig. 5.25 Sensitivity of model parameters in terms of final settlement

CHAPTER 6

THREE-DIMENSIONAL VISCO-PLASTIC ANALYSES OF PISA TOWER

6.1 Introduction

It is well known that for the past seven centuries the world famous Leaning Tower of Pisa has been tilting slowly but continuously toward its south side, under a increasing risk of a sudden collapse. In order to save this wonderful monument, there have been, on file, thousands of ideas and projects that are submitted, from time to time, from all over the world. Before these ideas and projects are implemented, the phenomenon of continuous movement with time under constant load needs to be fully understood. One of the possible explanations is creep. The term “creep” is used to describe the time-dependent deformation of soil under sustained loads or stresses. This phenomenon is especially pronounced in cohesive soil. The 30m thick of soft clay underneath the tower’s foundation and the well documented data over the period of 800 year provide an excellent case for studying the creep phenomenon.

Previous numerical investigations conducted by Burland and Potts (1995), Mitchell and Soga (1995), showed that in order to fully simulate the deformation behavior of the soil beneath the tower’s foundation, three-dimensional visco-plastic analysis is necessary. Even though, the tower structure itself is almost axisymmetric, the loading is non-axisymmetric. In this study, three-dimensional visco-plastic analyses of the foundation with and without the tower part were conducted through a time-dependent plastic model named the double-yield surface Cam-clay plasticity (DYSCP) model. This study represents the first application of the DYSCP model under a three-dimensional condition. It is also the first attempt for visco-plastic analysis to be carried out for the soil

underneath the tower's foundation. The capability of the numerical model in predicting the stress-strain-time behavior under a three-dimensional field case is illustrated. Creep effects on the deformation behavior and stress strain distribution of the soil beneath the tower' foundation are studied in detail. A better understanding of the deformation mechanism of the tower is obtained.

6.2 The constitutive model

6.2.1 Yielding surfaces

The DYSCP model was proposed by Borja and Kavazanjian (1985) and Hsieh et al. (1990). This model is adopted here for its simplicity and successful application in field cases (Borja et al. 1990 and Morsy 1994). To fully define the model, only thirteen material parameters are required. Seven of them are needed in the absence of creep; six more are required for the presence of creep. All parameters are readily obtainable from standard laboratory tests or from correlation with index properties of the soil, which are familiar to most geotechnical engineers. Figure 6.1 shows the projection of the yield surfaces on the p-q plane. It is represented by the ellipsoid of the modified Cam-clay model F and the Von-Mises cylinder G inscribed in the ellipsoid. This model is used to evaluate both time-independent and time-dependent components of strains. Because the stress levels at some small areas close to the footing exceed the valid range of the model (20% to 80% of their shear strength), as indicated in the two-dimensional plane strain analysis in Chapter Four, certain inaccuracy of the numerical results may be expected.

6.2.2 Numerical stability criteria

In visco-plasticity analysis with a variable time scheme, oscillating results can be obtained if time steps exceed a certain magnitude; which indicates the instability of the process. In the consideration of accuracy, some empirical rules have been proposed (Zienkiewicz and Corneau 1974, Corneau 1975). The first one relates the time step

magnitude to the anticipated changes of visco-plastic strain: the second one relates the change of time step between successive intervals.

A convenient scalar measurement of the visco-plastic strain is obtained by the second strain invariant defined as:

$$[6.1] \quad \bar{\varepsilon} = \sqrt{\frac{2}{3} \varepsilon_{ij} \varepsilon_{ij}} = \sqrt{\frac{2}{3} (\varepsilon_{11}^2 + \varepsilon_{22}^2 + \varepsilon_{33}^2 + 2(\varepsilon_{12}^2 + \varepsilon_{23}^2 + \varepsilon_{31}^2))}$$

where ε_{ij} is the strain tensor, $i=1,2,3$ and $j=1,2,3$. The maximum increment of this scalar visco-plastic strain will be limited to a certain fraction of the total accumulated strain at all integrating points, as follows:

$$[6.2] \quad \Delta t^n = \tau \left[\frac{\bar{\varepsilon}^n}{\bar{\dot{\varepsilon}}^n} \right]_{\min}^{1.2}$$

where Δt^n is the time increment at step number n ; τ is the time-increment parameter, its value must be specified by the user. For an explicit scheme, τ is in the range of 0.01 to 0.15; $\bar{\varepsilon}^n$ is the second total strain invariant at step n ; $\bar{\dot{\varepsilon}}^n$ is the second strain rate invariant at step n ; and \min is the minimum value of Δt^n (time step), which is taken over all integration points in the soils.

A further limit is generally imposed to relate the change of time step between successive intervals.

$$[6.3] \quad \Delta t^{n+1} \leq 1.5 \Delta t^n$$

where Δt^{n+1} is the time increment at step number $n+1$.

Previous investigations (Zienkiewicz and Corneau 1974, Corneau 1975) show that none of these empirical criteria are entirely satisfactory, and none prevent some forms of instability occurring.

The determination of the time-increment parameter τ is one of the major problems in visco-plastic analysis, especially under three-dimensional conditions. A large value of τ will result in numerical instability, while a too small value of τ will give a stable result but will result in computer cost inefficiency, especially for three-dimensional creep analysis. Since the creep process is non-associative in the DYSCP model, the stiffness matrix is non-symmetric. Currently, there are no satisfactory criteria available to prevent numerical instability in the double-yield surface case. In order to balance the problems between the numerical instability and the analysis time-consuming, a trial and error method is used here to optimize the value of τ .

For a selected value of τ , the analysis typically runs a couple of days in the IBM RISC System/6000 machine before the unstable results are observed. It is unrealistic to try many different values of τ . Here, three different values (0.05, 0.02, and 0.01) have been selected. τ of 0.05 has been tried first and unstable results were found. τ of 0.01 gave stable results but was very costly. Finally τ of 0.02 was found to be a relatively optimum value and was used in this study.

6.3 Ground profile and construction history of Pisa Tower

Figure 6.2 shows a cross-section of the Pisa Tower. It consists of a hollow masonry cylinder nearly 60m in height and 20m in footing diameter. At present, the footing is inclined toward the south side at about 5.5° to the horizontal and has been increasing by 6 arc seconds a year (Burland and Potts 1995). The average inclination of the axis of the tower is less than 5.5° due to its slight curvature.

Figure 6.3 shows the ground profile underlying the tower proposed by Calabresi et al. (1992). It contains three main formations: Formation A contains clayey silt and silty sand, and is about 10m in thickness. CPT tests reveal that its inhomogeneity is significant. The north side soil is more rigid than the south side which is believed to be of major significance as regards the lean; Formation B contains predominantly clay, and is

about 30m in thickness. It includes the upper clay or Pancone clay (B_1 to B_3), the intermediate clay (B_4 to B_5), the intermediate sand (B_6), and the lower clay (B_7 to B_{10}); and Formation C contains slightly silty sand. It is encountered at a depth of 40m, and extends to a depth greater than the deepest boring.

A series of drained triaxial creep tests conducted by Mitchell and Soga (1995) showed that creep deformation was important in the soil underneath the tower's foundation. Test samples from layer B_1 exhibited very large axial strain (up to 16%) due to its high plasticity and relatively large tower loads. Test samples from layer A_1 also exhibited large deformations (up to 9%) due to very large tower load increments.

The construction process of the tower contained three stages with two interruptions (see Figure 6.4). It started in 1173 and finished in 1370. The whole construction lasted about two hundred years. From the beginning of its construction, the tower has never been vertical. Not long after 1173, it began to lean toward the north side. From 1271, southward leaning became evident and has been continuous ever since. Detailed study shows that the tower would have fallen over during the construction period if there had not been any interruption.

6.4 Historic tilting and major disturbance of Pisa Tower

As mentioned by Burland and Potts (1995), it is necessary to learn as much as possible about the tilting history of the tower, since the only means to calibrate a model of the tower is to attempt to simulate the tilting history during, and subsequent to its construction.

Figure 6.5 shows the tilting history of the tower. The displayed data have been highly qualitative until 1817, when the first recorded measurement was made by Cressy and Taylor. From this figure it can be seen that significant tilting of the tower occurred only after the second construction stage. When the bell chamber was finished, the tilting was 1.6° . In 1550, the tilting increased dramatically, up to 4.7° . The tilting angle increased

more than 3.0° in this time period. What happened at that time which accelerated the tilting of the tower is not clear. There are no related historical records available. The only clue relates to the Meloria War during which Pisa city suffered a disastrous defeat by Genoa.

One possible explanation for the discontinuity of the tower inclination is that after the tower reached its full height, leaning instability occurred, which caused the tower to rotate around a center above the foundation (Burland and Potts 1995). This kind of pure rotation amplifies the tower's inclination.

Another possible explanation for this discontinuity is the possibility of the footing material failure at some area around the south side. The annular footing is made with an infill masonry structure. The thin inner and outer facings of the hollow cylinder are made of marble, while the annulus between the facings is filled with rubble and mortar within which some extensive voids have been found (Jamiolkowski et al. 1993). After the tower reached its full height, it was very possible that very high stress concentrations might occur at the south side of the footing and cause the footing material to fail. Thus, the tower had to rotate further to the south side to reflect this effect.

During the Second World War, Pisa city was subjected to notable destruction from heavy bombing raids. Some artistic treasures, including the Piazza dei Miracoli, were seriously damaged (Verlag La Torre s.r.l. 1984). Even though there is no detailed record available related to the direct damage of Pisa tower, it is almost certain that the tower suffered from bomb explosion shocks. This kind of dynamic influence may cause the tower to tilt more.

Among the recorded events, the excavation of the catino in 1834 appears to have caused an increase in tilting by 0.5° . The bottom of the excavation was below the groundwater table, and a substantial flow of water poured out on the south side of the tower, carrying with it noticeable quantities of solid material.

For most of this century, the inclination of the tower has been increasing, but these changes of inclination are extremely small compared with those that occurred during and immediately following the construction. Figure 6.6 shows the tower tilt in the North-South plane. Four major perturbations can be seen. The foundation masonry grouting in 1933 caused a sudden increase in tilt by 31 seconds. The soil and masonry drilling in 1966 caused 6 seconds increase. Ground water lowering from 1970 to 1974 caused 41 seconds increase. A masonry boring in 1985 caused an increase in tilt by 10 seconds. The current rate of tower inclination has doubled since the 1930s. The tower is very sensitive to even the smallest ground disturbance.

The systematic monitoring of the tower shows that temperature changes also have some influence on the tower's movement. Figure 6.7 shows daily movements of the tower obtained by means of an inclinometer named the Girometti-Bonacchi Pendulum. The tower expands as it is heated by the sun. It rotates in a loop as the sun moves across the sky (Wheeler 1995). Some of this motion causes the tower to screw into the ground.

A study by Croce et al. (1981) shows that apart from the tilting of the tower itself, the whole Pisa plain is subsiding, as shown in Figure 6.8. The differential subsidence occurring in the square might contribute to the present tilting of the tower.

Some other disturbances, such as earthquakes, wind, traffic, and visitors, also increase the tilting of the tower (Gabe and Gudehus 1992).

It must be kept in mind that the actual situation of the tower is very complex. There are many physical disturbances in the tower's history which contribute to its inclination. Moreover, there are maybe more than one mechanism controlling its deformation behavior. It is almost impossible to account for all the aspects in a single constitutive model. Nevertheless, sample tests on the Pisa clay already show the importance of its creep behavior. It is worth knowing how much this kind of effect will contribute to the tower's deformation.

6.5 Three-dimensional visco-plastic analysis

In this study, the finite element program named PISA-FORTRAN developed by Chan and Morgenstern (1992) and Morsy (1994) has been extended into the three-dimensional case. Through the ensuing numerical work, the capability of the DYSCP model in predicting the stress-strain-time behavior under a fully three-dimensional field case is illustrated. The deformation mechanism of the soil underneath the tower's foundation is subsequently better understood.

The double-yield-surface Cam-clay plasticity model has been used efficiently in time-dependent analysis of certain field cases under two-dimensional conditions (Borja et al. 1990, and Morsy 1994). Since the creep process is assumed to be fully plastic, the flow rule for creep strains is always non-associative. The corresponding stiffness matrix is non-symmetric. Solving the basic equilibrium equation becomes the most time-consuming part, especially under three-dimensional conditions. It typically takes 80% to 90% of total CPU time. The non-symmetric stiffness matrix is the major reason which causes creep analysis to be so computer costly.

In visco-plastic analysis, due to the stress path dependence of the material behavior, a realistic loading sequence is a fundamental requirement for obtaining reasonable results. In this study, the loading sequence composes an initial switch on gravity steps to obtain the pre-existing stress field before the construction of the tower, and the subsequent loads due to the construction of the tower. In order to get more accurate initial yielding surfaces before the construction of the tower, the switch on gravity process is repeated 10 times by applying 10% gravity each time. Then, the displacement and the strain are both set to zero to give the initial configuration of the soil beneath the foundation the same as the field. The tower loads are applied according to the construction history. For each loading step, a time value based on the real history is added to let the soil creep. The time period for each stage is specified in terms of years.

The soil material properties used here are the same as used in the two-dimensional case and are listed in Tables 6.1 to 6.3.

6.5.1 Finite element

The three-dimensional mesh without the super-structure is shown in Figure 6.9, which is the half of the soil beneath the foundation along the N-S direction and neglects the E-W ward deformation. The mesh extends vertically to 40m, with a horizontal radius of 60m. It contains a total of 708 elements. Two different kinds of elements have been used in this study: a 20-node block element, and an 8-node block element, as shown in Figures 6.10 and 6.11, respectively. The 20-node block element mesh has 3528 nodes and 9139 degrees of freedom. Its stiffness matrix size is very large, up to 12,002,115. The computer implementation showed that this amount of degrees of freedom was too large for computers such as the IBM RISC System/6000 and even the SP2. The analysis was unbelievably slow, therefore this mesh was used only for comparative study on the effect of element type. In order to reduce the computational time, 8-node block elements with a total of 949 nodes and 2345 degrees of freedom were used. The inclined soil layer in Formation A was modeled using the inclined 8-node block elements. The horizontally sliced 8-node block elements were used for the other soil layers. The tower footing was modeled as a ring-shaped rigid plate.

For the purpose of analysis, a coordinate system is selected with the origin at the left bottom of the mesh, which is 45m below the original ground level, 80m north from the tower axis and 5m in front of the tower axis, as shown in Figure 6.9 (not in scale). The formation C (dense sand), at the elevation of 40m below the ground surface, is assumed to be unaffected by the construction of the tower, thus the bottom fixed boundary of the finite element mesh is defined at this depth. The vertical roller boundaries with zero displacements at X and Y directions are defined at the surface with a horizontal radius of 60m. The vertical roller boundaries with zero Y direction are defined at the vertical surface along the N-S direction and through the tower axis.

After the switch on gravity process, the load and overturning moment were applied to the mesh to account for the tower weight and its inclination. Table 6.4 and Figure 6.12 show the loading history and overturning moment. The loads were reduced to an amount of 11589KN due to the weight of soil excavated for the tower's foundation. Then the reduced tower was converted to two loads acting at 6.02m south and north, respectively. The loading conditions for three-dimensional analysis are shown in Table 6.5.

In order to investigate creep effects on the stress and strain distributions, as well as on the deformation characteristics of the soil beneath the foundation, both plastic and visco-plastic analyses using 20-node and 8-node block elements were carried out. The results are discussed in the following section.

6.5.2 Simulation results

6.5.2.1 Stress and strain distributions in the soil beneath the foundation

Since sample tests show that creep is important in layers A_1 and B_1 (Mitchell and Soga 1995), creep effects on the stress and strain distribution in the soil beneath the foundation are investigated in detail in these layers, as shown in Figure 6.13. This figure also shows the locations of four elements. Elements 508 and 503 belong to Layer A_1 and locate underneath the south and north edges of the footing, respectively. Elements 331 and 326 belong to Layer B_1 and locate underneath the south and north edges of the footing, respectively.

Shear stress versus. strain relationship

Figure 6.14 (a) and (b) show the shear stress and strain relationships under both plastic and creep conditions for elements 508 and 503, respectively. It can be seen that for layer A_1 , plastic analysis gives a concave upward curve because as confining pressures increase, soil stiffness increases. Creep causes a convex downwards curve because as

shear stresses decrease, shear strains increase. Under unloading conditions, plastic analysis shows shear stresses, as well as shear strains, decrease as time progresses. Creep causes shear stresses to decrease but shear strains to increase.

The shear stress and strain relationships of layer B_1 (see Figure 6.15) show that both plastic and creep analyses give an almost linear shear stress-strain relationships. Creep causes q to be almost constant under loading conditions while q decreases under an unloading conditions.

Mean stress and deviatoric stress distributions at certain depths

Figure 6.16 (a) and (b) show mean stress distributions at 6.5m and 12m depths, respectively. For layer A_1 , creep causes mean effective stresses to decrease slightly within the footing area, but to increase under the area outside that range. The maximum increase is 84%, which occurs at 14m south from the footing center. For layer B_1 , creep increases mean effective stress at all locations. The maximum increase is 31%, which occurs at 14m south from the footing center.

Shear stress distributions at the depths of both 6.5m (Figure 6.17 (a)) and 12m (Figure 6.17 (b)) show that creep decreases shear stresses significantly within the footing area, up to 59% at layer A_1 and 53% at layer B_1 . Outside the footing area, creep drives q to almost zero, which is equivalent to the hydrostatic stress condition.

Volumetric strain and deviatoric strain distributions at certain depths

Volumetric strain distributions at depths of both 6.5m and 12m (Figure 6.18) show that creep increases volumetric strains at the area outside the footing range, but does not change or slightly decrease them within the footing range.

Deviatoric strain distributions at the depths of both 6.5m and 12m are shown in Figures 6.19 (a) and (b). Creep causes shear strains to increase as high as 100% at the

depth of 6.5m and 14m south from the footing center (see Figure 6.19 (a)), and 44% at the depth of 12m and 10m south from the footing center (see Figure 6.19 (b)).

Overall, strain distributions show that strain values are less than 10% in all the area, except for some local areas within or slightly outside the footing. Thus, small strain formulations are still valid for creep analysis under fully three-dimensional conditions.

p'-q plots at certain depths

Figures 6.20 (a) and (b) show the p' - q plots at the south edge of the footing, at the depths of 6.5m and 12m, respectively. They also show the p' - q plots for plastic and creep analyses based on the previous two-dimensional results. It can be seen that three-dimensional analysis predicts smaller p' and q values than two-dimensional does. Creep causes the stress state to move far away under the three-dimensional condition. For layer A_1 (6.5m deep), starting from stage three, deviatoric stress q slightly decreases even though the soil is under loading conditions, which gives a concave downward p' - q curve (see Figure 6.20 (a)). For layer B_1 (12m deep), the stress path goes almost horizontal since as p' increases, q keeps almost the same values (see Figure 6.20 (b)).

Figures 6.21 (a) and (b) show p' - q plots on the north edge of the footing, at the depths of 6.5m and 12m, respectively. The p' - q plots at 6.5m depth show that under unloading conditions, plastic analysis predicts a stress state above the original loading curve, while creep analysis predicts a stress state below the original one.

6.5.2.2 Displacement of the footing

Simulations results

Figure 6.22 shows the final settlement of the footing from the results of 20-node elements and 8-node elements plastic analyses. Figure 6.23 shows the results from creep analyses. Creep analysis with 20-node-block elements gives 3.0^0 tilting and 3.6m

settlement. Plastic analysis with 20-node-block elements predicts 1.5° tilting and 2.1m settlement. When comparing the results with both creep and plastic analyses, it can be seen that for the 20-node-block element case, the creep effect contributes to 1.5° of the tilting and 1.5m of the settlement. Creep analysis with 8-node-block elements gives 2.5° tilting, of which creep contributes 1.2° tilting. When comparing these with 20-node-block element results, it can be seen that the creep effect on the tilting loses 0.5° by using 8-node block elements.

An additional creep analysis was conducted by updating the coordinates at each step, and by starting from the second construction stage introducing 8 weak elements close to the south edge of the footing. The tilting versus time relationship is shown in Figure 6.24. It can be seen that, even under these conditions, the calculated tilting angle can reach up to 4.0° , but it is still smaller than the actual 5.5° . Moreover, the tilting history is not properly followed

Discussion

The three-dimensional results show that creep and the tower load increments cannot account for the total tilting angle of 5.5° . As mentioned earlier, the observed tilting history curve is not a continuous one (see Figure 6.5). Immediately after the last construction stage (1370 to 1550), the tilting angle increased more than 3.0° . Something other than creep happened and caused some additional tilting. Simulating these amounts of tilting is beyond the scope of the current model.

If part of the simulated curve is moved vertically after 1550 (see Figure 6.25), one can see that numerical simulation can follow the observed data fairly well. This suggests that if after considering some significant historic events, creep analysis could simulate the tilting history during the recent four centuries.

6.6 Sensitivity analyses

In order to investigate the possibility of improving the simulated tilting angle by changing some material parameters in the DYSCP model, sensitivity analyses were conducted for the Singh and Mitchell creep parameters $\bar{\alpha}$, m and the hyperbolic parameter a of layer A_1 . This is done based mainly on two-dimensional sensitivity results.

6.6.1 Influence of Singh and Mitchell creep parameter $\bar{\alpha}$ and m

The effect of the Singh and Mitchell creep parameter m on the total tilting angle was investigated through three analyses using m of 0.75, 0.89, and 0.95 while keeping the rest parameters the same values as before. The results give a concave upward curve in the tilting angle versus m plot as shown in Figure 6.26. m of 0.89 gives the smallest tilting, while m of 0.75 gives the largest tilting. The difference in tilting angle is within 0.5° .

Three more analyses were carried out using $\bar{\alpha}$ of 3.81, 5.81, and 7.81 to study the effect of this parameter. The results give a slightly concave downward curve in the tilting angle versus $\bar{\alpha}$ plot, as shown in Figure 6.27. $\bar{\alpha}$ of 3.81 gives the smallest tilting, while $\bar{\alpha}$ of 7.81 gives the biggest tilting. The difference is within 0.2° .

6.6.2 Influence of hyperbolic parameter a

As shown in Figure 6.28, which is the shear stress strain relationship under triaxial conditions, the hyperbolic parameter a influences the initial stiffness as well as the unloading stiffness. Under a 10 times increase in a value, shear strains change significantly. Under unloading conditions, shear strains decrease 0.92% for an a value of 0.046 while 0.13% for an a value of 0.0046 (reference case). Since starting from the second construction stage, north side soil is under unloading conditions, on the other hand, the sensitivity of the parameter a was not investigated in the previous two-dimensional study, it is necessary to conduct some analyses for different values of a .

Three-dimensional creep analysis shows that for a 10 times increase of parameter a , the total tilting angle increases from 2.3° to 3.3° (43% increase). Parameter a is relatively sensitive in terms of the tilting angle, but a 10 times increase in this parameter is an exaggerated case. Even under this case, the total tilting angle only can reach 3.3° .

As mentioned in the two-dimensional case, the deformation behavior of the soil beneath the foundation is not controlled by any single parameter. It is the combination of all the parameters in the DYSCP model. By changing material parameters such as the Single and Mitchell creep parameters $\bar{\alpha}$, m and the hyperbolic parameter a , the total tilting angle can only increase to 3.3° of the maximum. The actual 5.5° tilting angle cannot be reached by simply changing one of the material parameters. There are some other reasons which contribute to the tilting of the tower, such as physical disturbances and other deformation mechanisms which the current numerical model could not quantify.

6.7 Three-dimensional visco-plastic analysis with the super-structure

In order to avoid applying load and overturning moment directly to the tower's foundation, creep analysis of the soil together with the tower case, was conducted under three-dimensional conditions. The finite element mesh, shown in Figure 6.29, consists of 828 eight-node block elements with a total number of 1124 nodes. The soil part was modeled using the same mesh as without the super-structure case (see Figure 6.9). The tower part was modeled by adding 120 additional elements. The tower was assumed to have a uniform geometry, and the same inner and outer diameters, 4.5 m and 19.58 m, respectively. The equivalent unit weight γ was obtained through the volume and the weight at a different time period. A linear elastic model was used for the tower material, since only the stress in the soil beneath the foundation was of interest.

The loading sequence composed two parts: (a) an initial switch on gravity steps to get the initial stress field; and (b) subsequent layer construction to simulate corresponding

tower construction according to the actual construction process shown in Figures 6.2 and 6.4. During the construction period, elements were added at a mainly uniform rate. After that, no external loading was applied to the model. The soil beneath the foundation was undergoing creep process.

In order to improve the accuracy, layer construction process was repeated 10 times by applying 10% gravity each time. Node coordinates were updated after each time increment. For modeling the first construction stage, the footing and tower elements were added up to 29.8 m above the ground as shown in Figure 6.30; then the soil started to creep until the beginning of the second stage. For the second stage, the tower elements were added from 29.8 m to 47.9 m. To model the phenomenon that the southward leaning started at this stage and proceeded since then, weak elements were introduced close to the south edge of the footing. These weak elements were given two or three orders of lower stiffness. The last construction stage was modeled by adding up the tower elements from 47.9 m to 55.4 m above the ground. After that, the soil was allowed to creep until present time.

By including the super structure into the creep analysis, Figure 6.31(a) plots the tilting history of the tower while the stiffness of the weak elements is two and three orders lower respectively. Numerical results can follow the tilting history closely until the completion of the construction at 1370, but under-predict the tilting angle after that. The results could not indicate a sudden jump of 3.1° tilting from 1370 to 1550, although it was observed in the history. If the calculated curve from 1550 to the present is vertically moved up by 2.5° , it can provide a very close approximation for the observed data as shown in Figure 6.31(b). This phenomenon may suggest that between 1370 to 1550 something other than creep happened and caused some additional tilting. Simulating this part of tilting is beyond the scope of the current model.

Figure 6.32 presents both the calculated settlement profile and the measured data from borehole tests (Calabresi et al. 1992) along the N-S cross section on the top of the

upper clay layers, 10.4 m below the ground surface. The calculated maximum settlement of 2.82 m is very close to the measured value of 2.64 m. The figure also shows a fairly accurate prediction within the footing area, beyond which the accuracy is getting lower. The calculated profile range is within the radius of 35 m to the north and south of the axis of the tower comparing to the measured 25 m. This discrepancy may be due to the footing material failure or the larger elements being used in this region. If the footing materials in some area are in a failure condition, the stiffness of the whole footing would be decreased. Thus, the settlement profile range beneath the footing would be smaller comparing with no footing material failure case. On the other hand, the accuracy of the prediction might be improved if smaller elements were adopted.

6.8 Summary and conclusions

1. This study has quantified the creep effects on the deformation behavior and stress-strain response of the soil underneath the tower's foundation, which have not been achieved by others so far.
2. Results from creep analysis can predict the tilting history within a reasonable accuracy during the construction period and illustrate more or less the same trend for the last four centuries.
3. The numerical model is capable of calculating the settlement profile on top of the upper clay layers with a fair accuracy. The calculated maximum settlement of 2.82 m is very close to the measured value of 2.64 m.
4. Three-dimensional creep analyses gives a maximum of 3.0° tilting, of which 1.5° are due to creep alone. By updating node coordinates and introducing some weak elements underneath the south edge of the footing, the calculated tilting angle can reach 4.0° , which is still smaller than the observed value of 5.5° . Moreover, the tilting history is not properly followed

5. The actual 5.5° tilting angle cannot be reached by simply changing some material parameters in DYSCP model. Some other reasons may have also contributed to the tilting, but cannot be simply quantified due to the complexity of the tilting history of the tower. Based on surveyed results, the possible reasons include: (a) some influence of wars that took place in Pisa city. Pisa Tower might at least suffer from dynamic shocks due to bomb explosions; (b) the excavation of the catino in 1838; (c) temperature changes; (d) the subsidence subjected by the whole Pisa plain; and (e) other disturbances such as earthquakes, wind, traffic, and visitors, etc.
6. In summary, the final 5.5° tilting is the total result of many different causes. No single numerical model is able to consider all of them. The model studied here can only quantify the influence due to the weight of the tower and the soil creep.

Table 6.1 Cam-clay parameters for the clay layers

material No.	layer	γ (kN/m ³)	C_c	C_r	Φ' (degree)	e_a	a	b	R_f	C_α
1	made ground MG	9.09	0.205	0.021	33.67	1.290	0.0046	1.220	0.89	0.0051
2	clayey silts A ₁ and A ₁ '	9.09	0.205	0.021	33.67	1.290	0.0046	1.220	0.89	0.0051
5	upper Pancone clay B ₁	7.32	0.615	0.081	26.54	2.730	0.0063	1.548	0.89	0.0154
6	upper Pancone clay B ₂	7.32	0.615	0.081	26.54	2.730	0.0038	1.548	0.89	0.0154
7	upper Pancone clay B ₃	7.32	0.615	0.081	26.54	2.730	0.0057	1.548	0.89	0.0154
8	intermediate clays B ₄	10.21	0.297	0.062	28.62	1.524	0.0095	1.351	0.89	0.0059
9	intermediate clays B ₅	10.21	0.297	0.062	28.62	1.524	0.0055	1.351	0.89	0.0059
11	lower clay B ₇	9.21	0.421	0.053	25.84	2.053	0.0051	1.538	0.89	0.0098
12	lower clays B ₈	9.21	0.421	0.053	25.84	2.053	0.0039	1.650	0.89	0.0098
13	lower clays B ₉	9.21	0.421	0.053	25.84	2.053	0.0039	1.650	0.89	0.0098
14	lower clays B ₁₀	9.21	0.421	0.053	25.84	2.053	0.0039	1.650	0.89	0.0098

Note: Material No. 3, 4, and 10 are the sand layers, they are tabulated in the next table.

Table 6.2 Soil parameters for the sand layers

material No.	layer	γ (kN/m ³)	E * (MPa)	ν *	Φ'
3	Silty sand A ₁ "	8.39	13.0	0.12	34
4	upper gray sand A ₂	8.39	13.0	0.12	34
10	intermediate sand B ₆	9.29	18.0	0.12	34.3
15	rigid footing	9.09	1*10 ⁷	0.12	-

Note: All the rest of materials are clay and clayey silt. they are tabulated in the previous table.

*--from Calabresi et al. (1992) TAB5.XV.

Table 6.3 Singh and Mitchell parameters (from Mitchell and Soga 1995)

Sample	layer	$\bar{\alpha}$	m	A' (%/min.)	A (%/year)
4m	clayey silt A ₁	5.81	0.89	2.12*10 ⁻²	9.03*10 ⁻²
6m	clayey silt A ₁ '	5.86	0.95	2.19*10 ⁻²	4.23*10 ⁻²
10m	upper clay B ₁	6.33	0.83	1.62*10 ⁻²	15.21*10 ⁻²
14m	upper clay B ₂	6.39	0.86	8.35*10 ⁻³	5.279*10 ⁻²
19m	upper clay B ₃	8.82	0.75	2.15*10 ⁻³	5.789*10 ⁻²

Note: $A = A' * (365*24*60)^{(1-m)}$

Due to the lack of creep test data, and the fact that layer B₃ is highly structured soil, creep parameters from layer B₂ were assumed to represent those of B₄ to B₁₀.

Table 6.4 Weight, overturning moment and rigid tilt versus time

Year	Weight (MN)	Moment (MNm)	Tilt (degree)
1178	94.80	-	-
1272-1278	137.28	5.51	0.103
1285	137.28	59.99	1.112
1360-1370	144.53	97.7	1.611
1550	144.53	284.72	4.684
1758	144.53	293.54	4.831
1817	144.53	310.98	5.103
1911	144.53	318.98	5.246
1990	144.53	332.56	5.469

Table 6.5 Three-dimensional loading increments

Year	increment		Δp (kPa)		Creep (years)
	Weight (MN)	moment (MNm)	at North	at South	
1173	32.211		8052.8	8052.8	-
1173	39.411		9852.8	9852.8	
1173-1178			-	-	6 (stage 1)
1178-1272			-	-	94
1272	42.48	5.51	10391.2	10848.8	-
1272-1278			-	-	6 (stage 2)
1278		27.185	-1128.9	1128.9	-
1278		27.185	-1128.9	1128.9	-
1278-1285					7
1285		18.91	-785.3	785.3	-
1285		18.91	-785.3	785.3	-
1285-1360			-	-	75
1360-1370			-	-	10 (stage 3)
1370	7.25		1812.5	1812.5	-
1370		31.17	-1294.4	1294.4	-
1370-1430			-	-	60
1430		62.34	-2588.9	2588.9	-
1430-1490			-	-	60
1490		62.34	-2588.9	2588.9	-
1490-1550			-	-	60
1550		31.17	-1294.4	1294.4	-
1550		4.41	-183.1	183.1	-
1550-1758			-	-	208
1758		4.41	-183.1	183.1	-
1758		8.31	-362.1	362.1	-
1758-1817			-	-	59
1817		8.31	-362.1	362.1	-
1817		4.41	-183.1	183.1	-
1817-1911			-	-	94
1911		4.41	-183.1	183.1	-
1911		6.79	-282.0	282.0	-
1911-1990			-	-	79
1990		6.79	-282.0	282.0	(Stage 4)

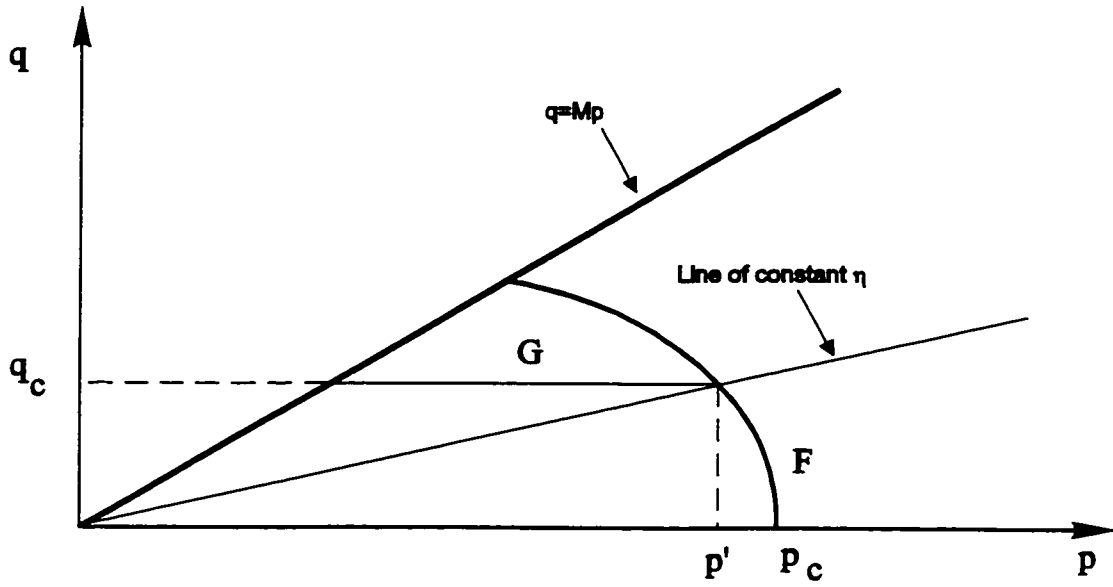


Figure 6.1 Projection of double yield surface on p-q plane

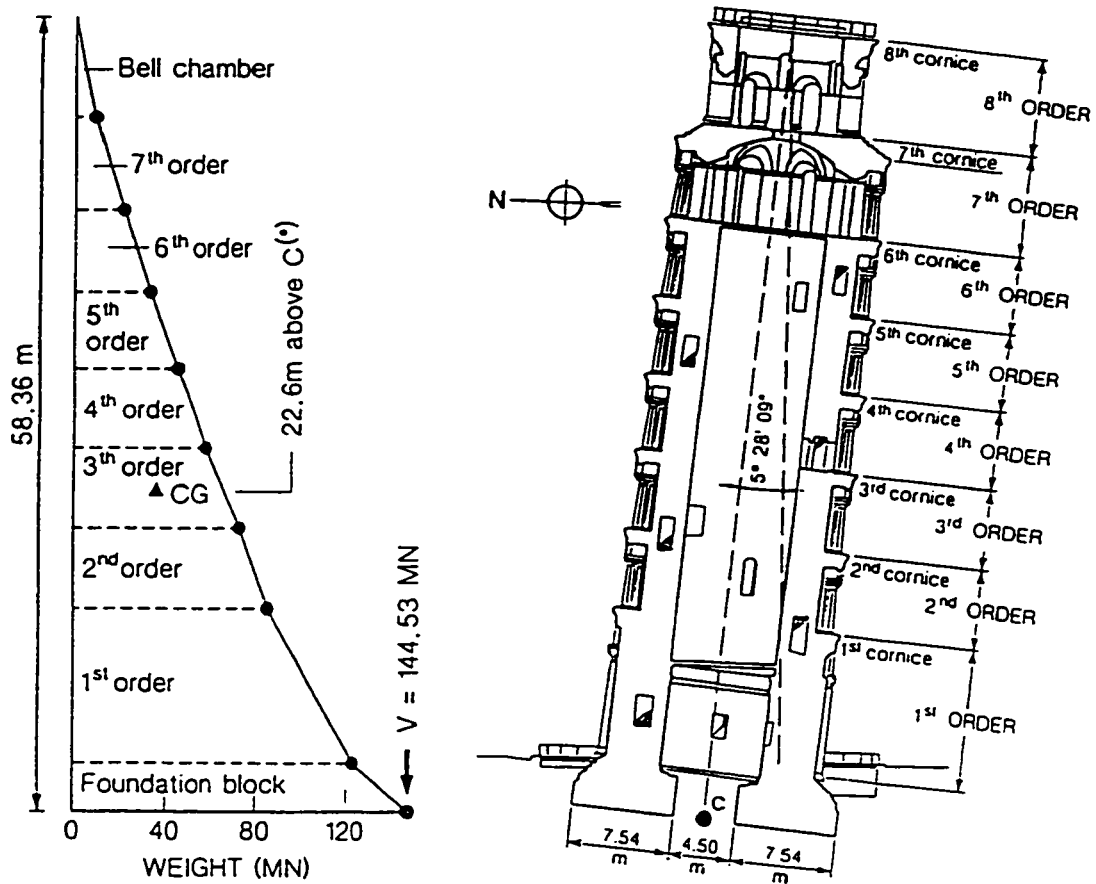


Fig. 6.2 Weight and geometrical characteristics of Pisa Tower (after Jamiolkowski et al. 1993)

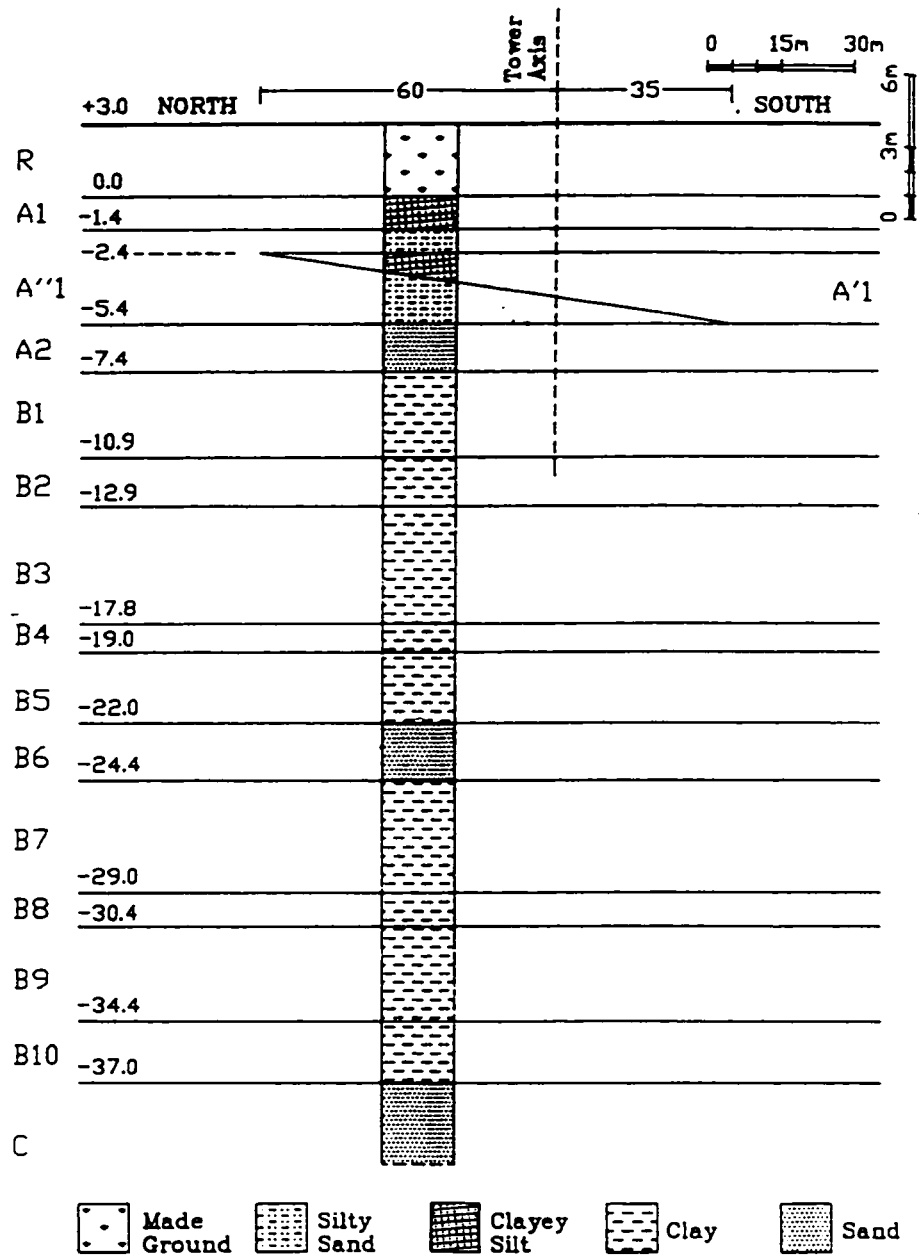


Fig. 6.3 Probable initial soil profile at the site of Pisa Tower (Calabresi et al. 1992)

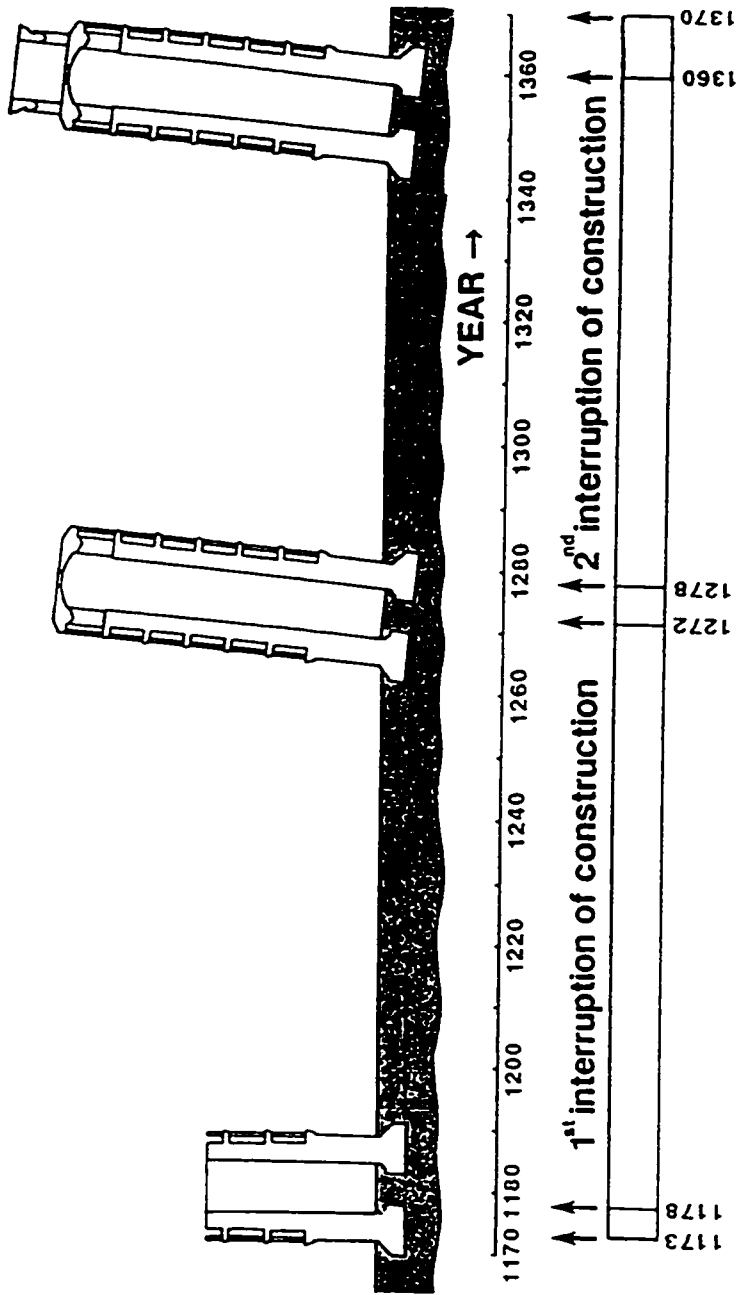


Fig. 6.4 Construction history (after Jamiolkowski et al. 1993)

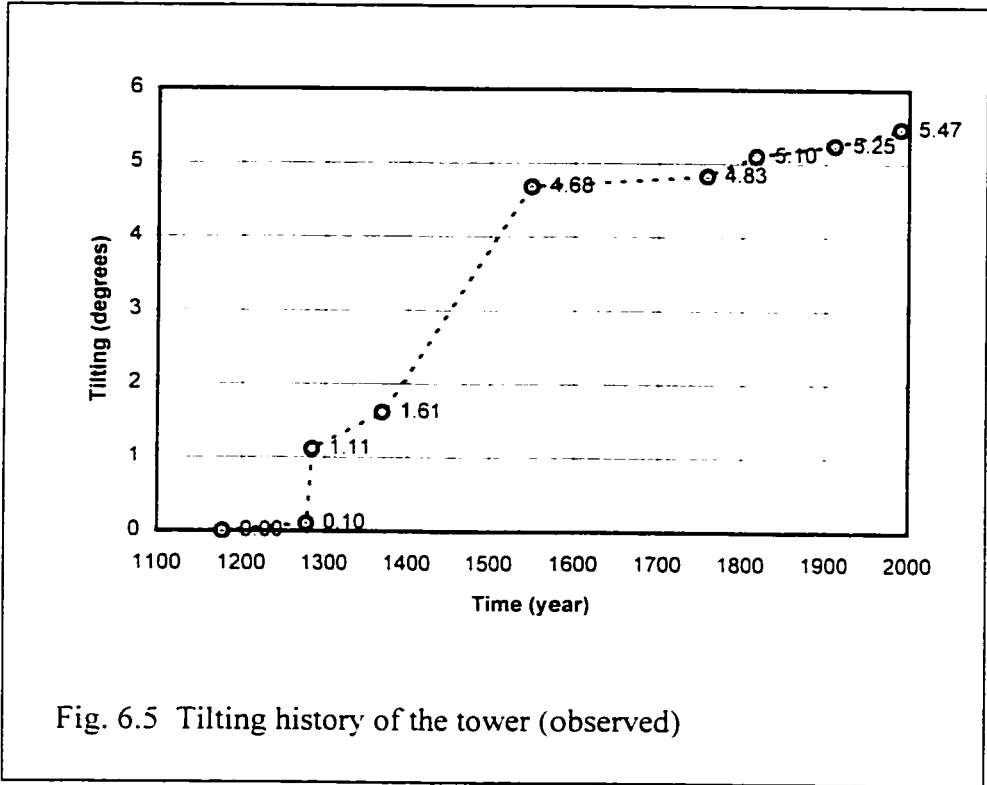


Fig. 6.5 Tilting history of the tower (observed)

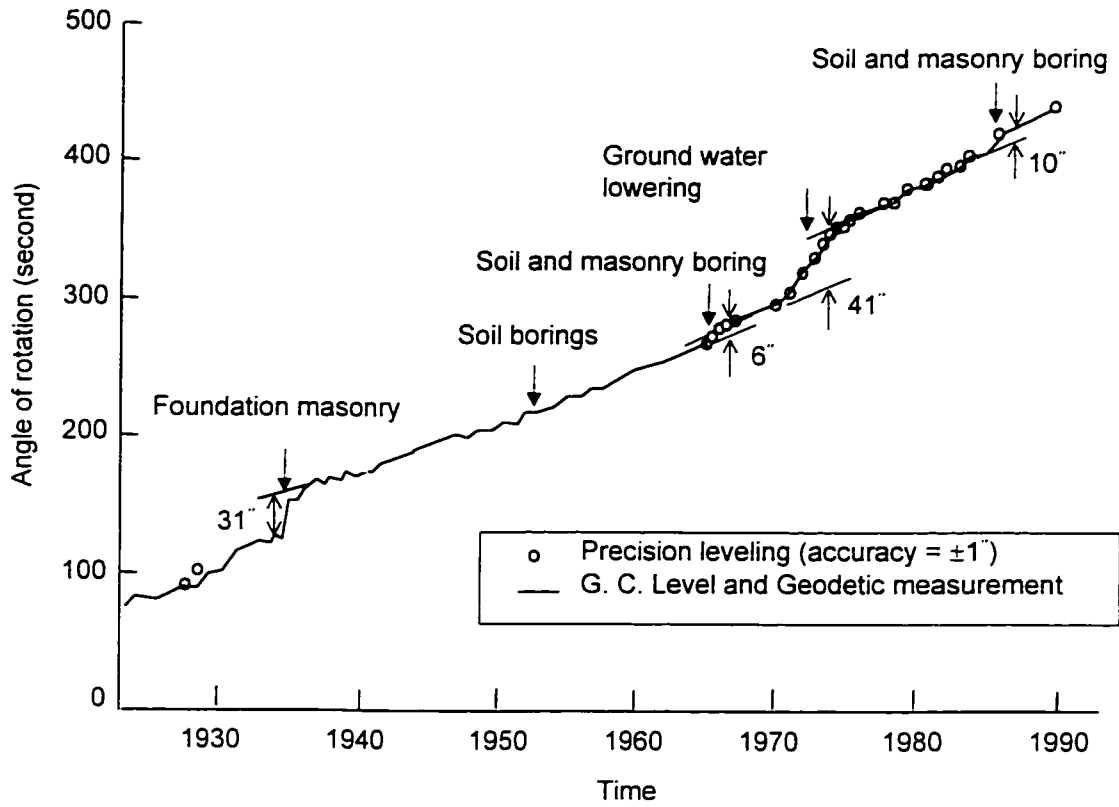


Fig. 6.6 Change in inclination of the foundation since 1911 (modified after Jamiokowski et al. 1993)

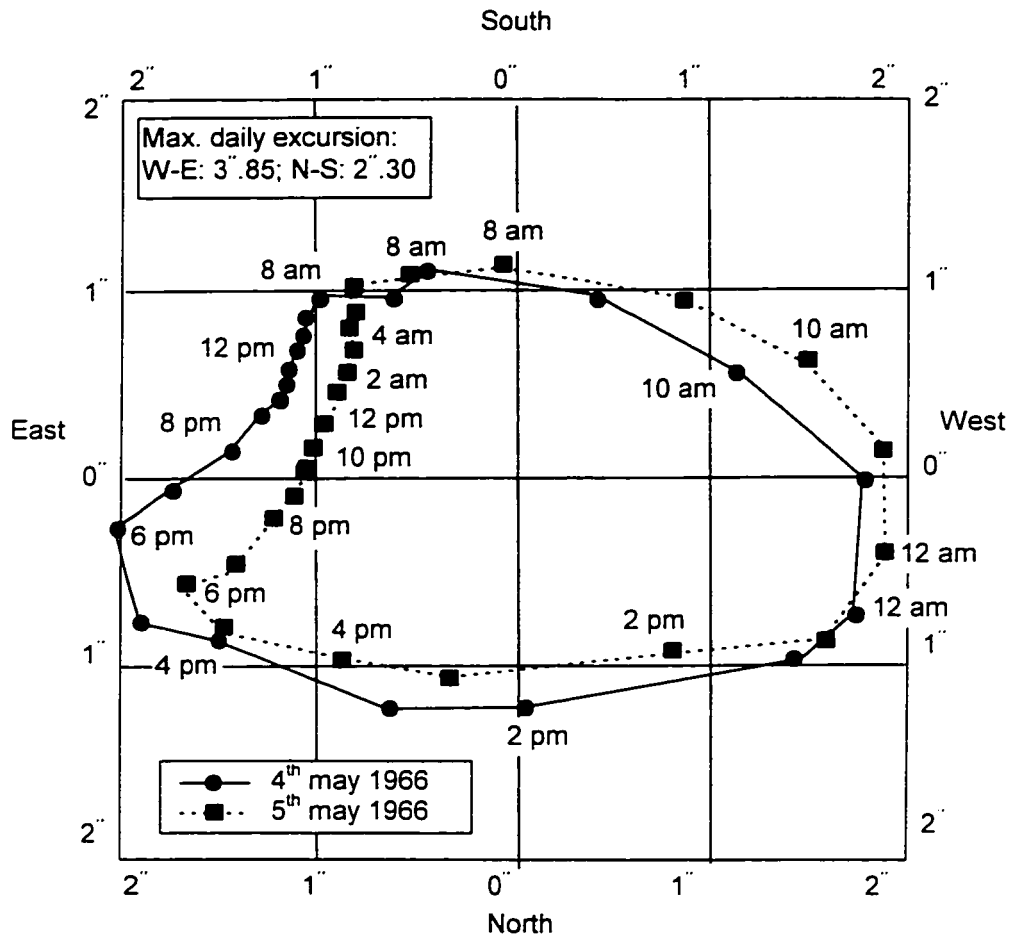


Fig. 6.7 Daily movement of the tower due to change of temperature (modified after Jamiolkowski et al. 1993)

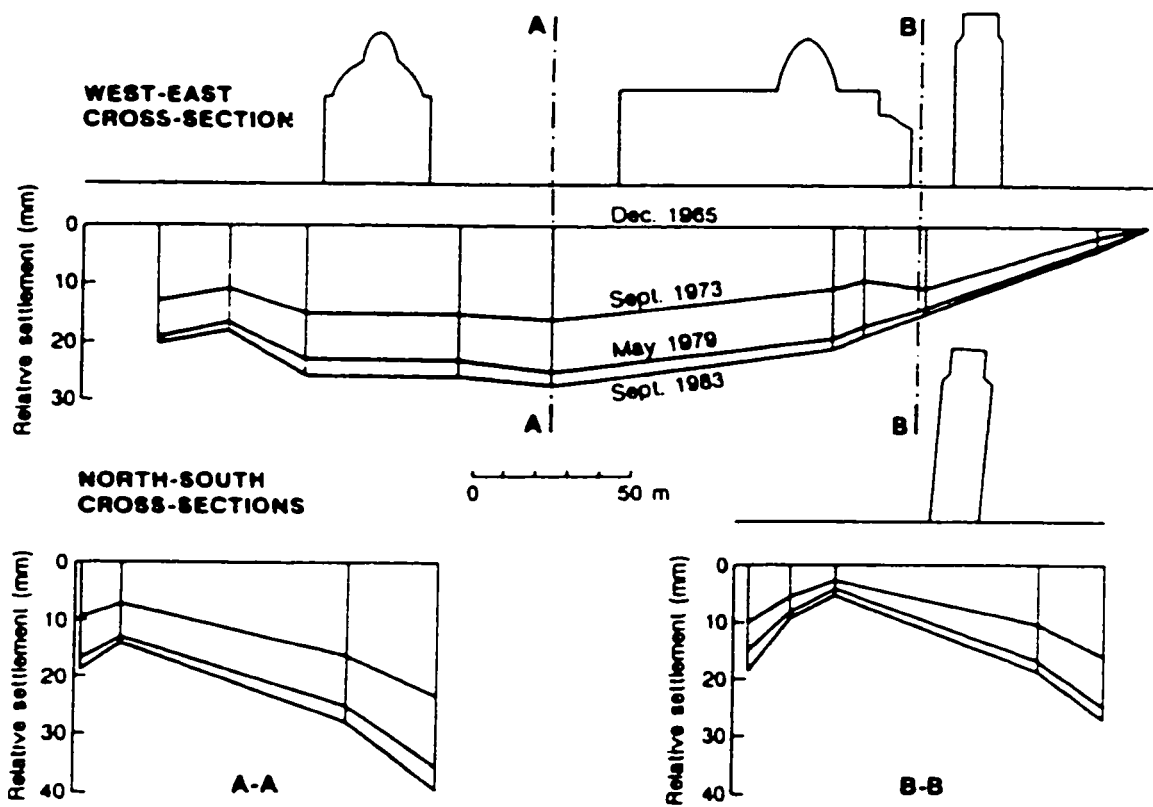


Fig. 6.8 Relative settlement over the Piazza dei Miracoli (after AGI 1991)

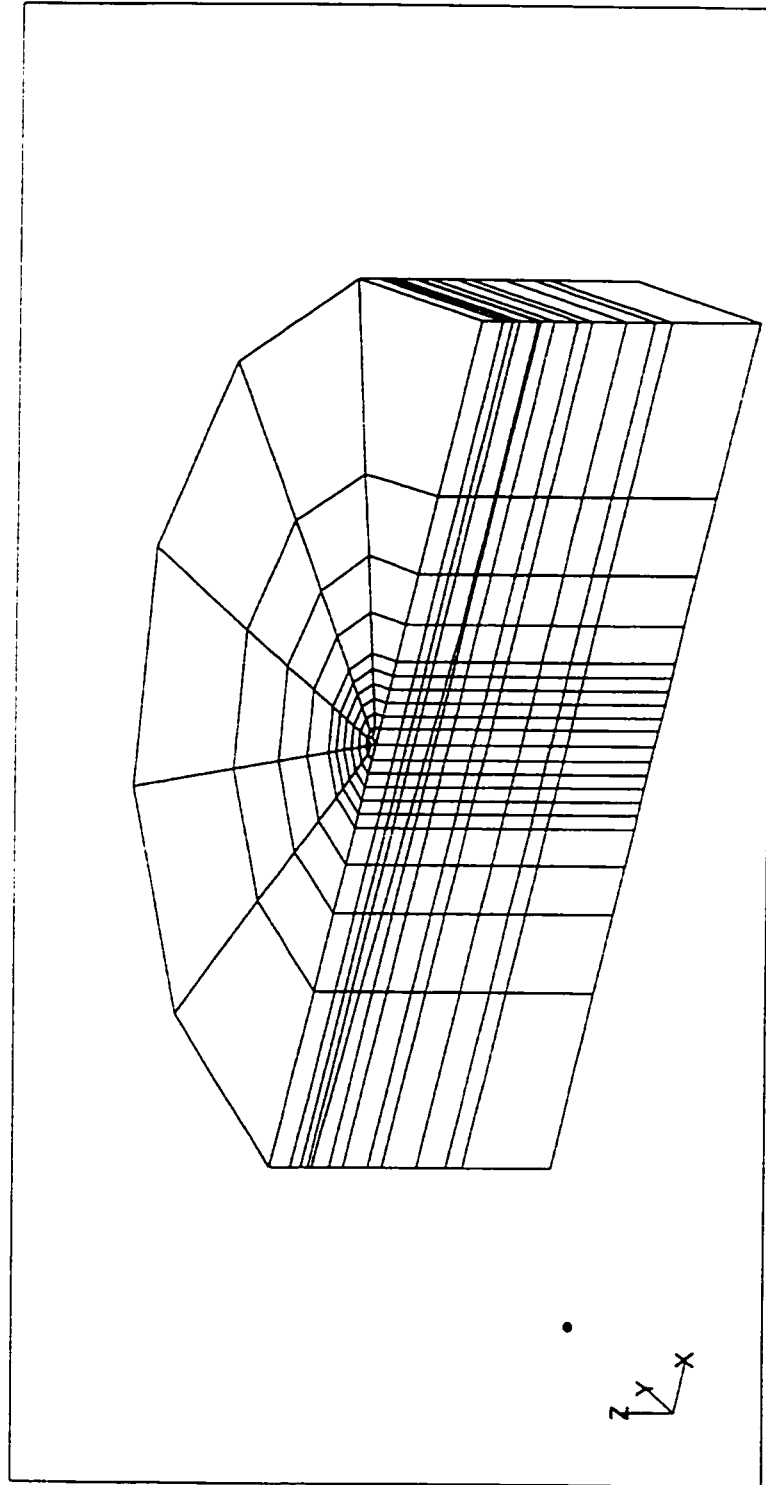


Fig. 6.9 Three dimensional finite element model of Pisa foundation

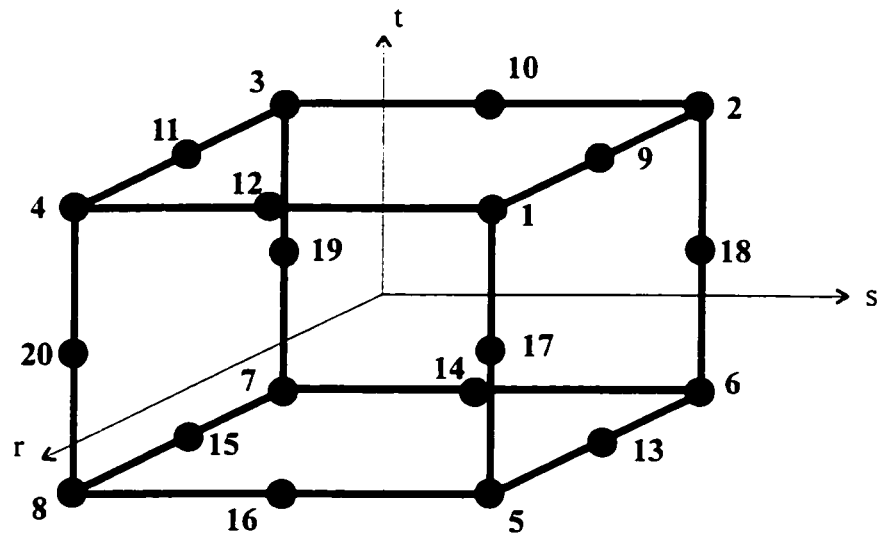


Fig. 6.10 20-node rectangular element for 3D analysis

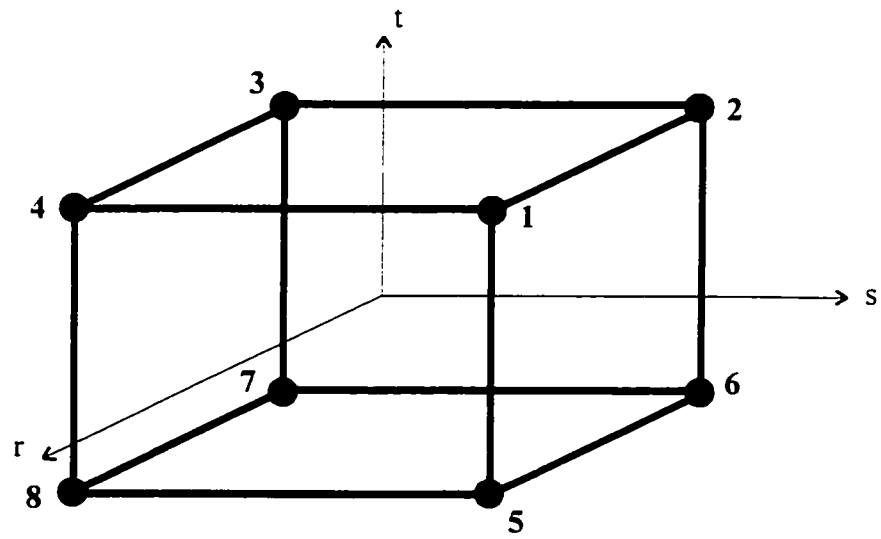


Fig. 6.11 8-node rectangular element for 3D analysis

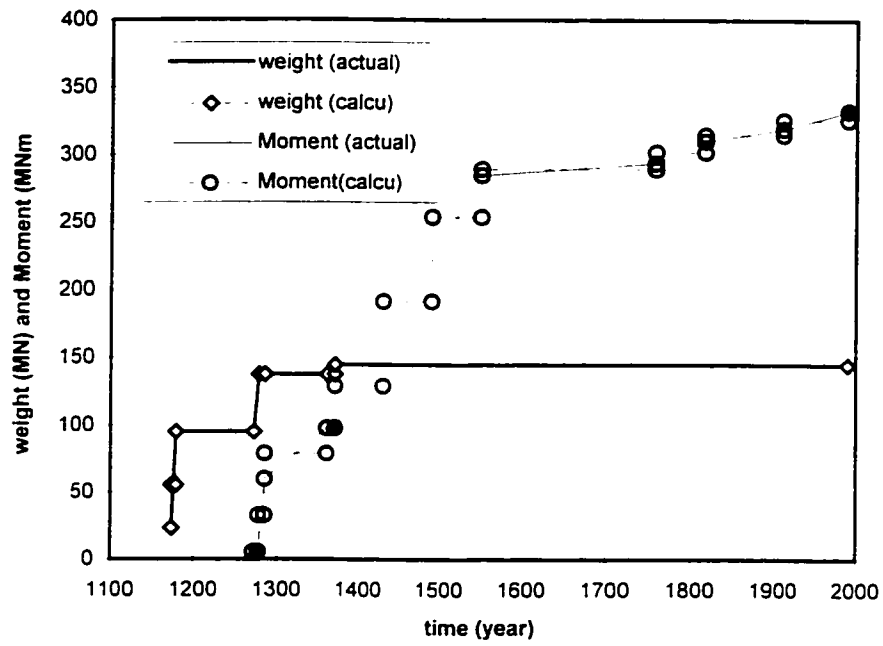


Fig. 6.i2 Pisa Tower weight and overturning moment versus time relationship

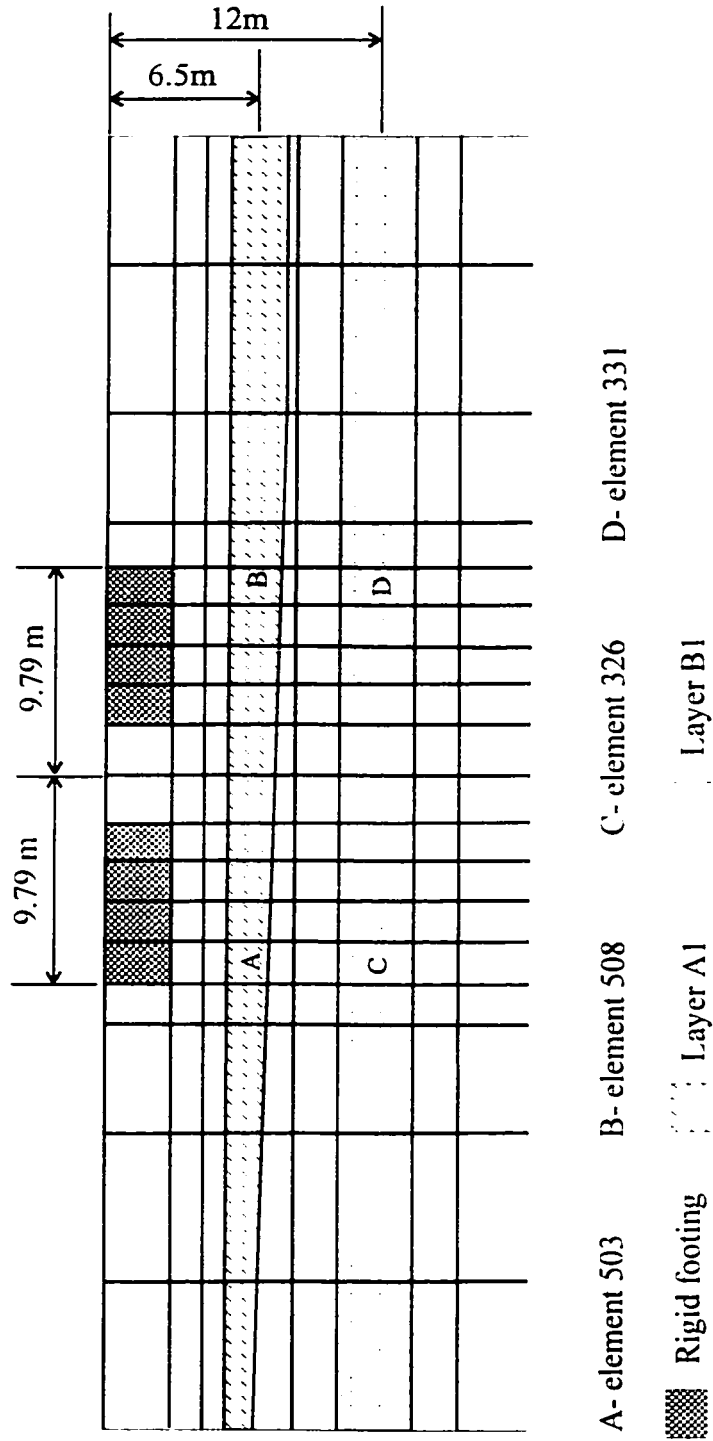


Fig. 6.13 Three-dimensional mesh of Pisa foundation (part)

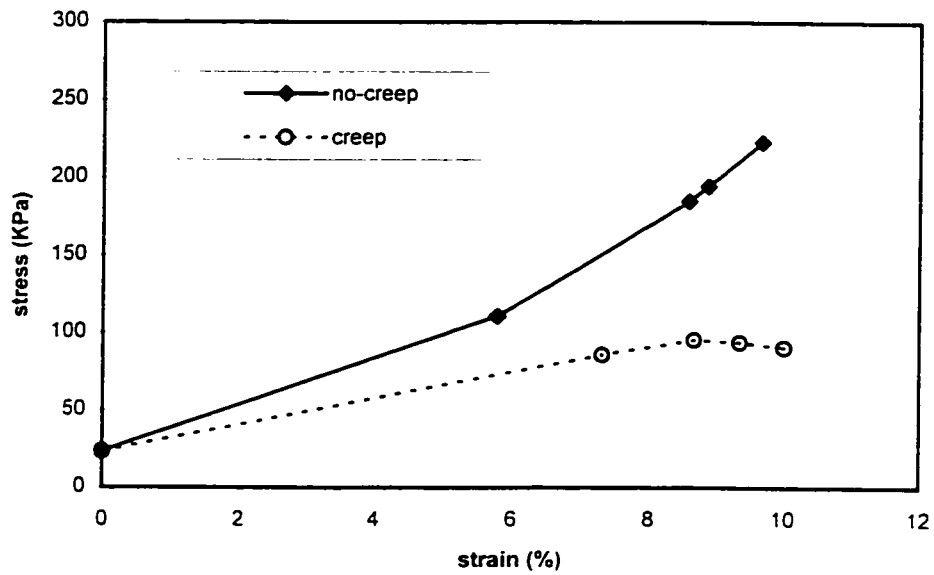


Fig. 6.14 (a) Shear stress-strain relationship at 6.5m deep (layer A1, element 508)

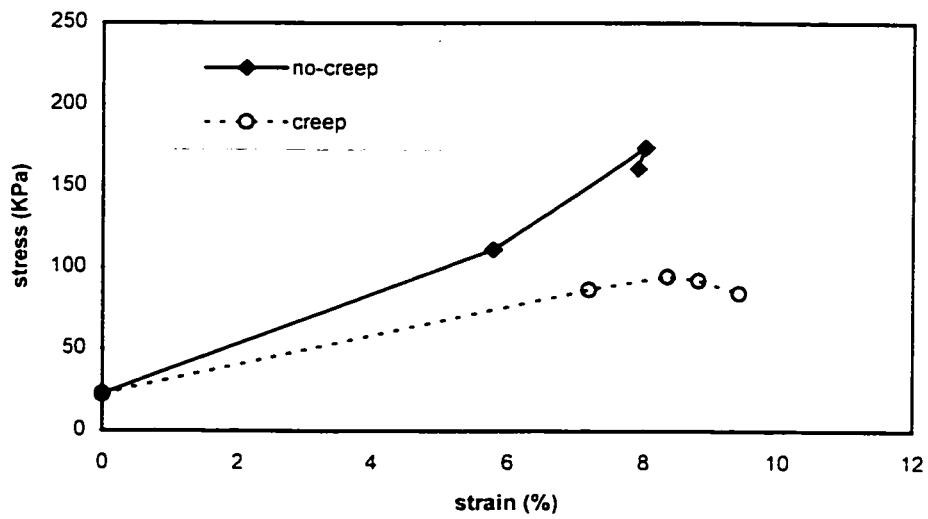


Fig. 6.14 (b) Shear stress-strain relationship at 6.5m deep. (layer A1, element 503)

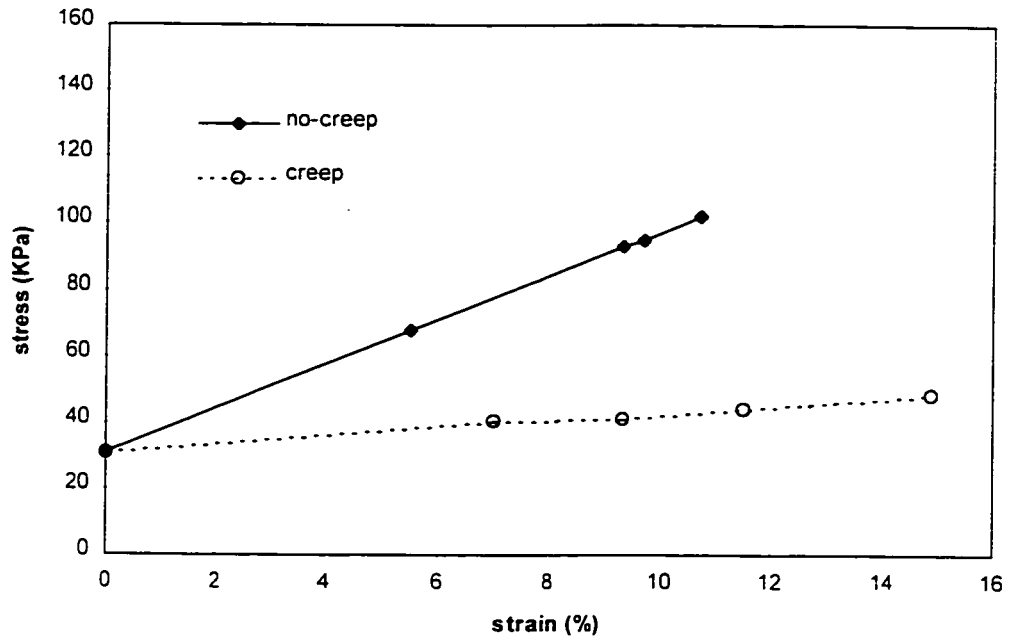


Fig. 6.15 (a) Shear stress-strain relationship at 12m deep (layer B1, element 331)

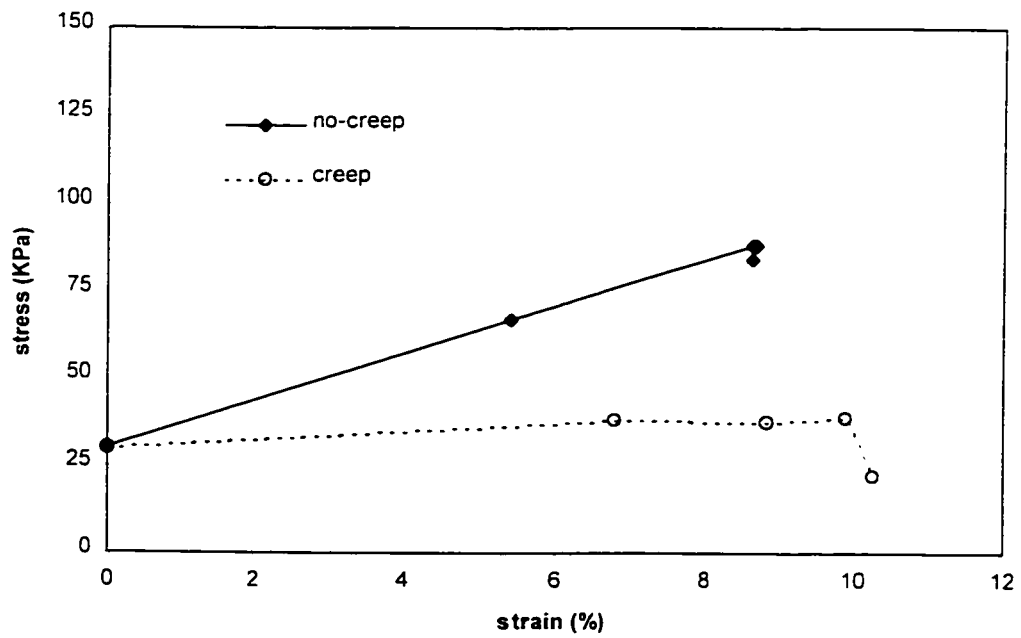


Fig. 6.15 (b) Shear stress-strain relationship at 12m deep (layer B1, element 326)

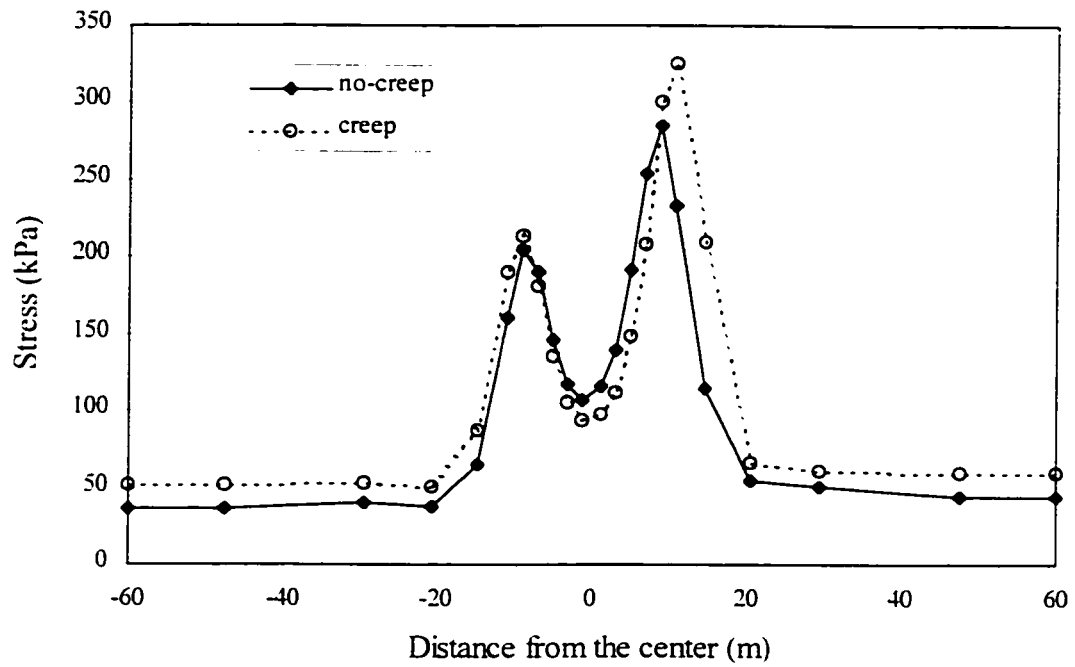


Fig. 6.16 (a) Mean stress distribution at depth of 6.5m (Layer A1)

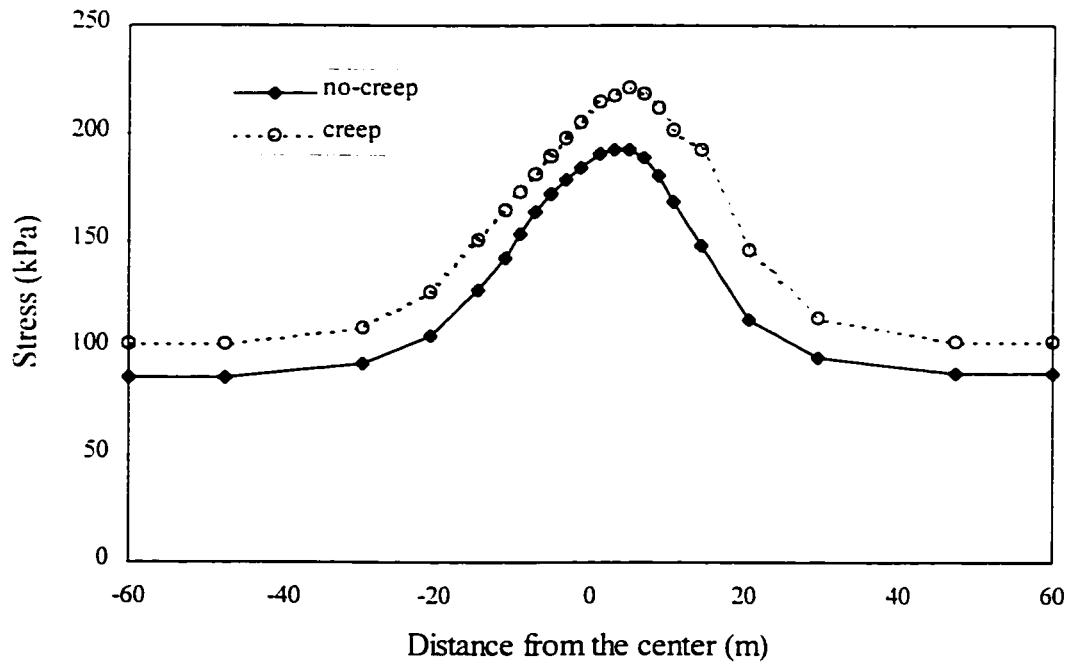


Fig. 6.16 (b) Mean stress distribution at depth of 12m (Layer B1)

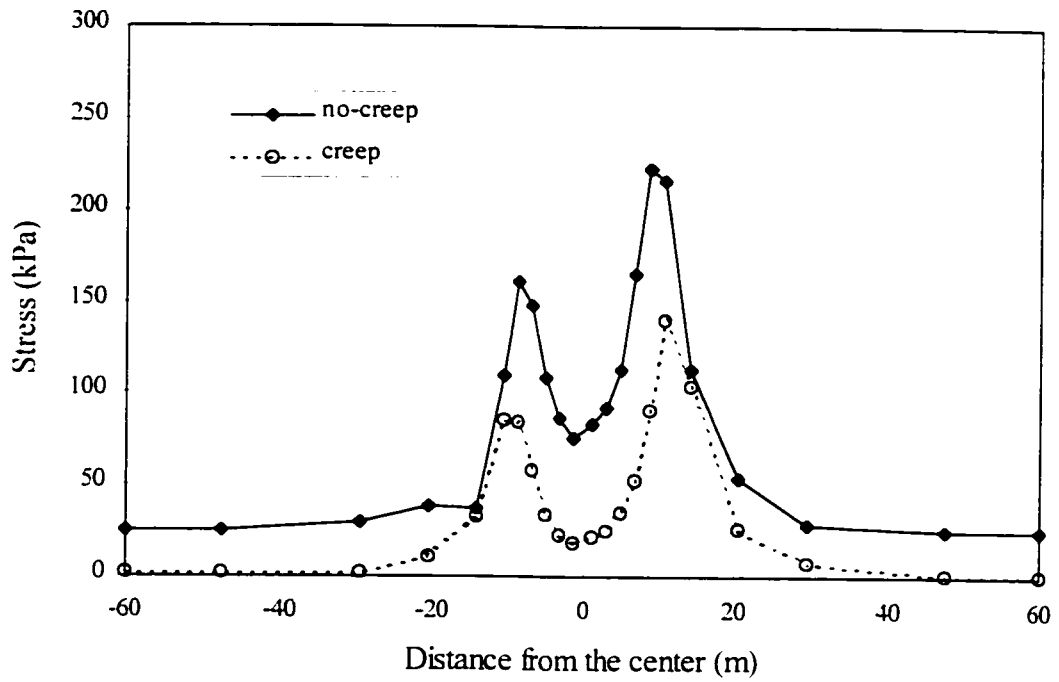


Fig. 6.17 (a) Deviatoric stress distribution at depth of 6.5m (Layer A1)

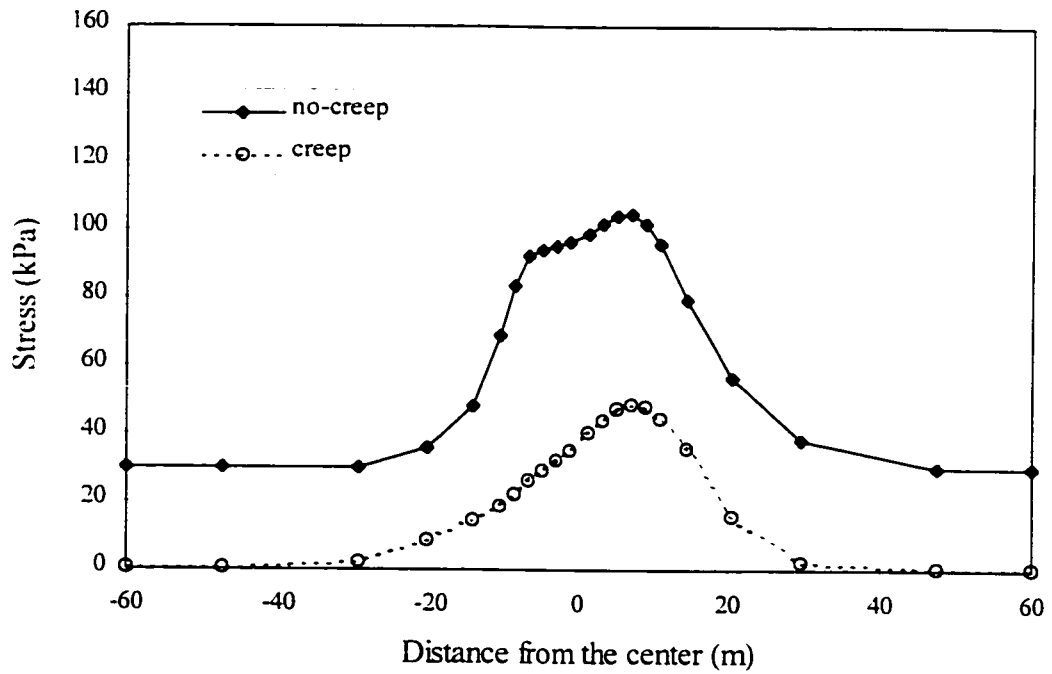


Fig. 6.17 (b) Deviatoric stress distribution at depth of 12m (Layer B1)

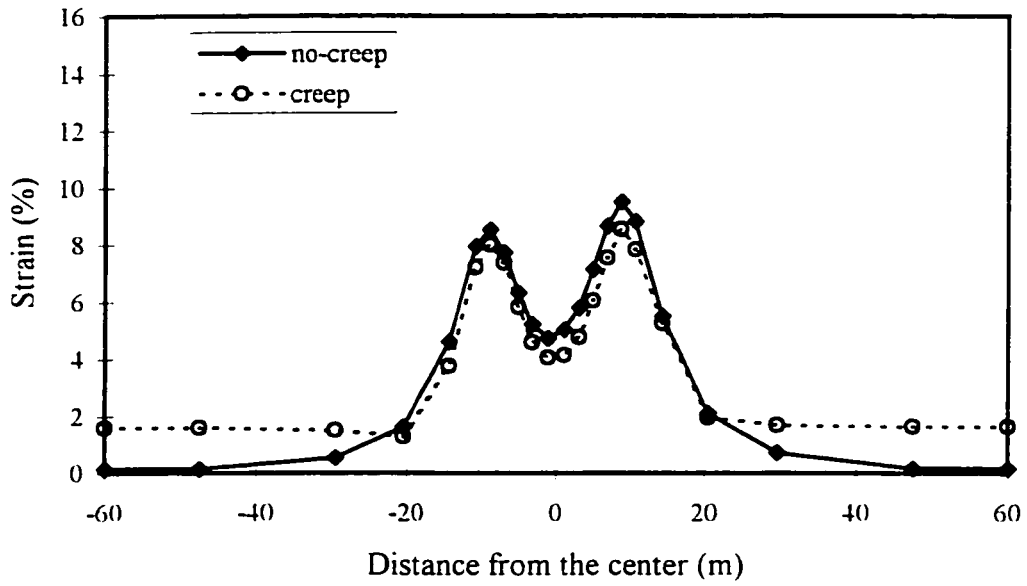


Fig. 6.18 (a) Volumetric strain distribution at depth of 6.5m (Layer A1)

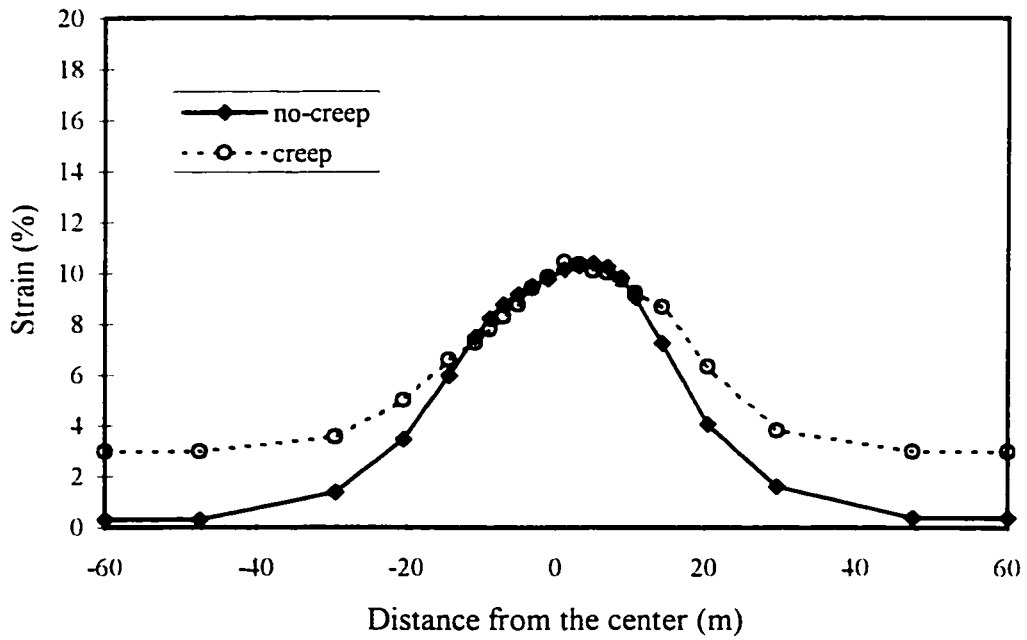


Fig. 6.18 (b) Volumetric strain distribution at depth of 12m (Layer B1)

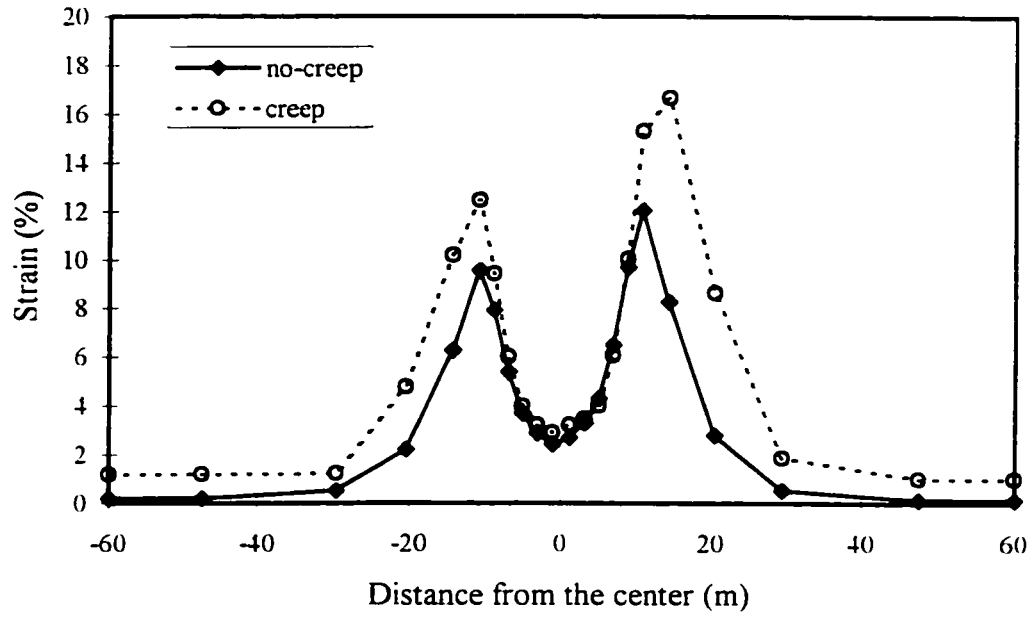


Fig. 6.19 (a) Deviatoric strain distribution at depth of 6.5m (Layer A1)

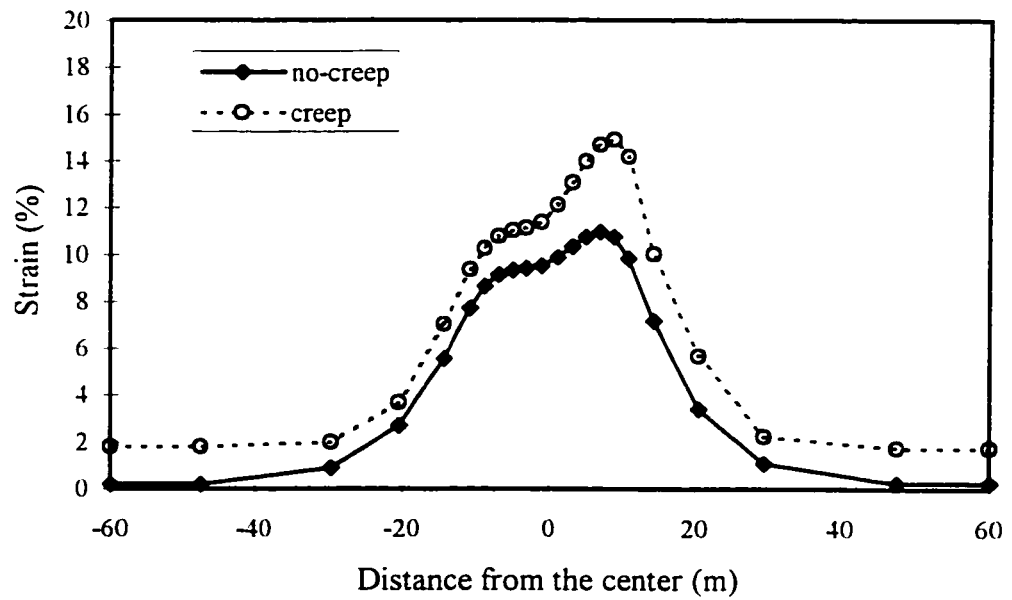


Fig. 6.19 (b) Deviatoric strain distribution at depth of 12m (Layer B1)

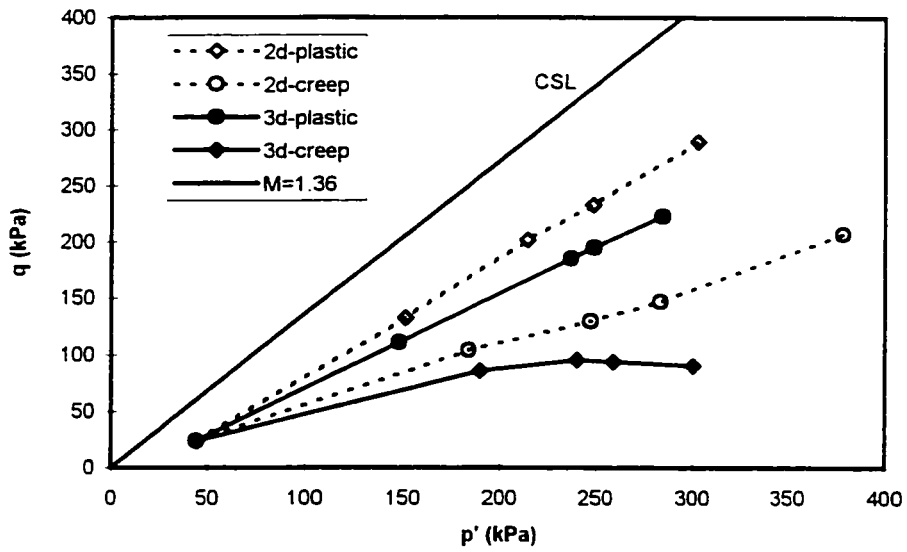


Fig. 6.20 (a) Stress path at 9.8m south of the footing center (Clayey silt A1)

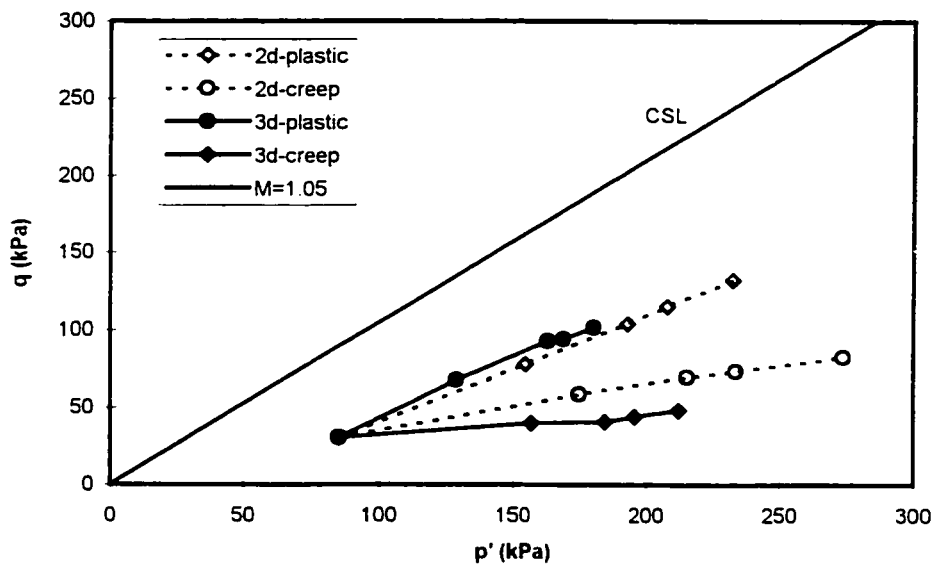


Fig. 6.20 (b) Stress path at 9.8m south of the footing center (Upper clay B1)

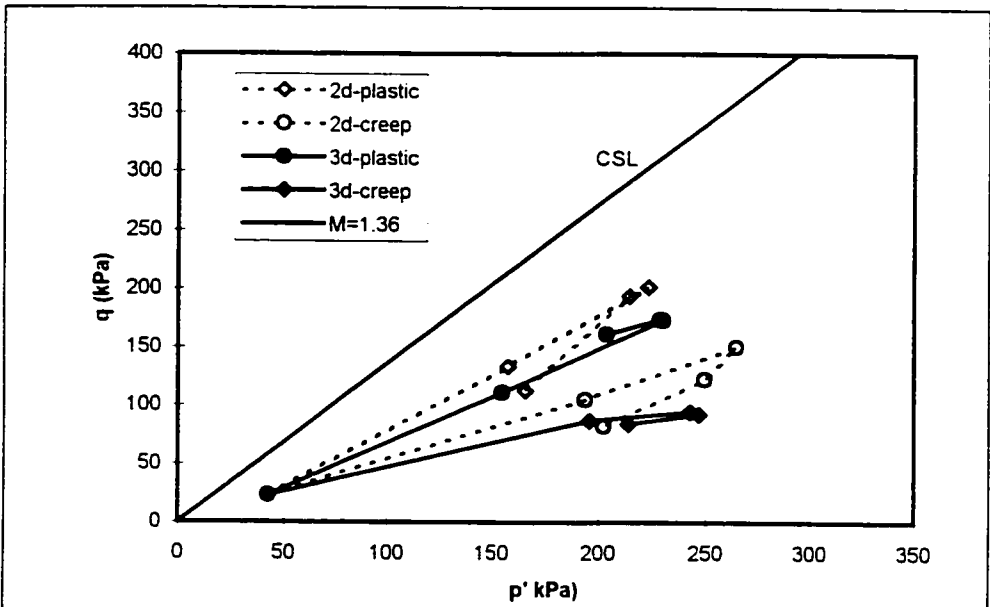


Fig. 6.21 (a) Stress path at 9.8m north of the footing center (Clayey silt A1)

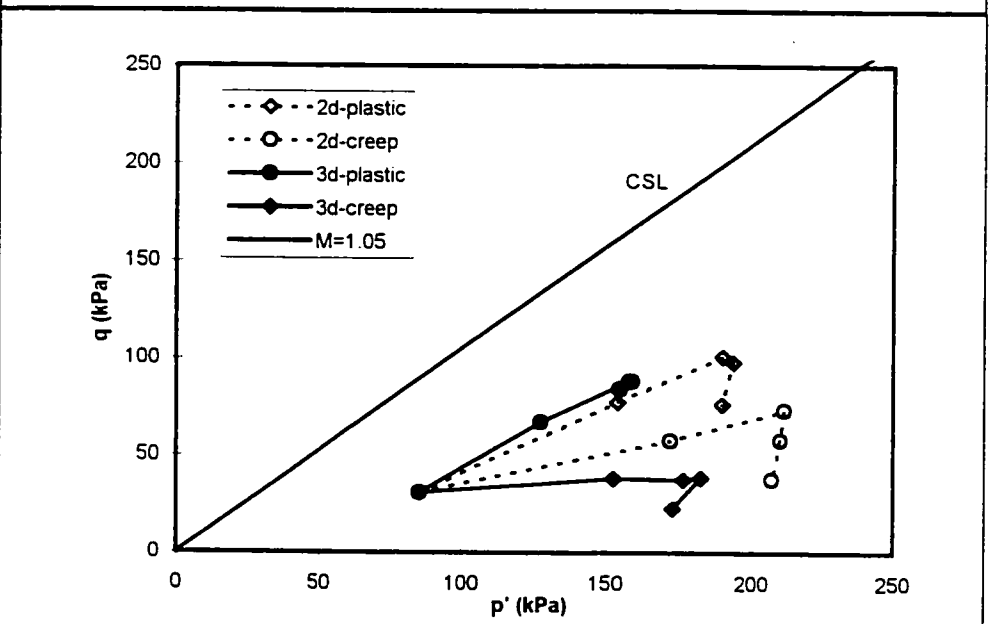


Fig. 6.21 (b) Stress path at 9.8m north of the footing center (Upper clay B1)

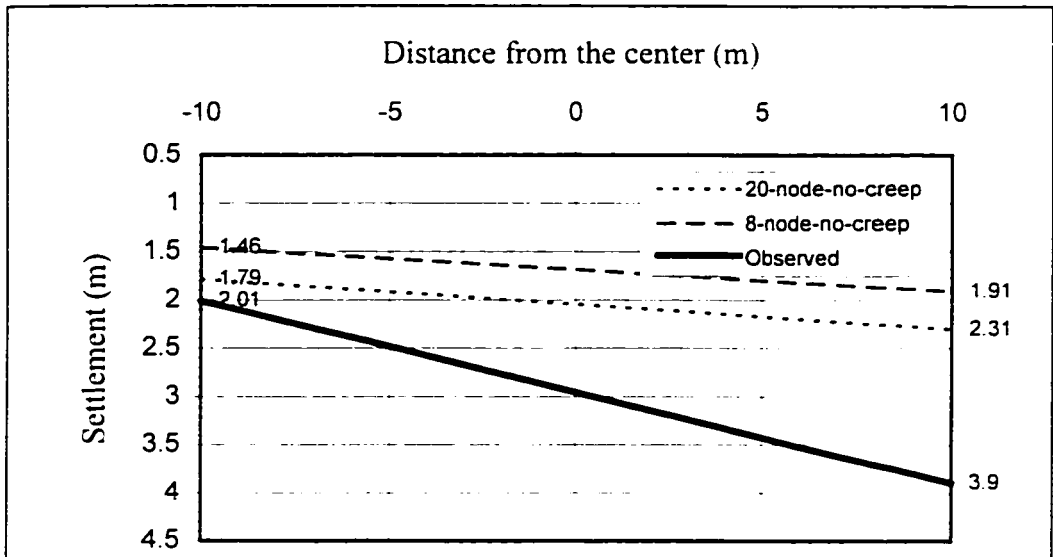


Fig. 6.22 Comparison for the settlement of the footing under different element types (plastic analysis)

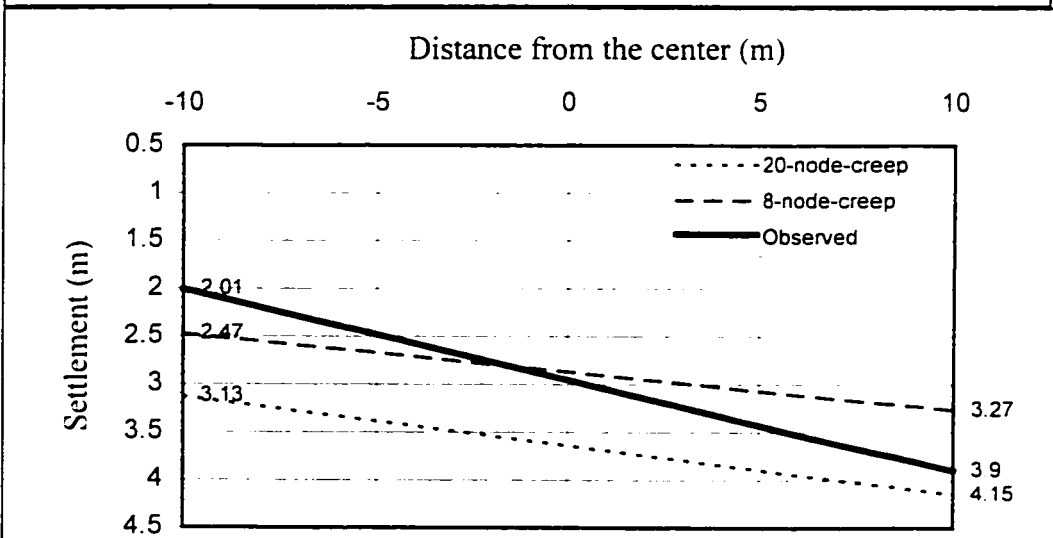


Fig. 6.23 Comparison for the settlement of the footing under different element types (creep analysis)

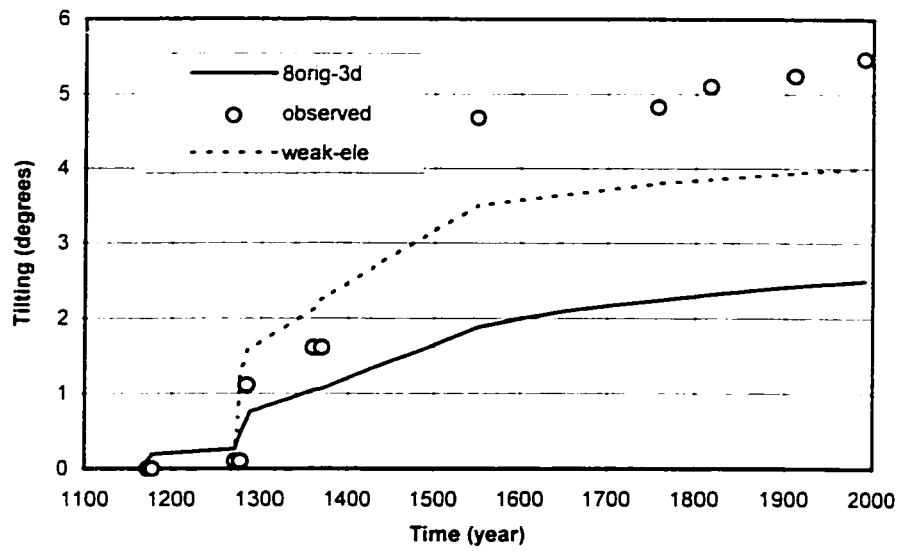


Fig. 6.24 Tilting history of the tower (original material, update coordinates, with 8 weak elements from stage two)

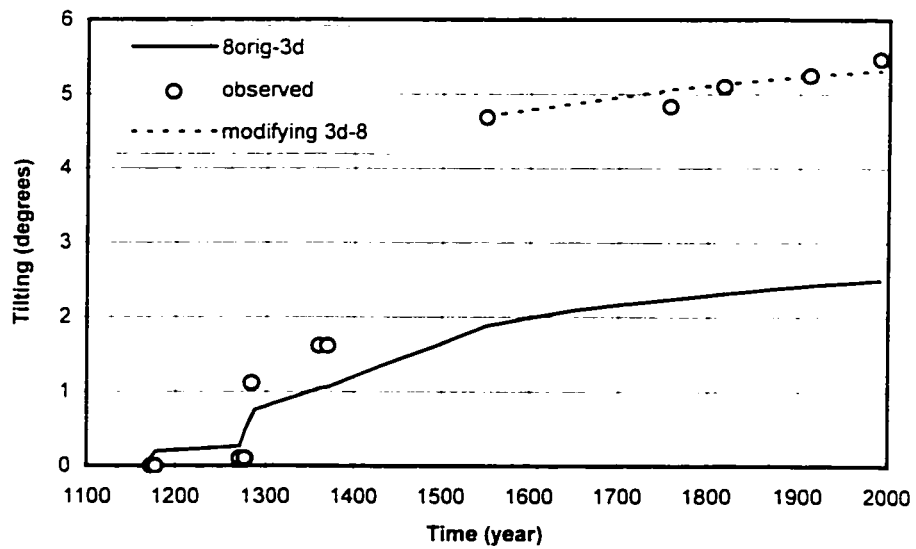


Fig. 6.25 Tilting history of the tower (original material parameters)

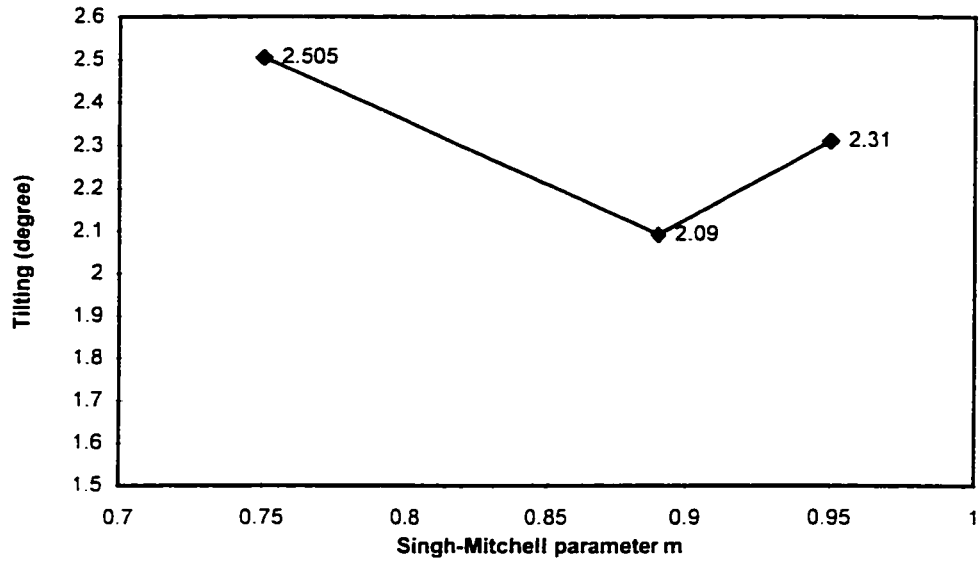


Fig. 6.26 Influence of Singh-Mitchell parameter m on tilting angle

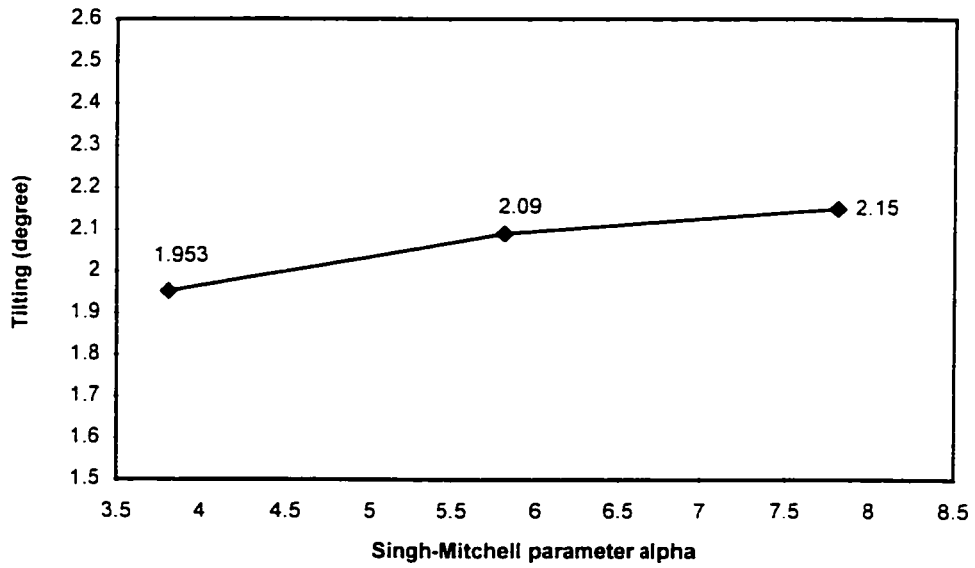


Fig. 6.27 Influence of Singh-Mitchell parameter alpha on tilting angle

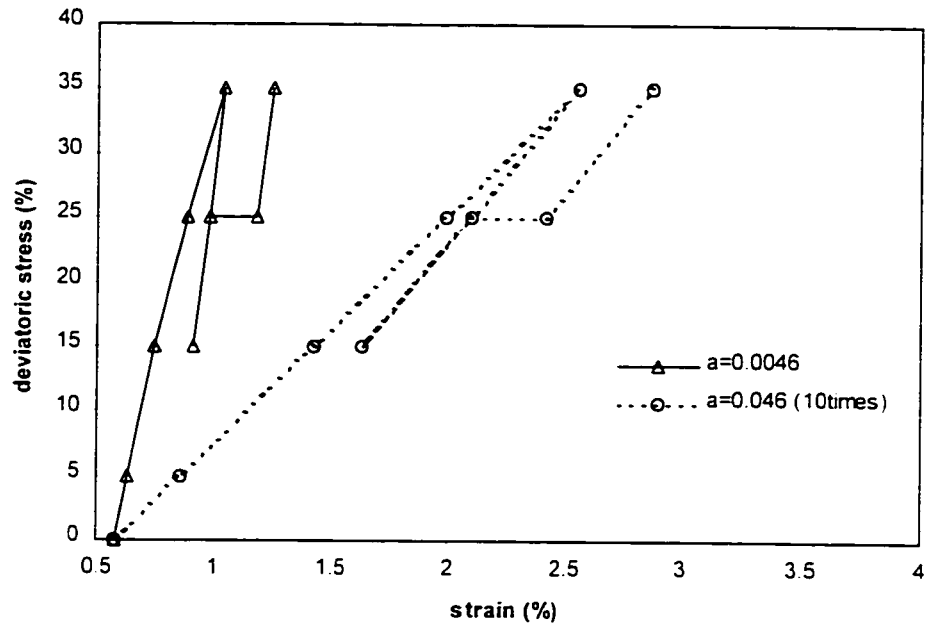


Fig. 6.28 Stress strain relationship under difference hyperbolic parameter a

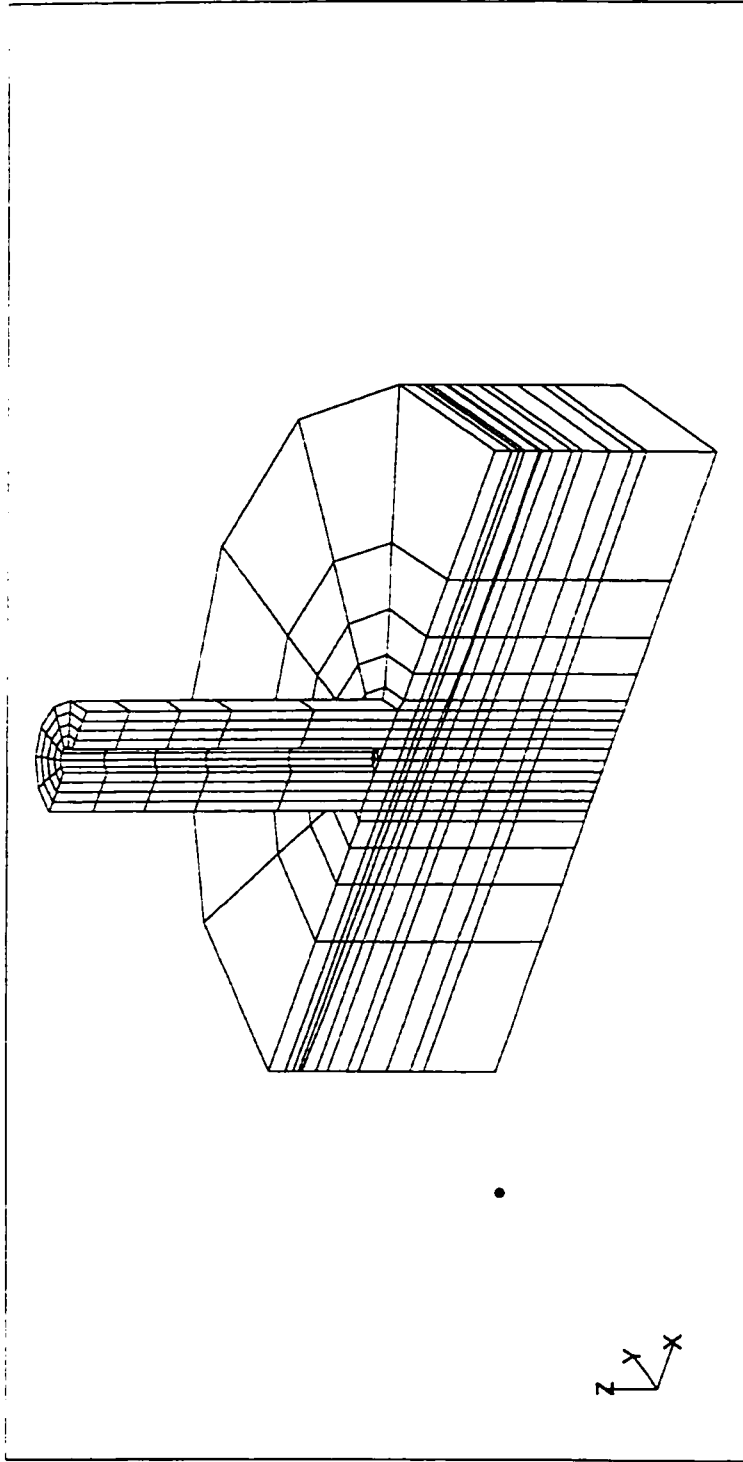


Fig. 6. 29 Three dimensional finite element model of Pisa Tower and its foundation

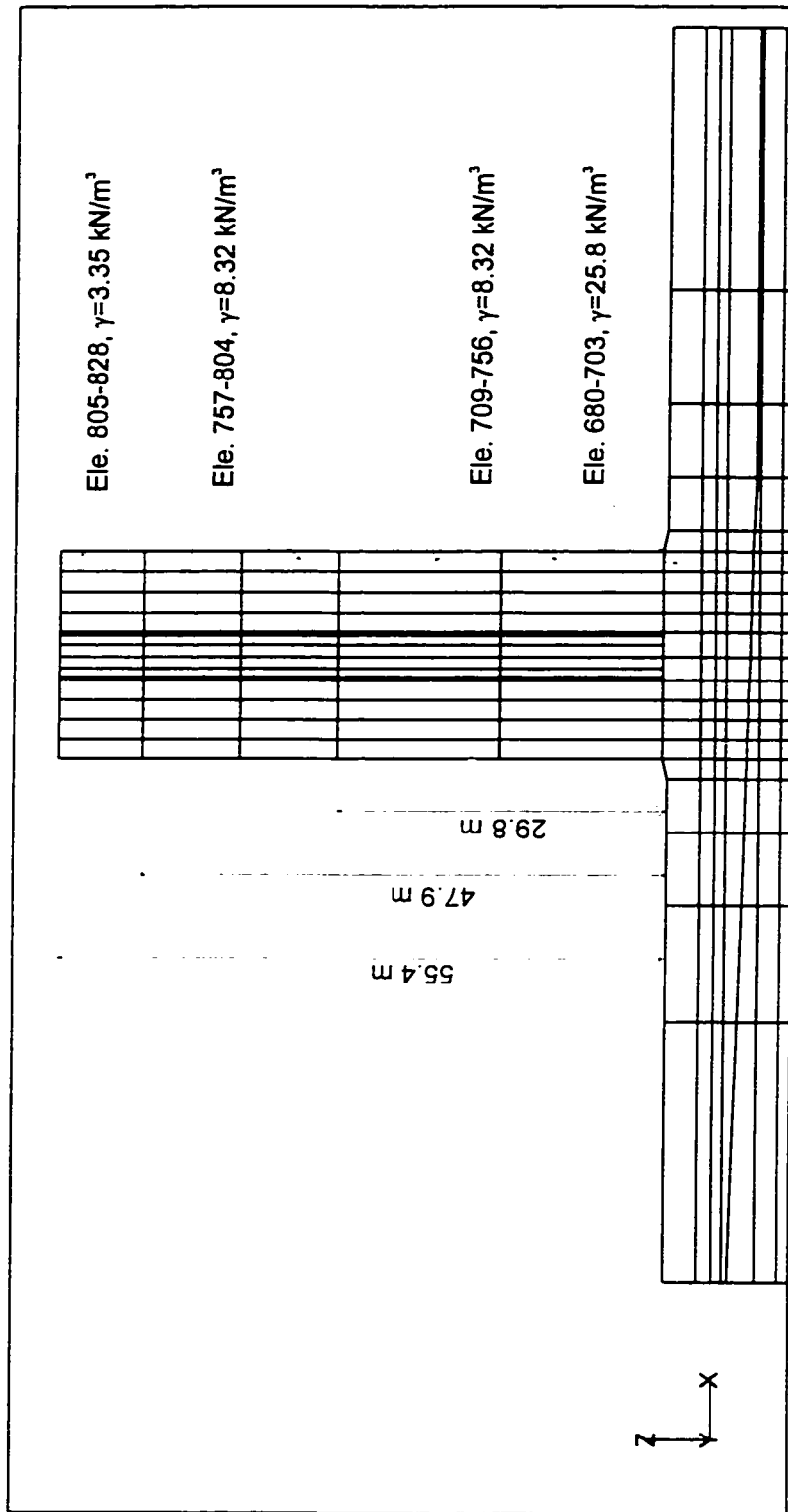


Fig. 6.30 Three-dimensional finite element model of Pisa Tower and its foundation (part)

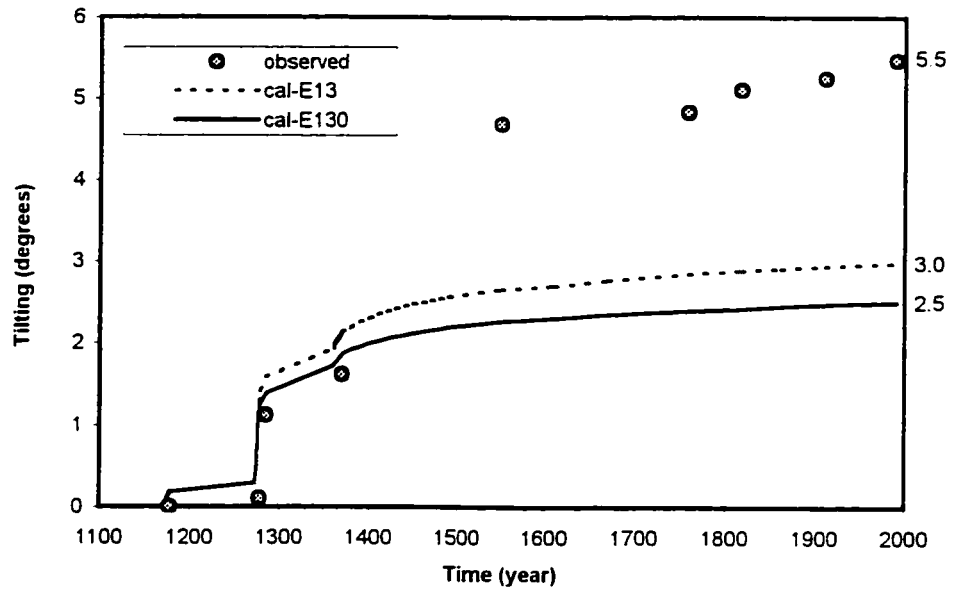


Fig. 6.31 (a) Tilting history of the tower
(8 weak elements from stage 2)

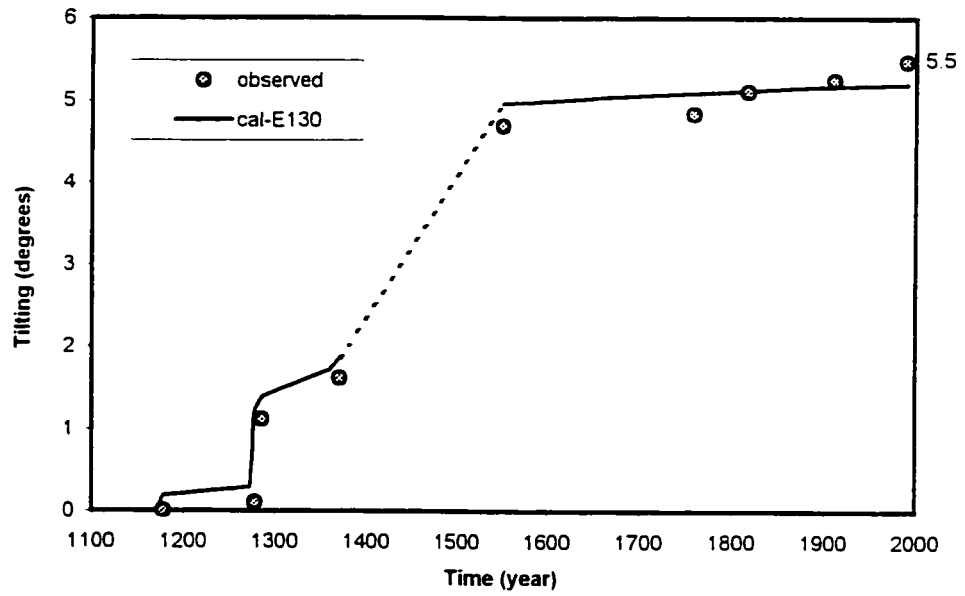


Fig. 6.31 (b) Tilting history of the tower
(8 two-order of weak elements from stage 2)

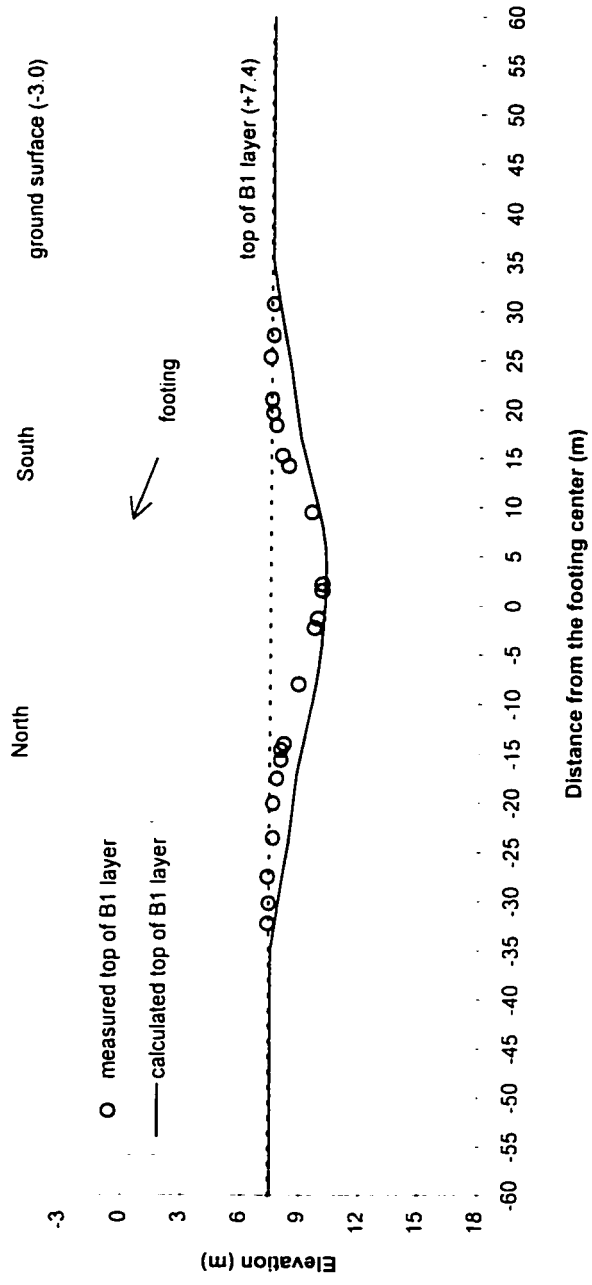


Fig. 6.32 Predicted final settlement profile at the top of upper clay layers

CHAPTER 7

CONCLUSIONS AND RECOMENDATIONS

7.1 Conclusions

This research studies the time-dependent deformation behavior of the soil underneath the Leaning Tower of Pisa. A double-yield surface Cam-clay plasticity model proposed by Hsieh (1987) is modified by changing the intrinsic time variables. Then the modified model is tested by simulating a series of drained creep triaxial tests conducted by Bishop and Lovenbury (1969) and Mitchell and Soga (1995). Results show that the modified model provides a more accurate and reasonable approximation in order to reflect the effect of the Singh and Mitchell parameter m . This model can be used to assess the stress-strain-time behavior of the soil beneath the Pisa Tower.

Two-dimensional plane strain results show that including creep in the model can predict the tilting of the tower much better than excluding it. The creep effect has contributed one meter of additional settlement and 1.7 degrees of additional tilting. Creep causes mean effective stresses to increase and deviatoric stresses to decrease in the clay layers. The impending instability of the footing may not be caused by the bearing capacity failure within the upper Pancone clay. The expected tilting angle of 5.5" could not be achieved by simply increasing the value of the correction factor I_c .

A comparison of the predicted tilting history with the measured one shows that creep may be an important factor during the construction period. After that, other factors may have contributed to the tilting of the tower, especially in the time period of 1370 to 1550. However, they are beyond the scope of the current numerical model.

An extensive model parameter sensitivity study shows that no specific model parameter is particularly sensitive compared with the rest. The angle of internal friction ϕ' and the Singh and Mitchell creep parameters m and $\bar{\alpha}$ are relatively sensitive in terms of the total settlement and the tilting angle. The deformation behavior of the soil beneath the foundation is not controlled by any specific parameter. It is the combination of all the time-independent as well as time-dependent parameters in the model. The stress level has more effect on the final results than the creep characteristics of material itself. Time-independent as well as time-dependent parameters become more sensitive under high stress levels. Increasing the accuracy of parameters of layer A_1 could improve the accuracy of analytical results.

The numerical model under three-dimensional conditions is capable of calculating the settlement profile on top of the upper clay layers with a fair accuracy. The predicted maximum settlement of 2.82 m is very close to the measured value of 2.64 m.

Three-dimensional creep analysis can predict the tilting history within a reasonable accuracy during the construction period and illustrate more or less the same trend for the last four centuries. The calculated maximum tilting angle is $3.0''$, of which creep effect contributes to $1.5''$. The actual $5.5''$ tilting angle cannot be reached by simply changing some material parameters in the DYSCP model. Many other reasons may have also contributed to the tilting, but cannot be simply quantified due to the complexity of the tilting history of the tower. Nevertheless, this study can quantify the creep effects on the deformation behavior and stress-strain distributions of the soil beneath the tower's foundation, which have not been achieved by others so far.

It must be kept in mind that the actual situation of the tower and the soil beneath its foundation is very complex. The current $5.5''$ tilting is the total result due to many different causes. Currently, no single numerical model could reasonably consider all of them. The model studied could only consider the influence due to the tower's weight and the soil creep.

7.2 Recommendations for further work

The application of new time-dependent numerical models, which can handle soils under high stress level conditions (more than 80% of their shear strengths), anisotropically consolidated soils or those stress paths that involve significant rotation of the principal-stress directions, and coupling between shear stress and volumetric strain on one side and the mean effective stress and shear strain on the other side, would improve the analytical results.

A model which can handle more than one mechanism, such as creep and leaning instability, will be helpful in simulating the deformation history of the tower.

Additional historical records related to what happened to the tower, especially during the years 1370 to 1550, would help to explain the difference between the predicted and the observed results.

Creep parameters used in this study were obtained based on creep tests with a duration of seven days for each load. When predicting the settlement and rotation of the tower over the 800 years period, uncertainty exists. A series of longer term drained creep tests are needed to further investigate the time dependency of Pisa soils.

BIBLIOGRAPHY

- Adachi T. and Oka F. 1982. Constitutive equations for normally consolidated clays based on viscoplasticity. *Soil and Foundations*, **22** (4): 57-70.
- Adachi T. and Okano, M. 1974. A constitutive equation for normally consolidated clay. *Soil and Foundations*, **14** (4): 55-73.
- Abdel Hadi, O.N., and Herrin, M. 1966. Characteristics of soil-asphalt as a rate process. *ASCE Journal of the Highway Division*, **92** (HW1): 49-69.
- AGI. 1991. The Leaning Tower of Pisa: Present situation. Deformation of Soil and Displacements of Structures. XECSMF, Florence, Italy. **4**: 1437-1445.
- Ansal, A.M., Bazant, Z.P., and Krizek, R. J. 1979. Viscoplasticity of normally consolidated clays. *ASCE Journal of the Geotechnical Engineering Division*. **105** (GT4): 519-537.
- Barden, L. 1965. Consolidation of clay with non-linear viscosity. *Geotechnique*. **15** (4): 345-362.
- Barden, L. 1969. Time dependent deformation of normally consolidated clays and peats. *ASCE Journal of Soil Mechanics and Foundation Engineering Division*. **95** (SM1): 1-31.
- Bazant, Z. P. and Krizek, R.J. 1976. Endochronic constitutive law for liquefaction of sand. *ASCE Journal of the Engineering Mechanics Division*. **102** (EM2): 225-238.
- Biot, M.A. 1941. General theory of three dimensional consolidation. *J. Appl. Physics*. **12**: 155-164.
- Bishop, A.E. and Lovenbury, H.T. 1969. Creep characteristics of two undisturbed clays. *Proceedings of the International Conference on Soil Mechanics and Foundation Engineering*, **1**: 29-37.
- Bjerrum, L. 1967. Engineering geology of Norwegian normally consolidated marine clays as related to settlements of buildings. *Geotechnique*, **17**: 83-117.

- Borja, R.I. 1984. Finite element analysis of the time-dependent behavior of soft clays. Ph.D. thesis. Stanford University, California.
- Borja, R.I. and Kavazanjian, E.Jr. 1985. A constitutive model for the stress-strain-time behavior of 'wet' clays. *Geotechnique*, **35** (3): 283-298.
- Borja, R.I., Hsieh, H.S., and Kavazanjian, E.Jr. 1990. Double-yield-surface model. II: Implementation and verification. *ASCE Journal of the Geotechnical Engineering Division*, **116** (GT9): 1402-1421.
- Borja, R.I. 1992. Generalized creep and stress relaxation model for clays. *ASCE Journal of the Geotechnical Engineering Division*, **118** (GT11): 1765-1786.
- Brandes, H. G., Silva, A. J., Sadd, M. H. and Veyera, G. E. 1994. Stress-strain-time modeling of submarine slopes. *Proc. 8th Int. Conf. On Computer Methods and Advances in Geomechanics*, **3**: 2435-2445.
- Brandes, H. G., Sadd, M. H., and Silva, A. J. 1996. Finite element modeling of a deep sea clay in long-term laboratory creep tests. *International Journal for Numerical and Analytical Methods in Geomechanics*, **20**: 887-905.
- Buisman K. 1940. *Grondmechanica*. Delf: waltman.
- Burghignoli, A., Chieppa, A., and Soccodato, F.M. 1994. A visco-plastic constitutive model for soft clay: implementation and validation. *Rivista Italiana Di Geotecnica*, **4**: 267-283.
- Burke, J.J. 1983. A non-linear finite element analysis of soil deformation. Ph.D thesis. Loughborough University of Technology.
- Burland, J.B. 1965. The yielding and dilation of clay. *Correspondence Geotechnique*, **15**: 211-214.
- Burland, J.B. 1991. Unpublished discussion reports to the Pisa Tower commission.
- Burland, J.B. and Potts, D.M. 1995. Development and application of a numerical model for the Leaning Tower of Pisa. Special Lecture. *International Symposium on Pre-Failure Deformation Characteristics of Geo-Materials, IS-Hokkaido*: 715-738.

- Calabresi, G. 1970. Creep di argille indisturbate in prove di taglio di lunga durata. Estratto Dalla, Rivista Italiana di geotechnica. Organo Dell'associazione Geotechnical Italiana. **1**.
- Calabresi, G., Rampello, S., and Callisto, L. 1992. Geotechnical characterization of the tower's subsoil within the framework of the critical state theory. Università di Roma. Dipartimento di Ingegneria Strutturale.
- Cambefort, H. 1978. Foundation performance of Tower of Pisa. Discussion. ASCE Journal of the Geotechnical Engineering Division. **104** (GT1): 156-160.
- Chang, C.Y., Nair, K., and Singh, R.D. 1974. Finite element methods for the non-linear and time-dependent analysis of geotechnical problems. Proc. Conf. Analysis and Design in Geotechnical Engineering, Austin. **2**: 269-302.
- Chan, D.H. and Morgenstern, N.R. 1992. User Manual of Program PISA. University of Alberta. Edmonton, Alberta, Canada.
- Christensen, R.W., and Wu, T.H. 1964. Analysis of clay deformation as a rate process. ASCE Journal of Soil Mechanics and Foundation Engineering Division. **90** (SM6): 125-157.
- Corneau, I.C. 1974. Viscoplasticity and plasticity in the finite element method. Ph.D. thesis. University College of Swansea.
- Corneau, I.C. 1975. Numerical stability in quasi-static elasto/visco-plasticity. International Journal for Numerical Methods in Engineering. **9**: 109-127.
- Croce A., Burghignoli A., Calabresi G., Evangelista A., and Viggiani C. 1981. The Tower of Pisa and the surrounding square: Recent observations. Proc. X ICSMFE. Stockholm. **3**: 61-70.
- Dafalias, Y.F. 1982. Bounding surface elastoplasticity viscoplasticity for particulate cohesive media. IUTAM Symp. on Deformation and Failure of Granular Materials. Rotterdam, Netherlands: 97-107.
- Darve, F. 1978. Une formulation incrementale des lois rheologiques; application aux sols. These de Docteur d'Etat. Institut de Mecanique de Grenoble.

- Darve, F. And Vuailat, P. 1982. A visco-elasto-plastic law for clays and its use. Proc. 4th ICONMIG, Edmonton, 1: 131-138.
- De Josselin De Jong 1968. Consolidation models consisting of an assembly of viscous element of a cavity channel network. *Geotechnique*, **18**: 195-228.
- Desai, C.S., and Zhang, D. 1987. Viscoplastic model for geologic materials with generalized flow rule. *Int. J. Num. Analytical Meth. in Geomech.*, **11**: 603-620.
- Desai, C.S., Samtani, N.C. and Vulliet, L. 1995. Constitutive modeling and analysis of creeping slopes. *ASCE Journal of the Geotechnical Engineering Division*, **121** (GT1): 43-56.
- Eyring, H. 1936. Viscosity, plasticity and diffusion as example of absolute reaction rates. *Journal of Chemical Physics*, **4**: 283-291.
- Feda, J. 1989. Interpretation of creep of soils by rate process theory. *Geotechnique*, **39**: 667-677.
- Gade J. and Gudehus G. 1992. The Leaning Tower of Pisa: Geotechnical theory and model tests. *Soils and Foundations*, **32** (3): 130-136.
- Hirst, T.J. 1968. The influence of compositional factors on the stress-strain-time behavior of soils. Ph.D thesis, University of California, Berkeley.
- Holzer, T.L., Hoeg K., and Arulanandan, K. 1973. Excess pore pressure during undrained creep. *Canadian Geotechnical Journal*, **10** (1): 12-24.
- Hsieh, H.S. 1987. A non-associative Cam-clay plasticity model for the stress-strain-time behavior of soft clays. Ph.D. thesis, Stanford University, California, U.S.A..
- Hsieh, H.S., Kavazanjian, E.Jr., and Borja, R.I. 1990. Double-yield-surface model. I: Theory. *ASCE Journal of the Geotechnical Engineering Division*, **116** (GT9): 1381-1401.
- Hvorslev, M.J. 1960. Physical components of shear strength of cohesive soils. ASCE, Research Conference on Shear Strength of Cohesive Soils, Boulder, Colorado, June: 169-273.

- Jamiolkowski, M., Levi, F., and Lancellotta, R. 1993. Leaning Tower of Pisa - updated information. Third International Conference on Case Histories in Geotechnical Engineering, St. Louis, Missouri, **2**: 1319-1330.
- Kaliakin, V.N., and Dafalias, Y.F. 1990. Theoretical aspects of the elastoplastic-viscoplastic bounding surface model for cohesive soils. *Soil and Foundation*, **30**: 11-24.
- Katona, M.G. 1984. Evaluation of viscoplastic cap model. *ASCE Journal of the Geotechnical Engineering Division*, **110** (GT8): 1106-1125.
- Katona, M.G. and Mulert, M.A. 1984. A viscoplastic cap model for soils and rocks. *Mechanics of engineering materials*, C.S. Desai and R.H. Gallagher, eds., John Wiley and Sons: 335-349.
- Kavazanjian, E. Jr., and Mitchell, J.K. 1977. A general stress-strain-time formulation for soils. *Proceedings, Specialty Session 9, 9th International Conference on Soil Mechanics and Foundation Engineering*, Tokyo, Japan: 113-120.
- Kavazanjian, E. Jr. 1978. A general stress-strain-time formulation for soils. Ph.D. thesis, University of California, Berkeley.
- Kavazanjian, E. Jr., and Mitchell, J.K. 1980a. Time-dependent deformation behavior of clays. *ASCE Journal of the Geotechnical Engineering Division*, **106** (GT6): 611-630.
- Kavazanjian, E. Jr., and Mitchell, J.K., and Bonaparte, R. 1980b. Stress-deformation predictions using a general phenomenological model. Position paper for the NSF/NSERC workshop on Limit Equilibrium, Plasticity and Generalized Stress-Strain in Geotechnical Engineering, McGill University, Montreal, Canada, May: 461-491.
- Kerisel, J. 1975. Old structures in relation to soil conditions. The Fifteenth Rankine Lecture. *Geotechnique*, **25** (3): 433-483.
- Kolymbas, D. 1987. A novel constitutive law for soils. 2nd Int. Conf. Constitutive Laws for Engineering Materials, Tucson, **1**: 319-326.
- Konder, R.L. 1963. Hyperbolic stress-strain response: Cohesive soils. *ASCE Journal of Soil Mechanics and Foundation Engineering Division*, **89** (SM1): 115-144.

- Kuhn, M.R. and Mitchell, J.K. 1993. New perspectives on soil creep. *ASCE Journal of the Geotechnical Engineering Division*, **119** (GT3): 507-524.
- Kulaway, F.H. and Mayne, P.W. 1990. Manual on estimating soil properties for foundation design. Final Report. Project 1493-6. EL-6800, Electric Power Research Institute, Palo Alto, California.
- Kutter, B.L., and Sathialingam, N. 1992. Elastic-viscoplastic modeling of the rate-dependent behavior of clays. *Geotechnique*, **42** (3): 427-441.
- Ladd, C.C., and Preston, W.B. 1965. On the secondary compression of saturated clays. Research report R65-59, Research in Earth Physics, Phase Report No. 6. Department of Civil Engineering, MIT, Cambridge, Massachusetts.
- Ladd, C.C. and Foott, R. 1974. New design procedure for stability of soft clays. *ASCE Journal of the Geotechnical Engineering Division*, **100** (GT7): 763-786.
- Lade, P.V., and Musante, H.M. 1976. Three-dimensional behavior of normally consolidated cohesive soil. Research Report *UCLA-ENG-7626*. University of California, Los Angeles..
- Lancellotta, R. And Pepe, C. 1990. Pisa Tower. A preliminary report. Polotecnico di Torino, Dipartimento Ingegneria Strutturale. Rapporto di Ricerca. No. 2.1. 2.2.
- Lancellotta, R. 1993. The Leaning Tower of Pisa: Geotechnical theory and model tests. Discussion. *Soil and Foundation*, **33** (3):155-156.
- Leonards, G.A. and Girault, P. 1961. A study of the one dimensional consolidation test. Proceedings, 5th International Conference on Soil Mechanics and Foundation Engineering, London, England, **1**: 213-218
- Leonards, G.A. 1979. Foundation performance of Tower of Pisa. Discussion. *ASCE Journal of the Geotechnical Engineering Division*, **105** (GT1): 95-105.
- Lizzi, F. 1990. The consolidation of the Leaning Tower of Pisa and the preservation of the Venice Lagoon. *Geotechnical Aspects of Restoration Works*. Balasubramaniam et al. (Eds). Bakema, Rotterdam: 17-33.
- Loudon, P.A. 1967. Some deformation characteristics of Kaolin. Ph.D. thesis. Cambridge University, England.

- Lovenbury, H.T. 1969. Creep characteristics of London clay. Ph.D thesis. Imperial College.
- Matsui, T. and Abe, N. 1985. Elasto-viscoplastic constitutive equation of ICONMIG. Nagoya, **1**: 407-413.
- Mayne, P.W. and Kulhawy, F.H. 1982. K_0 - OCR relationships in soil. ASCE Journal of the Geotechnical Engineering Division, **108** (GT6): 851-872.
- Mesri, G. 1973. Coefficient of secondary compression. ASCE Journal of Soil Mechanics and Foundation Engineering Division, **99** (SM1): 123-137.
- Mesri, G. and Goldewski, P.M. 1977. Time stress compressibility relationship. ASCE Journal of the Geotechnical Engineering Division, **103** (GT5): 417-430.
- Mesri, G., Febres, C.E., Shield, D. R., and Castro, A. 1981. Shear stress-strain-time behavior of clays. Geotechnique, **31**: 537-552.
- Ministero dei Lavori Pubblici. 1971. Ricerche e studi su la Torre pendente di Pisa ed I fenomeni connessi alle condizioni di ambiente. I.G.M. Firenze.
- Mitchell, J.K. 1964. Shearing resistance of soil as a rate process. ASCE Journal of Soil Mechanics and Foundation Engineering Division, **90** (SM1): 29-61.
- Mitchell, J.K. 1977. Additional comments and written discussions. Proceedings, Specialty Session 9, 9th International Conference on Soil Mechanics and Foundation Engineering, Tokyo, Japan: 296-298..
- Mitchell, J.K., Vivatrat, V., and Lambe, T.W. 1977. Foundation performance of Tower of Pisa. ASCE Journal of the Geotechnical Engineering Division, **103** (GT3): 227-249.
- Mitchell, J.K., Vivatrat, V., and Lambe, T.W. 1979. Foundation performance of Tower of Pisa. Discussion Closure. ASCE Journal of the Geotechnical Engineering Division, **105** (GT11): 1361-1365.
- Mitchell, J.K. 1991. Conduction phenomena: from theory to geotechnical practice. 31st Rankine Lecture. Geotechnique, **41**: 299-340.

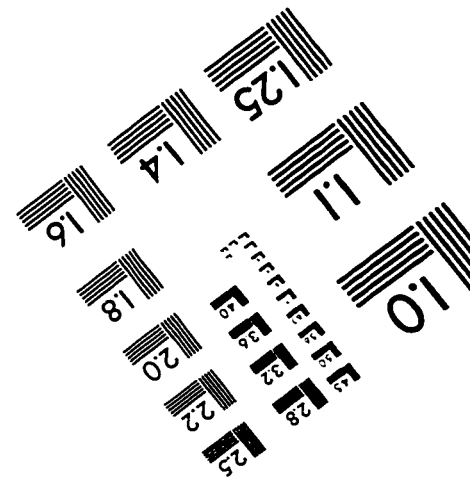
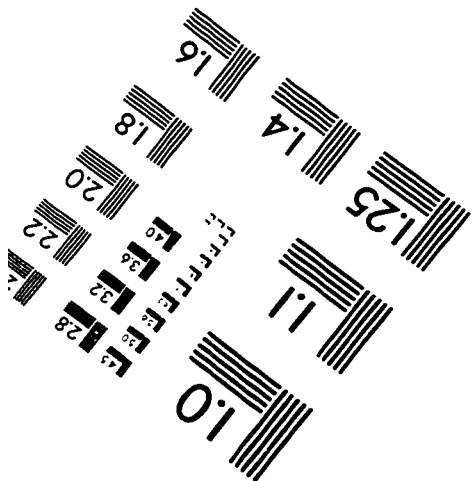
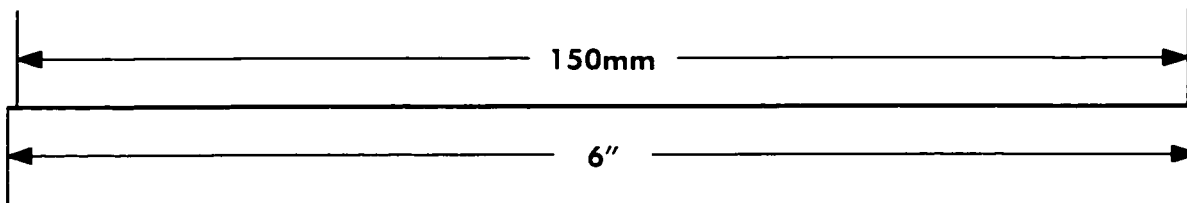
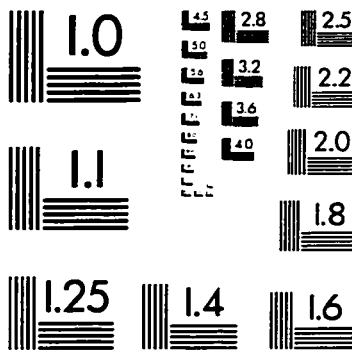
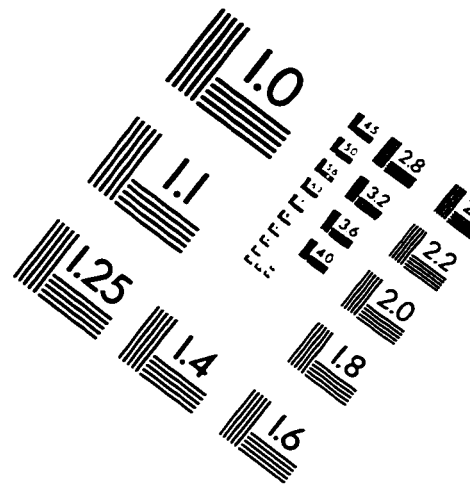
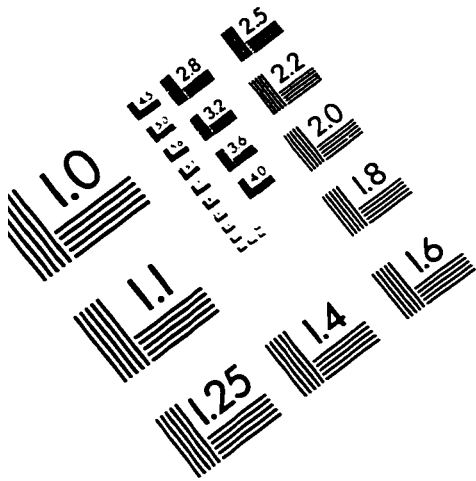
- Mitchell, J.K. and Soga, K. 1995. Numerical and experimental studies related to the performance and stabilization of the Tower of Pisa. Report to the Consorzio Progetto Torre di Pisa.
- Morsy, M.M. 1994. Effective stress modeling of creep behavior of clay. Ph.D. thesis. University of Alberta, Edmonton.
- Morsy, M. M., Chan, D. H., and Morgenstern N. R. 1995. An effective stress model for creep of clay. *Canadian Geotechnical Journal*, **32**: 819-834.
- Morsy, M. M., Morgenstern N. R., and Chan D. H. 1995. Simulation of creep deformation in the foundation of Tar Island Dyke. *Canadian Geotechnical Journal*, **32**: 1002-1023.
- Murayama, S.. and Shibata, T. 1958. On the rheological characters of clay. part 1. Disaster Prevention Research Institute, Kyoto University. *Bulletin*, **26**.
- Murayama, S.. and Shibata, T. 1961. Rheological properties of clay. *Proceedings, 5th International Conference on Soil Mechanics and Foundation Engineering, Paris, France*, **1**: 269-273.
- Nathan, S.V. 1978. Foundation performance of Tower of Pisa. Discussion. *ASCE Journal of the Geotechnical Engineering Division*, **104** (GT2): 296-298.
- Nova, R. 1982. A viscoplastic constitutive model for normally consolidated clay. *IUTAM Conf. Deformation and Failure of Granular Materials, Delft*: 287-295.
- Oliver, A. 1995. Pisa problems. *Civil Engineering News*, Nov.: 16-17.
- Parker, D. 1995. Work starts on Pisa foundation collar. *Civil Engineering News*, May: 6.
- Pepe, m.. 1995. Torre Pendente di Pisa. Analisi teorico-sperimentale della stabilita dell' equilibrio. Ph.D thesis, Politecnico Di Torino.
- Perloff, W.H. 1962. The effects of stress history and strain rate on the undrained shear strength of cohesive soils. Ph.D. thesis, Northwestern University, at Evanston.
- Perzyna, P. 1963, The constitutive equations for work hardening and rate sensitive plastic materials. *Quart. Appl. Math.*, **20**: 321-332.

- Pusch, R., and Feltham, P. 1980. A stochastic model of the creep of soils. *Geotechnique*, **30** (4): 497-506.
- Pusch, R., and Feltham, P. 1981. Computer simulation of creep of clay. *ASCE Journal of the Geotechnical Engineering Division*, **107** (GT1): 95-104.
- Roscoe, K.H., Schofield, A.N., and Turairajah, A. 1963. Yielding of clays in state wetter than critical. *Geotechnique*, **13**: 211-246.
- Roscoe, K.H., and Burland, J.B. 1968. On the generalized stress-strain behavior of "wet" clay. *Engineering Plasticity*. Edited by J. Heyman and F.A. Leckie. Cambridge University Press. Cambridge, England.
- Samtani, N.C., and Desai, C.S. 1991. Constitutive modeling and finite element analysis of slowly moving landslides using the hierarchical viscoplastic material model. Rep. To National Science Foundation. Dept. Of Civil Engrg. And Engrg. Mech., University of Arizona. Tucson, Ariz.
- Sekiguchi H. 1977. Rheological characteristics of clays. *Proceedings of 9th International Conference on Soil Mechanics and Foundation Engineering*. Tokyo, Japan. **1**: 289-292.
- Schiffman, R.L. 1959. The use of visco-elastic stress-strain laws in soil testing. *ASTM special technical publication* **254**: 131-155.
- Schultze, E. 1973. *Der schiefe Turm von Pisa*. Mitt. Tech. Hochschule, Aachen Germany, 1973.
- Singh, A., and Mitchell, J.K. 1968. Generalized stress-strain-time function for soil. *ASCE Journal of Soil Mechanics and Foundation Engineering Division*, **94** (SM1): 21-46.
- Tamagnini, C. 1993. Private communication with Mitchell, J.K..
- Taylor, D.W. 1942. Research on consolidation of clays. Report Serial No. 82. Department of Civil Engineering, MIT, Cambridge, Massachusetts.
- Taylor, D.W. 1948. *Fundamentals of soil mechanics*. New York, Wiley.
- Terracina, F. 1962. Foundations of the tower of Pisa. *Geotechnique*, **12** (4): 336-339.

- Terzaghi, K. 1934. Die Ursachen der schiefstellung des Turms von Pisa. Der Bauingenieur, No. 1/2: 1-4 (Reprinted in From Theory to Practice in Soil Mechanics. Bjerrum et al., eds., John Wiley and Sons, Inc., New York, N.Y., 1960)
- Terzaghi, K. 1941. Undisturbed clay samples and undisturbed clays. Journal of the Boston Society of Civil Engineering, **15** (3): 645-660.
- Terzaghi, K. 1943. Theoretical Soil Mechanics. John Wiley and Sons. New York.
- Valanis, K.C. 1971. A theory of viscoplasticity without a yield surface: Part I. General theory; Part II. Application to mechanical behavior of metals. Archives of Mechanics (Archiwum Mechaniki stosowanej), **23**: 517-555.
- Verlag La Torre s.r.l. 1984. Pisa in the centuries.
- Vulliet, L., and Desai, C.S. 1989. Viscoplasticity and finite elements for landslide analysis. 12th Int. Conf. On Soil Mech. And Found. Eng., International Society of Soil Mechanics and Foundation Engineering, Rio de Janeiro, Brazil, **2**: 801-806.
- Walker, L.K. 1969. Secondary compression in the shear of clays. ASCE Journal of Soil Mechanics and Foundation Engineering Division, **95** (SM1): 167-188.
- Wedage, A.M.P. 1995. Influence of rate effects on the residual strength of moving slopes. Ph.D. thesis, University of Alberta, Edmonton.
- Wheeler Paul. 1995. Work suspended as Pisa delivers surprise. Ground Engineering, Oct.:4.
- Wroth, C.P., and Loudon, P.A. 1967. The correlation of strains within a family of triaxial tests on overconsolidated samples of Kaolin. Proceedings, 1st Geotechnical Conference on Shear Properties of Natural Soils and Rocks, Oslo, Norway, **1**: 159-163.
- Wu, T.H., El Rafai, A.N., and Hsu, J.R. 1978. Creep deformation of clays. ASCE Journal of Geotechnical Engineering Division, **104** (GT1): 61-76.
- Yin, J.H., and Graham, J. 1991. Axisymmetric elastic visco-plastic modeling of compacted sand-bentonite. Proc. 3rd Int. Conf. On Constitutive Laws for Eng. Materials, Tucson, **1**: 337-340.

- Yoshikuni, H., Kusakabe, O., Hirao, T., and Ikegami, S. 1994. Elasto-viscous modeling of time-dependent behavior of clay. Proceedings. 13th International Conference on Soil Mechanics and Foundation Engineering. New Delhi, India. 1: 417-420.
- Zienkiewicz, O.C., and Corneau, I.C. 1974. Visco-plasticity, plasticity and creep in elastic solids--A unified numerical approach. International Journal for Numerical Methods in Engineering, 8: 821-845.

IMAGE EVALUATION TEST TARGET (QA-3)



APPLIED IMAGE, Inc
1653 East Main Street
Rochester, NY 14609 USA
Phone: 716/482-0300
Fax: 716/288-5989

© 1993, Applied Image, Inc., All Rights Reserved